



Durham E-Theses

Studies of distant clusters of galaxies

MacLaren, Ian

How to cite:

MacLaren, Ian (1987) *Studies of distant clusters of galaxies*, Durham theses, Durham University.
Available at Durham E-Theses Online: <http://etheses.dur.ac.uk/6891/>

Use policy

The full-text may be used and/or reproduced, and given to third parties in any format or medium, without prior permission or charge, for personal research or study, educational, or not-for-profit purposes provided that:

- a full bibliographic reference is made to the original source
- a [link](#) is made to the metadata record in Durham E-Theses
- the full-text is not changed in any way

The full-text must not be sold in any format or medium without the formal permission of the copyright holders.

Please consult the [full Durham E-Theses policy](#) for further details.

Studies of Distant Clusters of Galaxies.

by

Ian MacLaren

August, 1987.

An account of work done at the Department of Physics and submitted to the University of Durham in accordance with the regulations for admission to the degree of Doctor of Philosophy.

The copyright of this thesis rests with the author.
No quotation from it should be published without
his prior written consent and information derived
from it should be acknowledged.



Abstract

A technique of constructing crude, low-resolution Spectral Energy Distributions (SEDs) for galaxies in distant clusters, using a set of intermediate bandwidth filters and a CCD detector, is developed which is capable of redressing many of the problems which have previously beset work in this field. The technique has been used to study galaxies in the distant clusters 0016+16 ($z = 0.54$) and Abell 370 ($z = 0.37$).

These SEDs are then used to individually classify each object in the CCD field, ascribing both an estimated redshift and a galaxy type. The SEDs have been extended into the rest-frame ultraviolet (~ 270 nm) by imaging high redshift galaxies in blue passbands. Monitoring the behaviour of the Colour-Magnitude effect in the optical and ultraviolet (uv) regions, indicates the presence of a new class of object which exhibits excess emission in the uv, whilst having optical colours similar to nearby E/S0 galaxies.

The significance of this uv-excess is addressed by examining the available uv spectroscopy of nearby early-type galaxies obtained from observations carried out on the *International Ultraviolet Explorer* satellite. This study, in conjunction with a series of crude evolutionary models, leads to the conclusion that the uv-excess is most likely a manifestation of evolutionary differences in the spectral properties of galaxies at high redshifts, resulting from increased levels of star formation.

Having developed such methods for using distant clusters of galaxies as evolutionary probes, a catalogue of candidate distant clusters is constructed from high contrast copies of deep 4m photographic plates. Finally, a series of possible future observations based on such a resource, combining a wide range of techniques, is outlined.

'S treasa tuath 'na tighearna!

'Bùrn is moine 's coirc'

*“ An cridhe ri bacan, car ma char aig an fheist
's i fàs goirid,
's an inntinn saor.
Is daor a cheannaich mi a saorsa. ”*

Ruaraidh MacThomais.

Contents

Preface	6
1. Galaxy Evolution and Studies of Distant Clusters.	
1.1 Introduction	7
1.2 What kind of evolution can we expect?	8
1.3 What can nearby galaxies tell us?	9
1.4 Looking Back	12
1.5 Distant Clusters of Galaxies	13
1.6 Aims and Outline	19
2. Multicolour Photometry of Distant Galaxies	
2.1 Introduction	21
2.2 Spectral Energy Distributions of nearby galaxies	22
2.3 Modelling Galaxy Type and Redshift	24
2.4 Observations	33
2.5 Conclusions	37
3. CCD Photometry of the Distant Cluster 0016+16	
3.1 Introduction	38
3.2 Observations	39
3.3 Data Reduction	39
3.4 Colour Distributions	50
3.5 Spectral Energy Distributions	55
3.6 Spectral Evolution	69
3.7 Spectroscopy	77
3.8 Summary and Conclusions	79

4.	CCD Photometry of the Distant Cluster Abell 370.	
4.1	Introduction	81
4.2	Observations and Data Reduction	84
4.3	Errors	86
4.4	SEDs and Object Classifications	90
4.5	Spectral Evolution	114
4.6	Spectroscopy	119
4.7	Summary and Conclusions	124
5.	Ultraviolet Colours and Spectral Evolution	
5.1	Introduction	125
5.2	UV Colour-Magnitude Relation	125
5.3	Galaxy Evolution in Distant Clusters	141
5.4	Discussion	157
6.	A Catalogue of Distant Clusters of Galaxies	
6.1	Introduction	162
6.2	Detection Method	165
6.3	The AAO Deep Cluster Catalogue	175
6.4	Spectroscopy and Further Observations	175
6.5	Discussion	183
6.6	Conclusions	203
7.	Summary and Future Work	
7.1	Summary	204
7.2	Suggestions for Future Work	205
7.3	Postscript	206
	References	208
	Acknowledgements	212

Preface.

The work described in this thesis was undertaken between 1983 and 1987, whilst the author was a SERC sponsored research student under the supervision of Prof.R.S. Ellis. None of this work has been submitted for any degree, diploma, or other qualification at any other university. Some of the research was carried out in collaboration with Prof.R.S. Ellis and Dr.W.J. Couch, but the majority is the author's own work. Certain results have been presented in the following papers:

Ellis,R.S., Couch,W.J., MacLaren,I., & Koo,D.C., 1985, *Mon. Not. R. Astr. Soc.*, **217**,239.

Ellis,R.S., Couch,W.J., MacLaren,I., Malin,D.F., 1985, Conference Poster (Santa Barbara), & Preprint.

MacLaren,I., Ellis,R.S., Couch,W.J., 1986, *Space Telescope Preprint Series*, **130**, *Stellar Populations*.

MacLaren,I., Ellis,R.S., Couch,W.J., 1987, *Mon. Not. R. Astr. Soc.*, submitted, July 1987.

1. Galaxy Evolution and Studies of Distant Clusters.

1.1 Introduction

An understanding or appreciation of the nature of how galaxies have evolved from their epoch of formation to the present-day will provide us with important clues to some of the fundamental problems of cosmology and astrophysics.

For example, if we could accurately determine the ages of galaxies, we would have a key foothold on theories of the formation of structure in the universe. Such structure, observed over a wide range of scales (globular clusters, galaxies, groups of galaxies, clusters, superclusters) is presumed to have arisen as a consequence of fluctuations in the density of the matter and radiation present in the early universe, differing theories leading to a variety of predictions regarding galaxy formation.

A further problem of cosmological interest is the value of the deceleration parameter, q_0 , which describes the rate at which the universe's expansion is slowing down. The standard tool used in such studies is the Hubble diagram which is a plot of magnitude versus redshift for a specific type of object. Two possible 'standard candles' for such observations are the brightest member galaxy in a rich cluster, or the characteristic luminosity defined by the position of the 'knee' in the cluster's luminosity function (see, eg, Bahcall, 1977). However, one of the problems in using galaxies as such 'candles' is that we must be able to sufficiently account for the change of luminosity with time that arises in galaxies due to the evolution of their constituent stellar populations.

Galaxy evolution studies should also provide an understanding of why, at the present-day, we observe a variety of different types of galaxy, such as ellipticals, lenticulars, and spirals. Furthermore, we should also hope to understand the reasons for the observed (Oemler, 1974, Dressler, 1980) relation between a galaxy's morphology and the density of its local environment; with early-type systems (E/S0s) predominating in dense regions such as the cores of rich clusters, whereas spirals are most commonly found in the field. The debate as to whether such segregation is due to 'nature' or 'nurture' has not yet been satisfactorily resolved and continues to date (see, e.g., Godwin, 1976, Gisler, 1980, Dressler, 1980, 1984).

Knowledge of the rate of star formation in galaxies and its change with time may also shed light on the physical processes involved in large-scale star formation itself, such as its relation to gas supply, shock waves, and galaxy interactions. It is also of interest to investigate how the star formation in a galaxy can be related to activity in the nucleus, and speculation as to any possible connection between phenomena such as quasars and primeval galaxies.

Clusters of galaxies are an invaluable probe of evolutionary behaviour since they provide us with large samples of galaxies at a fixed distance, over a wide range of luminosities. Furthermore, by studying increasingly distant objects we are looking further back in time in the history of the universe. Comparison of the properties of distant galaxies with those at epochs closer to the present-day will illustrate the nature and extent of any evolution that has taken place.

This is the basis of the subject addressed by this thesis. Such a variety of topics shows just how significant would be any major progress in our understanding of the evolution of galaxies. In this chapter I shall describe our basic present-day knowledge of the subject both from theory and observation, concentrating on those aspects which are most directly relevant to photometric and spectroscopic studies of distant galaxy clusters.



1.2. What kind of evolution can we expect ?

Firstly I shall consider the evolutionary synthesis approach originally pioneered by Tinsley (see Tinsley, 1979 for a review) and her co-workers, and subsequently developed by Bruzual(1981). Basically these workers have attempted to combine our knowledge of stellar evolution with simple analytic expressions for star formation rates, in order to predict changes in the spectral form (e.g. colours, strengths of spectral features) and luminosity of galaxies as they evolve. I shall now briefly outline the key points and results of such techniques.

The expected number of stars formed per unit mass, per unit time can be expressed as the product of the star formation rate (SFR) and the distribution of stellar masses (initial mass function, IMF). The IMF is usually taken to be of a power-law form, as for example $m^{-(1+x)}$, where $x = 1.35$ in the Salpeter (1955) case. More recent work, e.g. Miller and Scalo (1979), has given rise to a slightly more complicated form, but for the purposes of these models the only assumption about the IMF is that it be a simple function of stellar mass.

The simplest scenario arises from the observation that elliptical galaxies (and globular clusters) do not contain any significant amount of gas or ongoing star formation at the present day. A star formation history which could conceivably explain the known properties of such systems is that of a single burst of star formation (at the epoch of galaxy formation) lasting for a period (t) that was short in comparison to the galaxy's present age. Such simple models could qualitatively, at least, explain the observed red colours of ellipticals in comparison to spiral and irregular galaxies in which the bluer colours are indicative of substantial levels of ongoing star formation.

In what follows, I shall primarily be concerned with the early-type galaxies since these types predominate (at the present epoch) in the rich cluster environment. As an illustrative example let us consider Bruzual's (1981,1983) set of models. In his notation the single initial burst models are known as the constant or c-models and the SFR is analytically expressed as:

$$SFR = \frac{M_0}{\tau}, 0 \leq t \leq \tau, \quad (1.1)$$

where M_0 is the total mass of the system, and where no star formation takes place for times, $t > \tau$.

An alternative to this is that of initial maximum star formation with a subsequent exponential decline;

$$SFR = \frac{M_0}{\tau} \exp\left(\frac{-t}{\tau}\right) \quad (1.2)$$

These models are usually described by the parameter μ which specifies the fraction of the mass of the galaxy that would be in stars after 1 Gyr.

The combination of these analytical expressions with available evolutionary tracks, such as those of Ciardullo and Demarque (1977), allows us to predict the number of stars present in various stellar types at a given time during the system's evolution. We are then able, using observed stellar spectra, to construct a composite spectrum as a model for the galaxies under consideration. These crude synthetic spectra can provide us with predictions for the evolution of, for example, broad-band colours and various spectral features with time which can then be directly compared with observed galaxies, both local and over a large range of redshifts.

Note that a number of major simplifying assumptions (Bruzual, 1981) must be made in such attempts to model evolution. Bruzual's models take galaxies as being closed systems with no consideration given to infall or loss of material from the galaxy. Furthermore chemical evolution, dust and gas effects are all ignored.

As can be seen in Fig. 1.1, the c-models are much too red in comparison to a nearby observed galaxy spectrum. The reason for such a failure to match the blue end of the spectrum may largely be due to the fact that the stellar evolutionary tracks are limited by our current knowledge which is unable to fully understand the more advanced evolutionary stages beyond Helium ignition (e.g. Horizontal Branch). Only when such limitations are overcome can we address the likely realism of this particular evolutionary scenario.

The μ -models, in which star formation still continues (in exponentially decreasing amounts) up to the present day, apparently yield a much better fit to the observations. This better fit is simply due to the blue light from the current star formation in the models substituting for the stellar components that are missing from the c-models.

In summary, therefore, it should be noted that progress in this field can be achieved by, (a) improving our somewhat limited picture of stellar evolution, and by (b) using a series of observations of galaxies of a given type over a range of redshifts to help discriminate between various possible models and scenarios.

1.3. What can nearby galaxies tell us about their past histories?

A second approach to the study of galaxy spectral evolution is to look for relics of past star formation in nearby galaxies using the Population Synthesis method.

The ages of composite stellar systems such as globular clusters can be estimated from examination of the cluster colour-magnitude diagram. In such plots there is a termination point in the extent of the main-sequence whose presence can be understood by virtue of the fact that main-sequence lifetimes are shorter for more massive stars. This observable main-sequence turn-off (MSTO) point is a sensitive function of age and thus, by comparison with theoretically predicted isochrones (dependent on an assumed chemical abundance), we can in principle achieve an estimate for the ages of our observed clusters. In practice there are many difficulties and uncertainties in such a procedure (see Mihalas and Binney, 1981 for discussion). When we try to consider the ages of galaxies we are also faced with the difficulty of having to interpret measurements of the integrated light from the various stellar components.

In Population Synthesis (PS) we attempt to fit the observed integrated spectrum of the galaxy under consideration by a combination of all available stellar spectra, the actual relative numbers of the constituent populations being obtained from that combination which has minimal discrepancies (within observational error) with the observed spectrum in terms not only of continuum shape but also strengths of important spectral lines and features (O'Connell, 1973). At first glance this seems reasonably straightforward. Stellar spectra, however, do not form a mathematically independent set, and variations in relative numbers, luminosities, and spectral types severely limit the ability of such a technique to achieve a unique solution. The problem can be alleviated somewhat by the imposition of a set of constraints on the variety of possible combinations. These constraints are usually the minimum necessary to yield "astrophysically plausible" results. In order not to pre-determine the final synthesis, care must be taken to ensure that only as few constraints as possible are imposed and that these do not make a priori assumptions about the evolutionary states of the various components.

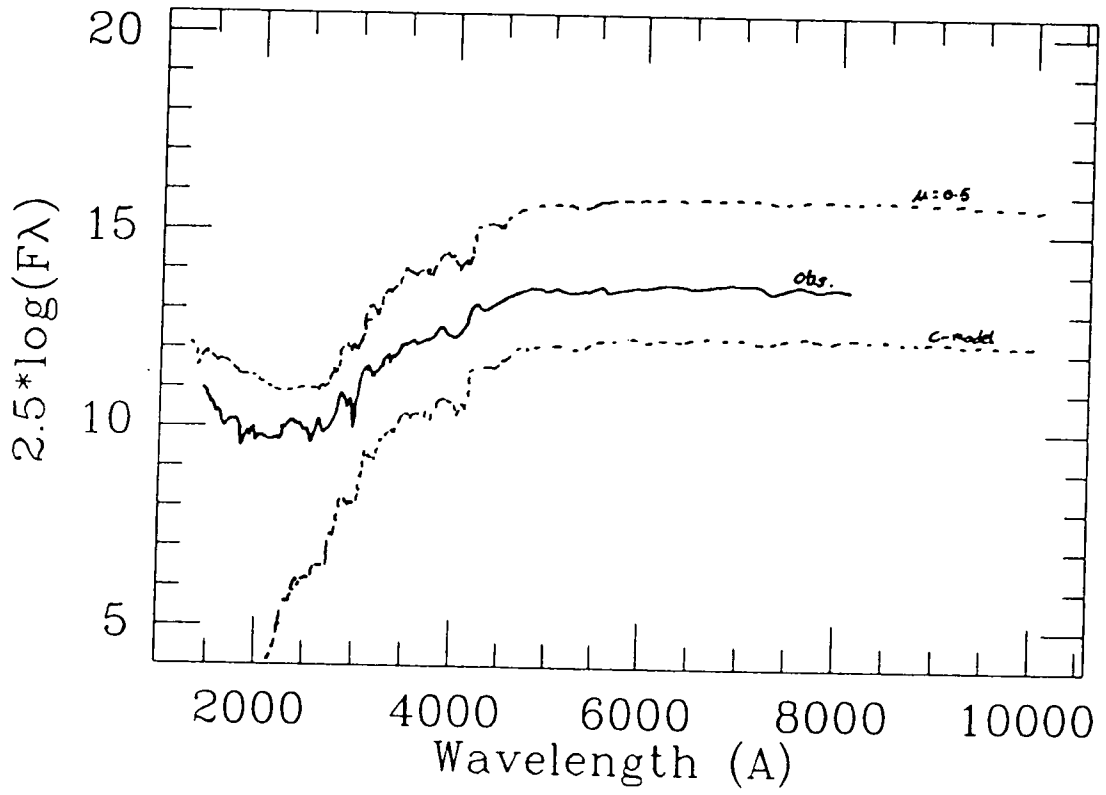


Figure 1.1: The Bruzual spectral evolution models compared to a nearby elliptical galaxy spectrum from Pence (1976).

A further precaution to be taken in the PS method is that since the technique is only capable of finding the best fit to the observations using mixtures of the supplied stellar spectra, the range of stellar types covered by the library of spectra should cover all possibilities. In recent studies, however, stellar libraries are usually fairly comprehensive. O'Connell (1986) even claims that in some cases the absence of an important stellar type from the library can be implicit in the poorness or extreme nature of the solution obtained. However, great care must be taken in such an interpretation.

It should be noted that one of the most severe difficulties is that the solutions obtained are dependent on the assumed metallicity. It is vital not to underestimate the importance of this effect; changes in metallicity can be approximated by changes in temperature, so that as the metallicity increases, the age inferred from a given main-sequence turnoff colour decreases.

These problems provide the most basic intrinsic difficulties of PS. Most of the early work was carried out at fairly poor resolution, but more recent work attempts to fit not only continuum colours but also important spectral features and by having as large a wavelength coverage as possible, as well as increased resolution. Let us now consider, the application of PS to bright, nearby early-type galaxies.

O'Connell (1976,1980) has carried out much of the ground-work in this field and has published results for the nuclei of three giant ellipticals in Virgo (NGC 4374, NGC 4472(M49), NGC 4552(M89)), the nucleus of M31, and the low-luminosity elliptical M32. The details of the linear programming technique employed by him to minimise the difference between syntheses and observations can be found in the references given, with a review of his and other workers' results in O'Connell (1986). In summary his conclusions are as follows.

For the galaxies he has considered there appears to be evidence of the presence of a significant intermediate-age population. That is, he finds that the best agreement is attained with relatively young ages (compared with those of the globular clusters) for the main sequence turn-off, suggesting that elliptical galaxies cannot simply be understood as single generation bursts with the same age as the globular clusters (15 Gyr.). Such models would fit the observed red colours of gEs but fail to match their blue ($<4300\text{\AA}$) colours, discussed in the previous section (such discrepancies were often compensated for in evolutionary models by simply adding groups of younger stars).

Obviously, information on the luminosity dependence of the age of the MSTO is of great importance. However, O'Connell (1980) has only considered M32 in detail as a low-luminosity elliptical and he concludes from its observed turn-off ($B - V \sim 0.5$ (F8 spectral type) that it was undergoing substantial star formation up to 5-6 Gyr ago. But objections have been raised that an extrapolation of this result to form a general model of luminosity-dependence may be invalid when one considers the nature of M32's dynamical relationship with M31.

An independent but similar procedure has been undertaken by Pickles (1985, Pickles and Visvanathan, 1985) by performing syntheses for 12 elliptical and 5 lenticular galaxies covering a 6 magnitude range, all in the Fornax cluster. His results are in agreement with those of O'Connell to the extent that he also finds the presence of a young age for the MSTO in these galaxies.

It should be stressed here that a young age for the MSTO does not imply that the galaxy itself may have formed at such a late epoch, since any previous generation of star formation would have a redder turn-off and would prove largely undetectable; the latest MSTO being the bluest group, it would dominate the optical spectrum. This illustrates the problem of using PS for evolutionary studies in that it provides little indication of the evolution of the star formation rate, beyond indicating (a) the last epoch of significant star formation, and

(b) an upper limit on the level of ongoing star formation.

Rose (1984) has, by cleverly identifying a series of diagnostic ratios of stellar absorption line strengths, managed to alleviate the non-uniqueness problem of the PS approach. By using the relative central intensities of nearby lines his approach is free of reddening problems. The index derived from $\frac{(\text{Ca II H+Hc})}{\text{Ca II K}}$ is a sensitive indicator of the presence of hot stars and the use of an index formed from the Sr II 4077 Å and Fe I 4045, 4063 Å lines is highly sensitive to surface gravity and hence provides a distinction between dwarfs and giants.

He has (Rose, 1985) subsequently obtained high (2.5 Å) resolution optical (3400-4500 Å) spectra for 12 elliptical galaxy nuclei and a number of integrated light observations of Galactic globular and open clusters. By making direct comparisons with the observations of the globular clusters his approach is able to highlight directly age differences between the clusters and the galaxies without recourse to semi-theoretical modelling procedures. His two principle conclusions are as follows.

- (a) Hot stars can contribute only as little as 2% to the integrated spectra of elliptical galaxy nuclei at $\sim 4000\text{Å}$, thus there is little scope for ongoing star formation in such systems.
- (b) The spectra of elliptical galaxies are dominated by dwarfs providing as much as 75-80% of the light at $\sim 4000\text{Å}$. This is in stark contrast to globular clusters. This is most easily explained by an intermediate-age population in the elliptical galaxies that is not present in the globular clusters. Thus O'Connell's original claims have apparently been vindicated by this approach.

In summary therefore, we can conclude that by extending our observations of the light from galaxies over as large a range of lookback times (and hence redshift) as possible, we should be able to begin to tackle the problem of galaxy evolution. Not only will such observations provide useful constraints on our simplistic evolutionary models, but they should also help to resolve the controversy over the population synthesis predictions of significant amounts of star formation in early-type galaxies at epochs far later than had previously been supposed.

1.4. Looking Back - extending the redshift baseline.

Modern detector systems such as CCDs can reliably probe to previously unattainable faint limits, enabling us to extend the redshift baseline over which galaxies can be studied. By observing increasingly distant objects we are looking further back into the history of the universe. For example, the lookback time corresponding to a redshift of 0.5 is 6 Gigayears, ($H_0=50, q_0=0.1$ — these values will be used throughout the present work unless otherwise stated) which is the epoch at which Rose and O'Connell claim there was significant star forming activity in the galaxies they have studied. By comparison of the colours and luminosities of distant galaxies to those at epochs closer to the present, we may then hope to find some evidence of the evolutionary changes described above.

A variety of means can be used to find samples of galaxies at various redshifts to use in these studies.

- (a) Spectroscopic observations of all galaxies in a selected area of sky down to a chosen magnitude limit will constrain ideas on the distribution of galaxies as well as indicating the nature of evolution in the field, as distinct from the rich cluster environment. Such deep field surveys, then, will prove particularly useful, and indeed many are now under way, pushing current spectroscopic detector systems to their limits. I will not be concerned with such an approach here, but details can be found in Ellis(1987).
- (b) Alternatively, we can study known distant objects such as radio galaxies, which is the method used by Lilly(1983) and others. The claim is that the apparent evolution of these

objects can be matched by Bruzual models with $\mu=0.5$. However, there is a serious problem with this approach which has recently been discussed by Yates *et al* (1986). This is that there is possibly a correlation between the radio emission of these galaxies and their infrared colours. Inadequate removal of the non-stellar contribution to the galaxy's light will then result in misleading evolutionary interpretations. Furthermore, the physical processes which lead to the radio emission may not be unrelated to the rates and mechanisms for star formation, suggesting that conclusions based on these objects may not be typical of elliptical galaxies as a whole. However, radio sources still offer some use in this field in that they often occur in clusters of galaxies and so could possibly be used as a detection method for distant clusters (see later, chapter 6).

- (c) Searching for distant clusters of galaxies which will provide us with a large number of galaxies over a range in luminosity, at various redshifts, is the approach with which I shall chiefly be concerned. There are a variety of different possible detection methods of candidate clusters and these will be reviewed in a later chapter.

Much of the work done on distant clusters has tended to concentrate mainly on the nature of the brightest member galaxy, in attempts to use such objects as standard candles with which to construct the Hubble diagram and hopefully obtain a value of q_0 , the cosmological deceleration parameter. From the point of view of the colour evolution of such galaxies we can see from the diagrams of Kristian, Sandage, and Westphal (1978) that the measured B-V and V-R colours as a function of redshift are well represented by the standard k-corrections as far as $z \sim 0.3-0.4$, suggesting that no major colour change of the galaxies has occurred over the last 4-5 Gyrs. At larger redshifts, though, the colours begin to get bluer, indicative perhaps of evolutionary changes.

However, there are arguments over the use of these objects in evolutionary studies; complexities being introduced to the picture when one considers that the central bright galaxies in clusters may not be undergoing purely stellar evolution. Indeed there is a large body of evidence to suggest that dynamical processes, such as cannibalism (Ostriker and Tremaine (1975) of other cluster galaxies, are important in such objects.

Might it not be preferable, therefore, to study the properties of the other, fainter, cluster members? In this way we may obtain information on the evolution of more 'typical' cluster galaxies. This indeed, is the approach I have chosen and which I shall discuss in more detail later. In the next section we shall review the most important work to date on distant clusters of galaxies.

1.5. Distant Clusters of Galaxies - The Butcher-Oemler Effect.

(a) *Properties of Galaxies in Clusters.*

So far we have only addressed the question of the evolution of individual galaxies and paid little attention to the more global behaviour of galaxies within clusters. Since we have concluded from the previous section that observations of distant clusters will be an important method of studying galaxy evolution, we should firstly consider the basic properties of nearby clusters.

One particularly interesting property to which we have already referred, is the morphology-density relation. Dressler (1980), from a study of nearby clusters, obtained a quantitative relation between the relative proportions of galaxies of each morphological type and the density of the local environment. Subsequent work has revealed that this relationship holds over a wide range of environments at the present day. Such an observation may be interpreted as reflecting that, since formation, a galaxy becomes aware of its neighbourhood, evolving in morphology towards the appropriate type. The alternative hypothesis is that such behaviour was somehow established by initial conditions when galaxies were formed.

This topic is discussed in detail in Dressler (1980, 1984), but the relevant point to note here is that at the present epoch, the cores of rich clusters of galaxies are dominated by early-type (E/S0s) galaxies, whereas in lower densities, spirals are the most common type.

A further 'global' characteristic observed in clusters, is the colour-absolute magnitude (CM) effect. Visvanathan and Sandage (1977) showed, from photometry of galaxies in Virgo, that for early-types (with no distinction discernable between ellipticals and S0s), the brighter galaxies are redder. This relationship has been observed in different clusters and in the field and is accepted as a universal phenomenon at the present epoch, arising from differences in galaxy metallicity (see references in Mihalas and Binney, 1981). As we shall see later in this thesis, the CM-effect can serve as a useful standard property against which distant clusters may be compared, with deviations in behaviour perhaps arising as a consequence of evolutionary changes.

These two aspects of galaxy clusters will form the basis of much of the discussion which follows. For a general review of the properties of nearby clusters of galaxies, including some discussion of dynamical considerations, see Bahcall (1977). For the present, we shall consider the observations that have been made to date on clusters at high redshifts.

(b) Photometry.

The main pioneers in the study of distant clusters are Butcher and Oemler who, in 1978, carried out photometry of two of the then most distant known clusters; 0024+1654 ($z = 0.39$) and the cluster around the radio source 3C295 ($z = 0.46$). Both of these rich, centrally concentrated clusters were seen to exhibit a far greater amount of blue objects in their V-r colours than would have been expected on the basis of the number of spiral galaxies observed in similar nearby clusters. This association of the blue objects with spiral galaxies, implied that in the available lookback time from redshifts of ~ 0.4 to the present (5 Gyr), spirals in clusters had undergone some form of drastic evolutionary change in order to constitute the red S0 population so common in such environments today. The ram-pressure stripping of the galaxy's interstellar material by the intracluster gas as it passes through the cluster core envisioned by Gunn and Gott (1972) was the favoured physical explanation.

However, subsequent, more detailed investigations highlighted the pitfalls of such an approach and indeed exposed inadequacies in our knowledge of even nearby galaxy clusters.

Firstly, a major problem was that of possible contamination of the cluster by field objects or overlapping foreground groups. Without spectroscopic information the removal of such field contamination can only be done on a statistical basis, and at large redshifts the problem is only exacerbated. Foreground galaxies being blue will inevitably, therefore, plague determinations of such quantities as Butcher and Oemler's blue fraction.

Indeed Matthieu and Spinrad (1981) tried an independent estimate of the field contamination in the case of 3C295 and concluded that Butcher and Oemler had seriously underestimated the problem. Spectroscopy by Dressler and Gunn (1982), which I shall discuss in more detail later, also confirmed that many of the supposed blue objects in this cluster were in fact foreground galaxies.

Another criticism was that of de Gioia-Eastwood and Grasdalen (1980) who objected to the insufficient regard that had been paid to the subtleties of the colour-magnitude (CM) effect. For early-type galaxies it has been known for some time (Visvanathan and Sandage, 1977) that brighter galaxies are redder, due to metallicity effects. Indeed it is presumed that such an effect is universal, being found in clusters (Visvanathan and Sandage, 1977) and also in the field. If one accounts for the effect of the cosmic scatter in the CM-effect (combined with observational error) their conclusion is that at higher redshifts the expected V-r colour distribution should widen substantially from the narrow peak characteristic of nearby clusters.

A further problem, discovered by Butcher and Oemler themselves (Butcher, Oemler, and Wells, 1983), lay in the association of morphology and colour. Butcher and Oemler had measured colours for the distant objects yet had compared them with morphologies of nearby objects, i.e. distant blue objects were assumed to be spirals. At first thought this may seem a reasonable assumption and that such criticism is somewhat pedantic. However, more detailed investigations of nearby clusters revealed this as a potential problem.

These authors found that the fraction of blue galaxies in low redshift clusters is much smaller than the fraction of spirals. The spiral/blue ratio was found to be 4/1 in these clusters and 4/3 in the field, i.e., spiral galaxies in clusters are redder than those in the field. Thus in order to have meaningful results, colour distributions at high redshifts have to be compared directly with colour distributions at low redshift.

In the light of these substantial criticisms, Butcher and Oemler refined their definitions and methods to more rigorous standards and have conducted a considerably more substantial investigation of colours in both nearby and distant clusters; thirty-three in all.

Selecting those objects in each cluster that are brighter than $M_V = -20$ within the circular area containing the inner 30% of the total cluster population and correcting for the colour-magnitude effect they were able to define the blue fraction as those galaxies lying at least 0.2 mag to the blue of the early-type peak of the J-F colour distribution.

Their results are shown in Fig. 1.2 which plots the blue fraction against redshift. Beyond $z \sim 0.1$ the blue fraction increases with z to reach a peak of 0.25 at $z \sim 0.5$. From observations of one less centrally concentrated cluster, 1447+26 at $z = 0.38$, Butcher and Oemler are tempted to conclude that the phenomenon is largely an environment independent effect. However it is also clear from the diagram that the underlying mechanism may be more complicated than the suggestion of a general decline of gas with time, 0016+16 lying well off the 'mean' relation. This cluster has indeed been problematic for some time, its intrinsically very red colours putting the tightest constraint on theory. I shall defer further discussion of this cluster until I describe my own work in chapter 3.

W.J. Couch (1981) undertook a similar photometric study of 14 rich clusters in the redshift range $0.18 < z < 0.39$ from J and F photographic plates. Although taking a somewhat different approach of classifying the 'blue' objects as being the excess number found over that expected, he largely verifies the existence of the BO-effect as a general property of clusters beyond $z \sim 0.26$.

The conclusions from these photometric studies therefore can be summarised by saying that there is a large amount of evidence for increasing numbers of blue objects in rich clusters of galaxies with increasing redshift, although the nature and origin of such objects is as yet unclear, possible explanations being required to explain not just the general trend but also the anomalous cluster 0016+16.

(c) Spectroscopy.

In order to verify that such blue objects are indeed cluster members, rather than a mere reflection of the increasing severity of foreground contamination with redshift, detailed multi-object spectroscopy is required. Dressler and Gunn (1982) have embarked on a long term programme to undertake such spectroscopy. Their first observations were of the two original Butcher and Oemler clusters, 3C295 and 0024+1654.

As mentioned earlier, in the case of 3C295 the initial spectroscopic result upheld the belief that many of the blue objects were foreground contaminants. Quite unexpectedly, however, it was noted that of those objects at the cluster redshift none had the spectra of 'normal' nearby spiral galaxies, exhibiting instead the high-excitation lines characteristic of active galactic nuclei (AGN), or strong Balmer absorption lines reminiscent of an A star

superposed on an underlying E/S0-type population.

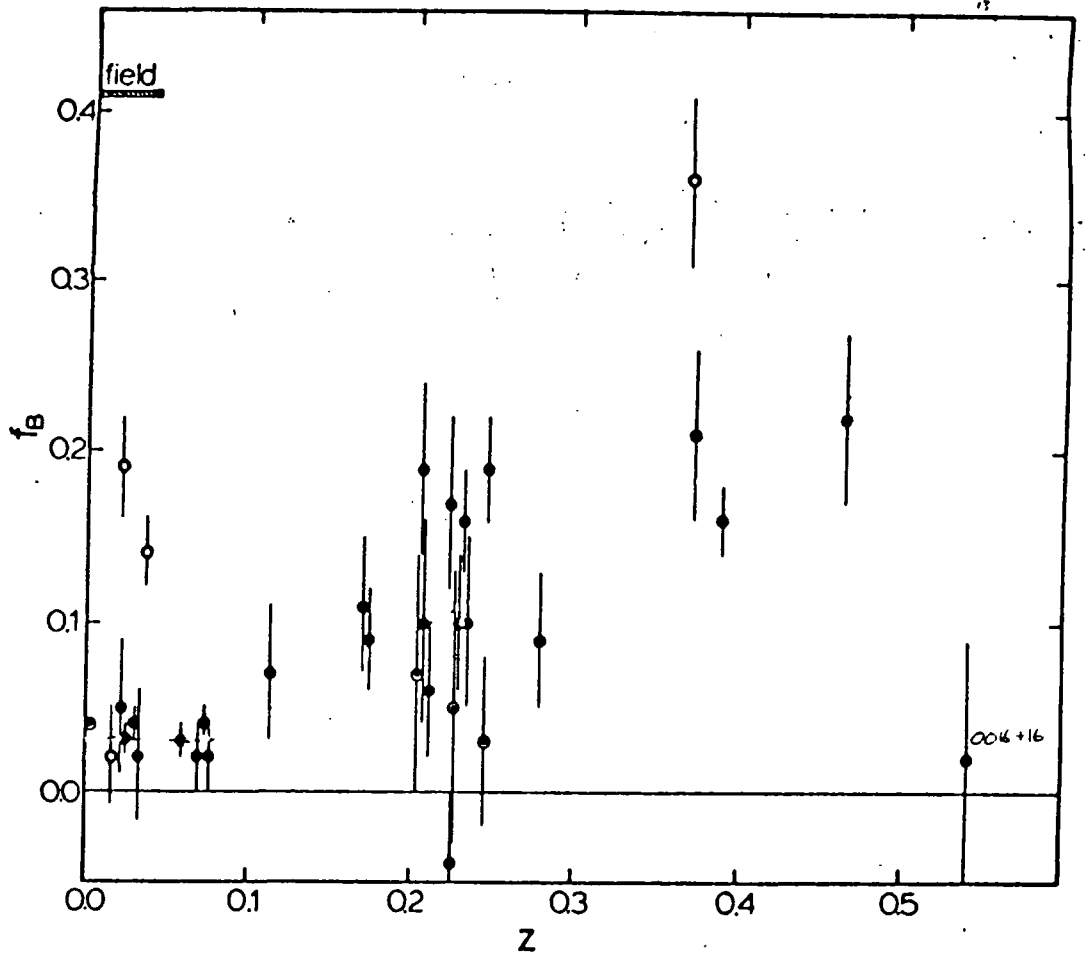


Figure 1.2: Butcher & Oemler's variation of blue fraction, f_b , versus redshift, for their sample of 33 clusters.

For 0024 on the other hand, no significant field contamination was found and the spectra of the blue objects were mostly typical of nearby spirals or a few AGN, with none of the Balmer-line objects found.

Objects of all these types have subsequently been found by other authors in more clusters. Sharples *et al.* (1985) found Balmer absorption line galaxies in AC103 at $z = 0.31$, as did Butcher and Oemler (1984) in 1447+26, and Lavery and Henry (1986) in three other clusters. The full results of all spectroscopy published to date are summarised in Table 5.2 and are further discussed in chapter 5.

Considering the AGN, Dressler and Gunn concluded that such activity was far more common in the past than at present. Whilst such a conclusion seems reasonable at least qualitatively from the observations, we must be cautious when attempting quantitative estimates for the scale of such an effect due to, probably large, selection effects and inadequate studies of a comparable nearby sample (see Dressler *et al.*, 1985).

(d) The Balmer Absorption Line Objects - Post Starburst Galaxies?

Let us turn our attention for the moment to the enigmatic Balmer absorption line galaxies. The reason they merit special attention is that such objects are very rare, their possible equivalents nearby being less dramatic (e.g. Sparke, Kormendy, and Spinrad, 1980, and Bothun & Dressler, 1986) and of much lower luminosity.

In the 3C295 cluster, Dressler and Gunn found three such objects, but in order to measure line strengths they found it necessary to co-add the three spectra to form a composite of reasonable signal-to-noise. This should be borne in mind when discussing the results. They measured an average absorption line strength $H = H\alpha + H\beta + H\gamma$ and the rest-frame (B-V) colour: $H = 7 - 8\text{\AA}$, $(B - V)_0 \simeq 0.74$.

Such a colour is typical of an Sb-type nearby galaxy, yet the extreme line strengths measured are considerably greater than expected for such a system. Indeed, although we are facing the problem of comparing spectra of distant galaxies which cover a large spatial area with nearby nuclear spectra, we can still conclude that it is extremely difficult to see how these Balmer line galaxies can be reconciled with nearby systems, particularly since they do not contain the [OII] 3727Å emission line, characteristic of ongoing star formation.

In conclusion, it is claimed that only a very narrow range of possible star formation histories are able to reproduce such spectra. Only a system in which there has been significant star formation in the last 1 Gyr or so will contain the necessary combination of A dwarfs and an older underlying population; the absence of the [OII] emission implying that star formation must have ended abruptly around 1 Gyr before the epoch of observation. The size of a burst of star formation that would be required to fit the observations is dependent on the IMF of the burst and could range from as high as 20% of the galaxy mass if the lower main-sequence is populated, to as little as 2% if only very massive stars were formed.

Subsequent spectroscopy (e.g. Sharples *et al.*, 1985, Butcher and Oemler, 1984, Lavery and Henry, 1986) in other distant clusters have also found examples of these objects. It is as well to point out that, in this model, the classification of such spectra as a distinct class of object is purely due to the stage at which the objects are observed. For example if star formation was ongoing the spectra would probably be more reminiscent of spirals with [OII] emission and the deep Balmer lines diluted and partially filled by emission.

One should be aware of the dangers of over-interpretation of such low quality spectra since the equivalent width measurements will contain a substantial error.

An interesting 'cautionary tale' to this effect can be illustrated by the case of 0024, in which no such objects were originally found by Dressler and Gunn's spectroscopy. Lilly and Gunn (1985) obtained infrared-optical photometry of these objects in order to construct

colour-colour diagrams with which to compare the observations with models of different star formation histories. Their conclusions largely echoed those of Dressler and Gunn by showing that the colours of most of the blue members were consistent with the extended star formation of spiral-type spectra. However, the extended baseline afforded by such photometry did allow more detailed investigation than the faint spectra. One interesting conclusion, being that one of the galaxies in Dressler and Gunn's sample exhibited photometric evidence of having undergone a burst of star formation. A result that was not originally obvious from the Dressler and Gunn spectrum, but by no means inconsistent.

The lesson to learn from this is that neither spectroscopy nor photometry on their own are capable of providing the full picture as regards the evolutionary state of galaxies in distant clusters. Broadband photometry suffering from contamination problems, and spectroscopy limited by its restricted wavelength coverage.

In conclusion, therefore, what have the observations of distant clusters told us? Firstly, such observations and analyses are difficult to carry out and lack of redshift information hampers photometry. Secondly, there do indeed seem to be larger numbers of blue objects in distant clusters than one would expect. The nature of these blue objects is considerably more exotic than originally suspected by Butcher and Oemler, indicating enhanced levels of star formation and nuclear activity at the earlier epochs studied than at the present time. Whether this is a general trend with redshift or is primarily an environmentally determined process can only be answered in the light of further observations.

1.6. Aims and Outline of the present work.

In the above review I have highlighted many of the major problems incurred in previous attempts to use distant clusters of galaxies in studies of galaxy evolution. Aside from the philosophical considerations of, for example, the significance of environmental processes and whether galaxies in rich clusters can be considered as 'typical,' we have come across a range of observational difficulties which have to be overcome before we can unveil the mysteries of galaxy evolution. In this thesis I shall address many of these topics and attempt to alleviate the difficulties. Three of the key problems are:

(1) Object Selection.

Firstly, there is the basic problem of the selection of suitable candidate distant clusters of galaxies. As we have seen, those objects observed previously have been found by a variety of approaches. For example, the 3C295 cluster was discovered by virtue of its radio source, yet 0016+16 was found as a density enhancement on red photographic plates. Should we therefore be surprised that 3C295 contains active objects and that 0016 is intrinsically red? Obviously, it would be misleading to derive general conclusions about evolution on the basis of such a heterogeneous sample. Not that any detection method is free of selection effects, but if the sample is chosen from a single well-defined source then comparison between various clusters is more legitimate. I shall discuss this issue in chapter 6.

(2) Contamination by non-members.

One of the key difficulties stressed in the earlier review was that of the possible non-membership of many of the excess blue objects found in distant clusters. Whilst I stress that such a problem can only be definitively solved by the use of spectroscopy, I will discuss a possible method to minimise the difficulties using multi-colour photometry in chapter 2.

(3) The Ultraviolet Spectra of Galaxies.

Proceeding to higher redshifts or bluer passbands than have previously been used demands that we have sufficient knowledge of the ultraviolet (uv) energy distributions of nearby galaxies. Such data is scarce, being only attainable from space-borne telescopes, although

the situation has been improved by the International Ultraviolet Explorer (IUE) satellite. These observations form the basis of the discussion in chapter 5.

In chapters 3 and 4 I use some of these techniques to study two previously known distant clusters, and I will attempt to model their observed properties via an evolutionary scenario developed in chapter 5. In chapter 6 I present a catalogue of distant clusters for future observations. Finally, in chapter 7, I shall outline possibilities for future study in this fascinating subject area.

2. Multicolour Photometry of Distant Galaxies.

2.1 Introduction.

The principal difficulty of searching for possible spectral evolution in distant clusters of galaxies is that of identifying a uniform class of object at each look-back time. Much of the previous work has been concerned with observations of the brightest cluster member. However, as we discussed in chapter one, it may not be possible to draw general conclusions about galaxy evolution from the use of a single, special type of object. In the core of a rich cluster effects other than those due to simple evolving stellar populations, such as dynamical friction (Richstone, 1976) and mergers (Hausman and Ostriker, 1978) may significantly affect the luminosities and colours of the most massive galaxies.

Even on purely observational grounds, the identification and selection of such objects can lead to difficulty and biases in the sample, particularly when we use only apparent magnitude as our selection criterion. Superimposed on distant clusters are foreground (and background) galaxies, and since foreground objects are often brighter than the cluster first-ranked galaxy, we ideally require a number of redshifts in the field before this object can properly be identified. The addition of a single colour allows some progress to be made in this problem.

Furthermore, at large redshifts the brightest object in a visible passband (say V) will be the most luminous in the rest frame ultraviolet which cannot easily be observed for low redshift clusters (see chapter 5). Care must therefore be taken when comparing objects over a wide redshift range.

In chapter one, I used the possible uniqueness of the cluster brightest member to argue for the use of a technique which identifies a population of objects at each epoch, providing us with a larger sample at luminosities closer to the characteristic magnitude of the galaxy luminosity function (LF). Rich clusters locally contain predominantly red E and S0 galaxies (Dressler 1980). A characteristic property of these objects is their colour-luminosity relation (Visvanathan and Sandage, 1977) which is not readily seen in galaxies with disc populations, thus the cluster colour-luminosity diagram should be able to isolate early-type galaxies at large redshift (Godwin, 1976).

Butcher and Oemler (1978), Couch and Newell (1981) used a single colour to broadly break the rich cluster population into two groups - the E/S0s and spirals but were only able to identify the latter statistically because a single colour is inadequate in separating both type (T) and redshift (z) (see figure 2.4 and later discussion). Baum (1962) and Koo (1985) have shown that the addition of more colours considerably improves the situation.

Spectroscopy can yield the definitive statement of a galaxy's redshift and an indication as to its current star formation rate, but, generally, detector systems have tended to limit the practical use of spectroscopic techniques to only brighter magnitudes, posing a serious constraint on the depth to which we can probe distant cluster luminosity functions. For example, Dressler and Gunn (1982) reached to $F \sim 22$ in their studies of distant clusters, but this was only achieved in 16000 secs on a 5 m telescope. In their observations of the cluster AC103, Sharples *et al* (1985), reached a limit of $R \sim 20$ at a resolution adequate for quite detailed spectral analysis ($\sim 5\text{\AA}$), however, this limit was inadequate to reach the magnitudes of most of the blue galaxies in this cluster field. Furthermore, until only fairly recently, spectroscopy could largely only be carried out on a single object per exposure.

Multi-object spectroscopy, whereby several ($\sim 10-50$) spectra can be obtained during a single exposure, makes far more efficient use of limited observing time. Consequently, this field has undergone much development in recent years, with the advent of several new

instruments. However, although such methods are undoubtedly exciting developments, as we have already discussed in the first chapter, spectroscopy by itself is not fully able to address the question of galaxy evolution, requiring a larger wavelength baseline (eg Lilly and Gunn, 1985).

In this chapter we examine how precisely multicolour photometry can determine both redshifts sufficient to determine likely membership and spectral type for identifying classes of galaxies for evolutionary studies. This technique has been studied also by Koo (1986) and Loh and Spillar (1986) and we shall compare our conclusions with theirs.

The approach will be to use present day galaxy spectral energy distributions (SEDs) and simulate colours at various redshifts. Since the field redshift distribution to a given apparent magnitude can be modelled using nearby field galaxy luminosity functions (Ellis, 1982), this provides an indication of the precision required in z space for the present work. The method initially assumes non-evolving SEDs but we shall discuss the effects of spectral evolution estimated on the basis of simple models.

By considering clusters at $z \sim 0.3-0.7$ we are probing to magnitude limits at $R_F > 21.0$. Using the simulations of Ellis (1987), we can plot the expected distribution of field galaxies down to these limits (Fig. 2.1). The peak of the distribution is fairly well separated from the distant clusters, with the median redshift ~ 0.25 . This implies, then, that for such distances the removal of foreground contamination should be a tractable problem given a redshift accuracy of $\sim \pm 0.05$ or better. Below $z \sim 0.25$ the clusters lie close to the field peak and individual object spectroscopy may be required to ascertain cluster membership.

2.2 Spectral Energy Distributions of Nearby Galaxies.

Firstly, we discuss the available SEDs of nearby galaxy types. The emphasis here is to examine a range of spectral properties and features that may be of some use for our purposes.

Initially, we seek a suitably prominent spectral feature common to all galaxy types, whose presence can be used to infer a probable redshift. The optical SEDs of nearby galaxies are shown in figure 2.2 from the work of Pence (1976). Clearly, the most obvious such feature in the optical region is the continuum break at 4000\AA , which increases in strength from late-type spirals to early-type galaxies.

This feature arises not only because of the CaII H and K lines, but also due to various other elements in a variety of ionisation states. As a consequence, we expect a dependence on stellar photospheric properties such as effective temperature, metallicity, and surface gravity. Hamilton (1985) discusses the behaviour of this feature in some detail with particular emphasis on its variation with stellar populations. His measured break strength, B_{4000} (defined as the ratio of the average flux density between 4050\AA and 4250\AA to that between 3750\AA and 3950\AA), in a sample of local galaxies (Heckmann, Balick and Crane, 1980) revealed that, whilst there is a general trend with morphology, there is also a fairly large intrinsic scatter, probably due to metallicity variations (Dressler, in Hamilton 1986).

Using the 4000\AA break as a redshift indicator, we still require galaxy type separation. If we increase our sampling over the full available optical region our chosen set of filters should become more sensitive to the underlying shape of the galaxy continuum. In particular, the differences from type to type become notably large at wavelengths shortward of the break.

Finally, we must not lose track of our ultimate goal, viz, to look for possible evolutionary changes in the colours of galaxies as a function of redshift. Simple modelling of galaxy evolution (Tinsley 1972, Bruzual 1981, and discussion in chapters 1 and 5) shows that variations in the rates of star formation should manifest themselves as changes in the galaxy rest frame uv colours. Consequently, we should aim to define the shape of the blue end of the observed galaxy SEDs as accurately as possible.

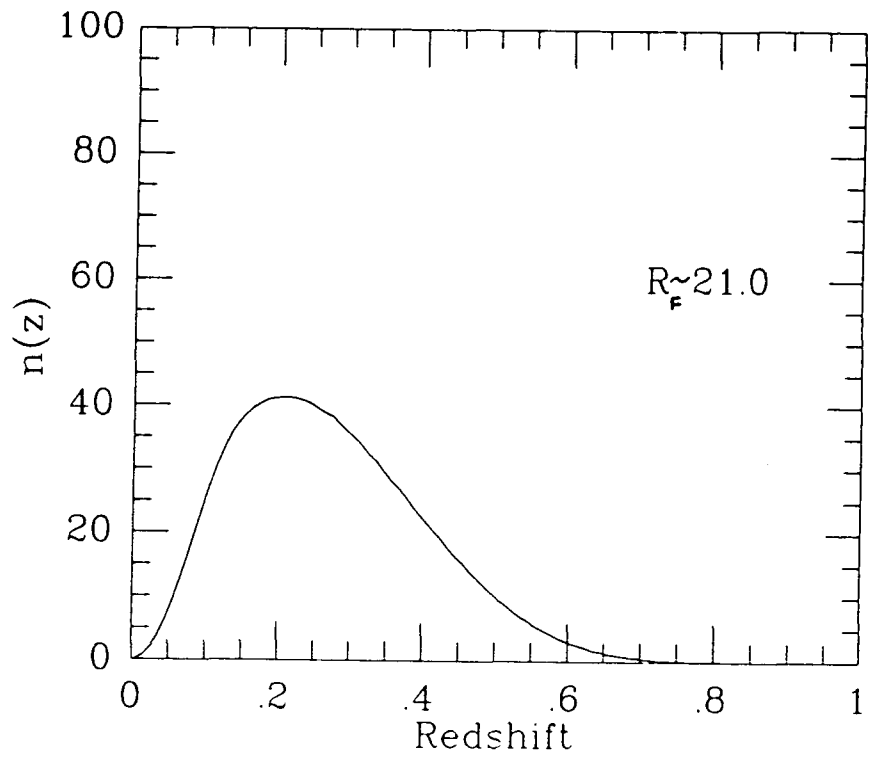


Figure 2.1: Expected $n(z)$ distribution for faint galaxies, down to the limits shown in the figure (Ellis, 1987)

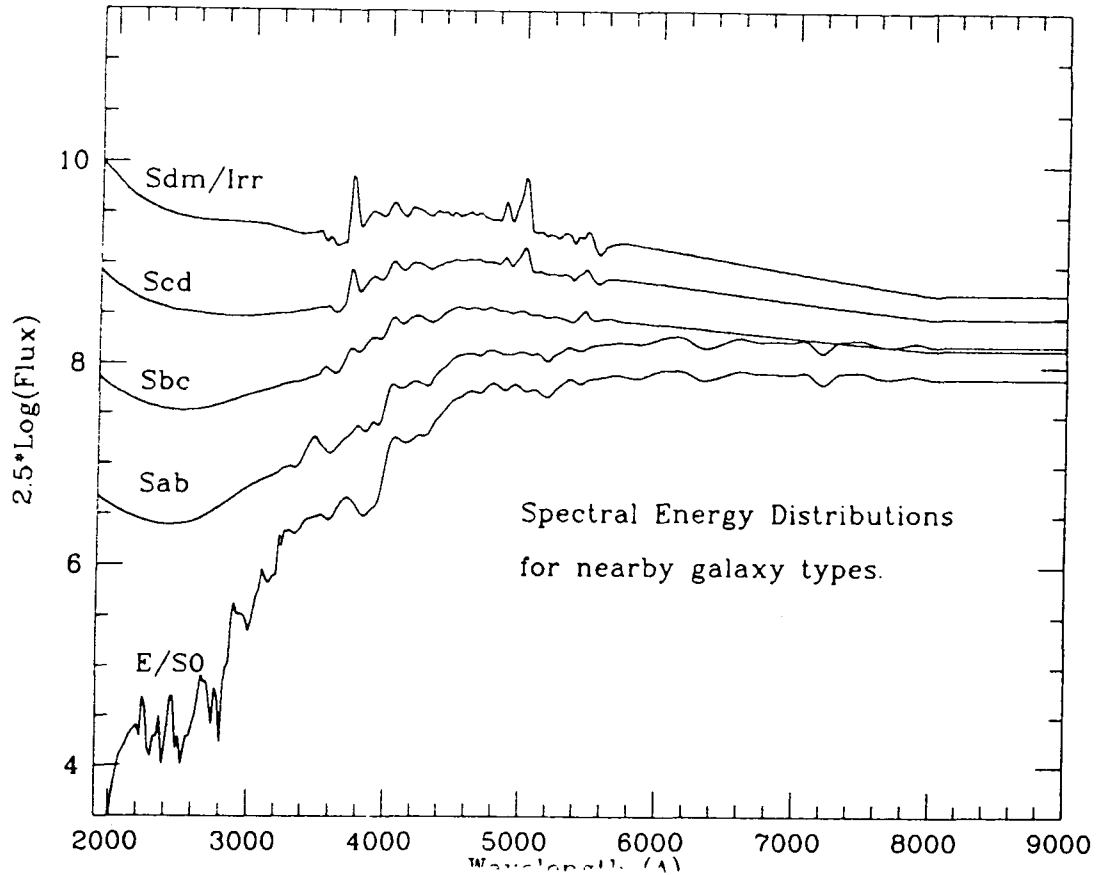


Figure 2.2: Pence's (1976) SEDs for nearby galaxy types.

Indeed, as we move to progressively higher redshifts our bluer passbands will become increasingly dominated by the galaxy rest frame uv spectrum. Studies of nearby galaxies at such wavelengths are only possible via satellite observations, and thus are somewhat limited. However, the International Ultraviolet Explorer (IUE) has proved particularly effective here and uv spectra of many galaxies have been archived over the last 8 years or so of the satellite's existence. We shall be analysing the IUE observations of early-type galaxies later in this thesis (chapter 5), but for the moment we shall summarise the key points that have emerged from such studies relevant to our immediate task.

It has been known for some time (Oke *et al*, 1981) that the uv spectra of nearby E/S0 galaxies show large variations in behaviour from object to object at short wavelengths. Various models have attempted to explain such behaviour, but the results have been largely inconclusive. In practice then this means that our simulations of galaxy colours at high redshifts should be limited by a lower wavelength limit at which these intrinsic uv variations become significant. The problem (as we shall see in chapter 5) is not quite so grave as it may at first seem, since we find that the SEDs of these galaxies are very well-behaved down to a rest wavelength of ~ 220 nm. Shortward of this, these variations rapidly dominate the form of the spectra. Bruzual and Spinrad (1980) and King and Ellis (1985) present mean uv spectra from observations of several galaxies.

For the purposes of the present models I shall then make use of the SEDs of the nearby galaxies presented in Pence (1976) and extended by Bruzual and Spinrad (1980). These SEDs are for 5 galaxy types and are the resulting composite behaviour of a sample of several nearby galaxies of each type. The ultraviolet end of the spectrum is determined in each of these cases from satellite observations. The uncertainties present in such 'template' SEDs are as follows. (a) The matching of uv spectra to optical data is uncertain, particularly when we consider that in each of these spectral regions the observations are often of different galaxies. (b) Furthermore, observations of nearby galaxies are obtained largely from the nuclear regions of each object (particularly with the small aperture of IUE) whereas spectroscopy and photometry of distant galaxies will be obtained from over a much larger area of the galaxy. This may result in uncertainty, if there are colour gradients present, or with variable bulge-to-disc ratios in spiral galaxies. (c) We must also correct for the effects of galactic absorption, or reddening. Here we use Pence's appropriately corrected SEDs.

Bearing these difficulties in mind, we shall here consider Pence's SEDs as representative of each object class, serving as our no-evolution 'templates' against which we can compare the distant galaxies.

2.3 Modelling Galaxy Type and Redshift Classifications.

In order to test the effectiveness of various filter combinations as redshift/type discriminators, we have developed the following procedure. We have constructed a series of simulated galaxy colours for any chosen set of filter/detector responses for a range of types as a function of redshift. These predicted colours can then be used to classify photometric observations of galaxies in terms of the most likely fit of our two parameters T and z .

To produce these simulations we require the following:

(a) knowledge of the present day rest frame galaxy SEDs as discussed above. Since, in reality, galaxy types form a continuum of possibilities rather than discrete steps, our set of 5 standard spectra have been interpolated to produce a range of some 20 spectral classes from E/S0 to Sdm/Irr.

(b) the filter response curves and detector sensitivities for various photometric systems. Here we shall chiefly consider Koo's set of photographic UJFN bands (Koo 1981,1985) and the intermediate band filter set of Couch *et al* (1983) which is used in conjunction with the

RCA CCD whose sensitivity is shown together with the filter responses in figure 2.3.

(c) the atmospheric transmission of 1 air mass (Allen, 1972).

Stepping through a range of redshifts of $z = 0.0$ to 1.0 (interval = 0.01) we shift each SED to the appropriate observed wavelengths and pass these through each filter and detector combination (including atmospheric absorption) producing an array of predicted colours.

To evaluate the accuracy to which we are able to classify each object we can make use of the properties of the χ^2 distribution. The best fit of observed to predicted galaxy colours is achieved by minimising the quantity,

$$\chi^2 = \sum \frac{(Obs - pred)^2}{\sigma_i^2} \quad (2.1)$$

where σ_i is the estimated photometric accuracy in each passband i . This minimum value then corresponds to the best choice of our two parameters, T and z .

Given that we have an error in each passband, defined by σ , our classification will not be an unique choice of T and z , but defines a range of permissible fits. If we choose those classifications which lie within the 1σ error limits of our χ^2 values, then we can use the property that all values of χ^2 lying within $\chi^2 + \Delta\chi^2$, where, for this case, $\Delta\chi^2 = 2.30$ are allowable (see, e.g., Press *et al*, 1986).

The technique can be effectively summarised by producing contour plots of χ^2 in the redshift-type plane. As an example, figure 2.4 shows five galaxy types observed at $z = 0.3$ using the UJFN system. The outermost contour in each plot shows the χ^2 , 1σ level for fits to the J and F passbands. The ambiguous nature of such single colour photometry is easily seen. Adding a further filter, N, leads to a reduced ambiguity, as in the second contour level. Finally, the U filter introduces a sensitivity to the shape of the galaxy continuum (ie type) as is represented by the innermost contour level.

Let us now consider the UJFN system in some detail. From Koo's own work he found that whilst the three passbands U, J, and F could provide fairly accurate redshift discrimination for relatively low redshifts, probing beyond $z \sim 0.35$ required the further addition of another filter, in this case his N band. Whilst this increases *sensitivity* to higher redshifts (ie, higher redshift galaxies can be detected on red plates), the errors now present in his two colour combinations (U+J-F-N and -U+J+F-N) considerably decreased the *accuracy* of each redshift estimate.

In table 2.1 I present estimates of the redshift error expected for each of the 5 primary galaxy types over a range of redshifts. The error is defined as half the range of redshift values encompassed by the projection of the $\Delta\chi^2 = 1.0$ contour on the z -axis of the type-redshift plane (Press *et al*, 1986). We have assumed a photometric accuracy of 0.05 m in each of our passbands. The general usefulness of each filter combination over all galaxy types and redshifts in the range 0.0 to 1.0 , can be approximately parameterised by the quantity F1 which is simply the fraction of object classes in each of the (redshift \times type) arrays in the tables that have redshift errors, $\Delta z \leq 0.05$.

The main conclusion to be drawn is that within the context of these models, the UJFN system is a fairly effective redshift estimator, particularly for early-type galaxies. However, for galaxies bluer than Sbc the Δz are all greater than our desired limit of ± 0.05 , and indeed for the bluest type (Sdm/Irr) the distinction between field and cluster objects is lost.

However favourable the results of table 2.1 may appear, we should be cautious about the details of these and Koo's own simulations. Chiefly we should express concern at the role played by the U passband at high redshifts.

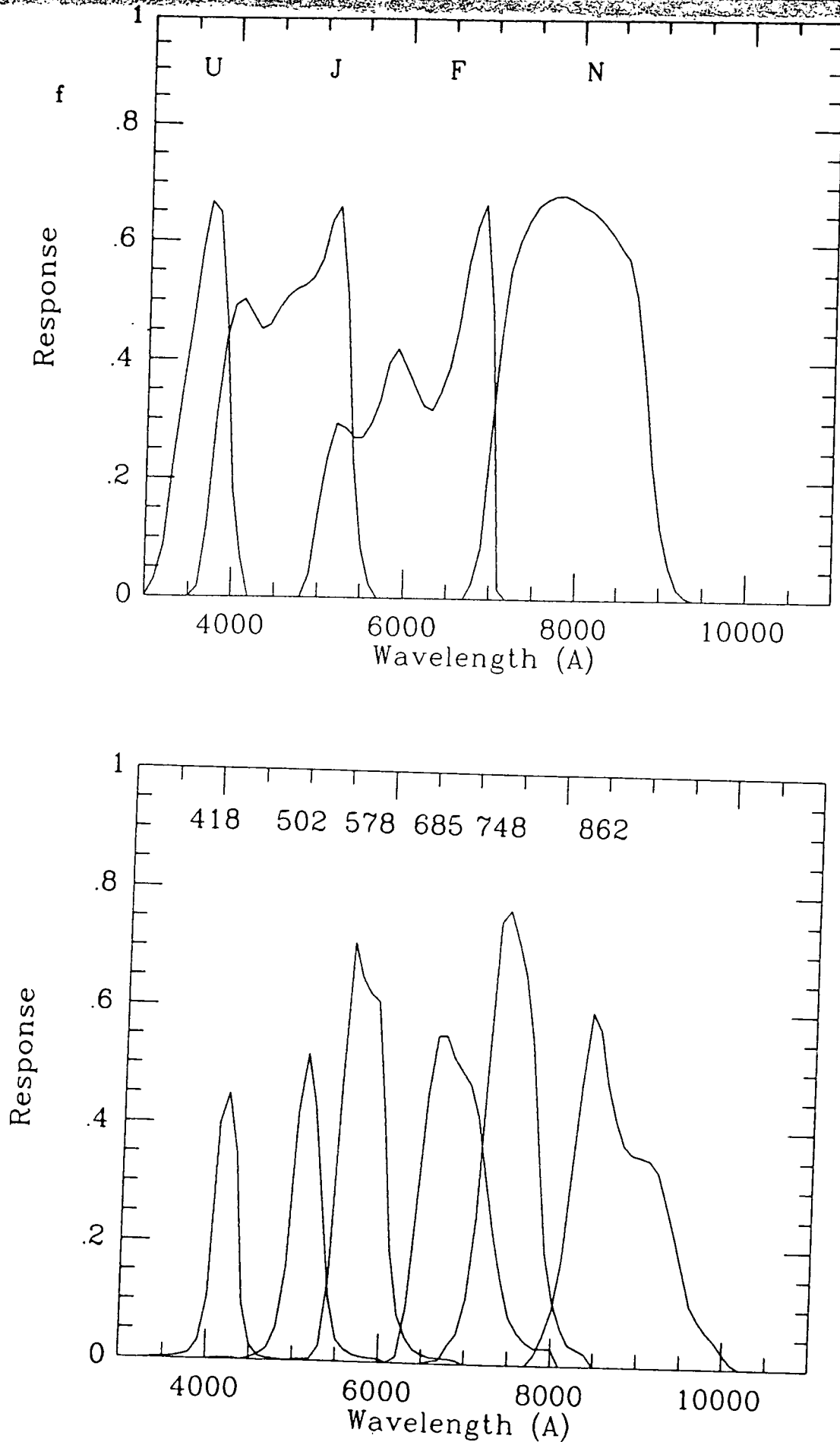
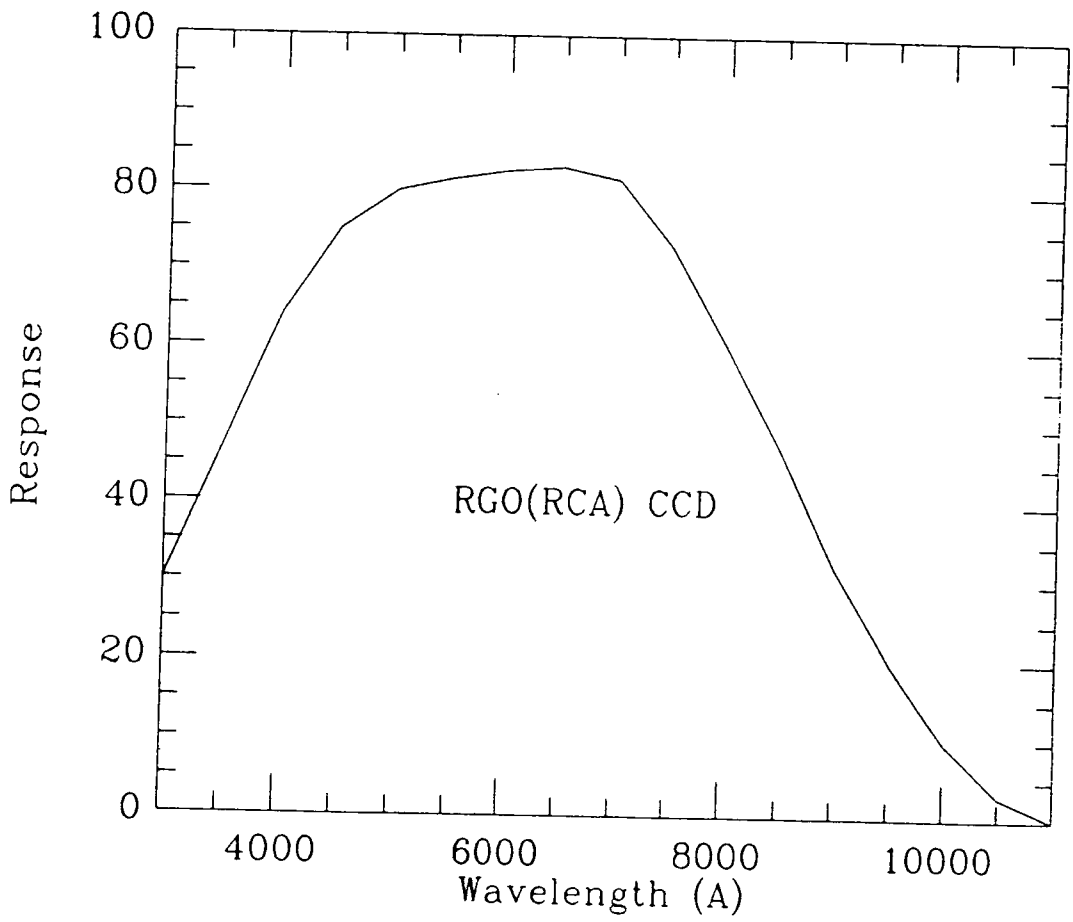


Figure 2.3: (a) Filter responses for Koo's UJFN system, and (b) Couch *et al.*'s intermediate bandwidths. Also shown is the response of the RCA CCD.



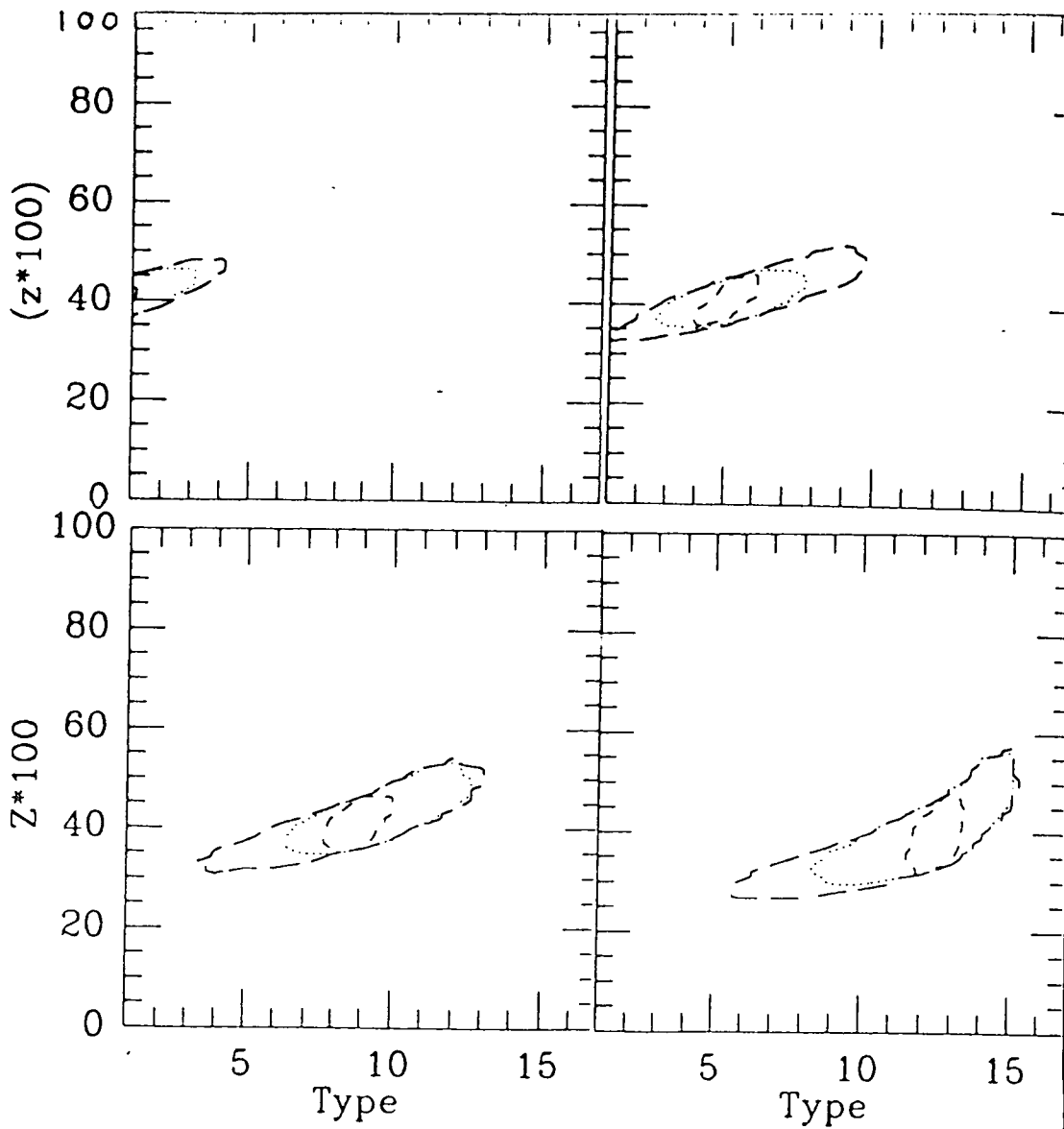
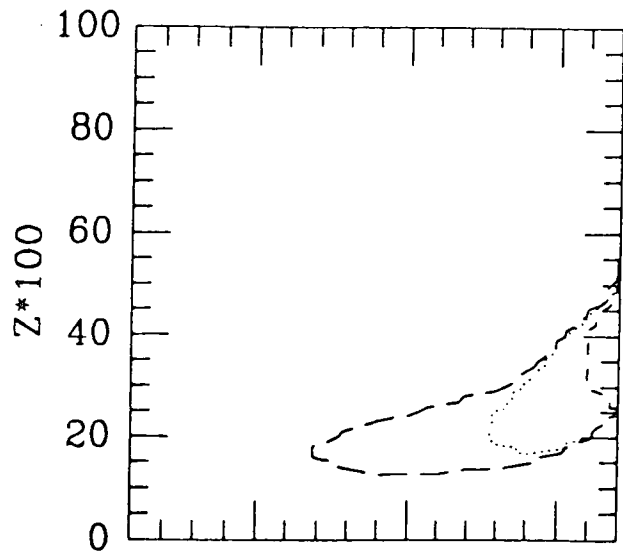


Figure 2.4: χ^2 -contours at the 1σ level in the UJFN system for 5 galaxy types at $z=0$.



Beyond $z \sim 0.45$ this filter reaches shortward of 220 nm in the rest frame, where, as discussed earlier, the large variations in early-type galaxy spectra occur. Koo argues that the error introduced by such an assumption is one of galaxy type misclassification rather than redshift uncertainty. Whilst this may well be so, our aim is not merely to assign redshifts to each of our galaxies. We must clearly be able to distinguish intrinsic uncertainties in the nature of galaxy SEDs from possible evidence of spectral evolution. With only these 4 rather broad passbands it is unlikely that such a distinction could be made.

Furthermore, since Koo includes spectra generated by Bruzual type evolutionary schemes his results are model dependent. Such an a priori assumption of the form of any underlying evolution is questionable.

The exclusion of the U band from this photometric system, as illustrated in Fig. 2.4 decreases our type and redshift accuracy. Expected errors on the basis of only the J, F, and N passbands are given in table 2.2.

To summarise, then, we have seen that for low redshifts ($z \leq 0.45$) Koo's UJFN system can provide useful classifications at least for the earlier types. Their use however is perhaps more 'statistical' in nature than on an individual object-by-object basis (We shall discuss some of Koo's actual photometry in the next chapter when we consider the cluster 0016+16). Beyond $z \sim 0.45$ intrinsic uncertainties in the spectra of nearby galaxies may begin to affect seriously the interpretation of colours based on the U filter.

Based on such considerations as these we prefer to seek a filter system that enables galaxy classification on the basis of rest frame optical colours, reserving uv passbands as probes of evolutionary behaviour. A set of narrower passbands enabling us to construct low resolution SEDs should prove a more powerful technique. The intermediate bandwidth filter set used by Couch *et al* (1983), was originally chosen for just such a purpose. Examples of galaxy SEDs constructed from this system are given later. Couch *et al* constructed mean SEDs for various populations of galaxies selected by colour criteria, I, however, shall consider the use of SEDs of the individual galaxies in each cluster field.

Thus we shall now perform similar tests to the above using this photometric system to outline its advantages and weaknesses. The transmission curves are shown in Fig. 2.3, along with the response of the RCA CCD which we shall use in these models. Although this is a unique, ie, non-standard, set of filters, comparison with photographic photometry is readily achieved due to the proximity of the 685 filter response to that of Couch and Newell's (1984) R_F passband. Note that we have replaced Couch *et al*'s original 722 nm filter with our 748 nm passband simply because of its reduced overlap with the 685 nm filter.

These filters cover the spectral region from 400–900 nm, which is equivalent to that encompassed by JFN. Comparison of our expected Δz values in these narrower bands (table 2.3) with those for JFN (table 2.2) provides an informative demonstration (see figure 2.5) of the advantages of the improved sampling afforded by the set of narrower passbands. Even with such increased resolution of the SEDs, however, the very flatness of Sdm/Irr type spectra makes redshift estimation difficult. Nevertheless, the errors in table 2.3 are a considerable advance over the previous work with most types having errors $\Delta z \leq \pm 0.05$.

Although this set of filters provides us with almost full coverage of the spectrum over the range 4000 – 9000 Å, imaging in all 7 bands can prove expensive of observing time. In practice we usually know the expected cluster redshift on the basis of spectra of one or two galaxies in the cluster field prior to photometric observation. It is worth asking, therefore, whether we can select a minimum set which still provides adequate object discrimination (ie typical error in $z \sim 0.05$)? We now pursue this possibility using our simulations to monitor the decrease in accuracy as we decrease the number, and vary the selection, of filters. Some examples are shown in table 2.4.

Table 2.1: UJFN system redshift accuracy.

z	E/S0	Sab	Sbc	Scd	Sdm/Irr
0.1	0.03	0.03	0.04	0.07	0.11
0.2	0.02	0.03	0.04	0.08	0.13
0.3	0.02	0.04	0.04	0.07	0.13
0.4	0.01	0.04	0.05	0.07	0.11
0.5	0.02	0.03	0.05	0.07	0.12
0.6	0.02	0.04	0.05	0.08	0.15
0.7	0.02	0.03	0.05	0.08	0.15
0.8	0.02	0.04	0.05	0.07	0.14
0.9	0.02	0.04	0.06	0.09	0.14

$$F_1 = 0.57$$

Table 2.2: JFN filters only, redshift accuracy

z	E/S0	Sab	Sbc	Scd	Sdm/Irr
0.1	0.03	0.04	0.06	0.10	0.12
0.2	0.03	0.04	0.06	0.11	0.14
0.3	0.03	0.04	0.07	0.14	0.15
0.4	0.04	0.05	0.08	0.11	0.15
0.5	0.03	0.06	0.07	0.11	0.21
0.6	0.04	0.06	0.08	0.10	0.17
0.7	0.02	0.05	0.06	0.09	0.15
0.8	0.02	0.06	0.05	0.08	0.15
0.9	0.02	0.04	0.07	0.09	0.12

$$F_1 = 0.35$$

Table 2.3: Intermediate band filter system (7 passbands).

z	E/S0	Sab	Sbc	Scd	Sdm/Irr
0.1	0.01	0.02	0.04	0.04	0.07
0.2	0.02	0.02	0.03	0.04	0.04
0.3	0.02	0.02	0.03	0.05	0.07
0.4	0.01	0.03	0.03	0.04	0.07
0.5	0.01	0.03	0.03	0.04	0.06
0.6	0.01	0.02	0.03	0.04	0.04
0.7	0.01	0.02	0.03	0.06	0.06
0.8	0.01	0.02	0.03	0.05	0.11
0.9	0.01	0.02	0.03	0.05	0.08

$$F_1 = 0.82$$

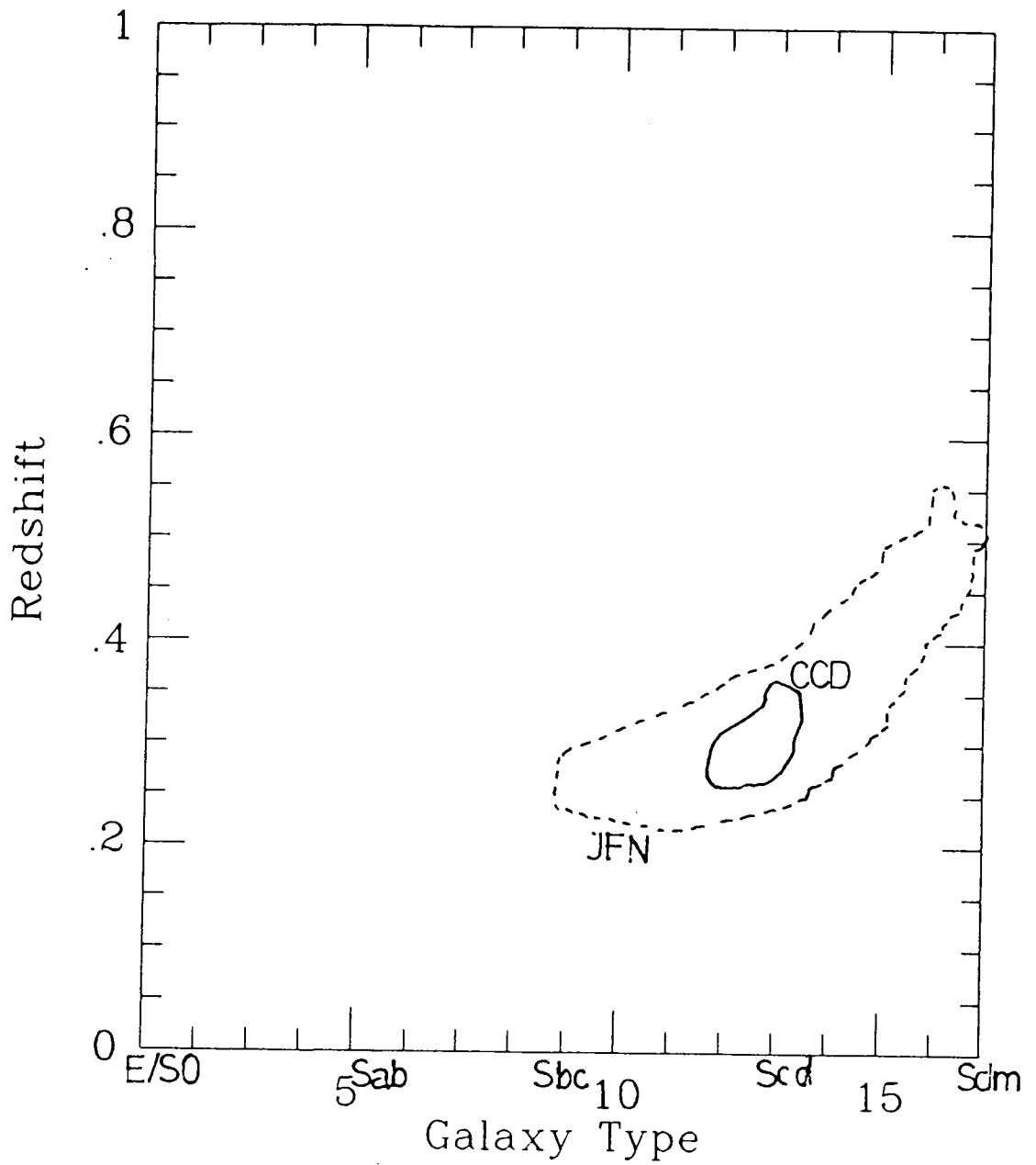


Figure 2.5: χ^2 -contours for JFN (solid line) system compared with that for the intermediate bandwidth filters. Both these systems cover the same wavelength range.

Table 2.4: Intermediate Bandwidth Filter Combinations.
(a) Filters: 418, 578, 748

z	E/S0	Sab	Sbc	Scd	Sdm/Irr
0.1	0.04	0.03	0.04	0.05	0.04
0.2	0.06	0.09	0.11	0.13	0.17
0.3	0.02	0.04	0.10	0.14	0.22
0.4	0.02	0.04	0.08	0.11	0.20
0.5	0.02	0.04	0.06	0.07	0.09
0.6	0.05	0.07	0.06	0.08	0.08
0.7	0.04	0.05	0.09	0.13	0.24
0.8	0.02	0.06	0.09	0.13	0.29
0.9	0.02	0.04	0.06	0.10	0.22

(b) Filters: 418, 502, 748, 868

z	E/S0	Sab	Sbc	Scd	Sdm/Irr
0.1	0.02	0.02	0.03	0.04	0.05
0.2	0.03	0.04	0.07	0.09	0.14
0.3	0.02	0.02	0.04	0.06	0.15
0.4	0.04	0.05	0.05	0.05	0.06
0.5	0.03	0.06	0.09	0.13	0.18
0.6	0.02	0.06	0.10	0.14	0.23
0.7	0.02	0.05	0.09	0.15	0.21
0.8	0.02	0.05	0.09	0.14	0.15
0.9	0.02	0.04	0.06	0.10	0.18

(c) Filters: 418, 502, 685, 868

z	E/S0	Sab	Sbc	Scd	Sdm/Irr
0.1	0.02	0.02	0.03	0.04	0.05
0.2	0.03	0.04	0.07	0.09	0.13
0.3	0.02	0.02	0.04	0.06	0.12
0.4	0.04	0.05	0.05	0.05	0.06
0.5	0.03	0.04	0.10	0.11	0.19
0.6	0.03	0.04	0.08	0.12	0.18
0.7	0.03	0.04	0.07	0.10	0.15
0.8	0.03	0.04	0.06	0.08	0.11
0.9	0.04	0.06	0.07	0.09	0.12

(d) Filters: 418, 502, 578, 685, 868

z	E/S0	Sab	Sbc	Scd	Sdm/Irr
0.1	0.02	0.02	0.03	0.04	0.04
0.2	0.02	0.04	0.07	0.09	0.12
0.3	0.02	0.02	0.04	0.06	0.11
0.4	0.02	0.04	0.04	0.05	0.05
0.5	0.02	0.02	0.04	0.06	0.09
0.6	0.02	0.04	0.04	0.06	0.09
0.7	0.02	0.04	0.06	0.08	0.14
0.8	0.02	0.04	0.06	0.08	0.11
0.9	0.02	0.04	0.06	0.08	0.12

Koo (1986) claims that a set of only three filters that are carefully chosen to monitor the 4000Å break over the redshift range of interest can provide useful z estimates. From our simulations, however, it is clear that object classification to our desired accuracy requires at least 4 passbands. The combination of 418, 502, 685 and 868 filters holds promise as an optimised minimum set of filters. These passbands cover a broad spectral range, straddle the 4000Å feature, and are sufficiently narrow to avoid ambiguous redshift and type identifications. For clusters with $z \leq 0.4$, the addition of a U passband to this set would then allow monitoring of the rest frame uv flux as desired. At higher redshifts our 418 and 449 passbands begin to enter the uv and the addition of further optical filters should help to better define the galaxy SED. Use of the full 7 filter set of passbands, however, will reduce the errors, particularly for later (bluer) spectral types, and hence yield more reliable indications of cluster membership for such flat spectra.

A few words of caution should be attached to the values quoted in these tables since these errors are most likely to be somewhat optimistic estimates. Being based only on the simplistic χ^2 model I have assumed that the nearby SEDs are well established and definitive for each type, whereas the reality may well be different. For example, as remarked upon earlier, since these are obtained from nearby galaxies the spectra are not representative of the total light from each object, but rather arise from only the nuclear regions. In the absence of integrated spectra of nearby objects we are unable to improve on the situation. The interpretation, then, of observational data should bear this in mind (I shall refer to this again in later chapters).

In the next section we shall compare observations of galaxies in three moderate redshift clusters, obtained using this intermediate-bandwidth filter set, with available spectroscopy to assess whether in practice our photometric object classifications are as reliable as our simulations indicate.

2.4 Observations.

Couch *et al* (1983), present results of CCD photometry of three moderate redshift clusters — A1942 ($z = 0.22$), A1525 ($z = 0.25$), and AC103 ($z = 0.31$) — in these 7 intermediate bands (table 2.5). Spectroscopy has also become available for many objects in each of these clusters (sources listed in table 2.6), so, in principle, it should be possible to directly check the accuracy of the photometric redshift estimates. In this section I will discuss the results of a study of the photometry of individual objects in each of these clusters and consider the consequences for future observations. In practice we find that some complications become evident when working with genuine observational data rather than mere simulations. The results of these studies are presented in table 2.6, where the object numbers are as in the finding charts provided in Couch *et al* (1983).

Firstly, in this particular case, the authors used two different CCDs for their photometry. Although they undertook a detailed comparison of the properties and relative behaviour of each detector, it is evident from detailed inspection of the data for individual galaxies, that the GEC (redder response) CCD provided poorer quality results than that obtained using the RCA chip. Indeed, a very large fraction of the observed galaxies had photometry of very poor quality, necessitating their rejection from further analyses.

Considering, the usable photometry, it was noted that the SED fitting algorithm can occasionally be 'misled'. This happens for quite understandable reasons. For example, photometry of a given object in one or more of the filters can be erroneous if the object is imaged on a defective pixel or column on the CCD, or if a cosmic ray event is detected nearby. Occurrences of the former type are not uncommon, particularly if the CCD is of poor cosmetic quality, whilst the effects of cosmic ray events can be minimised by taking shorter repeat exposures in each passband rather than single long integrations.

Table 2.5: Three Moderate Redshift Clusters.

Cluster	R.A.	Dec	z	No. of SEDs	No. of z_s
A1942	14 36 06	+03 51	0.224	39	6
A1525	12 19 30	-00 53	0.259	24	6
AC103	20 53 06	-64 51	0.311	31	17

Table 2.6: Comparison between spectroscopy and SED fits.

Cluster	#	z	SED	z_{phot}	Spectroscopy
A1942	26	0.145	Sab	0.2	(1)
	56	0.145	Sab	0.2	
	84	0.225	Scd	0.25	
	1	0.224	E/S0	0.2	
	33	0.307	E/S0	0.3	
	16	0.217	E/S0	0.15	
A1525	1	0.25	E/S0	0.25	(2)
	2	0.257	E/S0	0.25	
	3	0.1	E/S0	0.1	
	46	0.257	E/S0	0.25	
	61	0.26	E/S0	0.25	
AC103	16	M star	poor	-	(3)
	1	0.113	Scd	0.2	
	2	0.311	E/S0	0.3	
	3	0.312	E/S0	0.3	
	4	0.310	E/S0	0.3	
	13	0.310	E-Sab	0.3	
	36	0.309	E/S0	0.25	
	43	Star	poor	-	
	49	0.333(EM)	Scd	0.3	
	144	0.303	Sab	0.25-0.3	
	145	0.312	Sab	0.3	
	15	0.31	E/S0	0.3	
	39	0.31	E/S0	0.3	
	20	0.31	E/S0	0.3	
	12	0.31	Sab	0.25-0.3	
22	0.31	E/S0	0.3		
17	0.31	E/S0	0.3		
47	0.31	E/S0	0.3		

References:

- (1) Henry, 1984, private communication.
- (2) MacLaren, Ellis, Couch, unpublished.
- (3) Sharples et al, 1985.

The use of narrow bands could conceivably cause further difficulties if the observed galaxy SEDs contain very strong emission features, ie. stronger than in our adopted nearby template spectra. In the case of 0024+1654, Dressler *et al* (1985), purposefully chose a narrow filter to coincide with the [OII] emission line at 3727\AA at the cluster z to measure line strengths from galaxy to galaxy. This technique is rather valuable in that the strength of this line provides an indication of the level of ongoing star formation in these objects.

In our case the 3727\AA line lies near the centre of the 502 filter at a redshift $z \sim 0.35$. By modelling the change in magnitude in this filter as a function of change in the equivalent width (W_λ) of the line the results in table 2.7 were obtained. Because these filters, although considerably narrower than standard broad-band photographic bands, are still relatively broad ($\sim 600\text{\AA}$) compared to the line width, the contribution of the line to the overall magnitude is not large. In other words, significant changes will only occur if the line has a strength which is quite inconsistent with 'normal' local galaxies. Consequently this effect is not likely to be of any major significance.

Another discrepancy that can arise when comparing our simulations with genuine observational data is that objects in distant clusters may have continua that are different in form to those of our template objects, perhaps due to the nature of the rich cluster environment or evolution. In such a case the quality of the χ^2 fit may be rather poor, but without visual inspection it is not possible to know whether there are any systematic differences or simply large random errors.

Loh and Spillar (1986) using an almost identical set of filters to Couch *et al* (1983), have followed a similar procedure on the cluster 0024. However, they have relied solely on an automatic χ^2 fitting algorithm to analyse their data without comment on the visual appearance of individual SEDs. This may well result in a 'force-fitting' of the observations to the templates causing the observers to overlook any unusual SED forms.

Indeed in their sample of objects for which Dressler *et al* (1986) have spectroscopic redshifts, there are a number of objects with seriously discrepant photometric z estimates. Loh and Spillar argue the case in favour of their results quite strongly in many of these examples, but perhaps notable by its lack of comment in their paper, is the old starburst galaxy discovered by Lilly and Gunn (1985) for which their χ^2 fit is seriously wrong. This effect may well be very relevant to such high redshifts and indeed we shall return to it in chapter 3 with further examples from our own work. These problems illustrate the need to visually inspect the SEDs of each object for spurious features, or discrepancies. This is the approach we shall adopt in all subsequent observations.

The observed SEDs are easily constructed from the measured colours and zero points, as we shall discuss in the following chapters. For each object we plot the observed galaxy photometry on top of the expected (figure 2.6) SEDs of various galaxy types at a variety of redshifts, allowing us to choose the redshift and type that best fits the observations. The SEDs can also be matched automatically using the χ^2 method which forms the basis of the program SEDFIT. A comparison of SEDFIT classifications with visual checks by several authors has shown that the 'eyeball' fitting is a reliable approach. In our analysis of all subsequent multicolour photometry then we shall perform the χ^2 fitting and independently examine each SED by eye.

I have thus classified the individual objects in the 3 clusters studied by Couch *et al*, and the results are presented in comparison to the available spectroscopy in table 2.6.

In summary, the SEDs provide an excellent comparison with the spectroscopy in these clusters, with no serious discrepancies beyond our stated accuracy. It is also most re-assuring to note that the two stars present in this sample were noted as having SEDs which did not match the template galaxy spectra at any redshift.

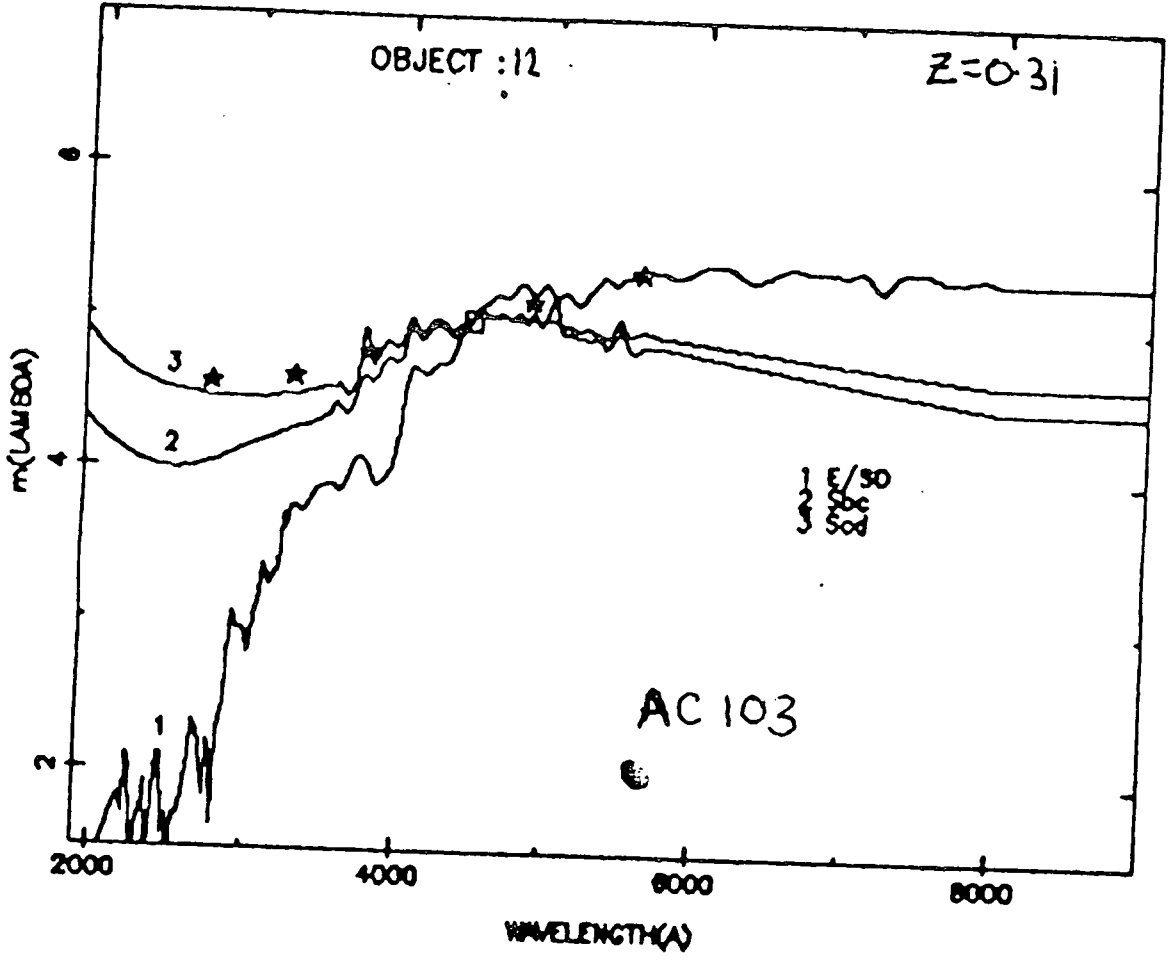


Figure 2.6: Example SEDs from Couch *et al*'s study of three nearby clusters.

f

Table 2.7: W_λ for [OII]

W_λ	Δm
10Å	0.03
20Å	0.05
30Å	0.08
40Å	0.10
50Å	0.12
100Å	0.23
200Å	0.43
300Å	0.60

Discrimination in the low redshift region, $z < 0.25$, is, however, fairly difficult, since our accuracy of $\sim \pm 0.05$ in z may be insufficient to separate field and cluster galaxies. The technique should, therefore, be expected to find its most successful role at higher redshifts. In the two following chapters we shall consider clusters of galaxies at such high redshifts, and once again compare with available spectroscopy to show just how valid our approach is in practice.

2.5 Conclusions.

This chapter has revealed that we can indeed estimate galaxy redshifts, albeit somewhat crudely, using photometric information. In particular we have found that a filter system similar in spectral coverage and resolution (with at least 4 passbands) to that of Couch *et al*, provides us with sufficient accuracy for our purpose of studying distant clusters of galaxies. Whilst the accuracy is a function of colour, we find that this filter set should provide $\Delta z \pm 0.05$ as a typical accuracy. Furthermore, our technique should be particularly valuable at high ($z > 0.3$) redshifts, allowing us to monitor the rest frame ultra-violet region of cluster members. We have also noted the need to inspect carefully the data for each object, since crude algorithms may yield misleading results.

3. CCD Photometry of the Distant Cluster 0016+16.

3.1 Introduction.

The photometric technique we developed in the previous chapter was specifically designed for observations of high redshift (i.e. $z > 0.4$) clusters of galaxies. At these distances, the corresponding look-back time of ~ 6 Gyr ($H_0 = 50, q_0 = 0.1$), is sufficiently long that we may expect to begin to see evolutionary differences in galaxy spectral properties. However, so far we have only observed clusters around $z \sim 0.25 - 0.3$. Before using our technique on a new set of candidate distant clusters, then, it will be important to test its effectiveness by comparison with a distant cluster which has previously been studied using a more traditional approach. This will directly reveal any inherent advantages or problems that such narrow-band imaging possesses.

An appropriate candidate is the rich, centrally-concentrated cluster 0016+16. Originally discovered by Richard Kron as a number density enhancement on red Kitt Peak 4.0 m photographic plates, the cluster was assigned a redshift of $z=0.54$ by Spinrad (1980), thus making it the most distant cluster then known. It is worth noting here, however, that whilst this redshift was obtained from spectroscopy of one of the central objects in the cluster core, another bright galaxy some 40 arcsec away had a z of 0.3.

These observations were subsequently followed up by Koo (1981), using his UJFN photographic system described in chapter 2. He obtained detailed photometry of a region of 4.0×4.0 arcmin around the apparent cluster centre, as well as a companion field area, and his results can be summarised as follows.

1. Observed colour-colour diagrams were used to argue that 0016+16 was a rich cluster with most galaxies at $z = 0.54$ and not $z = 0.30$.
2. The estimated richness of the cluster was found to be twice that of Coma and comparison of the luminosity function with Coma implied a luminosity evolution of $\Delta M_B \sim 0.6$ mag, as well as only a slight colour change of ~ 0.07 mag in (B-V).
3. Most of the galaxies were found to be intrinsically very red with no indication of any significant amounts of star formation for several Gyrs prior to the epoch at which they are observed. If we then reconsider the nature of the Butcher-Oemler effect discussed in chapter 1, we see that 0016+16 does not fit the standard picture of increasing blue fraction with redshift. In fact, as shown in figure 1.2, its dominant red population is akin to that of typical nearby rich clusters.

Studies of the X-ray emission from the cluster (White, Silk, and Henry, 1981) and the observation of a microwave continuum dip (Gull *et al*, 1981) apparently verified that this was a dynamically evolved rich system with the X-ray contours matching the elongation of the galaxy distribution.

To summarise, the cluster 0016+16 has properties similar to nearby rich systems, yet at such a high redshift we would expect to observe noticeable evolutionary differences if the Butcher-Oemler effect was a universal phenomenon. It thus constitutes an exciting candidate worthy of further detailed observation via our CCD intermediate-bandwidth imaging technique. With broadband observations, as we have seen in chapter 2, the level of ambiguity associated with individual object photometry, requires us to adopt only a statistical approach. We should, by using these narrower bands, be able to distinguish the level of foreground contamination and verify cluster membership, for each object or populations of object, as well as examining the form of object SEDs to look for any possible evolutionary effects not resolvable in a set of broader filters. In particular, our imaging in the rest frame ultraviolet (418 filter) should be more reliable than Koo's U photometry, not only because

of smaller photometric errors, but also for the arguments used in the previous chapter where we cast doubt on the applicability of the U passband at redshifts beyond $z \sim 0.45$.

In this chapter I shall present our observations of 0016+16, discuss in detail the data reduction process, and finally address these specific astronomical questions using our galaxy SEDs. The work presented in this chapter has been published in a less detailed form in Ellis *et al*, 1985.

3.2 Observations.

We have imaged the cluster through six of the intermediate bandwidth filters described in the previous chapter; 418, 502, 578, 685, 748, and 868 nm. The observations were made at the prime focus of the Anglo-Australian Telescope (AAT) during two nights in October 1983 by R.S. Ellis and W.J. Couch, but were reduced and analysed by the present author. A considerable improvement in the quality of the data over that in the original three moderate z clusters of Couch *et al* (1983) was achieved by using solely the RCA CCD for all passbands. Indeed, all the photometry presented in this thesis has been obtained using the RGO CCD camera which is based on the thinned 320×512 format RCA 53612 CCD. Full technical details of this device can be found in Jordan, Thorne, and van Breda (1982). The attractive feature of such a device, from our point of view, is its relatively high blue sensitivity (see Fig. 2.4).

A log of the observations made on these two nights is reproduced in table 3.1. Throughout both nights, the cluster observations were sandwiched between several exposures of the Oke (1974) spectrophotometric standard stars VMa2 and L870-2. The seeing value quoted in the table was measured from Gaussian fits to stellar profiles on each exposure using STARLINK software (written by R.F. Warren-Smith).

3.3 Data Reduction.

(a) Image Processing and Photometry.

Each of our raw image frames (figure 3.1(a)) was reduced in an identical manner, largely using the ASPIC image processing routines available on the Durham STARLINK VAX 11/750. The procedure is illustrated in Figs 3.1.(a)-(c).

The first stage is the removal of the bias level from each CCD exposure, determined using mean bias frames taken at the beginning and end of each set of observations. Next, cosmic ray events and chip cosmetic defects were removed (by replacing the affected pixels with a nearby mean value). The number of such cosmic rays was minimal (typically only a few per thousand seconds) and has little effect except in a few exceptional cases where the cosmic ray was incident on a galaxy image, but such events were noted and could be remedied on the basis of repeat exposures.

This CCD contains two central defective columns plus other smaller cosmetic flaws which were also cleaned from each image. The central columns are well established and their consequences were minimised by positioning our targets somewhat off-centre in each field.

To account for the intrinsic variations in sensitivity from pixel-to-pixel we construct a mean 'flat-field' frame for each filter from a series of exposures of light from a tungsten lamp reflected off the telescope dome. The individual frames are then divided through by the appropriate normalised flat-field response.

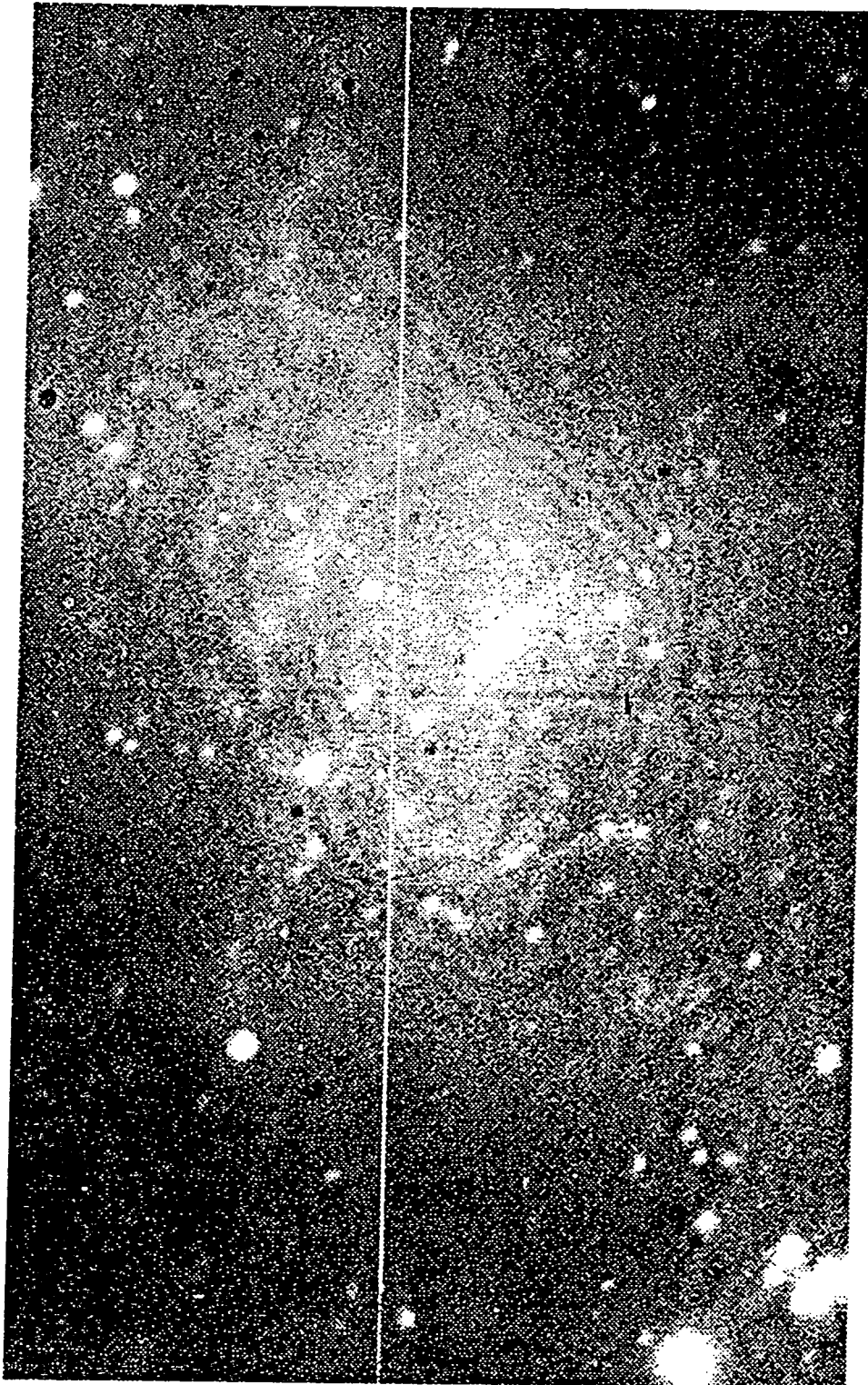
At this stage in the reduction procedure a faint fringing pattern can be seen on the frames taken longward of ~ 550 nm (Jordan *et al*, 1982, and figure 3.1(b)) resulting from interference in the thin substrate of the CCD. We correct for this effect by taking exposures of a blank region of sky (ie, devoid of bright objects) to obtain a template fringe pattern for each filter.

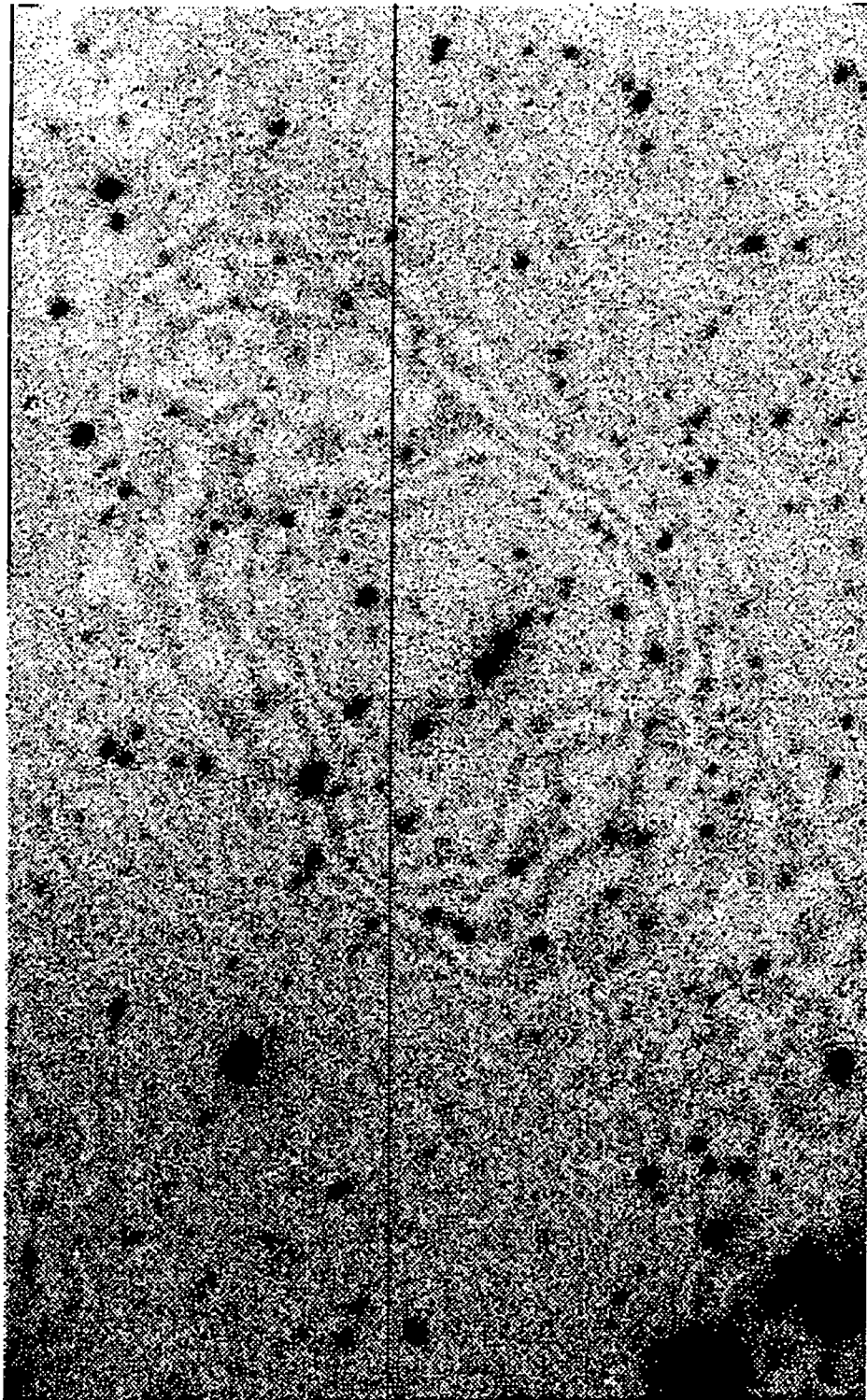
Table 3.1: *Log of Observations*

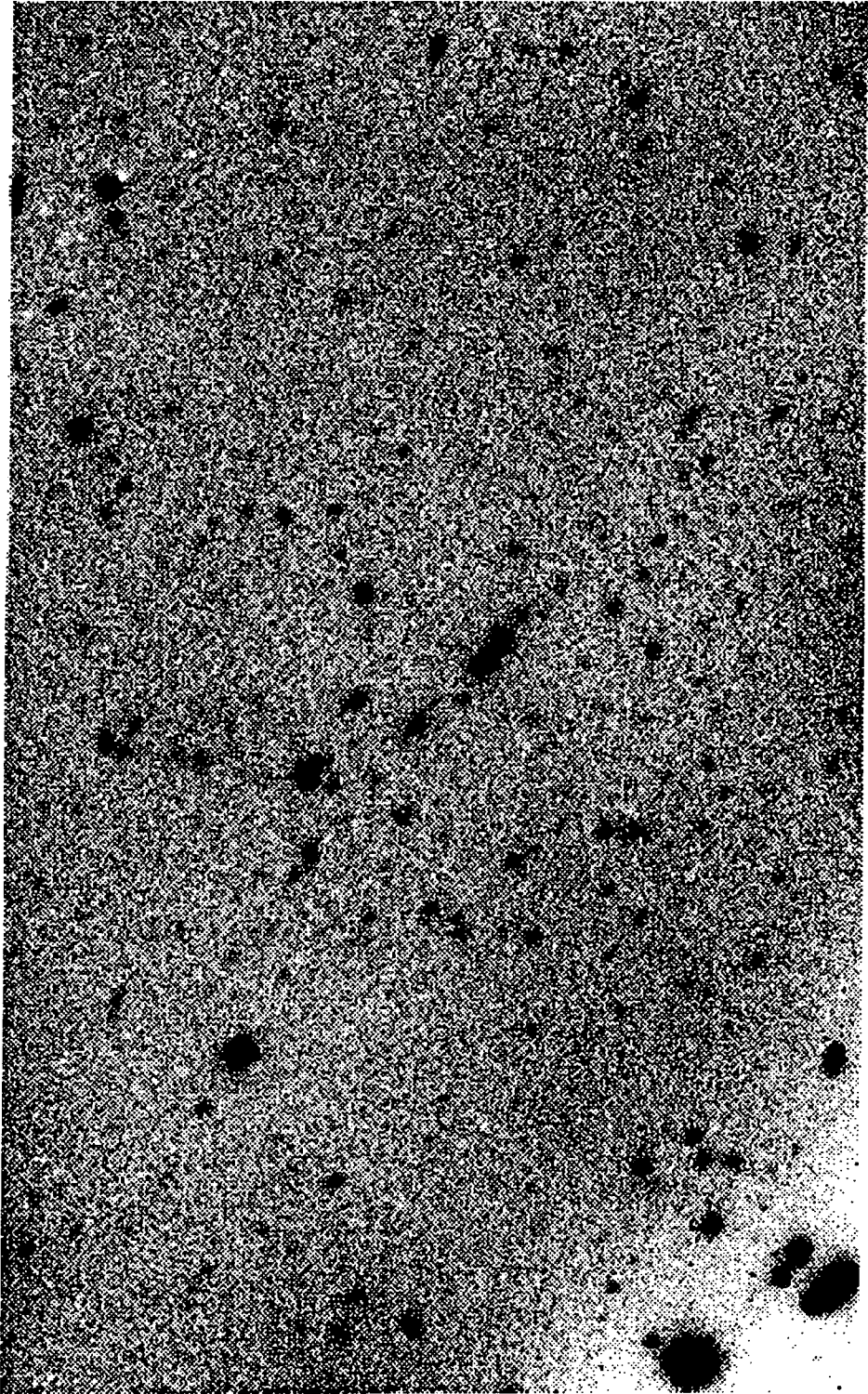
Object	Date	Filter	Dwell(s)	sec z	Seeing(arcsec)
0016+16	1983 October 2/3	685	2000	1.77	1.41
		862	2000	2.02	1.24
	1983 October 8/9	418	2000	1.55	1.03
		418	2000	1.50	1.21
		418	2000	1.49	1.18
		502	2000	1.54	1.04
		578	2000	1.68	1.06
		578	2000	1.70	1.25
		748	2000	1.91	1.52
		748	1000	2.26	1.52
		862	2000	1.87	1.12
VMa2	1983 October 2/3	418	50(1)	2.02	1.53
		502	25(2)	1.32-2.08	1.58
		578	25(1)	2.10	1.62
		685	25(2)	1.32-2.14	1.28
		862	50(2)	1.31-2.18	1.22
	1983 October 8/9	418	20(4)	1.25-1.83	0.96
		502	10(6)	1.25-1.82	0.79
		578	10(10)	1.25-1.80	0.93
		685	10(4)	1.25-1.79	0.83
		748	20(4)	1.25-1.87	1.00
		862	20(3)	1.25-1.84	0.81
L870-2	1983 October 8/9	418	20(1)	1.29	1.53
		502	10(2)	1.28	1.21
		685	10(2)	1.28	1.02
		862	20(1)	1.27	1.11

Figure 3.1: The CCD frame reduction process.

- (a) Raw image frame.
- (b) Flat-fielded frame, revealing fringe pattern.
- (c) Fully reduced frame, with fringes and dud column removed.







This template is then zero-measured and the appropriately scaled pattern removed from each image frame. Any residual fluctuations remaining after this procedure were very small and consequently posed little difficulty for our photometry.

To improve our signal in any passband we co-add multiple exposures to produce a final single frame. In this case we have repeat exposures in the 418, 578, 748, and 862 passbands. The frames were co-added (to the nearest pixel) after correcting for any positional offsets from exposure to exposure. Indeed because of positional offsets, the area of sky common to all exposures was reduced to some 6.2 arcmin² compared with the full CCD area of 9.2 arcmin².

With the finally reduced images in each passband we are now in a position to carry out detailed photometry of the individual objects. Several sets of photometric reduction software are available, each being limited in use by its own idiosyncracies. We have chosen for this work to use the APEX-based system of Newell (1979) and Couch and Newell (1984) since it is fairly flexible and well suited to our aims. The references given specify the details of the system but here we shall outline the basic key stages of the reduction procedure.

- (1) We selected objects from the fully reduced 685 nm frame (close in wavelength to Koo's F and CN's R_F) by visual inspection on an ARGS image display unit. Each object is selected using a cursor on the display (see figure 3.2 for our finding chart for 0016+16). The effectiveness of such a visual procedure will be seen later when we discuss the completeness limits of our photometry. To avoid any serious selection biases we have identified all objects on the frame, only rejecting obvious stars. The x-y positions are then stored in a file for later use whilst the program LEXTRACT extracts image sub-arrays centred on each cursor position, large enough to contain the object and a useful area of the surrounding sky.
- (2) In the next stage, the software examines each sub-array individually to determine a more exact object centre. This routine can be prone to error in the presence of nearby bright objects or defective pixels. Thus we checked each new centroid on the image display and interactively corrected any problems.
- (3) When all the object centres had been defined the program GALAXY was run on the sub-arrays to carry out the actual photometric measurements. The definition of magnitudes in the APEX system is

$$m = 25 - 2.5\log(I), \quad (3.1)$$

where I is the total object (ie, sky-subtracted) intensity in the specified aperture. This software can provide two types of magnitude for each object; a Kron (1978) type magnitude, and a series of 10 aperture magnitudes.

Kron's magnitude system was devised to measure the same fraction of galaxy light independently of redshift and profile. This is achieved by evaluating his r_1 statistic from magnitudes in a series of annuli over the whole object. Kron states that at least 90% of the galaxy's light should lie within a radius of $2r_1$. Using the aperture photometry APEX chooses that aperture which just includes the estimated Kron radius for each object as being a close estimate of the Kron size.

For estimates of galaxy colours we must be sure that the light we measure in one passband comes from the same physical area in the galaxy as that in the other filter. Thus all our colour values should be determined from aperture photometry. APEX produces magnitudes in a series of ten apertures from 1.6 arcsec to 16 arcsec in diameter, local sky values being determined from modal values in two annuli lying beyond the object apertures.



Figure 3.2: Composite CCD frame of 0016+16 created by co-adding the processed 578, 685, and 748 images. The numbered objects are those in the sample with $F < 22.0$.

Probing to such faint limits, we should like to determine our colours as accurately as possible. Consequently, we have chosen the relevant aperture size not on the basis of some predetermined metric size, but rather, by finding that aperture which provides us with the best signal-to-noise statistics on average over our sample. The signal in each aperture is simply obtained from the magnitude using expression 3.1. The noise associated with any such measurement is a combination of the CCD readout noise (ro), the noise in the sky background, and that in the object itself.

$$noise = \sqrt{ro^2 + sky + obj} \quad (3.2)$$

In this case we have $ro=73e^-$ per pixel and $1 \text{ ADU} = 15 \text{ photons}$ for this RCA CCD. After calculating the signal-to-noise for each aperture for a large number of objects in our sample, we found that the minimum noise contribution corresponded to an aperture of diameter 3.2 arcsec (denoted later as aperture(2)), which at this redshift is a physical diameter of $\sim 30 \text{ kpc}$, large enough then to include most of the light from the galaxy.

From a detailed study of various magnitude schemes on similar CCD data to that presented here, Couch *et al* (1983) have concluded that Kron-type magnitudes can be unstable (poor repeatability in separate exposures), the large error arising from the fitting of the outermost annuli. These authors expressed concern that this effect could pose a serious problem for faint galaxies. We shall thus only consider Kron type magnitudes in this work when directly comparing our photometry with other authors' work.

(b) *Comparison with Koo's photometry.*

D.C. Koo kindly made his J and F photometry of individual galaxies in this field available to us, enabling a direct calibration of our own CCD data obtained in the 685nm band on his F scale. Because of the relative width of the F band (see Fig. 2.3) we must correct our data for any possible colour equation. Of all the objects in our sample for which we have F magnitudes, down to a limit of $F=22.5$ we have plotted

$$\Delta m = 685 - F \quad (3.3)$$

(with the magnitudes measured in the aperture corresponding closest to the Kron radius — ie aperture 3, on average) versus the colour measured in 502-685, in figure 3.3. The least squares fit to this relation is also plotted in the diagram and found to yield

$$\Delta m = 0.587(502 - 685) - 0.959. \quad (3.4)$$

Using this relation we can convert our 685 magnitudes to F as in figure 3.4 The relation between the two sets of photometry is excellent considering the independent nature of the data with a random scatter about the 45 degree line of $\sim 0.17 \text{ mag}$ to a limit of $F=22.5$.

Now that the two sets of observations are calibrated we are in a position to directly compare Koo's findings with our new results. We can determine the completeness limits of our photometry by comparing the number of objects observed in our final CCD area down to Koo's claimed completeness limit of $F=22.5$. From such a comparison we can deduce that our CCD sample is also virtually complete (only 2 per cent discrepancy) to this limit. Table 3.2 contains estimates of field counts to various magnitude limits.

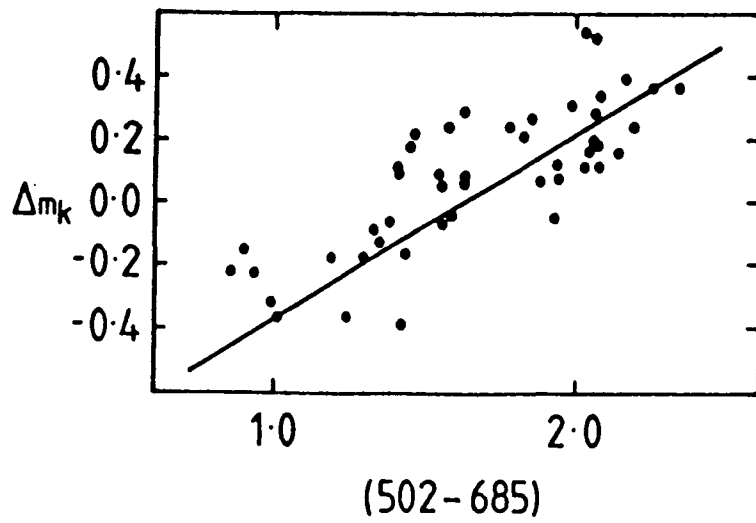


Figure 3.3: The colour equation between the 685 nm band and Koo's broad-band F, plotted as $\Delta m_K = 685_K - F_K$ versus (502-685). The filled circles represent the objects measured by both Koo and the present author with $F_K < 22.5$. The solid line is a least-squares fit through the data.

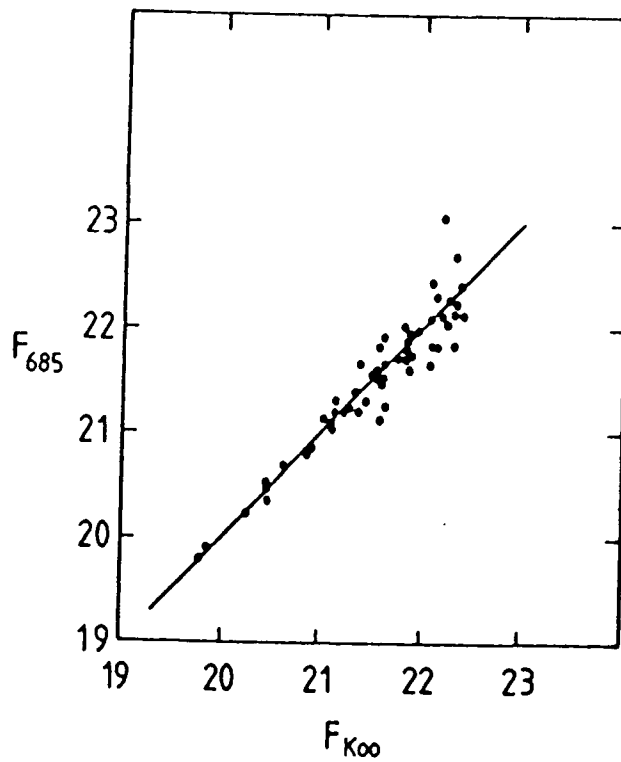


Figure 3.4: Comparison of the colour-corrected 685 magnitudes with Koo's F photometry for the objects plotted in Fig. 3.3. The solid line represents the one-to-one relationship.

Table 3.2: Photometric Samples and Field Contamination.

F limit	No. Measured	Expected Field
21.0	9	2
21.5	24	7
22.0	47	13
22.5	78	24

(c) *Standards and Colour Calibrations.*

To compare the observed galaxy colours with those predicted from suitably redshifted nearby galaxies (chapter 2) we must zero-point our APEX photometry onto the same colour scale as the models. Oke (1974) provides spectrophotometry for our two standard stars, VMa2 and L870-2, obtained using a multichannel spectrometer covering the range 3200Å to 10,500Å in bandwidths of 20Å – 80Å with an average accuracy of 0.02 mags at each wavelength. These standard star SEDs could then be passed through our models in the same manner as with the galaxy SEDs to produce predicted magnitudes in each passband, $p(i)$. The CCD frames of the standards were then reduced in an identical manner to the cluster exposures and the APEX determined Kron magnitudes were evaluated. We then calculate the offset,

$$T(i) = p(i) - o(i), \quad (3.5)$$

where $o(i)$ is the observed magnitude in the filter i , suitably corrected to the same zenith distance and exposure time of the finally reduced cluster frame. To each of our measured colour combinations we then add the value,

$$c(1 - 2) = T(1) - T(2). \quad (3.6)$$

The details of this procedure for each of our standard exposures are given in table 3.3.

In later discussions and for comparison with other workers we shall find it useful also to compare our photometry with R_{KC} (Kron-Cousins) magnitudes. Since our 685 filter response closely matches this passband (considerably closer than Koo's F) we can calibrate our photometry via the R magnitude of VMa2, found to be 12.129 ± 0.003 mags by H. Morrison (1985, private communication) of Mount Stromlo and Siding Spring Observatories (MSSO). From table 3.3 we have then,

$$R_{KC} = 685 + 4.225 \quad (3.7)$$

(d) *Photometric Errors.*

Since we have two separate exposures in the 578 nm passband and three at 418 nm we are able to carry out detailed tests of our random photometric errors to various limiting magnitudes. Each individual frame was reduced independently and the magnitudes obtained for every object were compared. As in Couch (1981) we can use Keeping's (1962) method of estimating the magnitude error $\sigma(m)$ from the range of magnitude values spanned by the individual exposures for each object, δm . In the case of two repeat frames the relation is

$$\sigma(m) = 0.886 \times \delta m, \quad (3.8)$$

whereas for three frames,

$$\sigma(m) = 0.591 \times \delta m. \quad (3.9)$$

This provides us with an estimate of the error on each frame and, by approximate scaling ($\sqrt{2}, \sqrt{3}$), that on the final co-added photometry.

These empirical values can then be compared with those expected on the basis of random noise considerations, which is simply estimated by obtaining a mean object magnitude in that particular passband down to our specified limit, and using expressions 3.1 and 3.2. The results of such comparisons are presented in table 3.4 which clearly show that our errors are essentially due to those expected from photon counting.

Table 3.3: Colour calibration using Oke standards.

Band	Std	Night	No. of exps.	Exp(s)	m_{ave}	σ	MAGS	T
418	VMa2	2	4	20	7.586	0.04	27.034	19.448
418	L870	2	1	20	7.892		27.289	19.397
502	VMa2	2	4	10	7.847	0.05	26.320	18.473
502	L870	2	1	20	8.400		26.754	18.354
578	VMa2	2	8	10	8.887	0.04	25.699	16.812
685	VMa2	1	1	50	7.904		25.777	17.873
748	VMa2	2	3	20	9.817	0.02	25.964	16.147
862	VMa2	1	1	50	11.594		26.757	15.163
862	VMa2	2	3	20	11.078	0.03	26.757	15.679

Note: 862, combined frames from both nights, $T=16.204$

Table 3.4: Random Photometric Errors.

Band	Sample	$\sigma_{observed}$	$\sigma_{Poisson}$
418	$F < 21.5$	0.123	0.080
	$F < 22.0$	0.148	0.111
	$21.5 < F < 22.0$	0.189	0.209
578	$F < 21.5$	0.039	0.021
	$F < 22.0$	0.082	0.028
	$21.5 < F < 22.0$	0.112	0.044
	$22.0 < F < 22.5$	0.166	0.074

The repeatability of our white dwarf colour calibrations are also of importance, providing an indication of the atmospheric conditions during our observations. Since we have only a limited set of observations of L870-2 we are only able to compare the offset for the colour 418-502 between the two standards, VMa2 and L870-2. However, since these colours are at the blue end of the spectral region it will play a major role in our conclusions about the nature of galaxy evolution. As is seen in table 3.4, the repeatability of individual exposures of each star in all passbands agree to within 0.05 mag, whilst the colour offset calculated from both standards agrees to ± 0.02 mag.

In conclusion our estimated photometric errors are ~ 0.07 m for $F=21.5$, and ~ 0.10 m to $F=22.0$ in all passbands except 418 for which the equivalents are ~ 0.13 m and 0.17 m respectively. Although complete to a limit of $F=22.5$, we define a prime sample down to $F=22.0$ which provides good quality photometric precision for our colour studies.

3.4. Colour Distributions.

Considering the colour distributions (ie histograms of the number of galaxies in colour bins) of galaxies in a rich cluster we would simply expect to find two basic components. Firstly, if evolution is small, we expect that there should be a narrow peak representing the position of the early-type member galaxies, which dominate in the cluster core. Together with this we should expect a tail in the distribution stretching bluewards, containing the other galaxy types present in the cluster as well as the foreground field objects. A small additional red tail may be produced if there are any background galaxies present.

As they are defined in a unique filter system, our colours will not be of general use in their raw form, thus we have zero-pointed them to the predicted colours of a present-day E/S0 SED at $z = 0.54$ with no evolution or reddening for ease of comparison and interpretation. These final values for the colours in aperture (2) are listed in table 3.5 and presented as a series of distributions in figure 3.5 (for our prime sample, $F < 22.0$). Note that we have as yet made no corrections for the colour-magnitude effect, but we shall return to this shortly.

Since there are two different redshifts ascribed to galaxies in our CCD area, we have indicated these separately in each panel of the figure. The filled box denotes the galaxy with a redshift of 0.3, whilst the two double cross-hatched boxes are the bright galaxies associated with Spinrad's spectroscopic determination of $z=0.54$. Spinrad obtained this value for only one of these galaxies (although which one was not entirely clear at the time) but as we shall see later, subsequent spectroscopy by Dressler(private communication) has confirmed that both of these galaxies are at this redshift. Above each histogram I have indicated (horizontal bars) the expected colours of the Hubble sequence at $z = 0.3$ and $z = 0.54$, the vertical ticks corresponding to the E/S0 colours.

It is interesting to compare Koo's previous broadband photometry with our new results. His J-F colour for each of the objects in our CCD sample is shown in panel (f). Koo also determined a field colour distribution (panel (e)) from photometry of a large adjacent area. Couch (1984, private communication) simulated the field distributions in each of our colours (solid curves in figure) from a model which successfully reproduces this observed J-F distribution.

Table 3.5: *Photometric Catalogue.*

No.	$F_{K_{00}}$	418 – 685	502 – 685	578 – 685	748 – 685	862 – 685
62	19.792	-1.453	-0.652	-0.802	0.004	-0.032
81	19.881	-1.445	-0.684	-0.910	0.293	0.094
148	20.196	-1.540	-0.853	-0.981	0.132	0.033
77	20.355	-2.310	-1.316	-1.066	0.438	0.635
2	20.483	0.042	-0.204	-0.105	0.055	-0.088
1	20.530	-0.421	-0.108	-0.201	0.078	0.055
63	20.683	-2.351	-0.804	-0.707	0.156	0.144
80	20.792	-1.535	-0.690	-0.839	0.187	0.180
144	20.838	-1.699	-0.614	-0.600	0.002	0.172
38	21.038	-1.532	-0.500	-0.473	0.067	0.121
7	21.079	0.696	0.091	-0.180	0.038	-0.229
6	21.123	1.300	-0.175	-0.212	-0.089	-0.295
11	21.129	-2.716	-1.618	-1.170	0.380	0.025
18	21.185	-0.901	-0.466	-0.414	-0.212	-0.371
59	21.200	-1.667	-0.904	-0.765	0.065	0.246
150	21.209	-2.312	-1.239	-1.072	0.052	0.180
49	21.228	-1.069	-0.612	-0.536	0.021	-0.036
88	21.246	-2.871	-1.239	-0.600	0.043	--
74	21.278	-0.975	-0.400	-0.408	-0.109	0.047
56	21.309	-2.136	-1.006	-1.042	0.428	0.038
30	21.384	-0.917	-0.179	-0.249	0.016	0.181
85	21.441	-3.438	-1.981	-1.575	0.065	0.368
3	21.469	-1.273	-0.087	0.025	-0.153	0.061
16	21.482	-0.895	-0.263	-0.445	0.113	-0.080
44	21.505	-0.233	-0.186	-0.351	-0.122	-0.224
113	21.547	-0.479	-0.364	-0.555	-0.236	-0.369
50	21.566	-0.438	-0.309	-0.538	-0.193	-0.248
45	21.571	-3.061	-1.372	-1.055	0.134	3.944
130	21.572	-0.884	-0.776	-0.977	-0.079	0.097
126	21.637	-1.298	-0.666	-0.492	-0.106	-0.013
37	21.648	-0.338	-0.186	-0.301	-0.105	0.365
61	21.649	-0.341	-0.341	-0.141	0.035	0.127
64	21.669	-0.744	-0.815	-0.697	0.180	0.154
116	21.696	-1.439	-0.700	-0.585	0.401	0.409
4	21.719	-2.751	-1.049	-0.754	0.643	0.444
43	21.726	-2.174	-1.397	-1.469	-0.418	-0.514
129	21.734	-0.444	-0.215	-0.487	-0.168	-0.415
24	21.770	-0.338	0.003	-0.515	-0.229	-0.018
147	21.826	-1.549	-0.296	0.062	-0.077	-0.281
21	21.829	-1.714	-0.181	-0.274	0.460	0.370
17	21.833	--	-0.612	-0.609	0.210	-0.322
55	21.833	-0.664	-0.373	-0.419	0.092	-0.029
22	21.859	-0.217	-0.042	-0.009	0.385	0.127
42	21.879	-0.810	-0.945	-0.650	0.040	0.925
131	21.889	-2.257	-1.484	-1.086	-0.346	-0.093
149	21.951	-0.919	-0.224	-0.153	-0.319	-0.126
57	21.979	-1.587	-0.309	-0.544	-0.071	-0.523

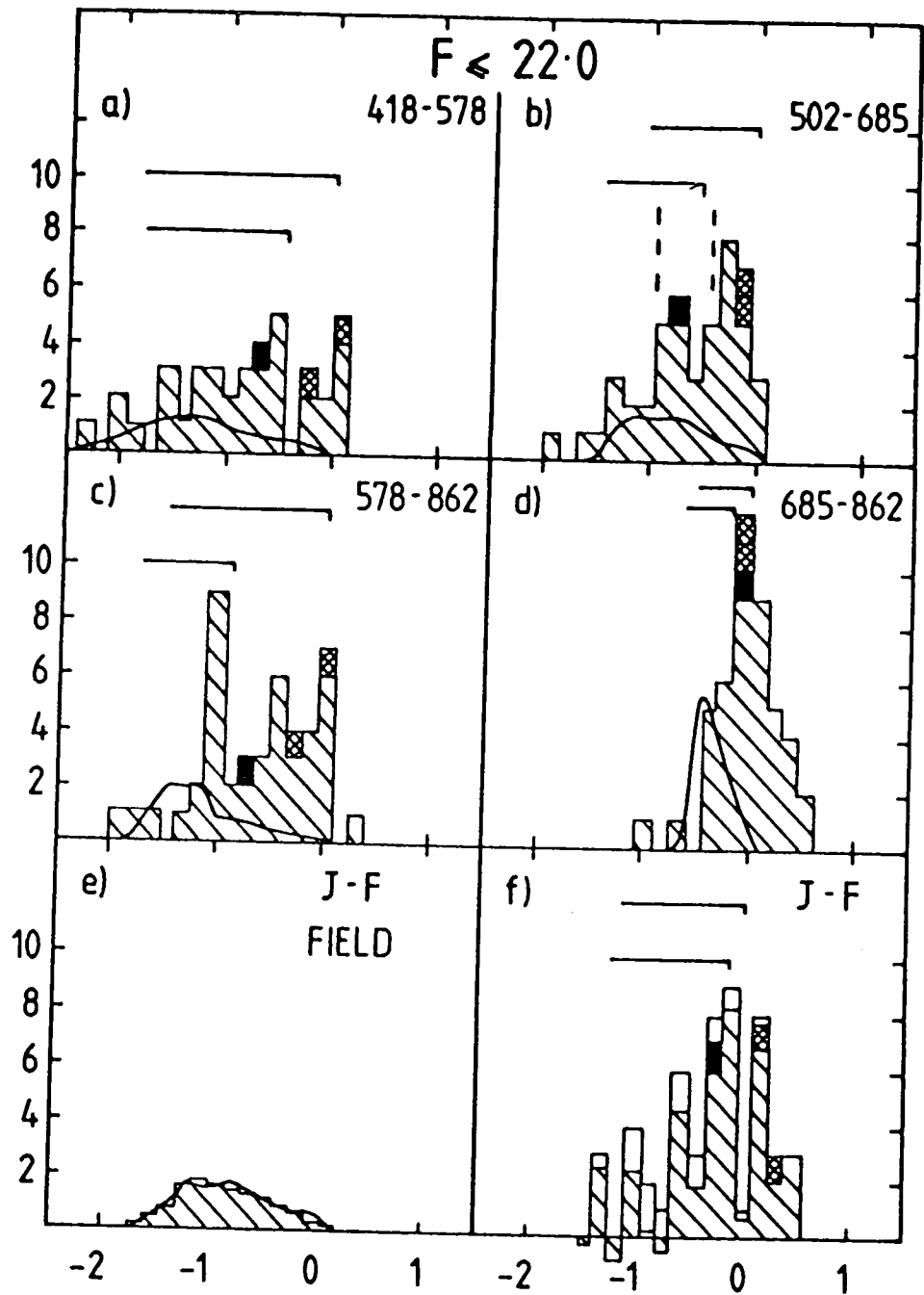


Figure 3.5: Representative intermediate-band CCD colour distributions for 0016+16. Also shown is Koo's J-F distribution for objects within the CCD area (f) together with his observed field distribution scaled to the same area (e). All distributions are limited to $F = 22$. The horizontal bars above the histograms indicate the predicted colour ranges for the non-evolving Hubble sequence (E/S0-Sm/Irr) at $z = 0.54$ (upper) and $z = 0.3$ (lower); the E/S0 is shown as the vertical tick. The double cross-hatched boxes are the two objects associated with the $z = 0.54$ spectroscopic observation of Spinrad, with the $z = 0.3$ spectrum represented as the filled box. The solid curves underlying the distributions (a)-(d) represent the predicted field component on the basis of a model which successfully reproduces the observed J-F field distribution (from Couch, 1985, private communication). In panel (f) the cross-hatched area represents the distribution after field subtraction.

It can be seen that Koo's J-F colour is fairly insensitive to redshift (see chapter 2), largely due to the width of the F band and the position of the 4000\AA break at $z \sim 0.2-0.6$. The resulting field subtracted colour distribution is consistent with a single but very broad peak. The separation of the two redshifts in the panel (f) is somewhat larger than expected from the predictions.

To improve sensitivity of colours to redshift differences, Koo added two further passbands, U and N as we remarked in the previous chapter, but these also introduce large errors to the photometry at these faint limits. We shall return to this later.

Our intermediate-band colour distributions reveal interesting behaviour which we now examine in detail. Firstly, our colours will each have different capabilities as redshift discriminators. For example, the 685-862 colour shows a single peaked distribution with no separation (within our errors) between $z = 0.3$ and $z = 0.54$, entirely consistent with the predictions. However, filter combinations which straddle the 4000\AA feature in our redshift range will allow more accurate discrimination (note that the 4000\AA feature is at 520 nm and 616 nm at $z = 0.3$ and 0.54, respectively). The details of this approach have already been discussed in chapter 2.

From our simulations we note that as the observations move further bluewards in the galaxy rest spectrum (in other words as we increase the wavelength baseline) our colours generally increase in sensitivity to redshift and galaxy type. The observed distributions spread to cover a broader range of colours with a flat blue tail, as can be seen in figure 3.5(b).

Summarising, these distributions imply that we are *not* observing a single homogeneous population of red galaxies at a redshift of 0.54. There is, rather, a significant population of blue objects which cannot be accounted for solely by possible errors in field subtraction in our small area (the blue tail contains more than twice the expected field contribution of 13 galaxies).

Furthermore, these blue objects are not uniformly distributed in that there is also evidence of 'clumping' around the colours expected for an early-type galaxy at $z = 0.3$, causing a second peak in the colour distributions, other than that at the $z = 0.54$ prediction. That this clumping is a genuine effect can be seen by examining the positions of individual galaxies from colour to colour. All the objects in both peaks generally maintain the same corresponding position in each of the histograms. This leads us to define three broad colour classes in one colour (502-685) distribution as follows (see panel (b)):

$$\text{Red : } 502 - 685 > -0.45$$

$$\text{Intermediate : } -0.45 > 502 - 685 > -0.95$$

$$\text{Blue : } 502 - 685 > -0.95$$

The mean colours of these samples are as in table 3.6. The red sample has a tight narrow distribution over all passbands, consistent with these objects largely being a population of E/S0 galaxies at $z = 0.54$. Indeed the colours of this sample agree to within ± 0.08 m (1σ) of the mean of the two spectroscopic candidates at $z = 0.54$. However, there is also evidence that these objects are bluer (~ 0.25 m) than present-day galaxies as we move to the rest frame uv (see later).

The intermediate component has colours which are incompatible with any galaxy type at $z = 0.54$. It too has a tight scatter of only 0.07 m (1σ) around the colour of the $z = 0.3$ galaxy. This strongly suggests that a large proportion of the galaxies in this group may well be explained as a group of E/S0s at this redshift.

Table 3.6: Mean Component Colours ($F < 22.0$) $m - m_{685}$

Subsample/Object	No.	418	502	578	748	862
Red	21	-0.442 (0.83)	-0.209 (0.12)	-0.286 (0.19)	-0.029 (0.19)	-0.076 (0.24)
#1,F=20.48		0.042	-0.204	-0.105	-0.055	-0.055
#2,F=20.53		-0.421	-0.118	-0.201	-0.078	-0.088
Intermediate	16	-1.342 (0.40)	-0.702 (0.13)	-0.685 (0.17)	0.074 (0.15)	0.092 (0.29)
#62,F=19.78		-1.450	-0.652	-0.802	0.004	-0.032
Blue	10	-2.703 (0.44)	-1.399 (0.27)	-1.104 (0.26)	0.170 (0.32)	0.586 (1.18)

Notes :

1. All colours are zeroed with respect to a present day $E/S0$ at $z = 0.54$.
2. Subsamples are defined in section 3.4 on the basis of the 502-685 colours.
3. Scatter shown in parenthesis (1σ).
4. Individual galaxies listed have spectroscopic redshifts. One of #192, #195 has $z = 0.54$; #62 has $z = 0.3$.

We therefore conclude that there resides in the 0016+16 field a significant population of galaxies bluer than E/S0s at $z = 0.54$ which are not field galaxies randomly distributed along the line of sight. Indeed, studies of separate components in the colour distributions strongly imply that there is an additional foreground component of galaxies at $z = 0.30$. The question arises as to whether a mixture of galaxies of various types at different redshifts could combine so as to mimic this effect. Whilst the tight colour scatter may argue against these results being due to a mixture of field galaxies at $0 < z < 0.5$, and say, spirals at $z = 0.54$, it is worthwhile to examine this point in more detail.

3.5. Spectral Energy Distributions.

Using the intermediate-bandwidths of our filter system we can construct SEDs for each of the selected populations in the manner described in chapter 2, calibrating the observations onto a relative flux scale using Oke's spectrophotometry of VMa2. Plotting these on the same scale as a series of SEDs for nearby galaxies, as in figure 3.6, we can see that the red galaxies do indeed agree with an early type $z = 0.54$ galaxy, and that the intermediate component is better fitted by a redshift of 0.30. Because of the quality of our photometric data we do not have to rely solely on such mean SEDs, but can in fact produce similar comparisons for each object. For example, the SED of galaxy #62, with a known spectroscopic $z = 0.3$, fits very closely the mean SED of the intermediate colour sample.

Every SED can thus be classified in terms of the best fitting galaxy type and redshift for the full range of colours. In the previous chapter we discussed the problems that can arise in automatic classification of such data using, for example, a χ^2 fitting procedure. We have seen that there are sometimes significant fluctuations in one of the six magnitudes which an algorithm would have difficulty rejecting. Another problem may arise when a filter lies close to a strong spectral feature, such as the 400 nm break, the deviation from the predicted SEDs may be large, but a small adjustment in effective wavelength can make a considerable difference. Finally, the use of non-evolving SEDs may lead to an incorrect classification.

For these reasons we decided (as stated in chapter 2) to independently classify each observed SED visually, by inspecting a series of plots (Fig. 3.7) similar to figure 3.6. for a range of redshifts (0.1 to 0.7) and Hubble types. Although the eye can also be misled such an approach can help to identify any significantly deviant filter measurements. A comparison between eye fits, the χ^2 procedure, and spectroscopy is presented in section 3.7. These classifications were carried out separately by the present author, Richard Ellis, and Warrick Couch and the agreement between each observer was excellent, confirming our estimated internal errors in chapter 2 of, on average, ± 0.05 in z and within one Hubble class (E/S0:Sab:Sbc:Scd:Sdm/Irr).

The final classification list is summarised in table 3.7, listing also the best χ^2 fits to each SED. Classifications for our selected colour samples are given in table 3.8, from which we see that 20 out of the 24 galaxies at $z = 0.54$ are contained within the red sample. In other words, we confirm Koo's result that this cluster does not show the Butcher-Oemler effect.

In what follows we shall use the classifications given in table 3.7. to analyse the physical properties of the 0016+16 cluster and its field contamination. We shall consider three basic problems; foreground contamination, cluster richness, and luminosity function.

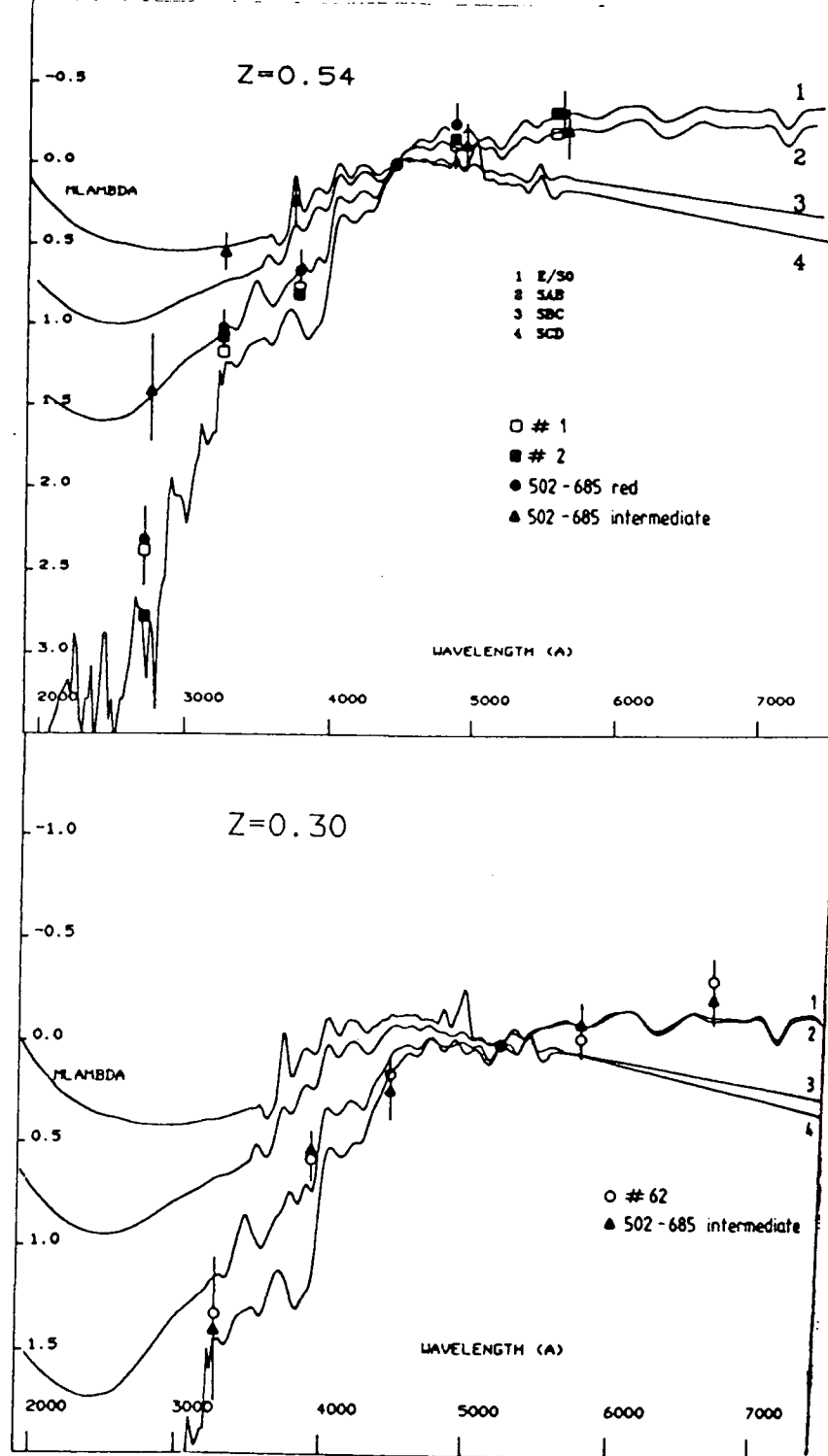


Figure 3.6: Mean SEDs for the red and intermediate components. The error bars indicate the mean individual scatter on the component objects.

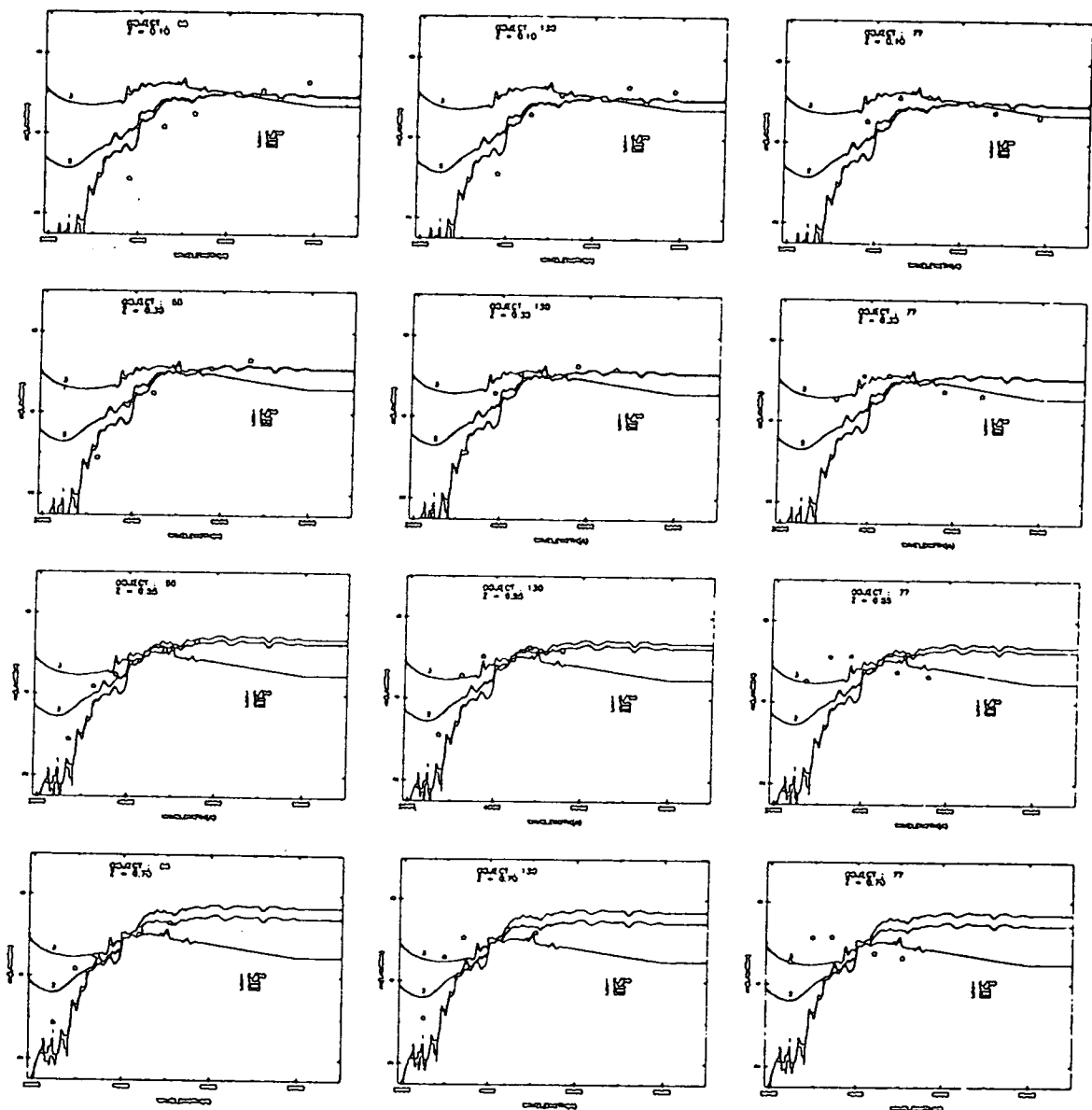
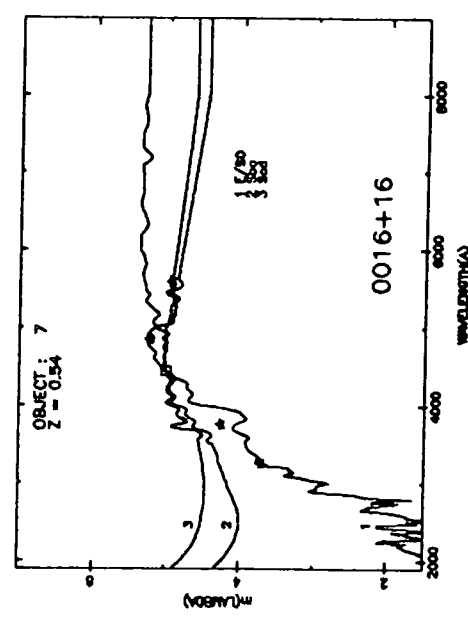
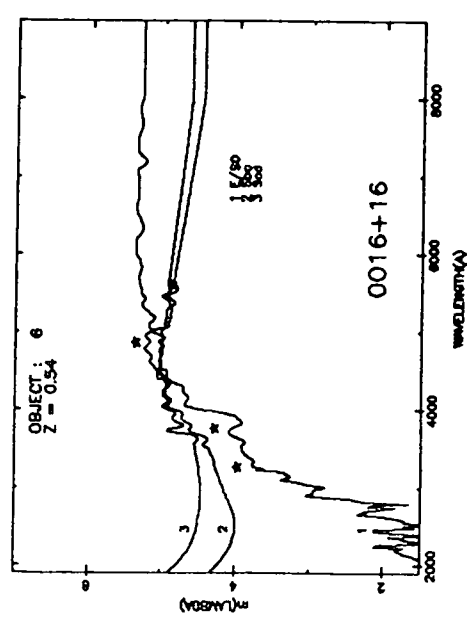
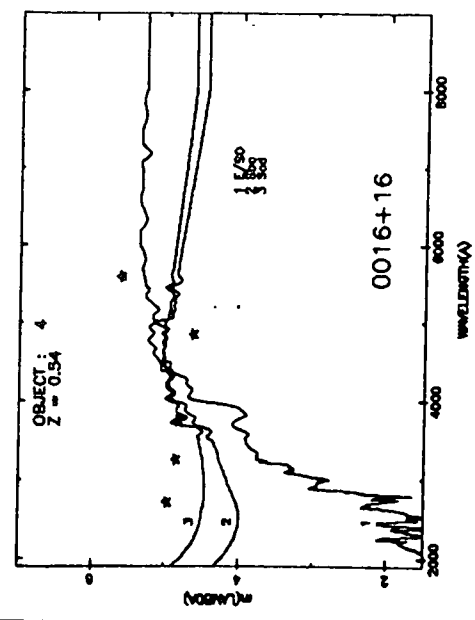
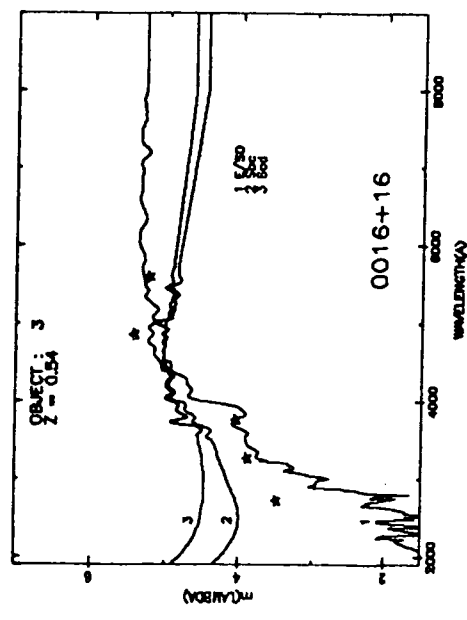
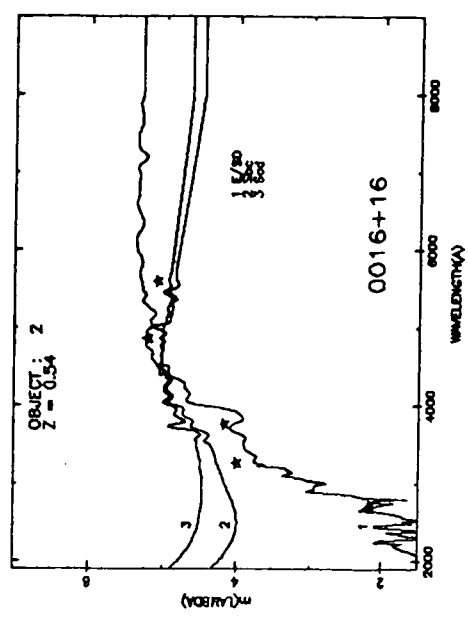
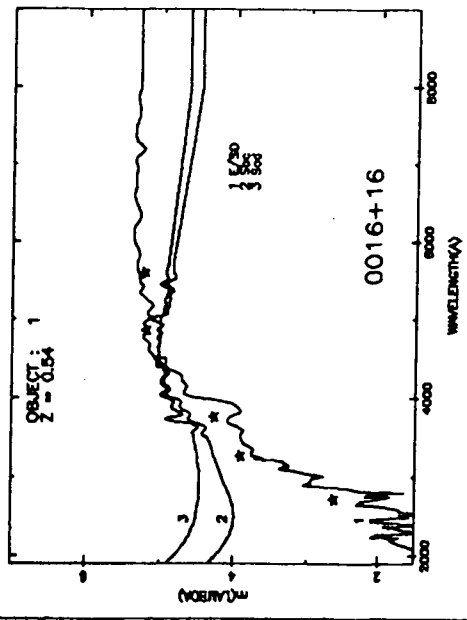
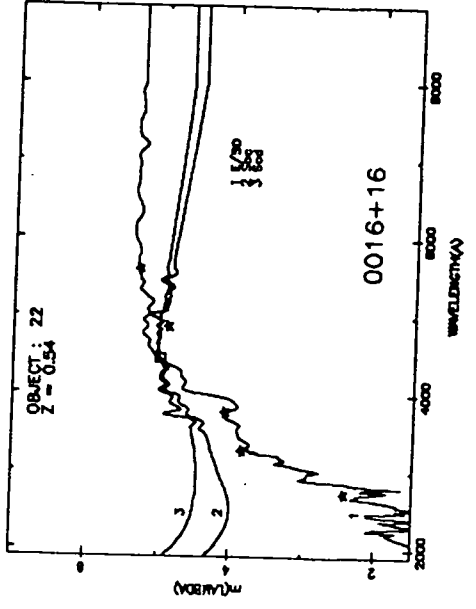
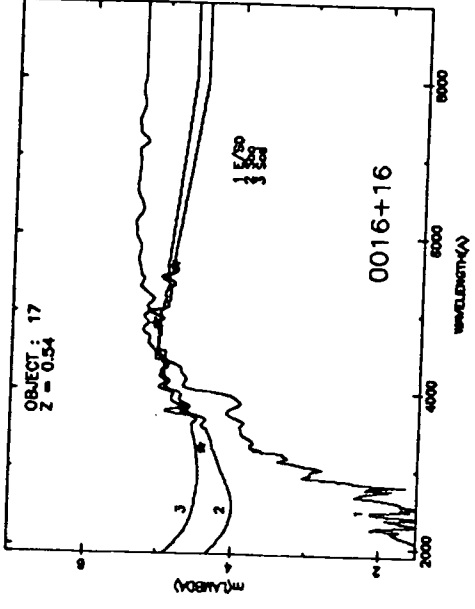
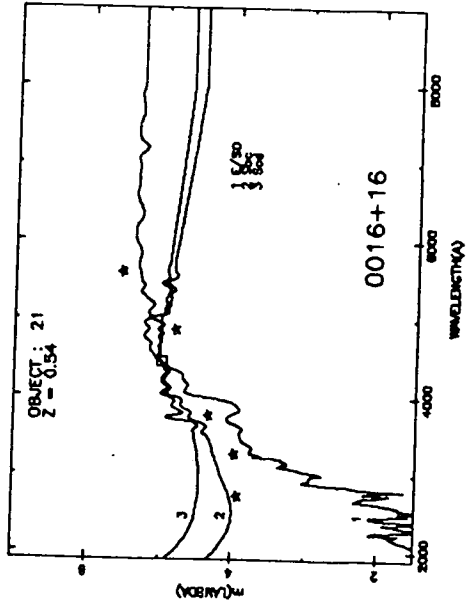
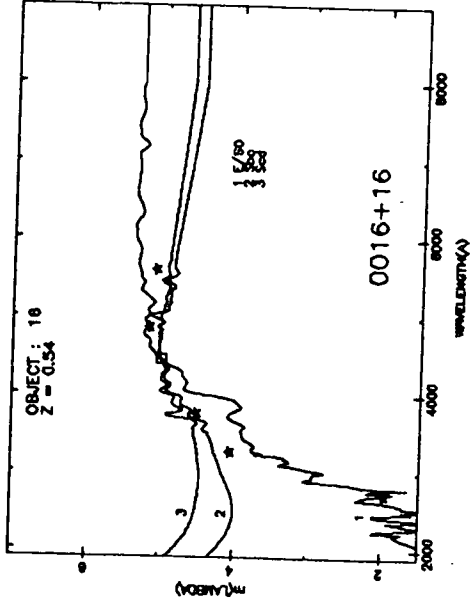
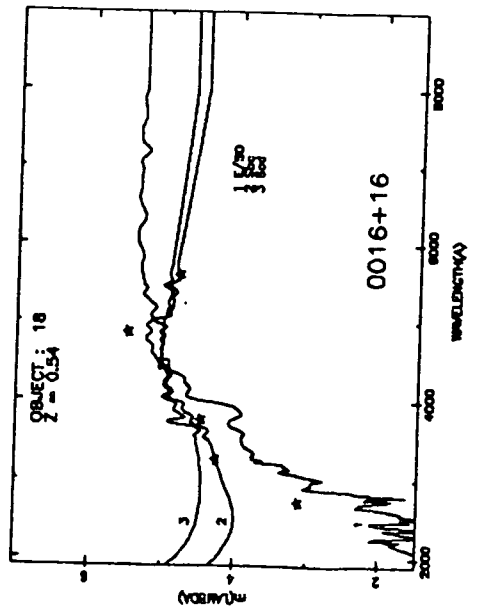
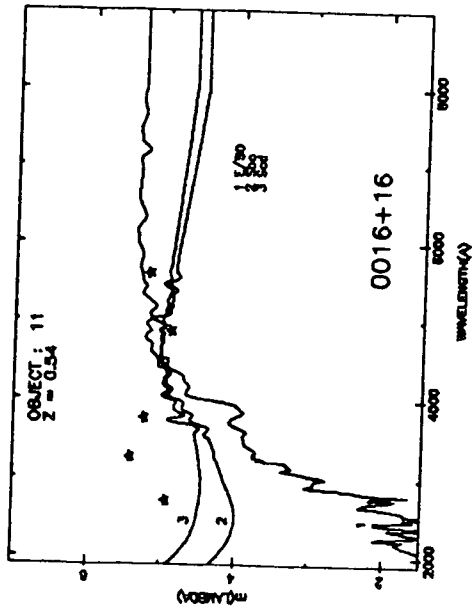
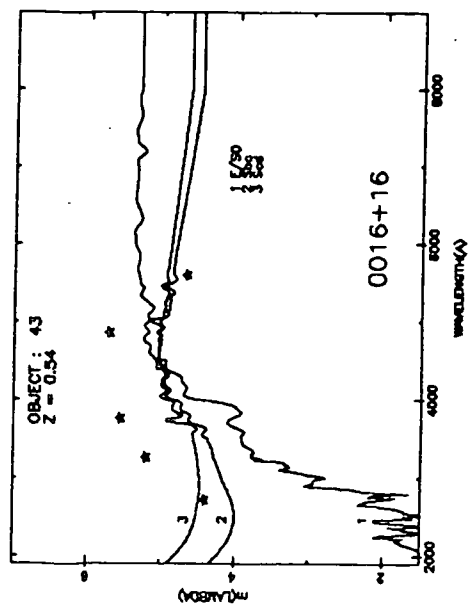
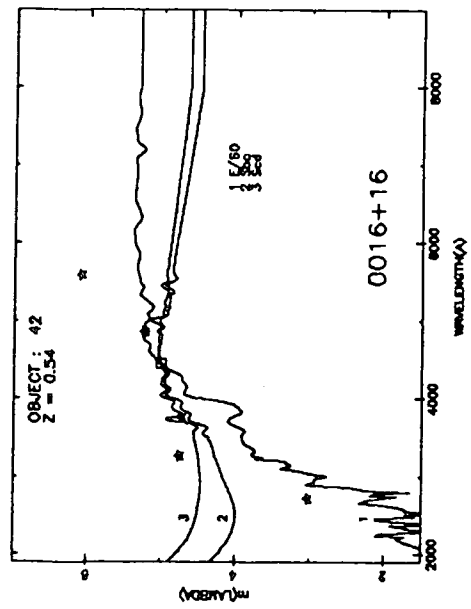
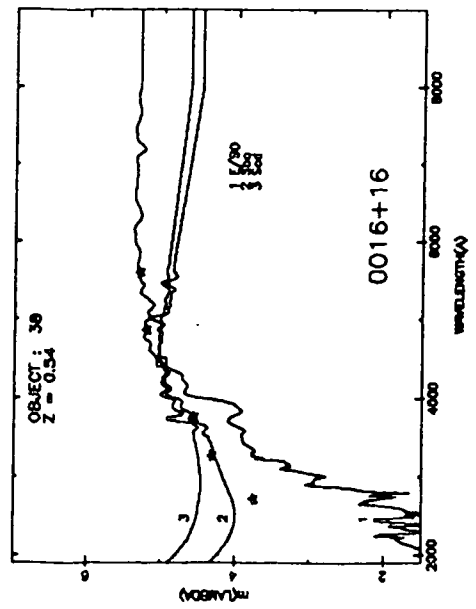
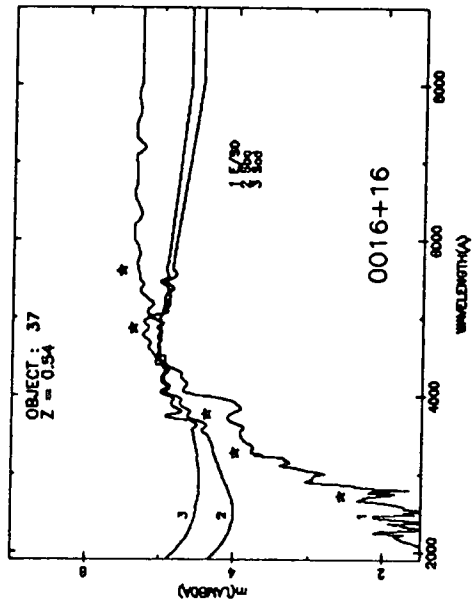
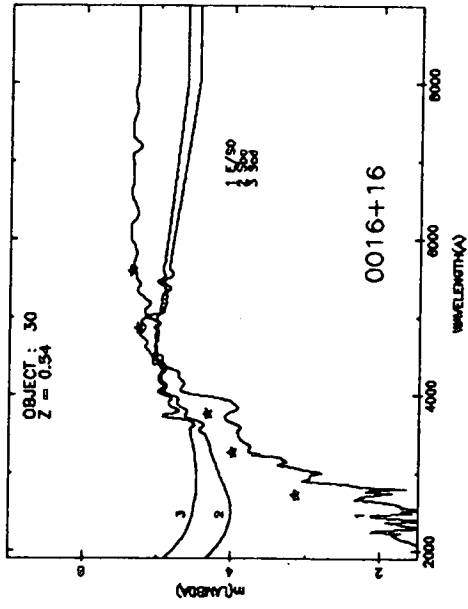
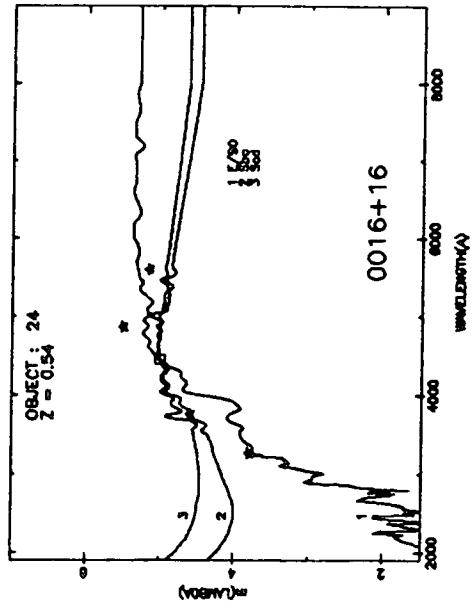
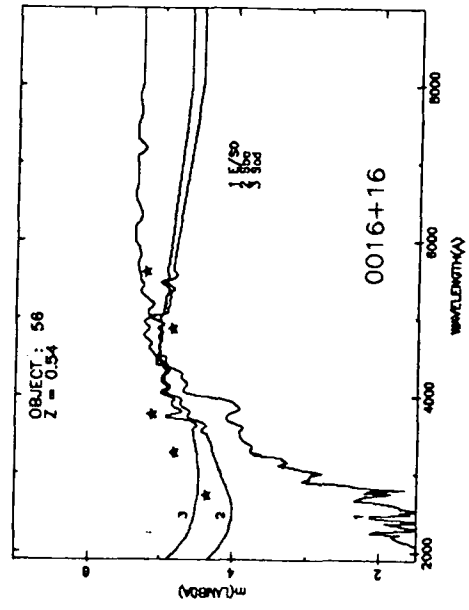
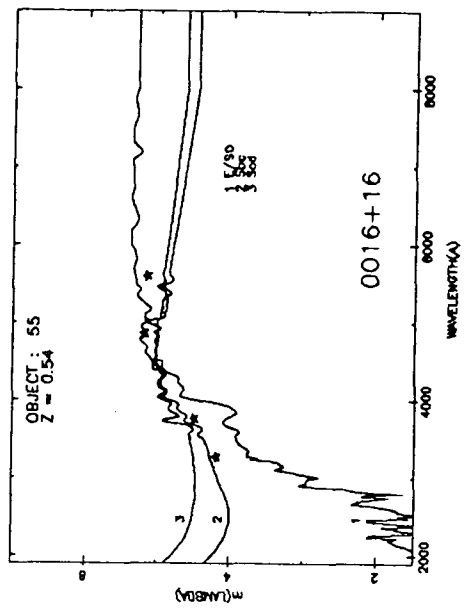
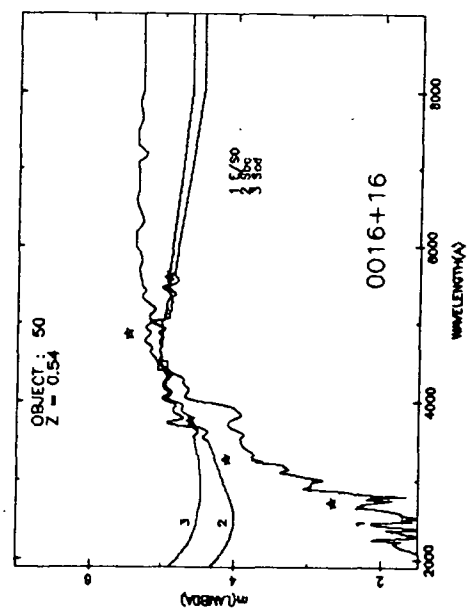
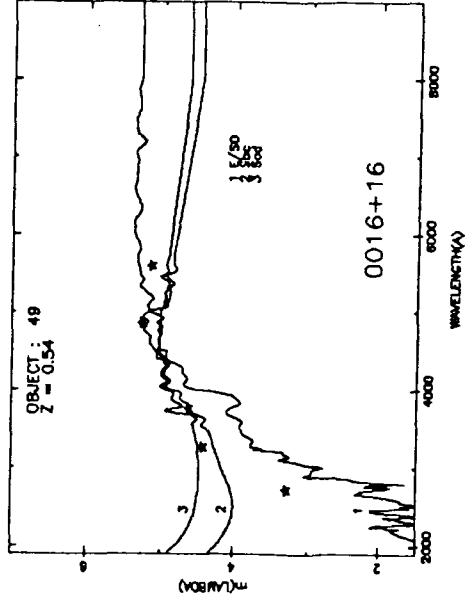
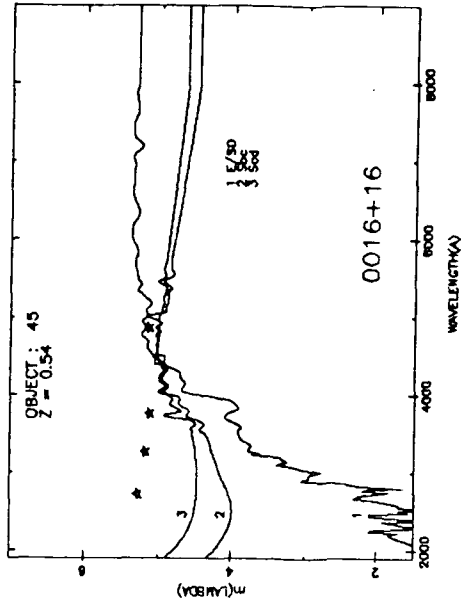
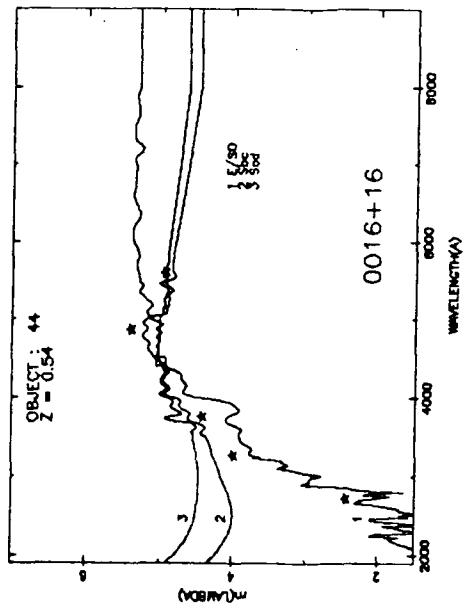


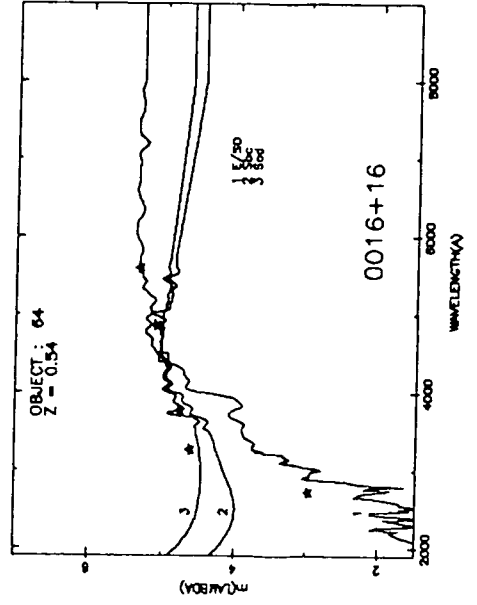
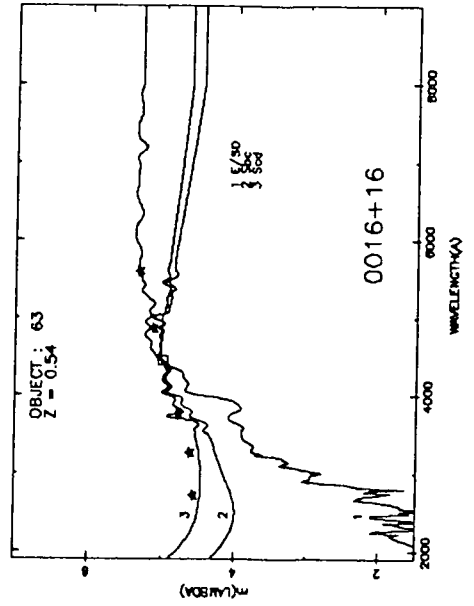
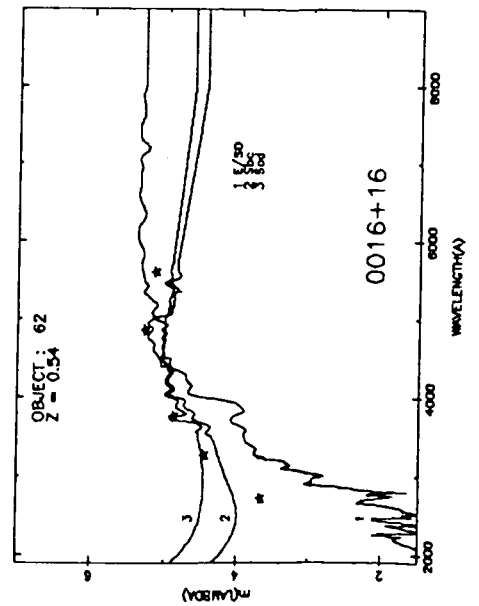
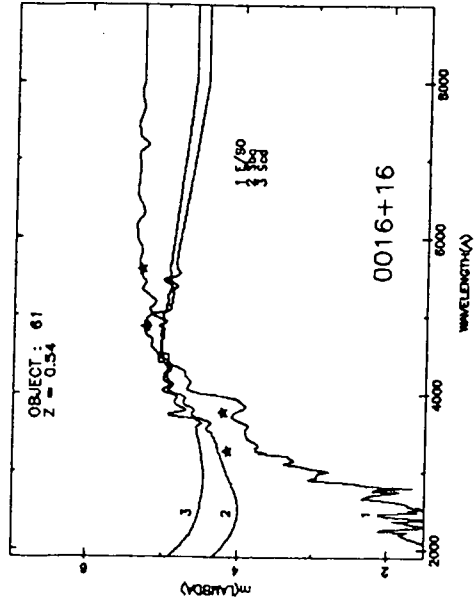
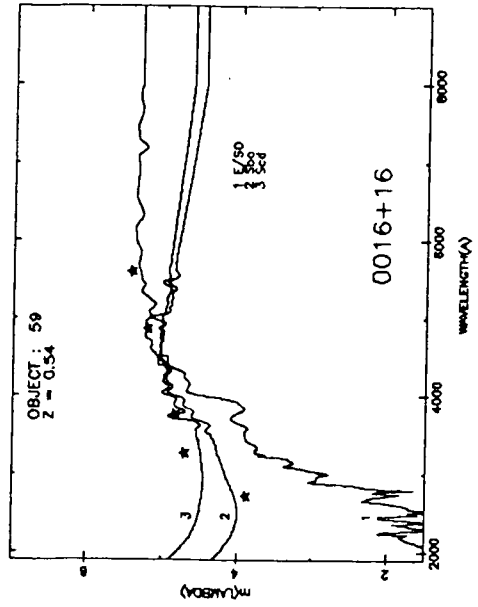
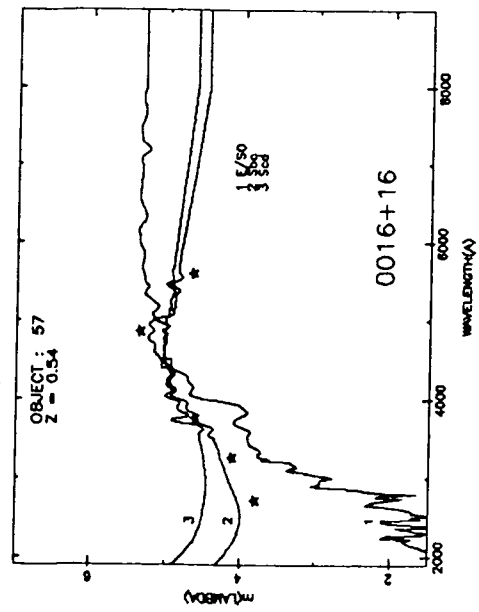
Figure 3.7: (a) An illustration of the redshift and morphological classification method for individual objects. The data for three examples are plotted in identical fashion to Fig. 3.6., at four different redshifts (0.1–0.7). Object 55 was classified as $z \sim 0.55$ E/S0 with slight colour evolution; galaxy 130 is also E/S0 but at $z \sim 0.3$; object 77 was classified as $z \sim 0.3$ Scd. (b) SEDs for all the galaxies in our present sample, plotted at $z = 0.54$.

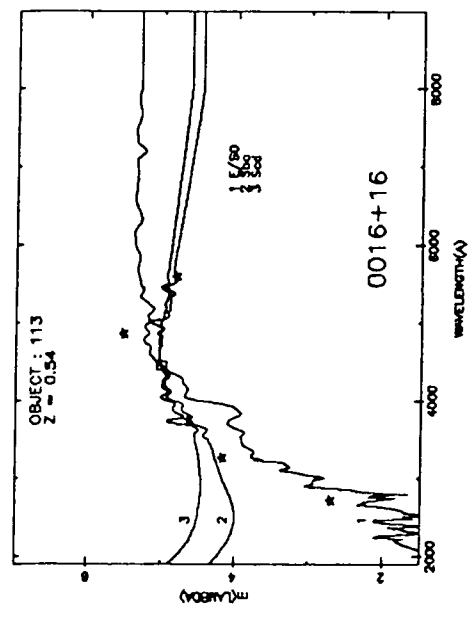
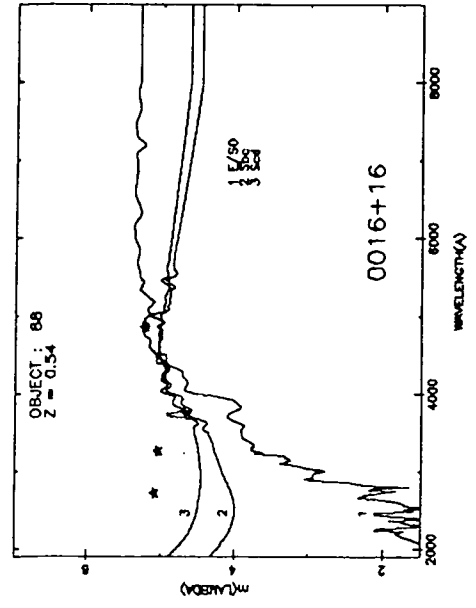
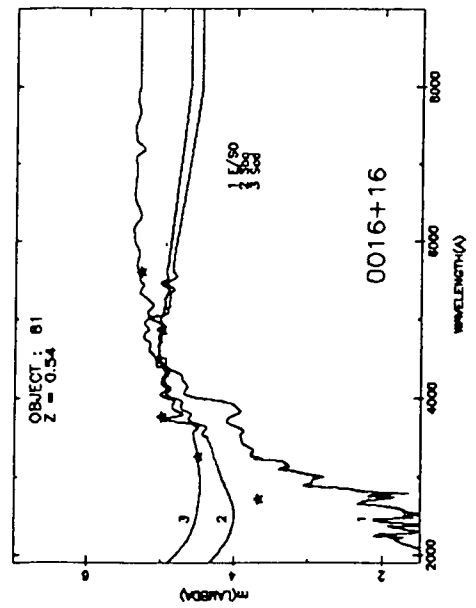
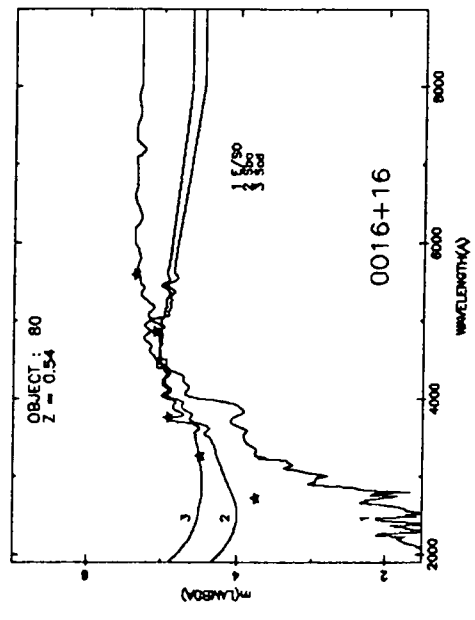
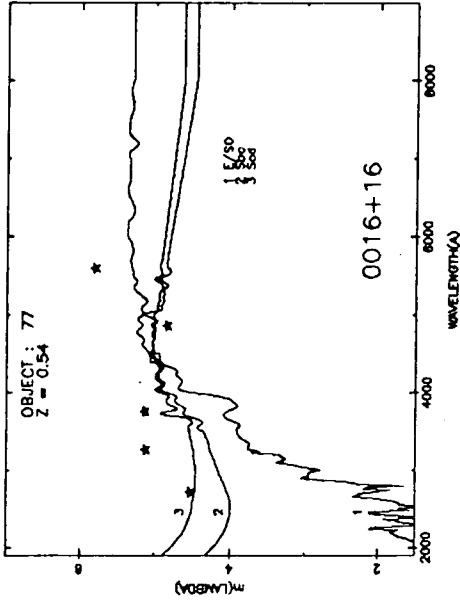
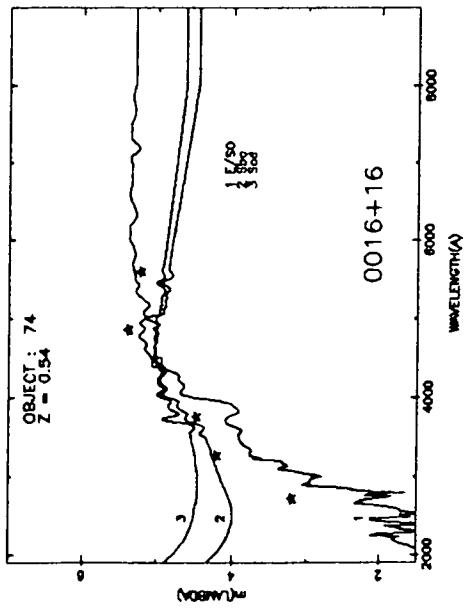


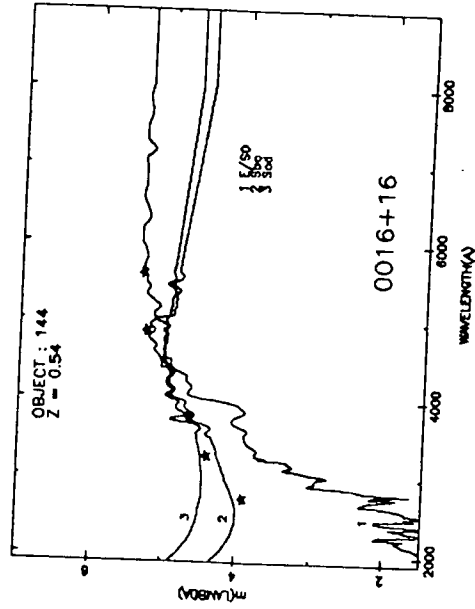
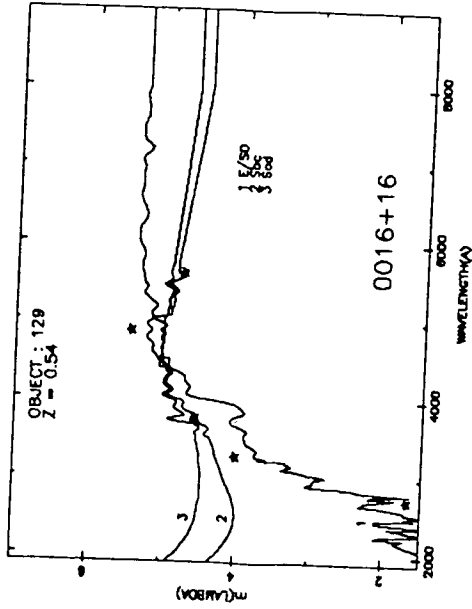
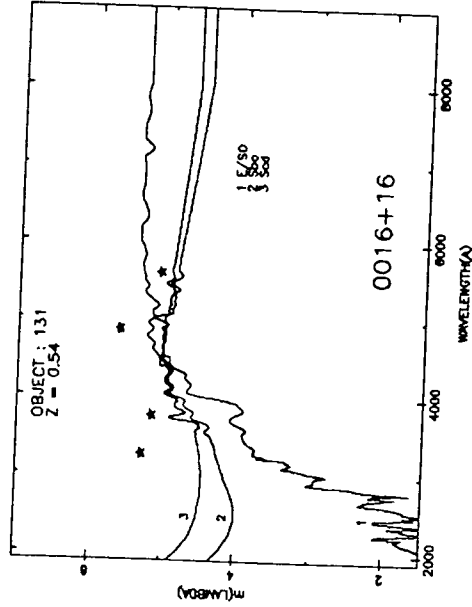
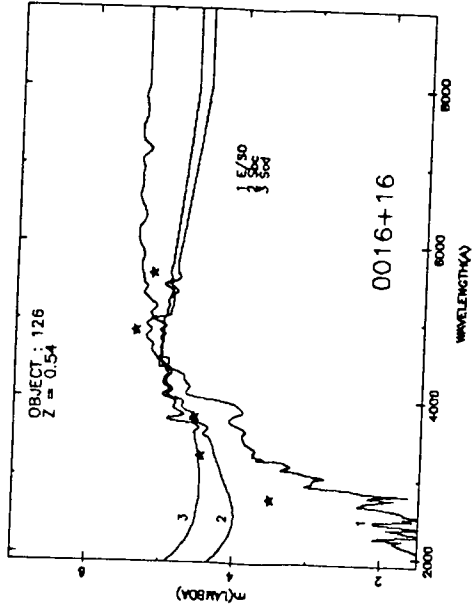
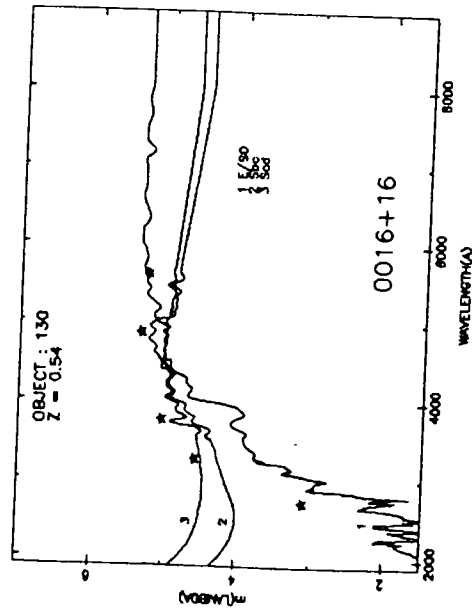
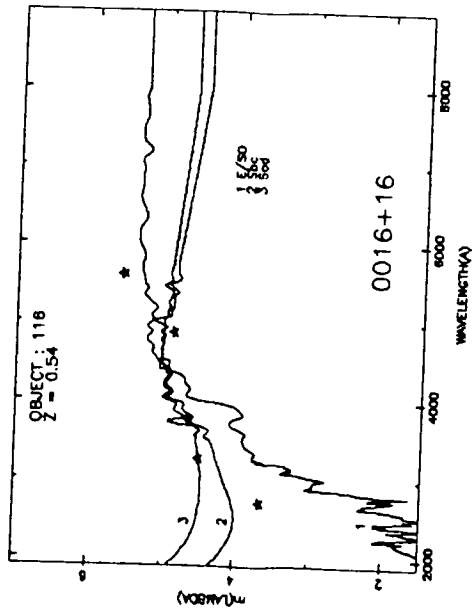


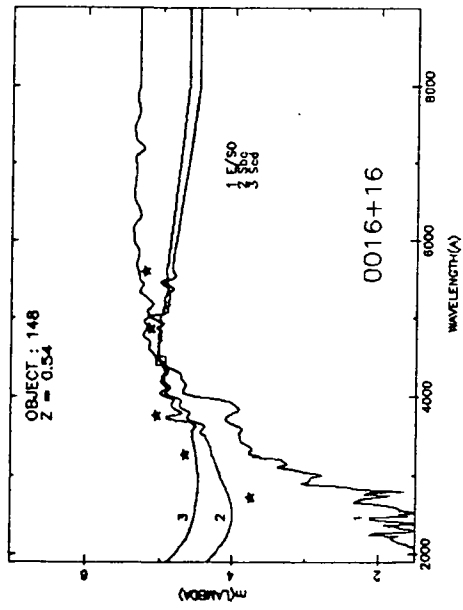
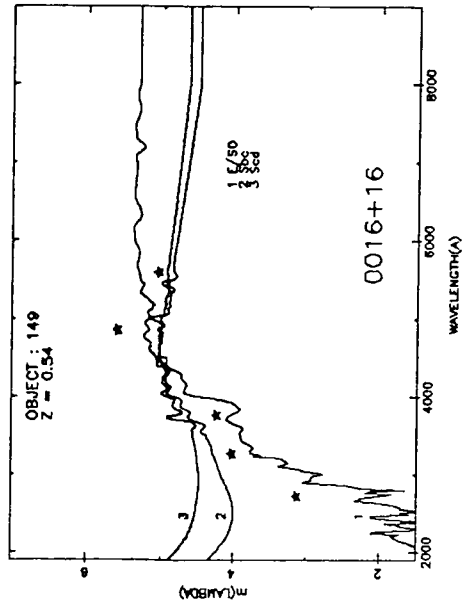
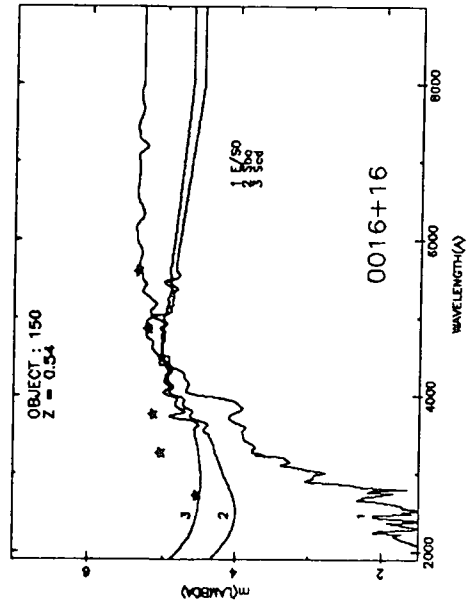












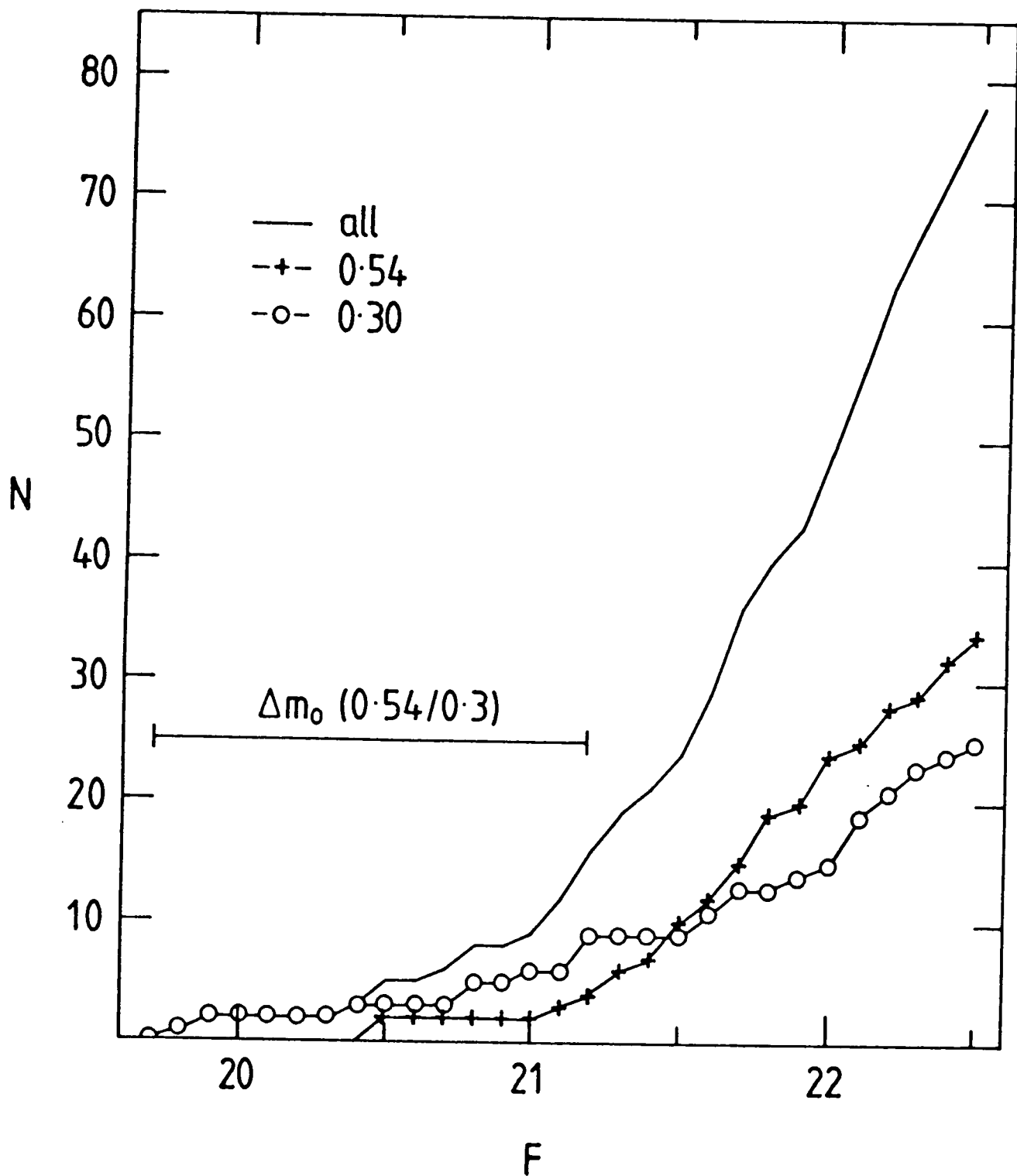


Figure 3.8: Cumulative F luminosity functions for the two ($z = 0.3, z = 0.54$) components. The horizontal bar indicates the expected separation in apparent magnitude between a fixed luminosity at $z = 0.3$ and $z = 0.54$.

Table 3.7: Object Classifications.

Object	Component	F	z_{phot}	Classification
62	I	19.79	0.3	E/S0
81	I	19.88	0.2 – 0.3	E/S0
77	B	20.36	0.2 – 0.3	Scd
2	R	20.48	0.55	E/S0
1	R	20.53	0.55	E/S0
63	I	20.68	0.4 – 0.6	Scd
80	I	20.79	0.2 – 0.3	E-Sab
144	I	20.84	0.3	Sab
38	I	21.04	0.3 – 0.4	Sab
7	R	21.08	0.55	E/S0
6	R	21.12	0.6 – 0.7	E/S0
11	B	21.13	0.1	Scd
18	I	21.19	0.6	E/S0
148	I	21.20	0.1(0.3)	E/S0(Sab)
59	I	21.20	0.2 – 0.3	Sab
150	B	21.21	0.2 – 0.3	Scd
49	I	21.23	0.3	E/S0
88	B	21.25	0.5 – 0.6	Sdm †
74	R	21.28	0.55	E/S0
56	B	21.31	0.1 – 0.2	Sab
30	R	21.38	0.55	E/S0
85	B	21.44	< 0.2	Scd-Sdm
3	R	21.47	0.55	Sab
16	R	21.48	0.55	E/S0
44	R	21.51	0.55	E/S0
113	R	21.55	0.6	E/S0
45	B	21.57	0.1 – 0.2	Scd
50	R	21.57	0.55	E/S0
130	I	21.57	0.3	E/S0
126	I	21.64	0.3	E/S0
61	R	21.65	0.45 – 0.55	E/S0
37	R	21.65	0.45 – 0.6	E/S0
64	I	21.67	0.3	E/S0
116	I	21.70	0.1 – 0.2	E-Sab
4	B	21.72	> 0.45	Sdm
43	B	21.73	0.2 – 0.3	E-Sab
129	R	21.73	0.6	E/S0
24	R	21.77	0.55	E/S0
147	R	21.83	0.55 – 0.6	Sab
55	R	21.83	0.55	E/S0
17	I	21.83	0.3(0.6)	Sab(Scd) †
21	R	21.83	0.5 – 0.55	Sbc
22	R	21.86	0.45 – 0.55	E/S0
42	I	21.88	0.3 – 0.4	E/S0
131	B	21.89	0.1	Sab
149	R	21.95	0.55	E/S0
57	R	21.98	0.55	Sab

Note : † indicates one of the 6 filter measurements was not available.

(a) *Foreground Contamination.*

We are now able to discuss the nature of the redshift distribution of the galaxies in the cluster field. Whilst we can readily distinguish between field contamination and galaxies at $z = 0.54$, at our magnitude limit of $F < 22.0$, the expected distribution of field galaxies (Chapter 2) peaks close to $z \sim 0.25-0.30$, thus some of our objects assigned photometrically to $z \sim 0.3$ may either be members of a physically associated group or merely field objects. From counts to $F=22.0$ we expect 13 field galaxies in our CCD area. In table 3.7 we classified some 8 or 9 objects as field galaxies at redshifts other than $z \sim 0.3$ or 0.54 . Thus there is no serious discrepancy between our photometric redshifts and the expected field distribution in this small area, if we assume that the relatively large number of $z \sim 0.3$ objects is due to the presence of a genuine foreground group.

(b) *The Foreground $z=0.30$ Component.*

The cumulative LFs of our total sample and the two redshift components are plotted in figure 3.8. The bright end is clearly dominated by galaxies at $z \sim 0.30$. The LF of the $z \sim 0.30$ component is by no means characteristic of that of a rich cluster. For example, the brightest member has $M_V \simeq -22$, ie close to the characteristic luminosity M^* , and the slope of the LF is very flat. The possibility of the group being part of a cluster whose brighter members lie outside the CCD area can be crudely investigated if we empirically calibrate the 502-685 colour against Koo's J-F. If we thus attempt a classification between $z = 0.30$ and 0.54 over Koo's larger area we find that the $z = 0.3$ component is apparently not clumped and extends all over the field area. The richness of this component is apparently only $\sim 20\%$ of Coma. Thus this extended foreground association probably artificially heightened 0016+16's contrast above the background, easing the cluster's detection (see chapter 6).

From the object classifications in the table it may seem that this loose group has rather a high proportion of early type members. Indeed, the morphology-density relation implies that early-types should become more prominent in dense environments. However, we have investigated this problem using Dressler's (1980) relations between morphological fraction and projected galaxy surface density, calculated by Couch (1984, private communication), using his 'tenth nearest neighbour' method (see Couch, 1981) for details). He has found that for the estimated density of the 0.30 component we should expect:

$$\%E: \%S0: \%Sp = 17: 43: 40.$$

From the SEDs we find that E/S0s constitute $\sim 57\%$ of this component, thus there is no unusual distribution of morphologies.

(c) *The $z=0.54$ Cluster Component.*

To estimate the richness of the cluster 0016+16, Koo used two different techniques. Firstly, a comparison of the bright end of the cluster LF with that of the Coma cluster (from Thompson and Gregory, 1980) to a limit of $F=23$, revealed that 0016+16 was some 3-4 times richer than Coma. This method however is affected by galaxy luminosity evolution. Bahcall's (1977) approach of counting the number of galaxies above (m_{3+2}) within a 1 Mpc diameter circle should be independent of luminosity evolution if all galaxies evolved by the same amount. Koo found that with this approach, 0016+16 was twice as rich as Coma.

Our findings, however, may affect these results since we will reduce the number of objects in the cluster considerably from Koo's number by virtue of the $z = 0.30$ component. If our ratio of numbers of objects in $z = 0.3/0.54$ applies over Koo's area then his richness should drop to only twice that of Coma in the first method. Since Metcalfe (1983) has now produced more careful photometry of Coma than that used in Bahcall's original visual counts, we find that using the second approach, 0016+16 is in fact comparable to Coma's richness. Within the considerable uncertainties the two estimates can be reconciled if galaxies were more

luminous in the past as Koo has discussed.

Again, from the morphology-density relation, Couch has estimated that the (non-evolved) population ratios for the $z = 0.54$ cluster density should be :

$$\%E: \%S0: \%Sp = 22: 44: 34$$

as compared to our classifications of $\sim 71\%$ E/S0s in table 3.7.

3.6. Spectral Evolution of galaxies in 0016+16

As we have seen above, our individual SED classifications allow us to select various populations of galaxy type for further detailed study. We will firstly consider the early-type galaxies at $z = 0.54$ to look for any signs of spectral evolution in the rest frame ultraviolet. These galaxies are of specific interest since, as we discussed in the first chapter, they are usually considered as having arisen from an initial burst of star formation some 16 Gyr ago.

Regarding our selection procedure, it may be argued that such objects were chosen to be E/S0s on the basis of their six colour SEDs and that this invalidates a search for differences between their colours and those of present-day E/S0s. Following the discussion in chapter 2 we have placed more emphasis on visually classifying our galaxies, where possible on the basis of the *optical* colours. Since our distinction in this case is only claimed to one Hubble class accuracy, then we are not severely constraining our fits from the 418 passband, but rather, use this uv passband primarily as a measure of the level of spectral evolution. In chapter 2 we showed much of the evolution we may expect to find (increased numbers of young stars) should arise at rest frame ultraviolet wavelengths. In practice, the classifications were relatively straightforward and each type was quickly identified. We shall discuss this further in section 3.7.

Before looking for evolutionary effects it is important to correct our observed magnitudes and colours for foreground reddening. The approach followed in Couch *et al* (1983) to separate these two effects was to match the red end of the early-type galaxies to the present day predictions, the assumption being that if evolution is due to a change in the main sequence turn-off point (chapter one), then the uv colours will be considerably more affected than the optical/ir (see chapters 1 and 5). At our redshift we have to reach to longer wavelengths to be insensitive to evolutionary complications when determining reddening. Fortunately the brightest red and intermediate galaxies (#192 and 62) have been studied at J ($1.25\mu\text{m}$) and K ($2.2\mu\text{m}$) using a 7 arcsec aperture at the Anglo-Australian Telescope by Ellis and Allen (1983). They found the J-K colour of #62 ($z = 0.30$) was slightly redder than that of #2 ($z = 0.54$), though both are within 2σ of the non-evolving SED prediction. We took the J flux of each galaxy, which is likely to be the more reliable i-r measurement, and converted the CCD magnitudes through a 7 arcsec circular aperture to flux using the white dwarf calibration discussed in section 3.3. The fluxes at 685, 748, 862 and 1250 nm are then compared with the redshifted present day SED and E_{B-V} derived by comparison using Seaton's (1981) representation of the Galactic law. Errors are calculated assuming photometric uncertainties of ± 0.1 m (the J magnitudes have a statistical error of ± 0.06 m). Using this method we determine

$$\begin{aligned} E_{B-V} &= 0.08 \pm 0.13, \#62 \\ &= -0.03 \pm 0.09 \#2, \end{aligned}$$

the agreement gives a further indication of the uncertainty involved. Certainly there is no compelling evidence for any positive reddening. Further constraints are imposed by the agreement between Koo's field counts in nearby SA68 (Koo 1981b) with those in SA57 (Ellis, 1984, private communication). In the discussion that follows we shall assume zero reddening for 0016+16.

(a) Luminosity Evolution.

It is possible to use our present data to test whether galaxies in distant clusters are brighter than their nearby counterparts. Previous tests of such luminosity evolution at high redshifts have been largely concerned only with the brightest cluster members. It is therefore informative to attempt a test of whether the 'typical' cluster member also evolves in a similar manner. Although our CCD photometry does not probe quite as deep as the characteristic magnitude of the cluster luminosity function (M^*), in principle we can use the average galaxy magnitude to our adopted photometric limit as a simple measure of evolution, by comparison with the equivalent quantity in a nearby rich cluster.

Metcalfe (1986, private communication) has kindly provided his luminosity function for the Coma cluster core in the Johnson R passband. These magnitudes can be transformed to $z = 0.54$ via the appropriate k-corrections and distance modulus, allowing a comparison with the CCD photometry obtained in the 685 filter (and calibrated onto the R (Kron-Cousins) system, see expression 3.7). By using aperture photometry of Coma galaxies (from Lucey, 1986, private communication, and Dressler *et al*, 1987), it is possible for us to correct Metcalfe's LF into magnitudes measured in the same physical aperture size as encompassed by our distant cluster photometry. Since the aperture we chose for our CCD photometry corresponded to the Kron radius for most of the galaxies, this aperture correction was only significant for the brightest galaxies (see figure 3.9).

Figure 3.10 shows the final comparison between the normalised cumulative luminosity functions for both clusters, whose use removes any richness dependence from our results. The R passband corresponds, at this redshift, to a rest-frame wavelength of $\sim 4700\text{\AA}$. We find that the average magnitude in this passband then is 20.87 for 0016+16 and 21.19 for Coma, implying some 0.32 magnitudes of evolution if the cluster 0016+16 resembles Coma after 7 Gyr. The uncertainties associated with this approach are, however, fairly large.

The major difficulty lies in the assumption that we can use the Coma LF as being representative of present-day galaxy clusters. Dressler (1980, 1984) claims to find significant variations in the form of the LFs of a sample of nearby clusters. Our conclusion regarding luminosity evolution is highly dependent on the expected shape of the bright end of the cluster LF. If, as Dressler suggests, this is not universal at the present epoch, then to address the question of luminosity evolution with any certainty, we must obtain deeper coverage of the cluster LF, in attempting to use M^* as a better probe.

Aperture photometry of the brightest member of this cluster is discussed in Shanks, Couch and McHardy (1986), revealing that this galaxy at least does exhibit a significantly enhanced luminosity. Koo's larger estimate of the amount of evolution in the cluster is partially due to his inclusion of the foreground, $z = 0.3$, galaxies in his luminosity function, as well as inaccuracy in transforming to his broad F passband.

(b) Colour Evolution

We shall now focus on the possibility of evolution in galaxy colours. Our primary tool in such investigations is the colour magnitude effect, discussed in the first chapter of this thesis. With our CCD photometry we can study changes in the observed colour magnitude relation as we move bluewards in wavelength from optical to uv colours, as shown in figure 3.11.(a)-(c). The predicted non-evolving slope, given as the solid line in the figures, was estimated using the method described in chapter 2. We have also plotted the scatter due to our photometric errors.

The 502-685 CM diagram shows a reasonably tightly defined relation. Because the CM slope is so flat at these wavelengths however, it's not possible to easily compare predicted and observed slopes. This colour is close to a rest-frame U-B so a useful comparison can be made with photometry of a nearby cluster. Metcalfe (1983) has provided his colours for

galaxies which lie on the B-R CM sequence in a nearby ($z = 0.048$) richness-class 2 centrally concentrated cluster, Shapley 8. As can be seen in fig. 3.11.(a) the mean scatter of this colour is virtually the same as that in fig 3.11.(b). In absolute terms however, our mean observed 502-685 is ~ 0.2 mag bluer than the predicted line.

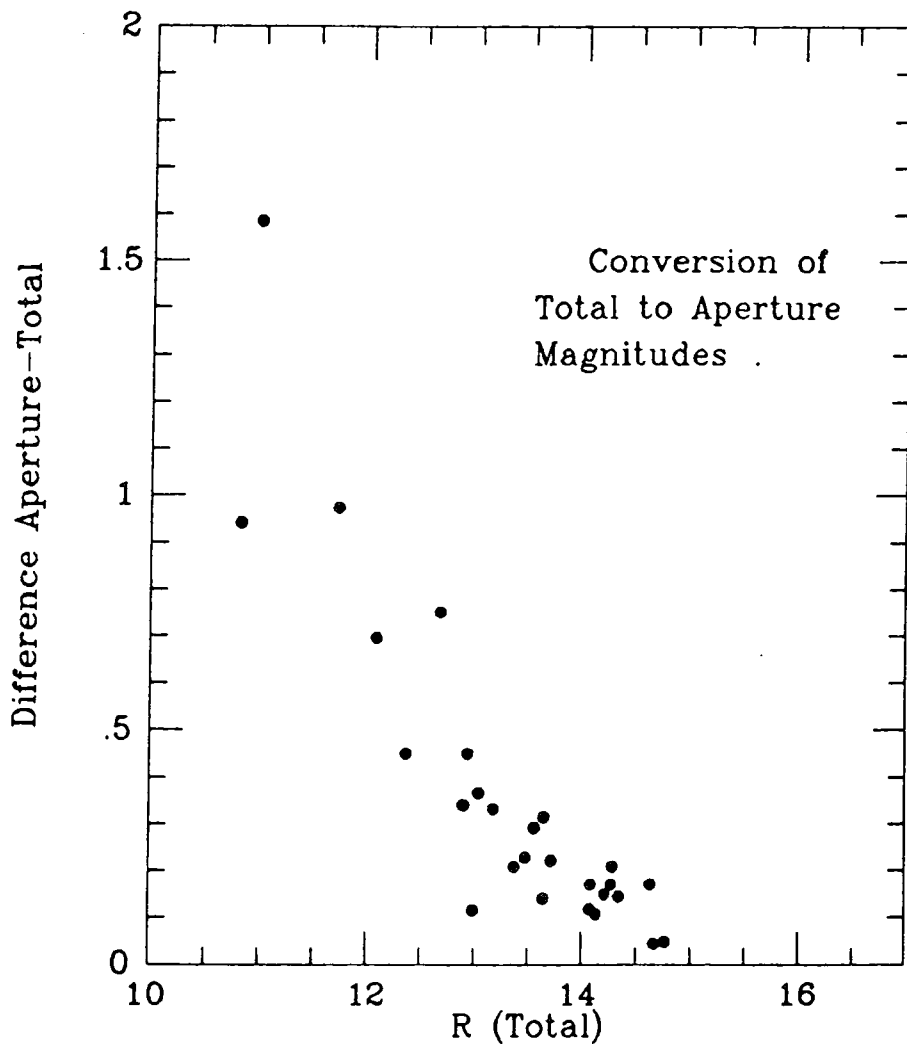


Figure 3.9: Correction between aperture and total magnitudes for Coma cluster galaxies, using Dressler's (1987) photometry.

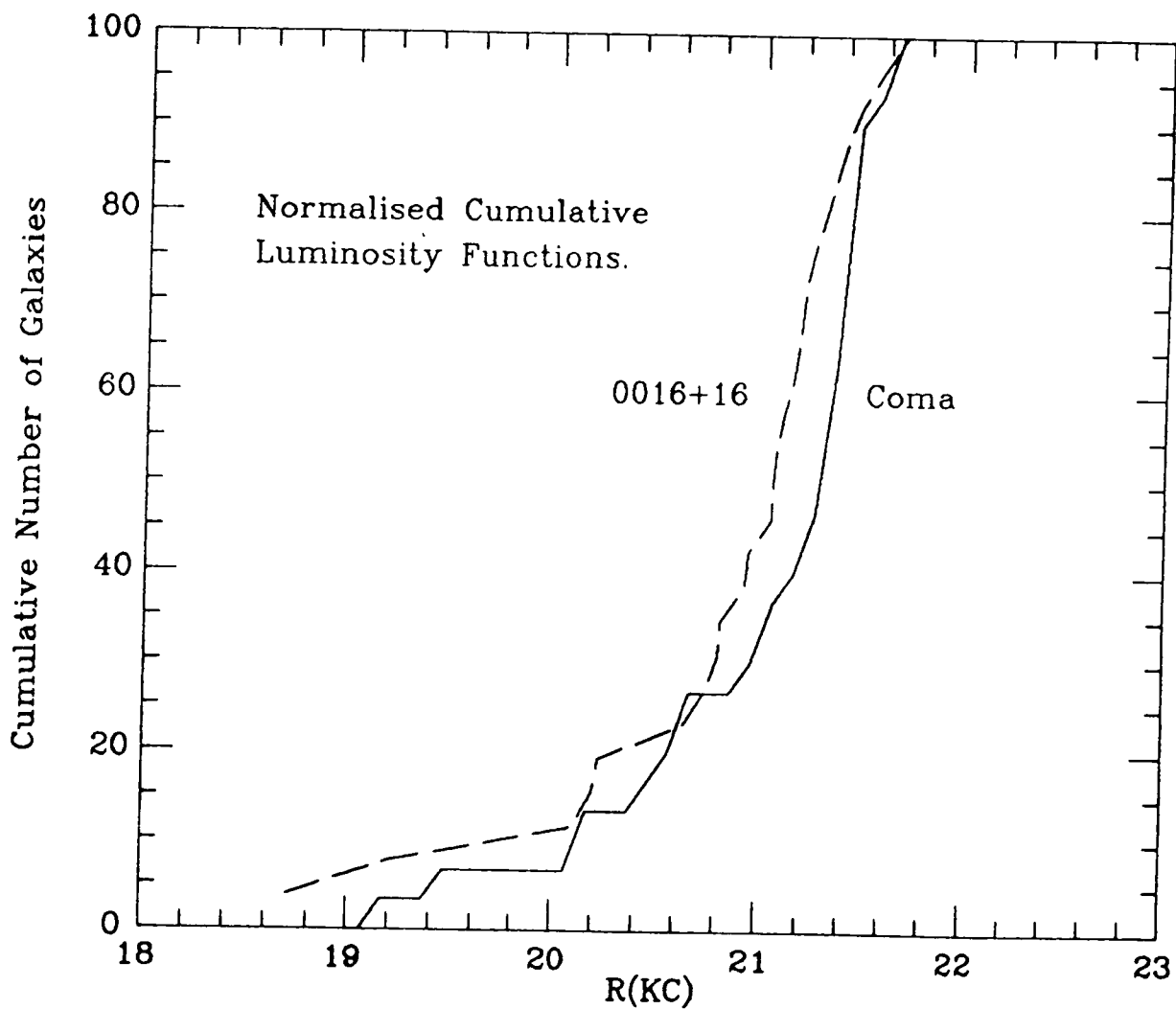


Figure 3.10: Normalised cumulative luminosity functions for the distant cluster 0016+16 and Coma (from Metcalfe, 1983).

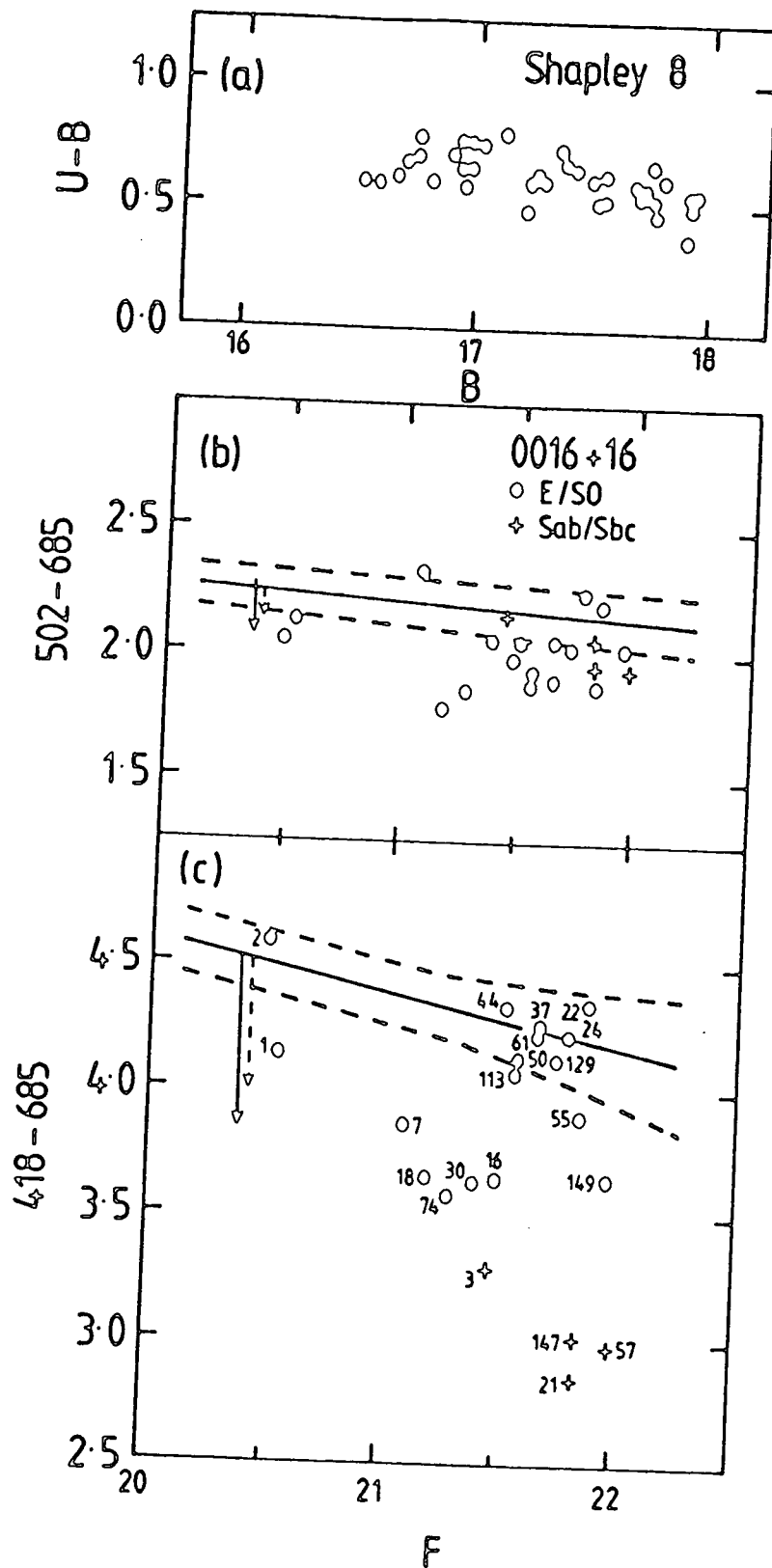


Figure 3.11: Colour-magnitude diagrams for both 0016+16 and the nearby rich cluster Shapley 8. (a) $U-B$ versus B for the objects in Shapley 8 which define the E/S0 sequence in B-R. (b) $502-685$ versus F for the 17 E/S0s (filled circles) and four Sab/Sbcs (crosses) at $z = 0.54$. The solid line shows the predicted non-evolving CM sequence at this redshift. The dotted lines represent a 1σ range of error about the prediction (from Couch, 1984, private communication). The solid arrows show the colour shift expected from Bruzual's $\mu = 0.5$ model at this redshift, the dashed arrow is for the c-model with a passive evolution of the initial population. (c) $418-685$ versus F .

For the rest-frame uv colour, 418-685, however, the situation is more complicated. Firstly, the scatter is very large (range of ~ 1.0 mag.). Some eight (out of 17) galaxies lie within the errors on the predicted CM relation, but the rest lie well outside (average deviation being ~ -0.27 mag, ie 2σ). Note also that the spiral galaxies in this diagram lie well away from the relation (~ 1.0 – 1.5 mag).

As a check that this dispersion in uv colour is not simply due to an underestimate of our photometric errors, we have compared our 418-685 colours with Koo's U-F photometry. Of our sample of 17 early-type galaxies at $z = 0.54$, Koo only has photometry of 9, although these show a similar range in U-F, as well as confirming the observed large difference in uv colour between the brightest two members. It would seem then that this scatter is a reflection of a genuine physical difference from galaxy to galaxy. Also plotted in figure 3.11(c) is the scatter expected from our uv studies of nearby early-type galaxies (chapter 2), revealing that the galaxies in 0016 are significantly different in uv colour range to our nearby sample.

If this uv-enhancement in many of these galaxies is genuine, as the evidence above suggests, then we should now seek to determine its nature. Firstly, we can ask whether there is any evidence for the uv light to be more centrally concentrated than the optical magnitudes, as is the case in, for example, active galactic nuclei. Although our CCD frames have only fairly low spatial resolution (due to the combination of the plate scale and the seeing profile), we can crudely construct azimuthally averaged light profiles for the bright galaxies using the series of apertures defined by the APEX software. Figure 3.12 shows some examples of profiles of uvx and other galaxies in the 685 and 418 filters (note that we measured these on a single exposure in 418, since addition of frames could have resulted in smoothing of the profiles). We can see that there is no indication that the uv light is centrally concentrated, and it would appear that the emission is distributed over the whole galaxy.

To explain these colours, then, we should investigate the possibility that these early type galaxies are bluer simply by virtue of an overall enhancement in the level of star formation in the manner expected from Bruzual-type models. We have plotted the expected positions for the colours of galaxies evolving under the two popular schemes, c-model, and $\mu = 0.5$ (Chapter 1), assuming an age of 16 Gyr. As mentioned earlier, studies of brightest galaxies (Lilly and Longair, 1984) in distant clusters have favoured this type of 'passively' evolving model.

Looking at the diagrams, we see that the models do indeed reach to colours almost as blue as these covered by our sample, but that the amounts of such evolution must vary from galaxy to galaxy. As we have seen (chapter 1 and Oke *et al*, 1981), nearby galaxies show a wide variation in the far uv ($\lambda < 220$ nm) which could possibly be attributed to small amounts of residual star formation today. Perhaps then, as we move to earlier epochs the number of young stars increases and these variations are seen at longer wavelengths. However, it must be borne in mind that almost half of our sample still display the rest colours, of nearby elliptical galaxies, arguing against such a general evolution picture.

An alternative explanation is that 0016+16 does indeed display the Butcher-Oemler effect but that the cluster is at a considerably more evolved stage than that of the other clusters studied by Butcher and Oemler at high redshift, so that the effect is manifest now only at uv wavelengths. The physical explanation here is akin to the early model discussed in chapter 1, whereby spiral galaxies in rich clusters constitute the precursors of the S0 population present in such environments at the present epoch.

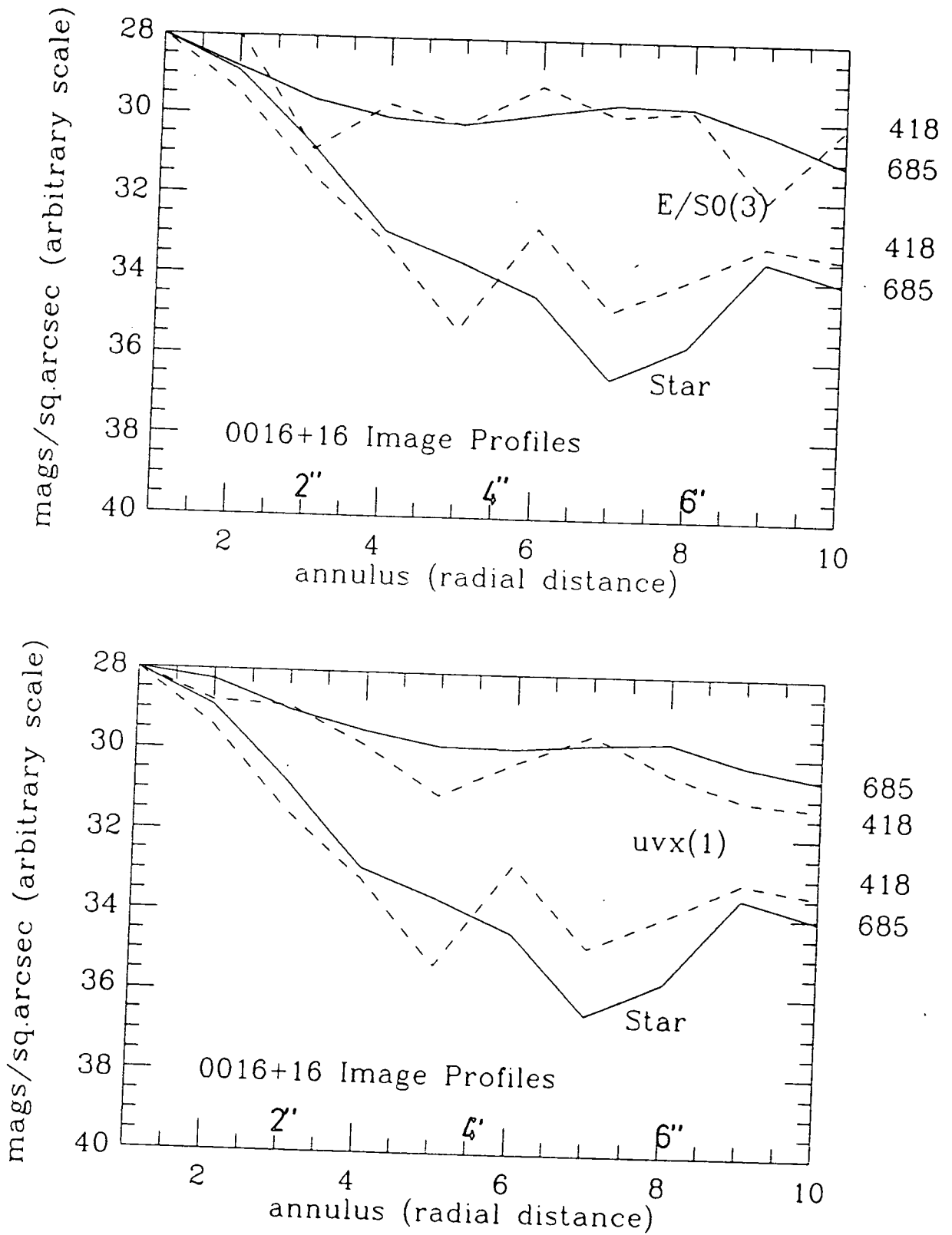
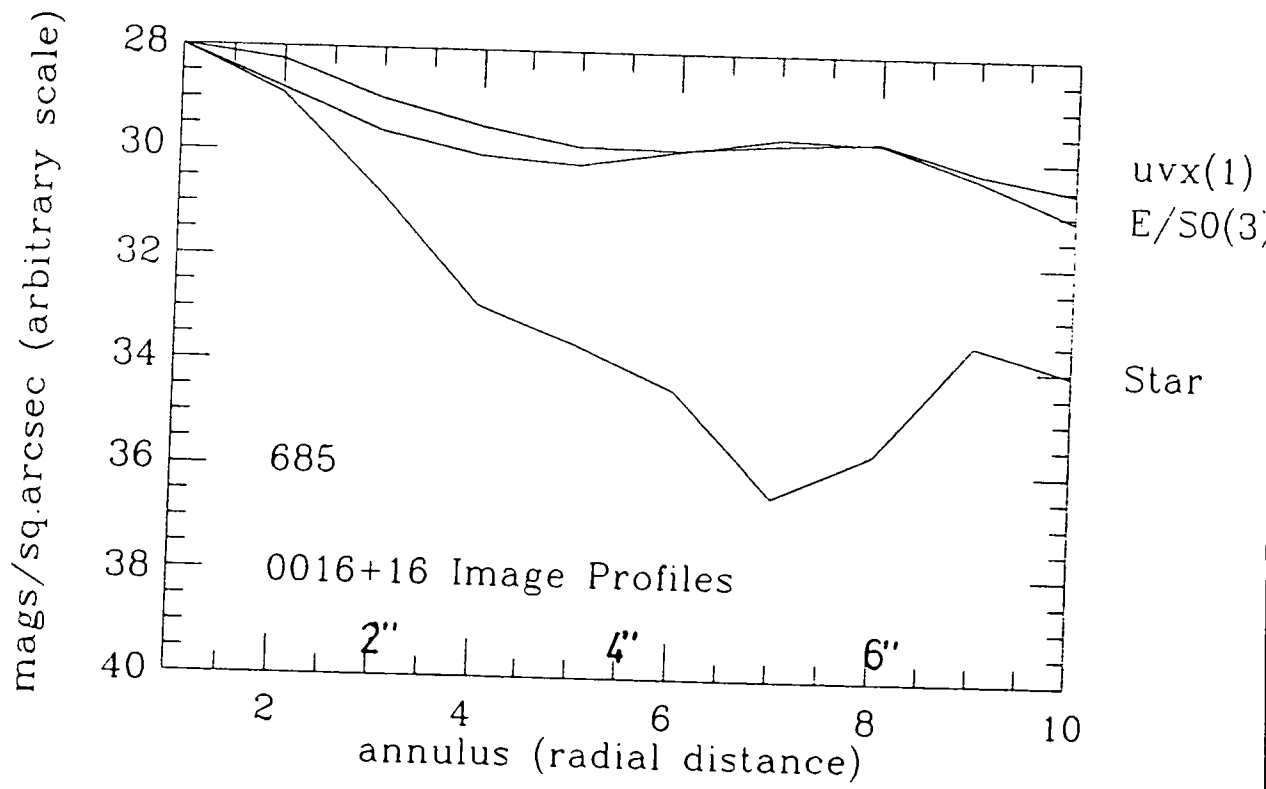


Figure 3.12: Crude image profiles for bright uvx and E/S0 galaxies in 0016+16. The surface brightness is in arbitrary units.



Some gas-depletion process such as stripping, evaporation, or large scale rapid star-formation causes a cessation of star-forming activity in these galaxies and their colours consequently evolve redwards. In this picture the bluest uv galaxies in our present sample (418-685 ~ 3.5) may be intermediate between Sa and S0 types. Using Couch's estimates (see earlier) of Dressler's morphology-density relation, we predict that this sample should be composed of 6 ellipticals and 11 S0 galaxies. Thus if the S0 galaxies are an evolving component we would expect to find them lying outwith the predicted CM region. In practice the division of objects within the predicted region to those outside is 8 to 9, and thus not inconsistent with such a scenario.

In chapter 5 we shall review these considerations, along with other work in the context of more detailed evolutionary scenarios and thus we defer any further interpretation of the colour magnitude diagrams till then, save to conclude that our uv observations, very strongly imply the presence of evolutionary changes having occurred in a large proportion of early-type galaxies from $z=0.54$ to $z=0.0$.

3.7. Comparison of Photometric Results with Spectroscopy.

After the results of our photometric study of this cluster were submitted for publication (Ellis *et al*, 1985), Dressler and Gunn (1985, private communication) kindly provided us with preliminary redshifts they had obtained in a recently begun study of the field of 0016+16. They have spectroscopy for 17 of the objects in our CCD area, such data providing an excellent opportunity to test the capabilities of our intermediate-band technique, which we shall consider here. The results are presented in table 3.8, in which we give object classifications based on the relatively quick eyeball fitting method described earlier, and the χ^2 minimisation routine described in chapter 2. In general these techniques are found to be in agreement. Discrepancies, however, can and do arise. In the case of the algorithm, we have already discussed the likely problems in the previous chapter, but we should note that it is also not inconceivable that eye-fitting can also be led astray. Thus we have found that, as we earlier suspected, accurate object classification is best achieved using both methods. Any discrepant objects can then be re-examined in detail to look for any possible causes for disagreement.

A few comments should be made about the spectroscopy. Firstly, we have only been provided with redshift estimates for these objects and have not been able to inspect the original spectra. Furthermore it would have been useful to have known which spectroscopic features were used to determine these redshifts. Consequently we are largely unable to estimate a level of confidence for any of these results, save for a few objects noted as having poor signal to noise spectra. Working at such faint magnitudes will prove difficult for spectroscopy, particularly if redshifts are being assigned using absorption features (see chapters 2 and 6).

A similar comparison has been carried out by Loh and Spillar (1986) on the cluster 0024+1654. These authors find in general an excellent agreement between the two methods, but there are still a number of discrepant objects. The advantage of imaging photometry is that the data can readily be re-examined to check for difficulties caused by overlapping nearby objects, or misidentification. Indeed in two cases, Loh and Spillar argue strongly in favour of their photometric redshift estimates, against the spectroscopy. As remarked in the previous chapter, however, one of the discrepancies, which is not commented upon in the text, is for the object that Lilly and Gunn (1985) have identified as a post-starburst galaxy in the cluster, whereas the photometry implied it was at a lower redshift. However, it should be re-emphasised that the spectroscopy in this case, whilst providing the redshift, did not originally reveal the post-starburst nature of this galaxy.

Table 3.9: Comparison of 0016+16 Observations.

#	Eye fit		χ^2 -fit		Spectroscopy	
	z	Type	z	Type	z	Dressler's Id.
62	0.3	E/S0	0.3	E/S0	0.30	184
81	0.2-0.3	E/S0	0.2	E/S0		
77	0.2-0.3	E/S0	0.17	Sbc		
2	0.55	E/S0	0.54	E/S0	0.54	149
1	0.55	E/S0	0.46	E/S0	0.54	144
63	0.4-0.6	Scd	0.7	Scd	0.54 [OII]	215
80	0.2-0.3	E-Sab	0.29	Sab		
144	0.3	Sab	0.32	Sab	0.53 Balmer	37
38	0.3-0.4	Sab	0.38	Sab	?0.65?	207
7	0.55	E/S0	0.62	E/S0	0.54	156+157
6	0.55	E/S0	0.62	E/S0	0.54	170
11	0.1	Scd	0.12	Scd	0.21	116
18	0.6	E/S0	0.33	E/S0	M Star	114
148	0.3	Sab	0.26	Sab		
59	0.2-0.3	Sab	0.24	Sab	0.21	198
150	0.2-0.3	Scd	0.20	Sbc		
49	0.3	E/S0	0.28	E/S0		
88	0.5-0.6	Sdm	0.40	Sdm †		
74	0.55	E/S0	0.32	E/S0		
56	0.1-0.2	Sab	0.30	Sbc	0.39	232
30	0.55	E/S0	0.36	E/S0		
85	< 0.2	Scd/dm	0.1	Sdm		
3	0.55	Sab	0.58	Sab	0.54	135
16	0.55	E/S0	0.54	E/S0		
44	0.55	E/S0	0.70	E/S0		
113	0.6	E/S0	0.74	E/S0		
45	0.1-0.2	Scd	0.32	Sdm		
50	0.55	E/S0	0.39	E/S0	0.55	217
130	0.3	E/S0	0.25	E/S0		
126	0.3	E/S0	0.67	Sab		
61	0.55	E/S0	0.63	E/S0		
37	0.45-0.6	E/S0	0.45	E/S0	0.54	203
64	0.3	E/S0	0.27	E/S0	0.56	Balmer 224
116	0.1-0.2	E-Sab	0.18	E/S0		
4	0.45	Sdm	0.41	Sdm		
43	0.2-0.3	E-Sab	0.23	Sbc		
	129	0.6	E/S0	0.64	E/S0	
24	0.55	E/S0	0.63	E/S0		
147	0.55-0.6	Sab	0.65	Sab		
55	0.55	E/S0	0.63	E/S0		
17	0.6	Scd	0.63	E/S0 †		
21	0.5-0.55	Sbc	0.44	Sab		
22	0.45-0.5	E/S0	0.48	E/S0		
42	0.3-0.4	E/S0	0.19	E/S0	0.53	200
131	0.1	Sab	0.63	E/S0		
149	0.55	E/S0	0.59	Sab		
57	0.55	Sab	0.70	Sab		

In the case of 0016+16, as can be seen in the table, we find excellent agreement between the SED-based classifications and the spectroscopy for 12 out of the sample of 17 galaxies. Of the remainder, one was identified spectroscopically as an M star. Indeed the large disagreement between the eyeball fit and the χ^2 algorithm had already drawn our attention to this object, although such stars are generally difficult to separate from galaxies using colours. A further two objects were noted as having very poor signal-to-noise spectra, and without further information it is difficult to follow these up. In one case, the SED is also of poor quality, with two out of the six passbands showing discrepant colours.

Most significantly, however, two of the galaxies that were photometrically assigned a redshift of ~ 0.3 (both by visual inspection and χ^2 fits) were found spectroscopically to have $z = 0.55$, and show strong Balmer absorption lines indicative of Dressler and Gunn's post starburst evolution. As discussed above, galaxies which have undergone such an evolutionary change will indeed be expected to have SED shapes that are different from our non-evolving templates, thus, a priori, we may expect some difficulty in the attempted χ^2 fitting of these objects. However, our SED method is largely based on the use of the 4000\AA break as a redshift indicator, and it is therefore somewhat surprising to find such a large discrepancy.

Examining these two objects in detail (Fig 3.13), it can be seen that they give very close fits at all wavelengths to our original SED classifications. If these objects really are at 0.54 as is claimed, then their SEDs are considerably distorted, with a larger enhancement at optical wavelengths than in the uv. Indeed it seems a somewhat remarkable coincidence that the colours of these two galaxies should conspire to mimic so closely the unevolved SED of a lower redshift galaxy. Nevertheless, we must seriously consider these examples as a warning to the potential dangers of relying solely on our technique. Such behaviour is not clearly understood in the context of an additional burst of star formation added to an older population and merits further study as we shall discuss in chapter 5.

In summary we can conclude that the SEDs provide an excellent estimate of galaxy type and redshift with the caveat that extremely unusual evolved galaxies may yield misleading results, demanding spectroscopic confirmation. This merely reiterates our conclusion in chapter 2 that multicolour photometry is complementary to spectroscopy, rather than a replacement, allowing us to select classes of object for further scrutiny.

3.8. Summary and Conclusions.

In conclusion we have obtained several valuable and surprising results from our intermediate band observations of the cluster 0016+16, many of which were not suspected from the earlier broad-band photometry of Koo. Indeed it is informative to re-examine Koo's data in the light of our findings. In particular, if we consider his reasons for choosing a redshift of 0.54 for the cluster rather than considering $z = 0.3$, we find that his colour technique was not able to rule out the possibility of a large contaminating foreground contribution. Indeed, even in his two colour plots (his figure 2) we can see that many of the objects lie near to the $z = 0.3$ track. His large errors and poor level of spectral resolution made individual galaxy classification impractical. In chapter two, it may be remembered that we also criticised the use of the broad band U filter at such redshifts.

The main conclusions of our study then are the following:

- (1) The colour distributions derived for 0016+16 are not indicative of a single uniformly red population of $z = 0.54$ early type galaxies. A substantial bluer component is also present with colours close to those expected for a foreground group of galaxies at $z \sim 0.3$. These different populations would be difficult to resolve using broad-band photometry alone.
- (2) Low resolution SEDs constructed from our 6-colour data have allowed us to classify galaxies individually according to redshift and morphology. We have demonstrated that

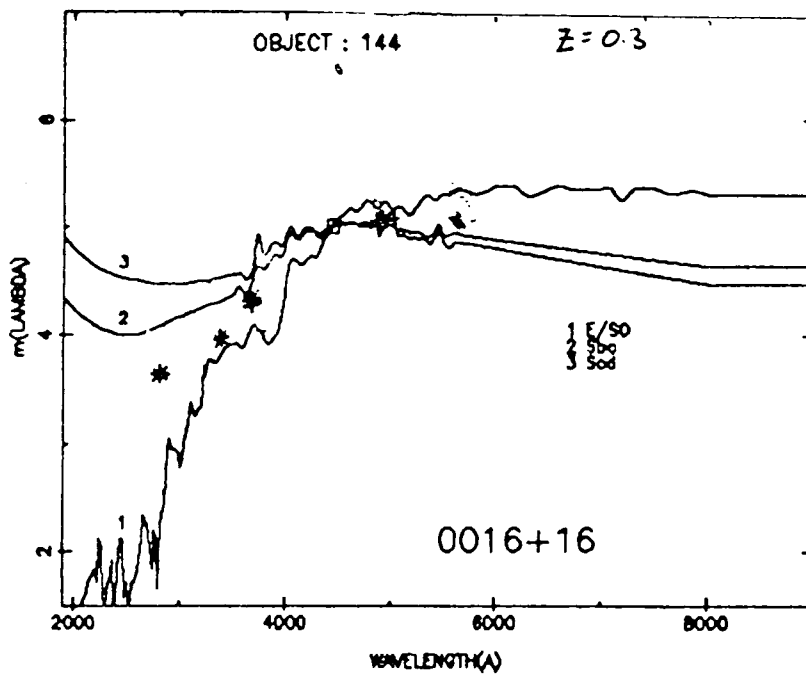
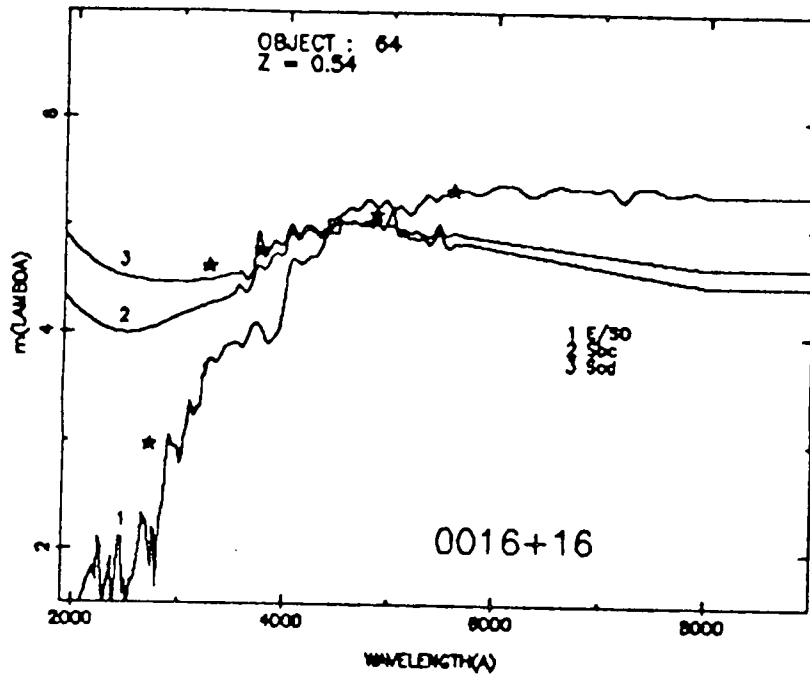


Figure 3.13: SEDs of the objects noted as having spectroscopic identifications discrepant with the photometric classifications.

this can, in most cases, be done unambiguously to $\Delta z \sim \pm 0.05$, and ± 1 Hubble type.

- (3) The classifications show that there is indeed no excess population of blue galaxies at $z = 0.54$ in agreement with Koo's earlier conclusion. However, the discovery of the foreground component at $z \sim 0.3$ reduces the cluster richness by $\sim 2/3$.
- (4) Using our classifications we collate a uniform complete sample of early type galaxies expected to be at $z \sim 0.54$. Their ultraviolet colours show a considerable range with some objects as red as present day E/S0's but about half are substantially bluer. A possible interpretation for such behaviour is that we are witnessing the effects of stellar evolution in the early type galaxies. This is addressed in chapter 5.

Now that we have demonstrated the potential wielded by our multicolour photometric system, we can begin to apply it to a larger sample of distant clusters. In the next chapter I will discuss observations of another distant cluster using a smaller number of filters with the intention of comparing the results with those obtained here.

4. CCD Photometry of the Distant Cluster A370.

4.1. Introduction.

The previous chapter has demonstrated the effectiveness of our multicolour approach to the study of distant galaxy clusters. In particular, our high success rate for individual object redshift/type determination modified considerably our understanding of the red cluster 0016+16, revealing substantial foreground contamination. Furthermore, our study of the rest-frame ultraviolet colours of E/S0 members provided evidence for the spectral evolution of such galaxies during the past 7 Gyr. In this chapter I further develop this technique by application to another previously studied cluster. The reason for not immediately obtaining observations of a new sample of homogeneously selected clusters (see chapter 6) is threefold.

Firstly, since 0016+16 contains predominantly red members to which photometric redshift estimates can be more accurately ascribed (see chapter 2), it is of value to test the effectiveness of our SED fitting scheme also on a cluster expected to contain a large population of blue objects. Secondly, we suggested in chapter 2 that it is possible in principle to minimise the number of intermediate band filters needed for such observations whilst not substantially decreasing the accuracy of our galaxy classifications, providing we make a careful choice of passbands based on the cluster's known (or suspected) redshift.

Furthermore the unexpected discovery of the new class of uvx galaxies found in 0016+16 may prove an important clue as to the nature of galaxy evolution. Thus it is important to check how universal this phenomenon is and whether it is also apparent in clusters with large blue fractions. Such an observation could then provide a link between 0016+16 and the other bluer Butcher-Oemler clusters.

The cluster A370 ($z = 0.37$) has a somewhat striking appearance (Fig. 4.1), being dominated by two bright members, separated by 37 arcsecs (249 kpc at the cluster redshift), each surrounded by a tight concentration of galaxies. Couch and Newell (1984) and Butcher and Oemler (1984) have independently obtained single colour broad-band photographic photometry of the cluster as part of their studies of the fractions of blue galaxies in distant clusters. Couch and Newell's photometry is in the B_J and R_F passbands from AAT 4m photographic plates, whilst Butcher and Oemler's data (from Kitt Peak 4m plates) is in their J and N passbands. Since J_{BO} is identical to B_J it is instructive to compare the two sets of photometry, particularly since both groups used quite different data reduction procedures. This comparison is shown to be quite favourable in figure 4.2. We found that in the area common to both samples almost all of CN's galaxies, to their limit of $R_F = 21.2$, were identified in Butcher and Oemler's data, verifying the claimed completeness.

The conclusions from both these studies indicated that A370 has a fraction of blue members which is considerably larger than that found in nearby clusters of similar richness and concentration ($f_b \sim 0.2$, in Butcher and Oemler's notation). Bautz, Loh, and Wilkinson (1982) have also obtained CCD photometry of this cluster, but only for the brightest ~ 20 galaxies in the cluster field. Even so they tentatively claim to uphold the Butcher & Oemler result.

In conclusion, then, A370 satisfies our requirement for a distant cluster with apparently contrasting properties to those of 0016+16. Furthermore, it should prove an excellent candidate on which to further refine our SED fitting technique, in that with a large blue fraction it may be more 'typical' of distant rich clusters. The availability of previous broadband photometry and the cluster's inclusion as a target for multi-object spectroscopy by several groups, including our own, will provide much valuable information.

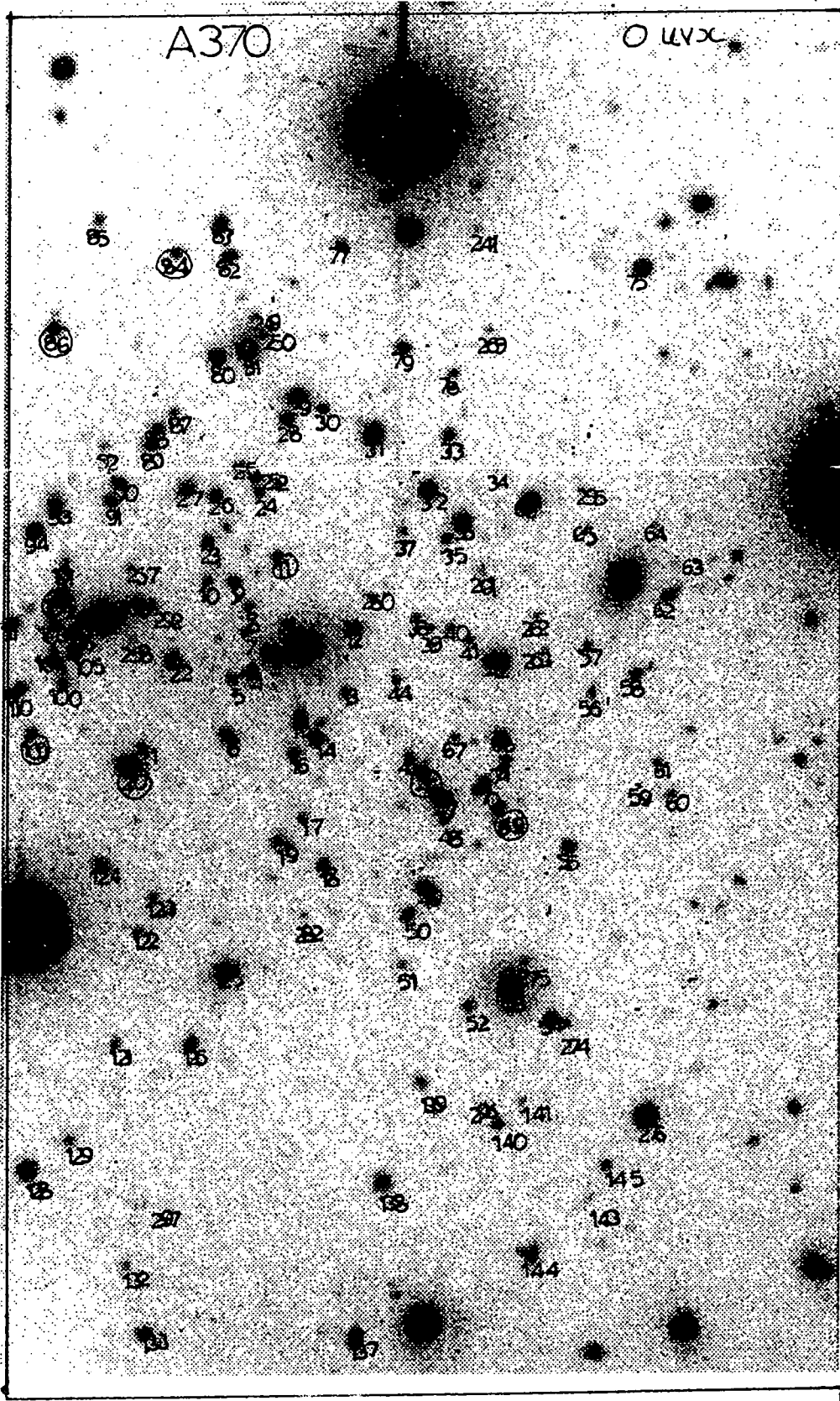


Figure 4.1: The 685 nm CCD frame of the cluster Abell 370. The numbering scheme follows that of Couch (1981).

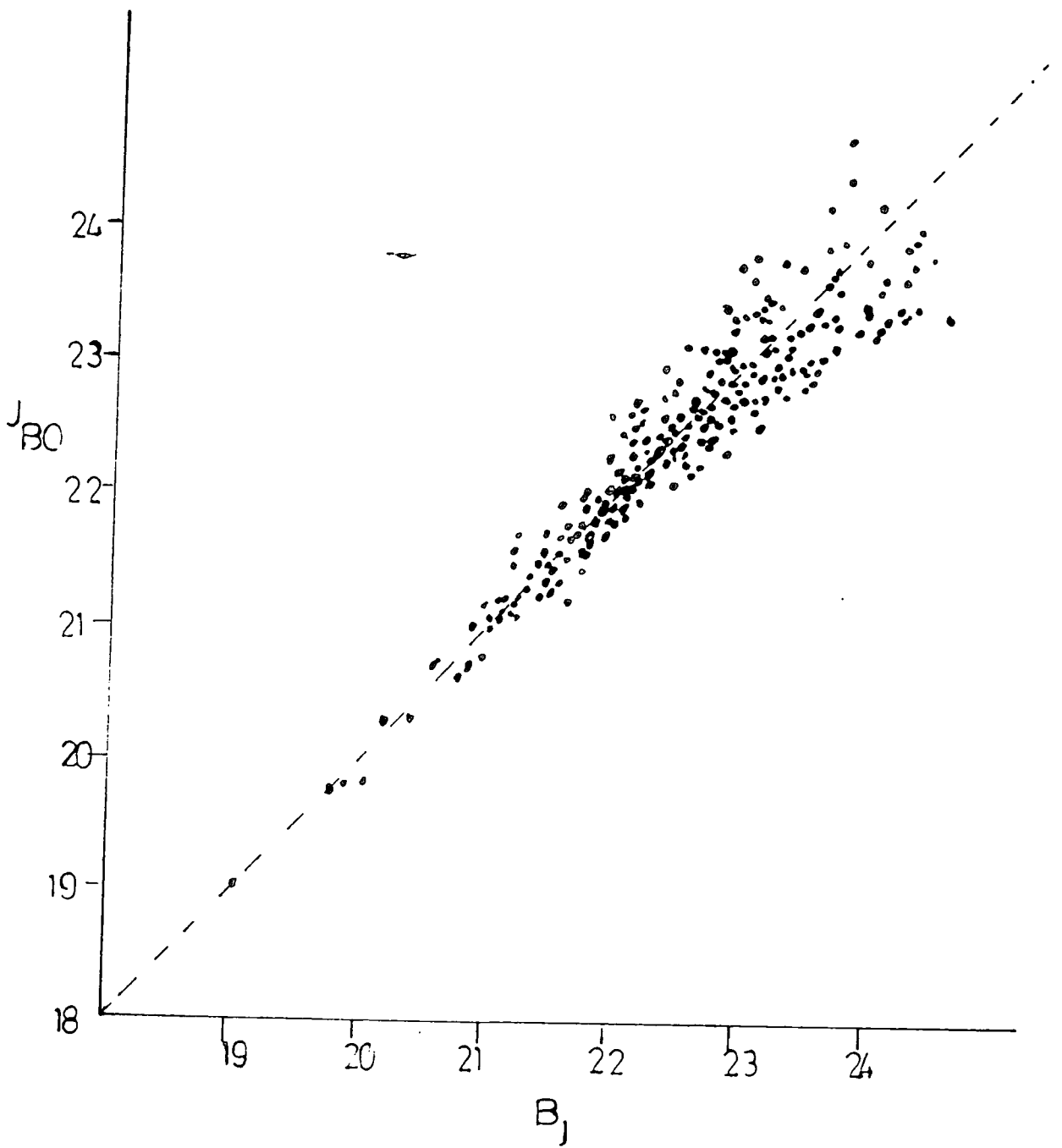


Figure 4.2: Comparison between Butcher & Oemler's (1984) J band photometry and that of Couch & Newell (1984).

4.2 Observations and Data Reduction.

Once again our photometry is based on observations made at the prime focus of the AAT using the RCA CCD. Whereas in chapter 3, we imaged the cluster 0016+16 in six filters, here we adopted the approach of rationalising the number of exposures to the minimum necessary to obtain reasonable object classification, ie to discriminate populations of cluster members from field galaxies as described in chapter 2. At this redshift we used the 4 filters, 418, 502, 685, and 862 nm, noting that our previously bluest band (418) does not penetrate sufficiently far into the rest-frame ultraviolet to test, for example, for the presence of uv enhancements of the sort we found in 0016+16. Consequently we have also imaged the cluster in the Johnson *U* band which reaches similar rest wavelengths (~ 260 nm) to those attained in 0016. This filter is somewhat broader than our intermediate bands, but we shall use it as an indicator of the uv flux from galaxies selected using the other 4 passbands.

Table 4.1 summarises our observations, made during two runs in October 1983 and December 1985. Repeated observations of Oke (1974) spectrophotometric standard stars (VMa 2 and Feige 24) throughout each night provided zero-points for our photometry as well as a useful monitor of the stability of the photometric conditions. I have reduced these observations in a manner identical to that in chapter 3 and consequently refer back for further details.

Our finally reduced 685 nm frame is shown in figure 4.1, with the objects we selected visually (using a cursor on the ARGS display) labelled according to Couch and Newell's numbering scheme (except for object number 110, and numbers greater than 250). Unfortunately, we have a slight positional offset between the two observing runs, decreasing the area common to all passbands to 3.75×2.0 arcmin.

The similarity of the 685 filter to Couch and Newell's R_F , allows us to calibrate our 685 magnitudes against their photographic photometry. A comparison of the Kron magnitudes derived from both sets of photometry is most appropriate but suffers from the complication of image-crowding. Contamination of objects by close neighbours is quite a severe problem in A370 and in order to deal with it (as in all their clusters) CN applied a cleaning algorithm to their data before magnitude measurement. We are not able to apply this algorithm in these reductions as it is not suited to CCD-type data (Newell, 1982). As a consequence the Kron magnitudes for many of our objects are systematically too bright due to neighbours falling within the Kron radius (in practice, the algorithm used to estimate the Kron radius can fail when faced with severely contaminated images, in that it defaults to the largest of our series of 10 apertures). This effect is seen in figure 4.3(a) where we plot CN's R_F Kron magnitudes against the equivalent 685 values measured here. The contaminated objects form a clear group which scatter upwards from a ridge line of objects which define a one-to-one relationship between the two scales (solid line in the figure). Visual inspection of these high scattering objects confirms that they all have crowded images.

As a further check on this conclusion, we also have R band CCD exposures of the cluster taken by Ellis, Couch, and D'Odorico (1986, private communication) during September 1986 on the ESO 3.5m telescope at La Silla. Whilst standards taken on this occasion reveal the data to be non-photometric we can at least verify the quality of our CCD photometry by plotting this R vs 685 (Fig. 4.3(b)). The tight relationship then confirms that the discrepancy in figure 4.3(a) lies within the photographic data and is not a consequence of dubious CCD data.

Table 4.1: *Log of Observations*

Object	Date	Filter	Exposure(s)	Airmass	Seeing(arcsec)
A370	1983 Oct 8/9	502	1400	1.22	1.02
		685	1200	1.27	1.52
		862	1200	1.33	1.14
VMa2	1983 Oct 8/9	502	10 (x6)	1.25-1.82	0.79
		685	10(x4)	1.25-1.79	0.83
		862	20(x3)	1.25-1.84	0.81
A370	1985 Dec 13/14	U	1000(x2)	1.15-1.17	1.57
		U	2000	1.15	1.60
		418	1000	1.20	1.6
		685	800	1.26	1.66
VMa2	1985 Dec 13/14	U	25(x2)	1.32	1.8
		418	50(x2)	1.34	1.98
		685	30(x2)	1.34	1.70
Feige 24	1985 Dec 13/14	U	25(x2)	1.22	1.86
		418	30(x2)	1.22-1.43	1.80
		685	30(x4)	1.22-1.42	1.80

In order to avoid this problem of crowding it is necessary to consider magnitudes determined within a much smaller aperture than required to measure Kron's total-type magnitudes. If, for example, we plot the 685 magnitudes measured in the third smallest (4.8arcsec) aperture (see above) against the R_F magnitudes CN measured through a similar sized aperture (figure 4.3(c)) we see a very much tighter relation with no sign of the behaviour seen in figure 4.3(a). The one-to-one relation fitted to this data (solid line) can then be adopted as the calibration between 685 and the R_F Kron scale.

$$685(3) = R_F(\text{Kron}) - 3.92 \pm 0.05 \quad (4.1)$$

We are also able to calibrate our photometry using the observed white dwarf standard, VMa 2, which has been found by H. Morrison (1986, private communication) to have an R magnitude (after accounting for the colour equation between R_{KC} and Couch and Newell's R_F band) of 12.129 ± 0.005 , yielding a transformation

$$685(\text{Kron}) = R_F(\text{Kron}) - 4.04 \pm 0.07 \quad (4.2)$$

The two relations (4.1) and (4.2) are thus found to be consistent and total magnitudes may be safely estimated from the 685(3) measures.

We can also use Couch's data to test our completeness. He claims completeness in his photographic photometry to a limit of $R_F = 21.2$. All of his objects within our CCD area down to this magnitude limit with the exception of one galaxy (WJC #43) are in our sample. This object is not present on any of our frames and we conclude that it is probably a spurious detection. To this magnitude limit we detect 7 new objects in our CCD field for which there is no corresponding photographic photometry. With a total of 102 objects to this limit, we can conclude that Couch's sample is incomplete at the 6% level at $R_F = 21.2$.

The completeness of the CCD data beyond $R_F = 21.2$ can be assessed in two ways. Firstly, Couch (1986, private communication) has assessed the number magnitude counts within the cluster and compared these with those in 0016+16 where the completeness limit is known to be $F = 22.5$ ($R_F = 22.1$). Table 4.2 shows the measured counts in the CCD area and the expected level of field contamination (based on Couch's, 1981 work). The cluster luminosity functions can be compared allowing for the difference in distance modulus (also Couch, private communication). Ignoring evolutionary differences there is slight evidence for a flatter slope in A370 beyond $R_F = 21.5 - 22.0$. This limit also agrees with that derived from the 685 exposure times used for A370 and 0016+16 (1200 and 2000 sec respectively) indicating a completeness limit of $R_F = 21.7$ to the same S/N. This is therefore a reasonable estimate for the completeness of the present data. However, as in the previous chapter we shall restrict the SED analysis to a sample of objects limited some 0.5 magnitudes brighter than the completeness limit, ie $R_F = 21.2$, providing 102 objects for detailed study.

4.3 Errors.

In our previous work we have conducted comparisons of repeat exposures in our various passbands to determine our photometric random errors. In summary we concluded that the errors are not significantly larger than the expected Poisson value so that our data is essentially limited by photon-noise considerations (Chapter 3). Errors in the intermediate-band filters determined for 0016+16 were found to be approximately 0.07 mag (and 0.12 mag in 418) down to a limit slightly deeper than that attained here in A370 (Note that the 1983 observations of A370 were obtained on the same night as many of the 0016 exposures of the previous chapter).

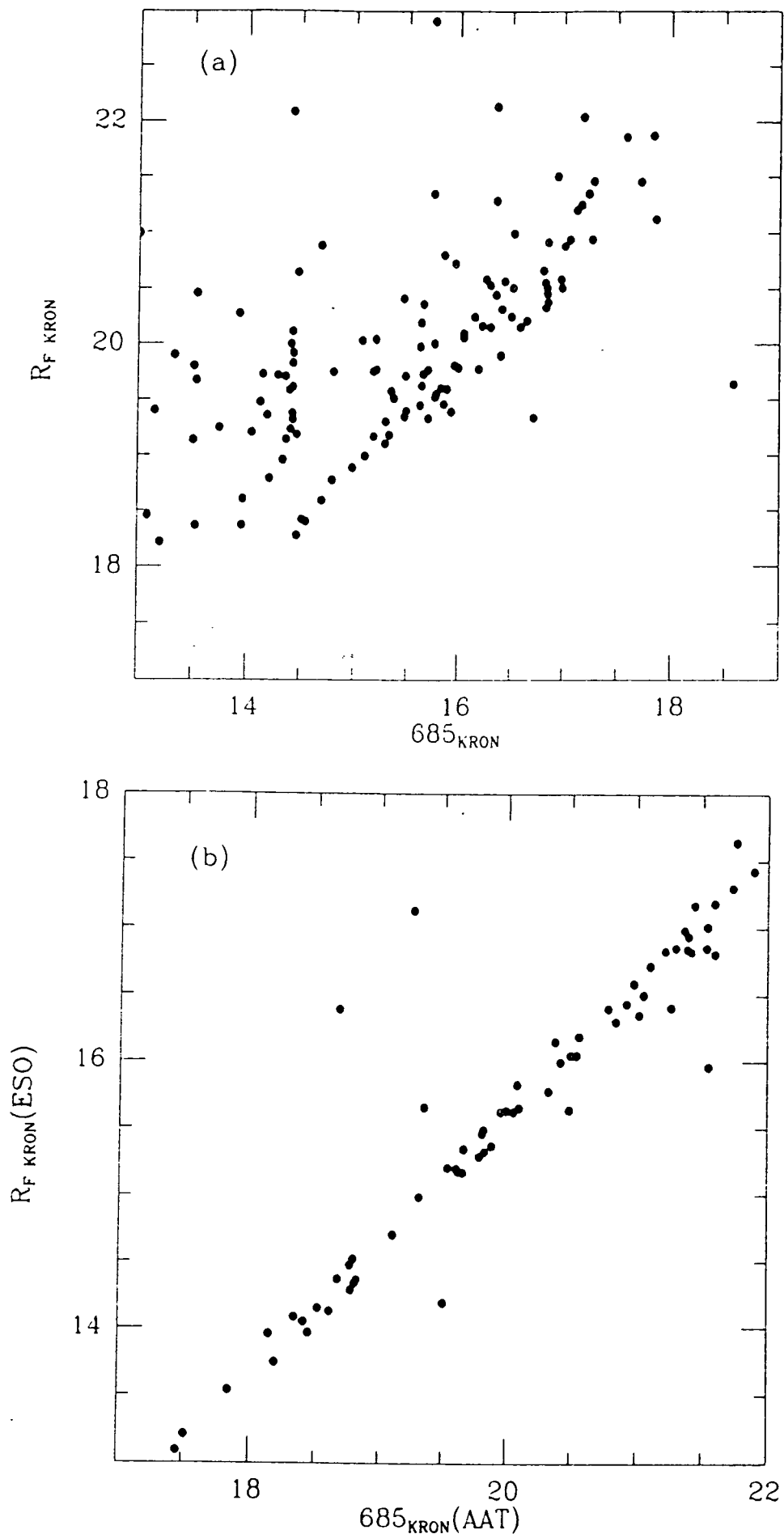


Figure 4.3: (a) Couch & Newell's photographic R_F photometry compared with that in the CCD 685 nm filter; both Kron-type magnitudes. The large scatter is due to crowding problems. (b) ESO 3.6 m R CCD magnitudes compared with AAT 685 nm mags, justifying the high precision of the CCD photometry. (c) 4.8 arsec diameter aperture magnitudes (AAT 685 nm) compared with Couch and Newell's Kron mags. The solid line represents the adopted calibration.

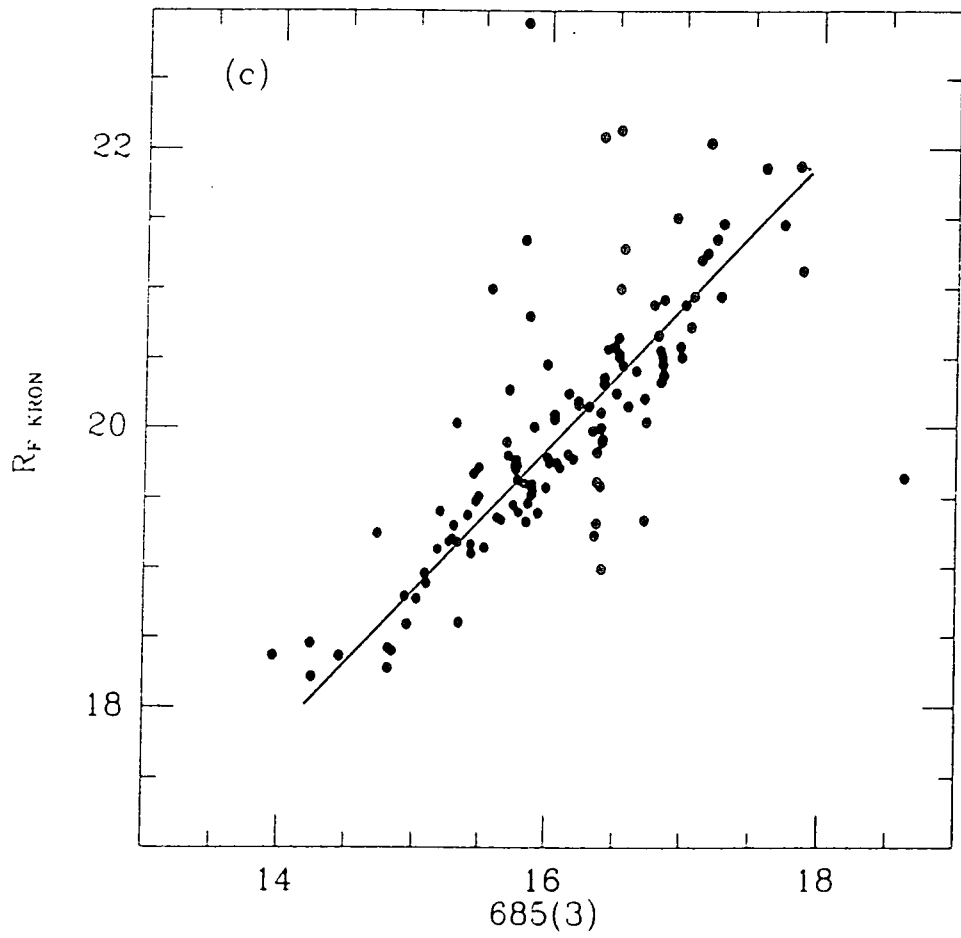


Table 4.2: *Integral Number Counts in CCD Field.*

R_F	Number measured	Expected field
20.0	50	5
20.5	75	8
21.0	97	13
(21.2	102	18)
21.5	110	19
22.0	130	-

Note: Photographic incompleteness beyond $R_f = 21.5$ makes it difficult to predict fainter field counts.

For our investigation of the form of SEDs at high redshift, the U passband is of most importance. Thus it is crucial to ensure accurate error determination for this filter. Consequently we obtained three individual exposures (one at 2000 s and two at 1000 s) of the cluster in U , which we can compare with the expected magnitude scatter on the basis of random noise. In our $R_F = 21.2$ limited sample we find a scatter on U of $\sigma = 0.21$ mag, whereas the expected Poisson value is $\sigma = 0.20$. Note, however, that the errors in U are not a straightforward function of R_F magnitude since these bands are well separated in wavelength. Thus for a fixed R_F an object with bluer colours has a more well-defined U magnitude than a red object. It is more meaningful, therefore, to talk in terms of the error for various regions in our colour magnitude diagrams. This will be discussed in detail in section 4.5.

The photometric quality of the data can be assessed by noting that the repeat exposures of the spectrophotometric standards taken on both runs yield results in good agreement. In U , 418, and 685 the two standards, VMa 2 and Feige 24, give colour offsets consistent to between 0.01 to 0.04 mags.

4.4 SEDs and Object Classification.

(a) *SED Construction.*

The method for constructing low resolution SEDs from our magnitudes has already been described at length in chapter 3. To briefly recap, however, we use the zero-points determined from the photometric standards and their published spectrophotometry to compare our observations directly with colour predictions obtained on the basis of appropriately k -corrected spectra of nearby galaxies of various spectral types as shown in figure 4.4. Whilst we include the U -colour for each galaxy on our SED plots it should be stressed here that our approach is based on the use of intermediate bandwidth filters, and consequently the U magnitudes are excluded from our object classification criteria. The classifications obtained in this manner are only accurate to, on average, approximately ± 0.05 in z and to the nearest Hubble type (see chapter 2), but this is sufficient in most cases to determine the likelihood of membership of a given object. Spectroscopy of galaxies in the area covered by our present imaging will be discussed later (section 4.6). Our classifications for the A370 galaxies are listed in table 4.3.

(b) *Foreground Contamination and the Butcher-Oemler Effect.*

In the primè sample ($R_F = 21.2$) of 102 galaxies in the A370 field, there are 78 cluster members, a further 13 with uncertain membership (classified as $z \sim 0.2 - 0.4$), 9 non-members, 1 unclassified steep-spectrum object and 1 star. The total field galaxy contamination lies between 10 and 24 objects depending on the status of the uncertain members. Couch and Newell's (1981) photometry predicts an expected contamination of 18 galaxies. Since our errors in redshift are estimated as being ± 0.05 it is possible that some field objects with redshifts around $z \sim 0.33 - 0.41$ will be classified in the present work as being cluster members. However, predictions using models based on local field luminosity functions have shown this effect to be small and only 18% of field galaxies at $R_F = 21.2$ could lie in this region (Ellis, 1987 and private communication). Our present observations, therefore, verify the level of field contamination expected from Couch's photometry.

As discussed earlier, the previous studies of this cluster have indicated the presence of a substantial proportion of blue objects in the cluster population. Indeed, Butcher and Oemler estimated f_b to be 0.21 ± 0.05 where f_b is the fraction of objects bluer by more than 0.2 magnitudes in rest-frame $B - V$ than an E/S0 galaxy of the same absolute magnitude. Couch (1981) undertook a different approach to analysing his data, decomposing his cluster colour distribution into spiral and E/S0 components.

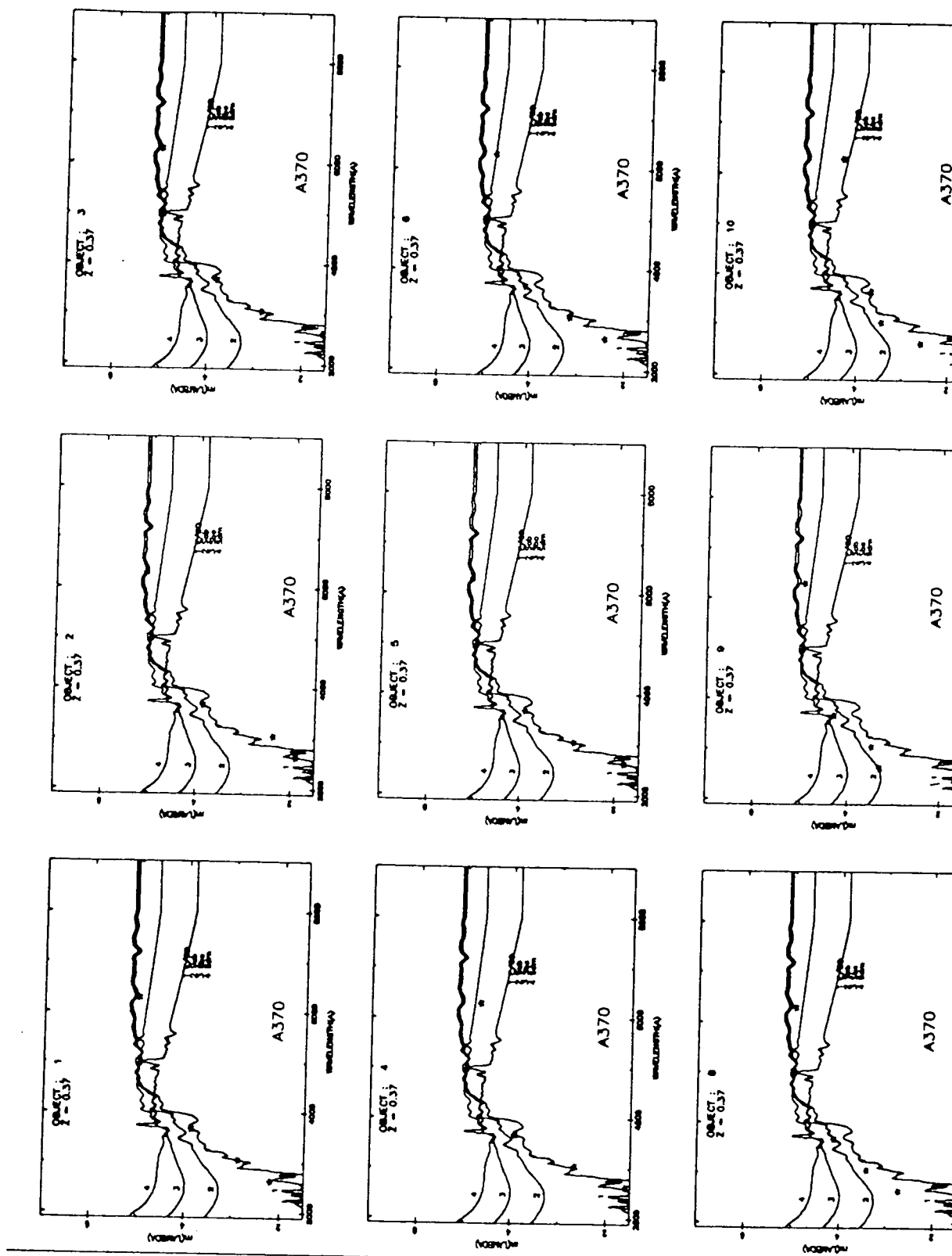
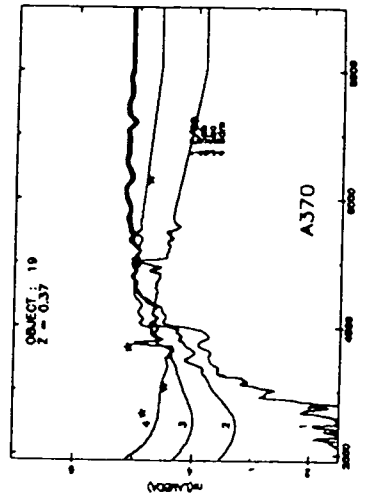
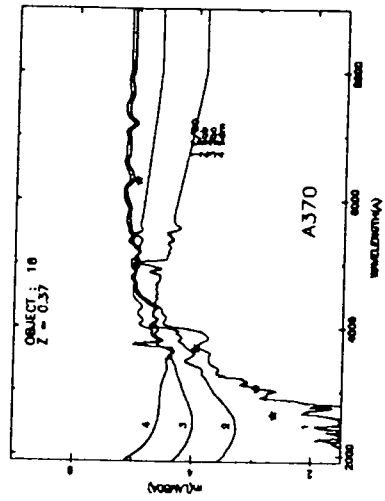
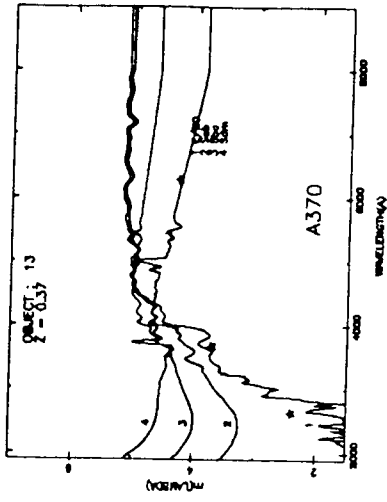
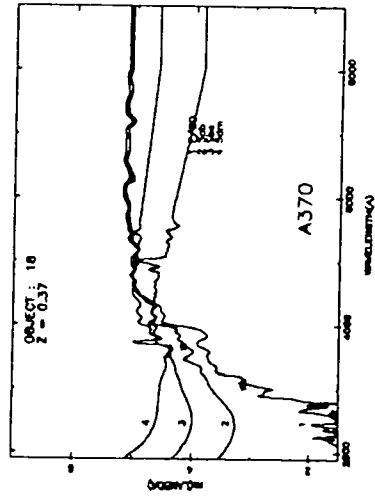
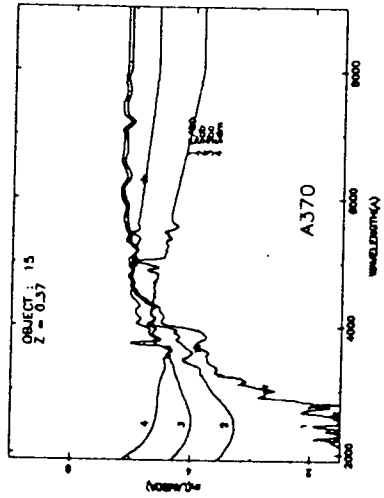
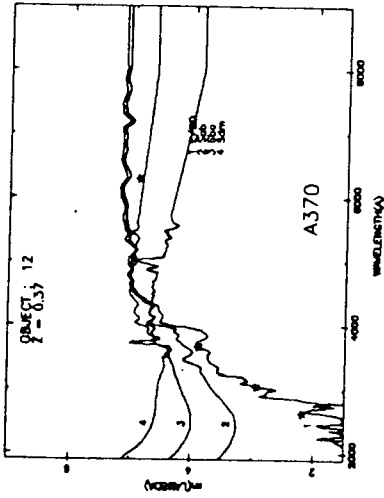
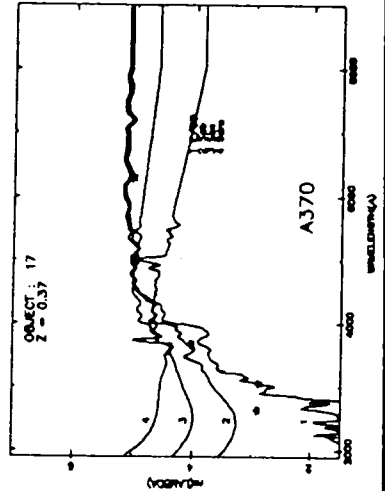
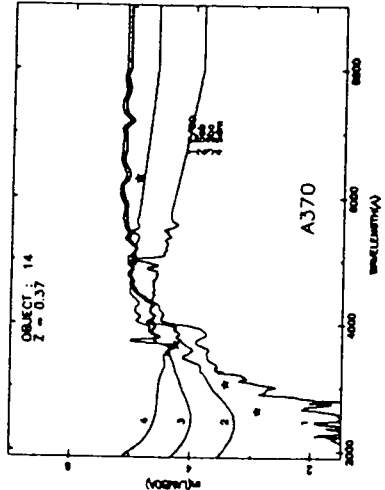
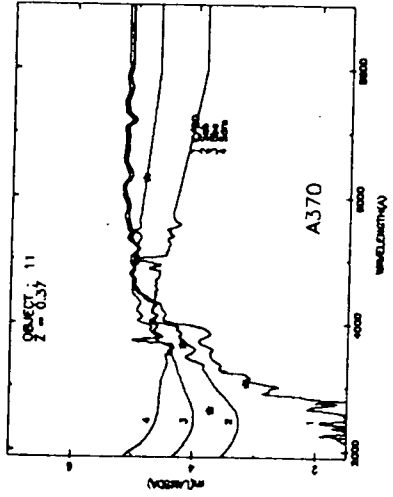
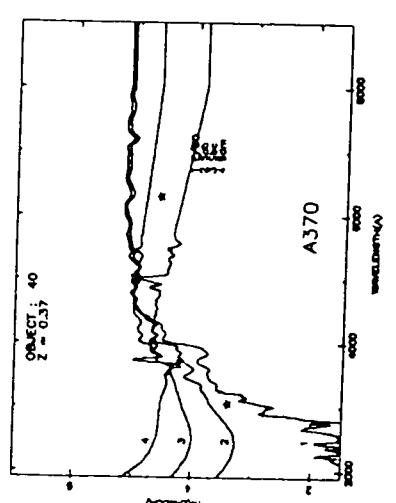
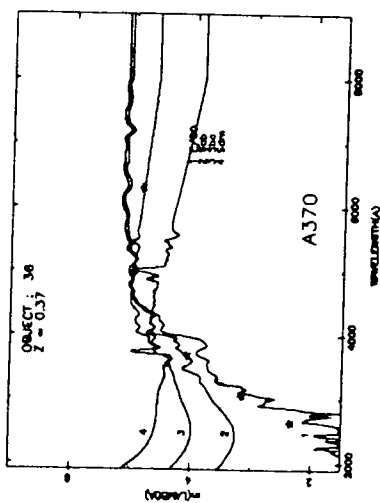
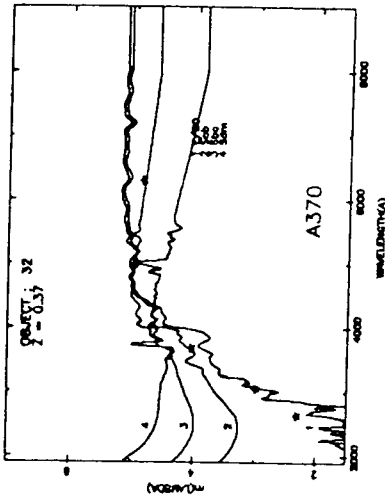
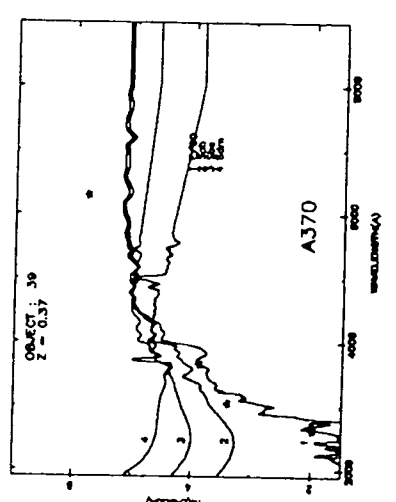
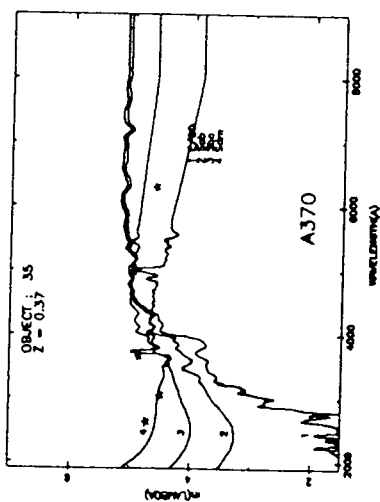
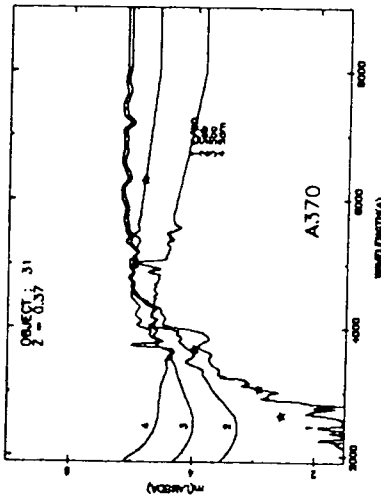
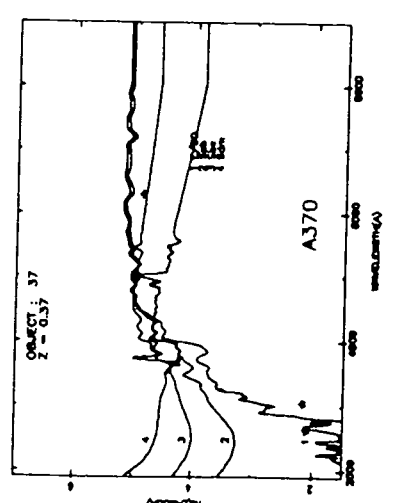
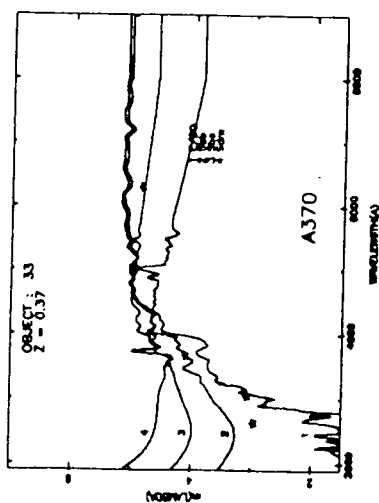
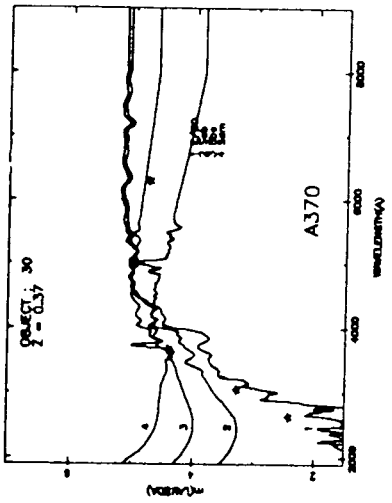
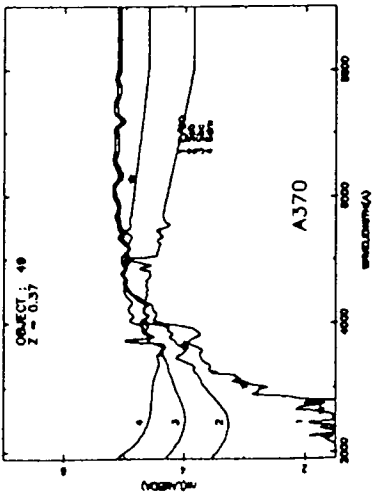
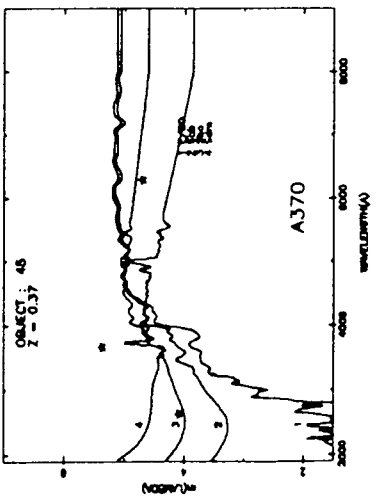
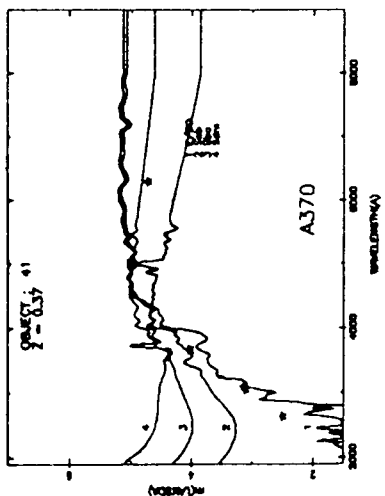
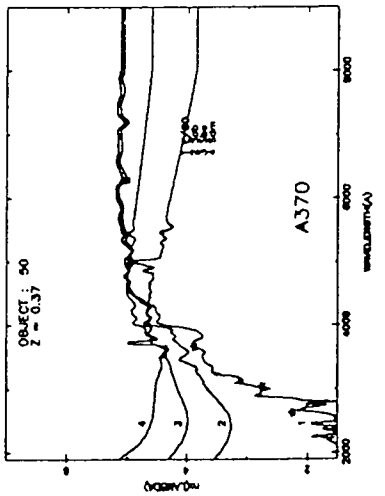
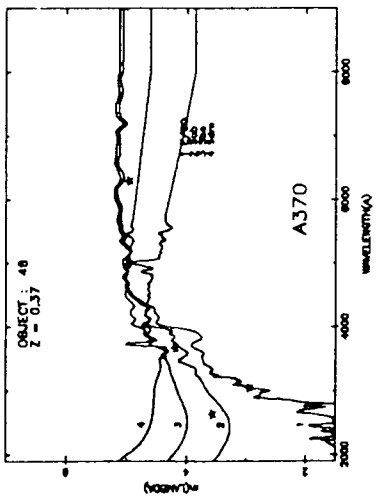
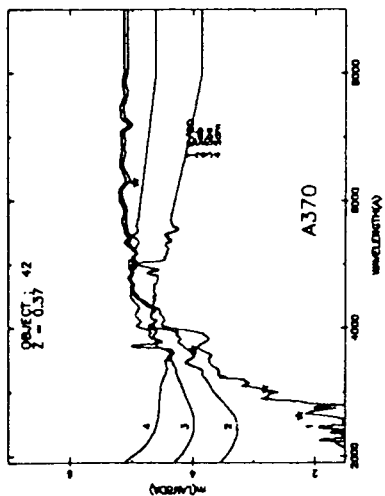
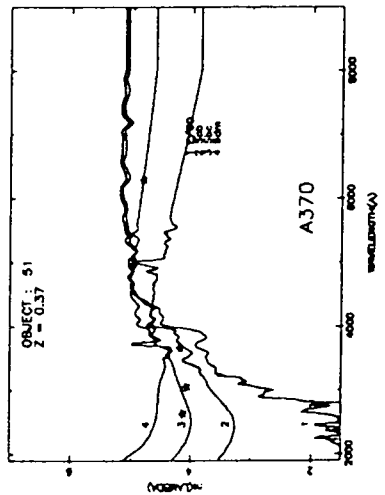
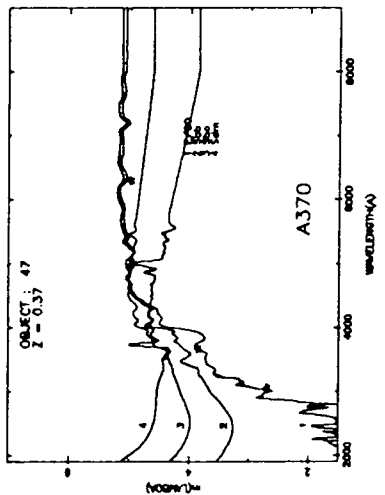
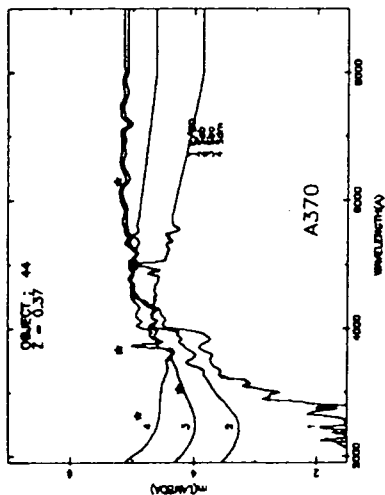
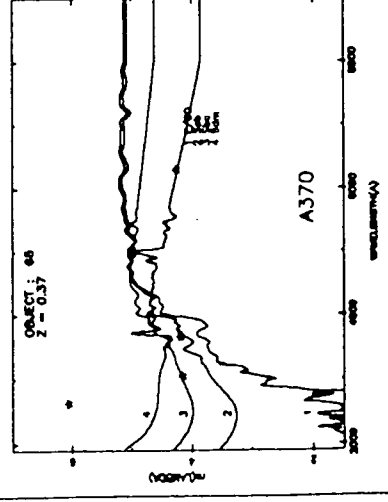
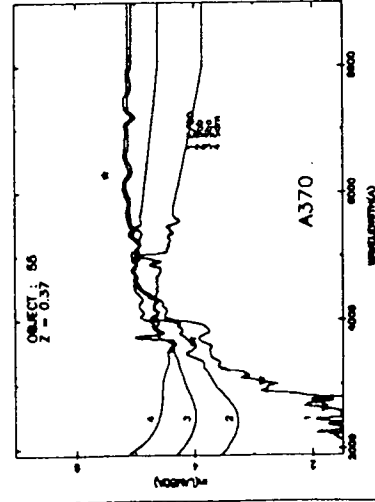
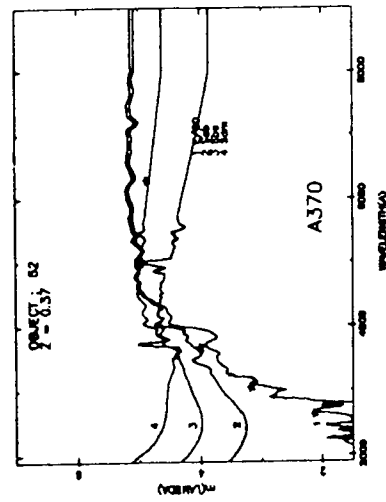
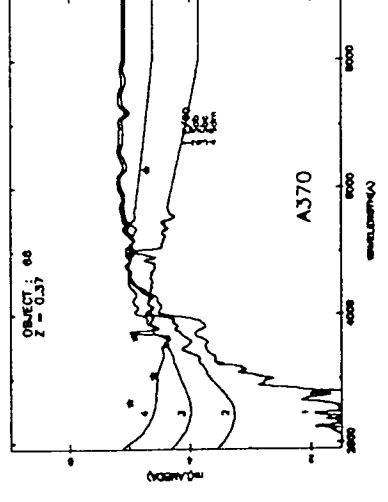
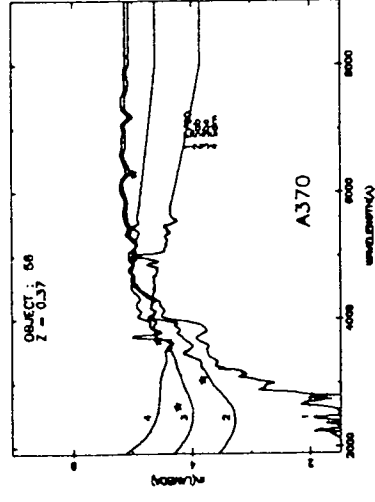
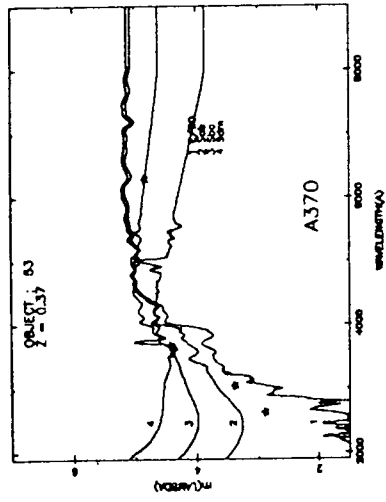
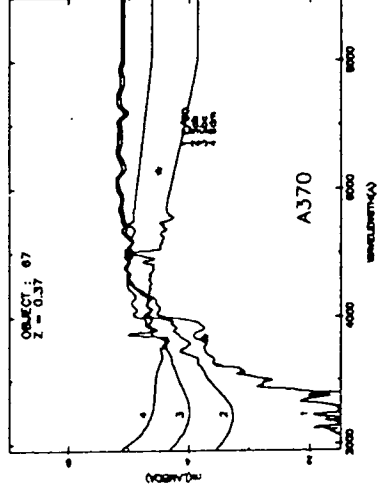
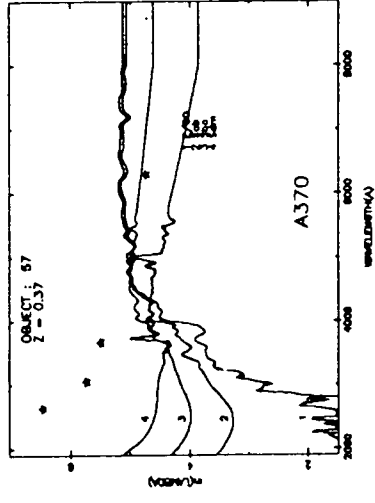
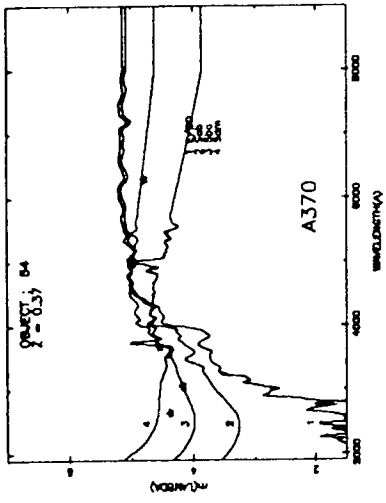


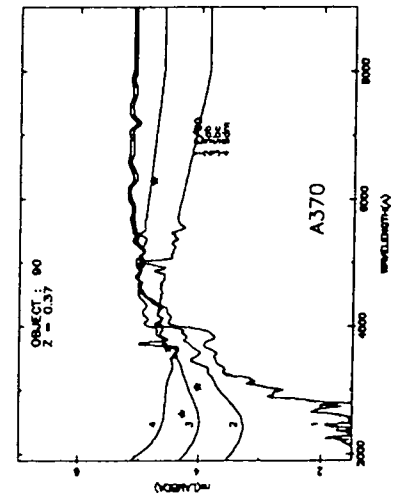
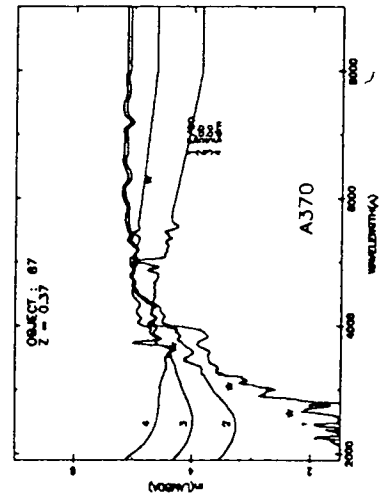
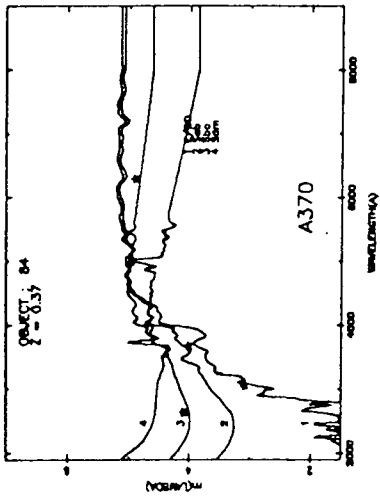
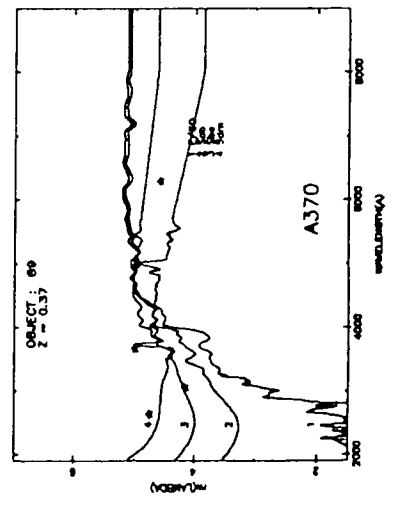
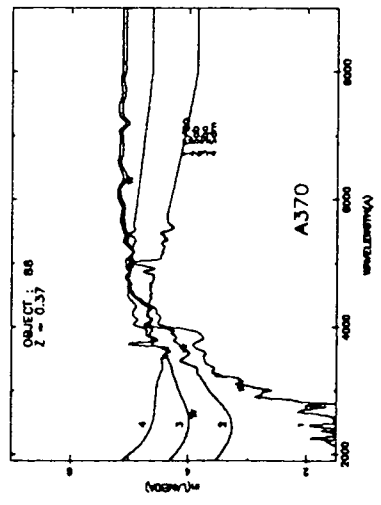
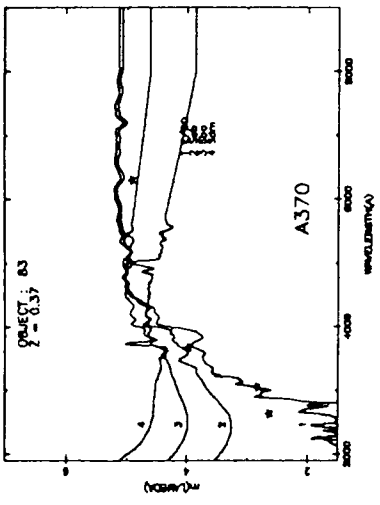
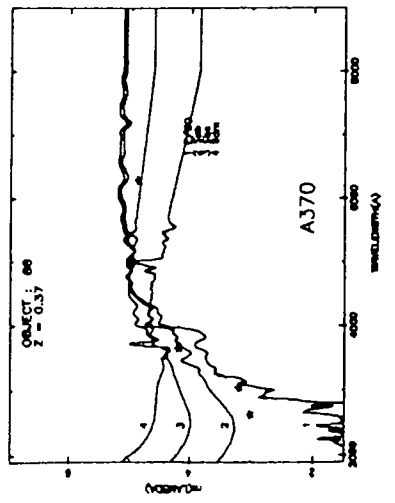
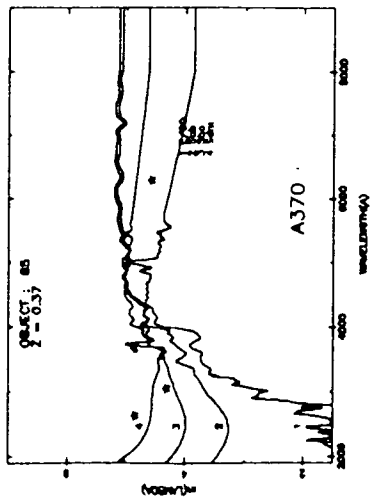
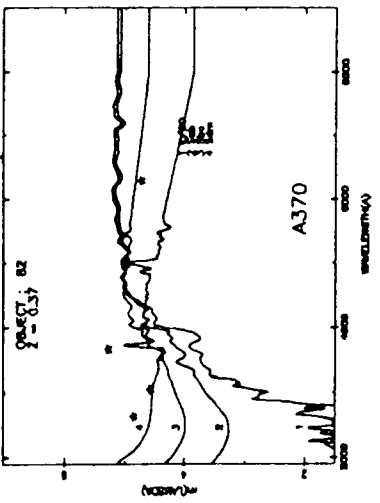
Figure 4.4: SEDs for galaxies in A370 CCD area, plotted at the cluster redshift.

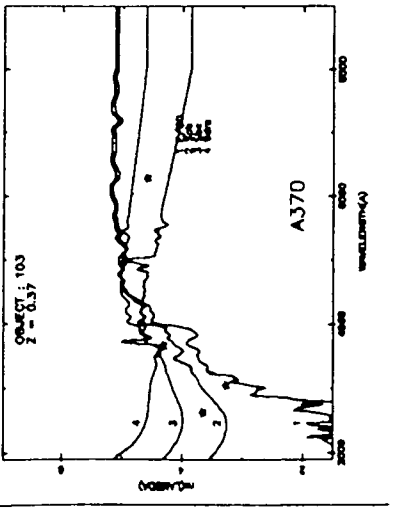
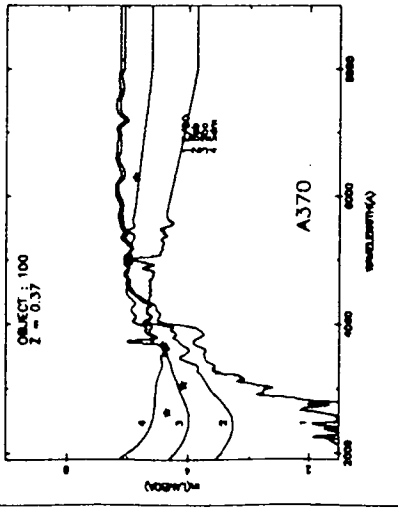
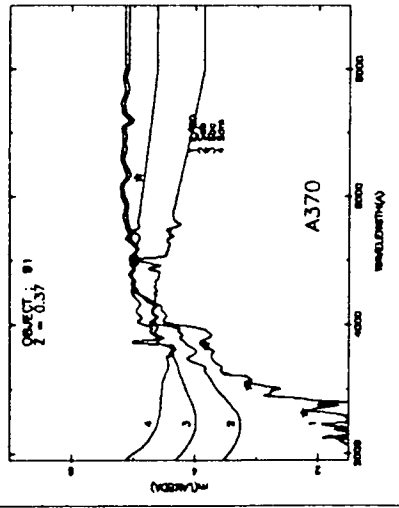
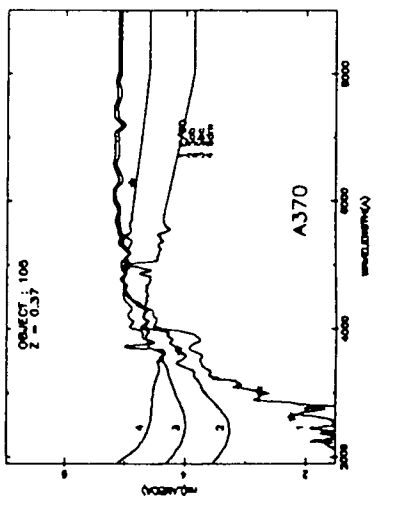
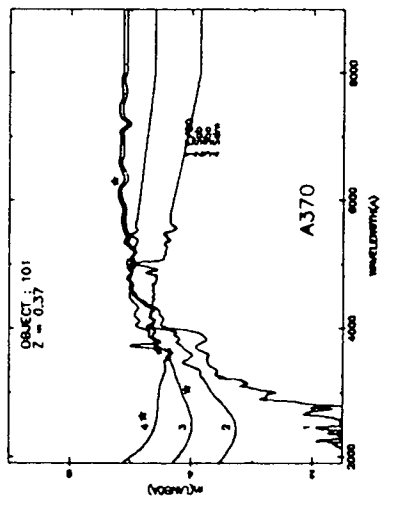
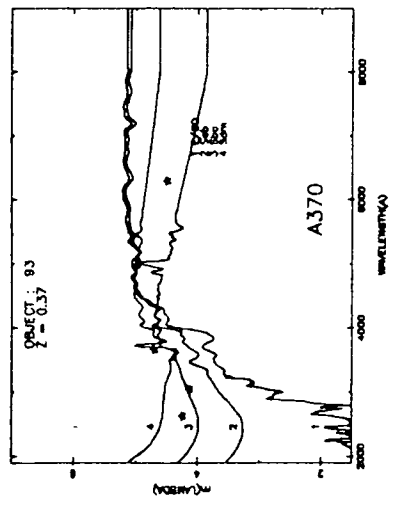
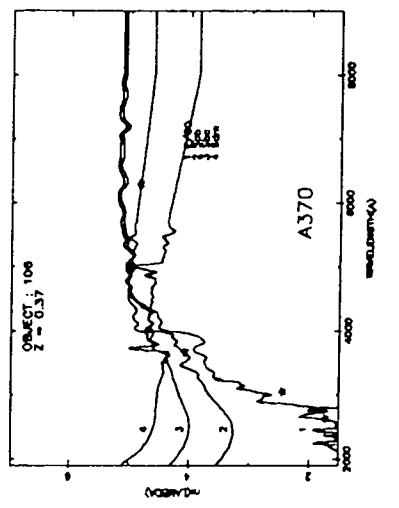
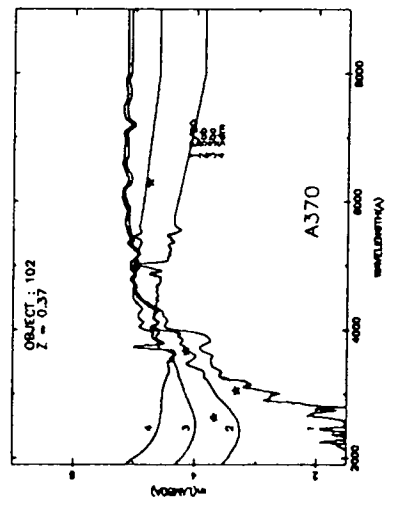
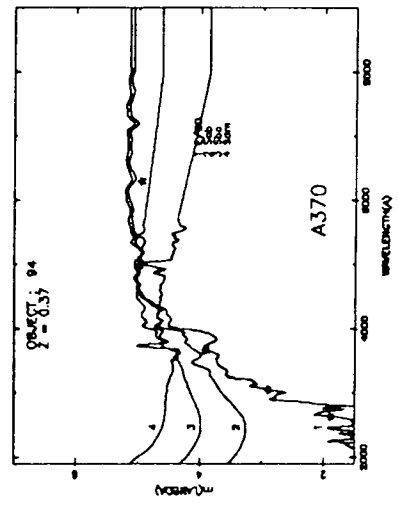


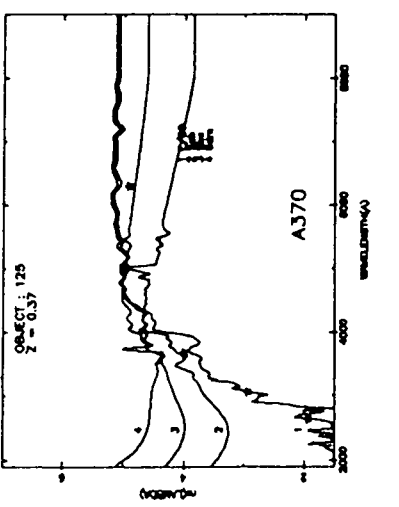
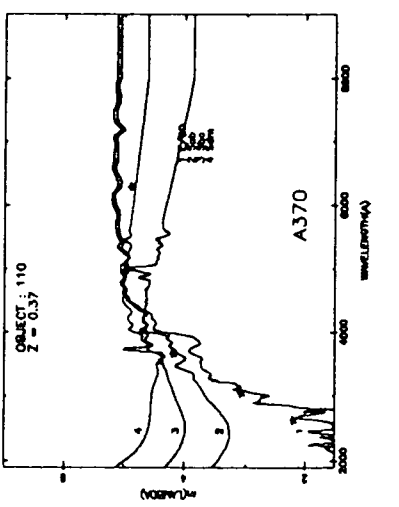
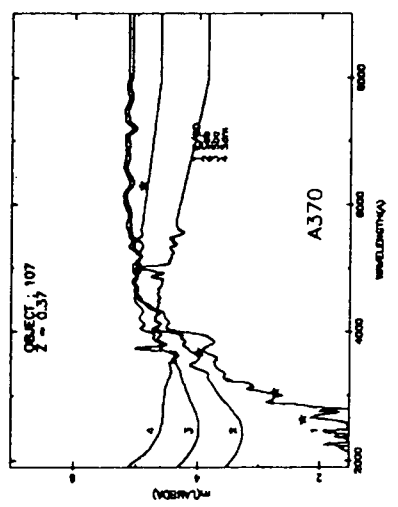
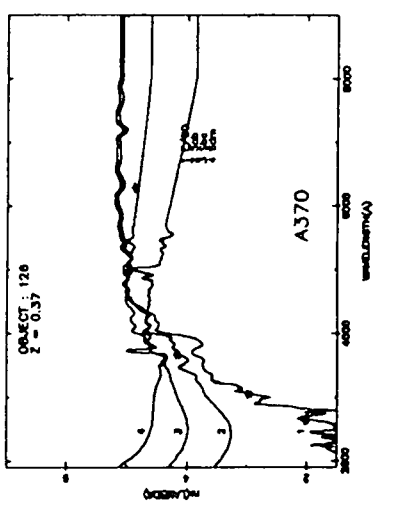
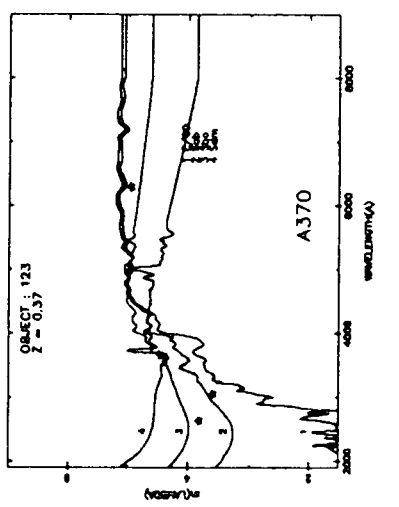
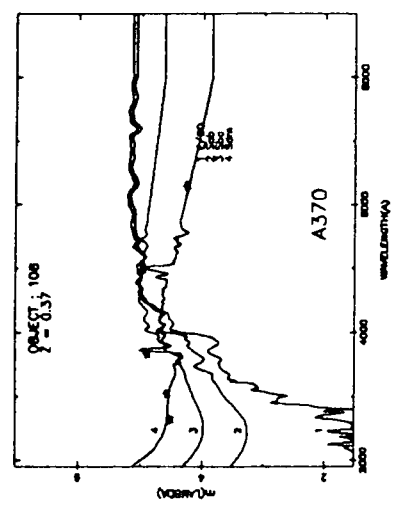
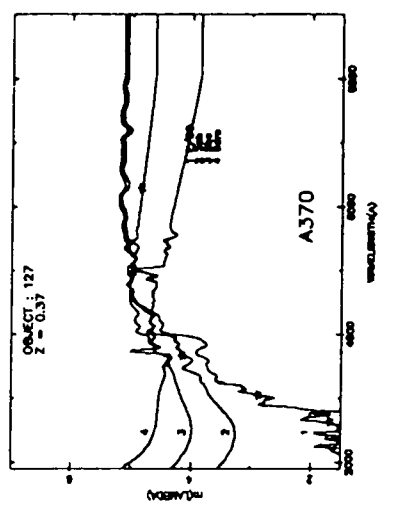
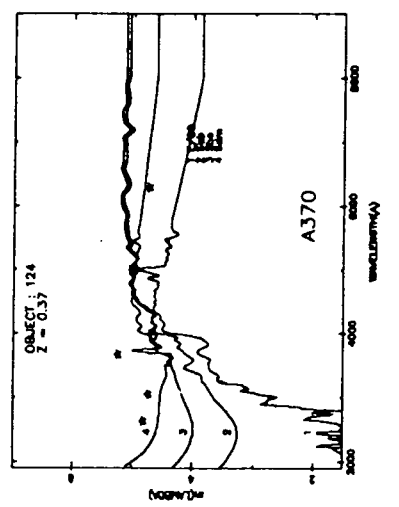
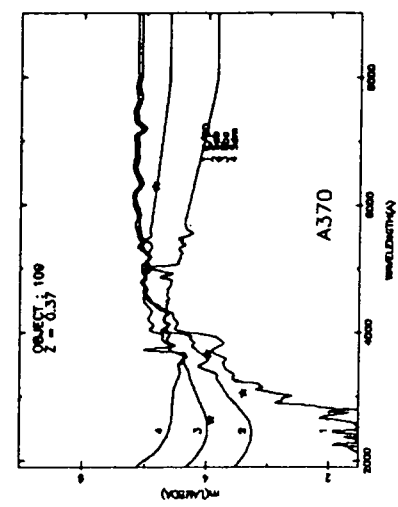


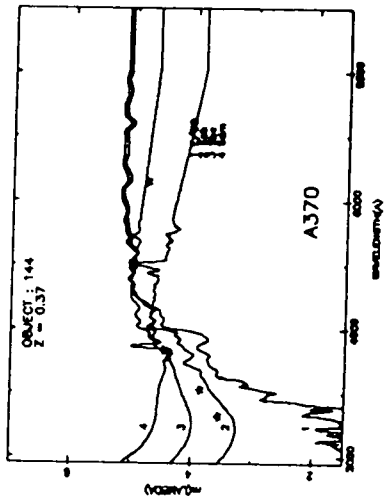
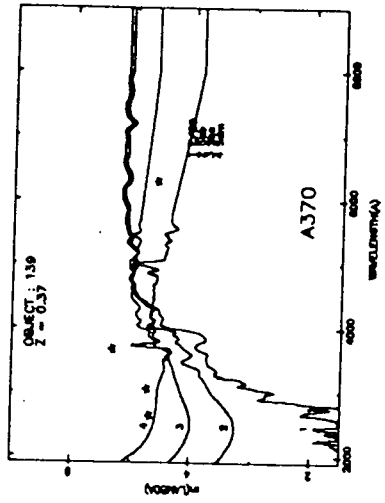
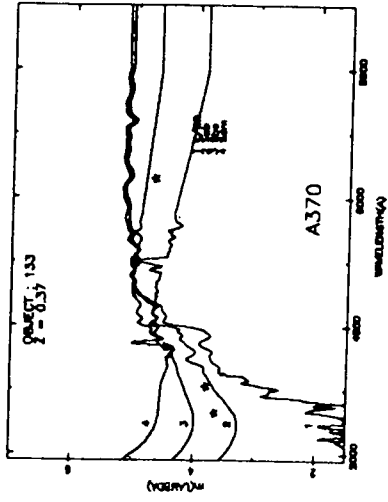
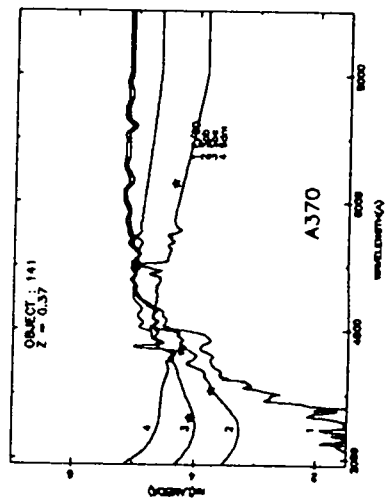
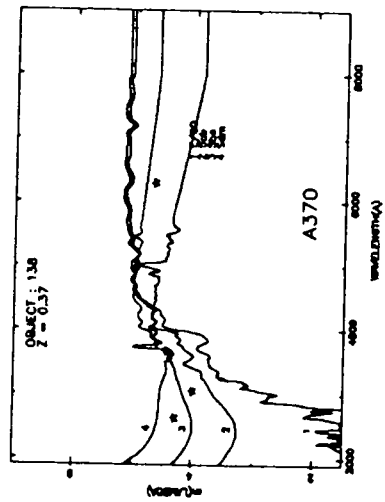
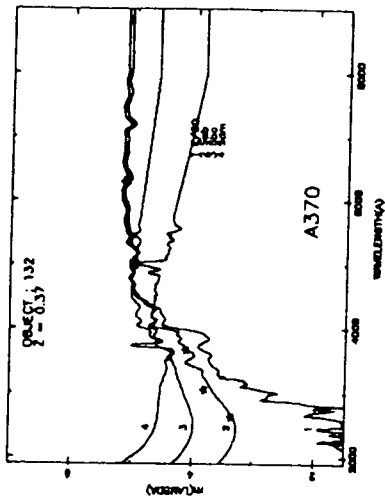
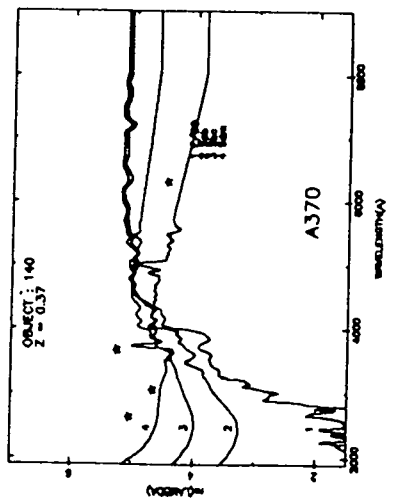
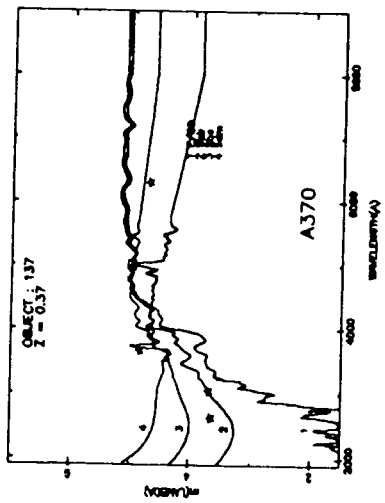
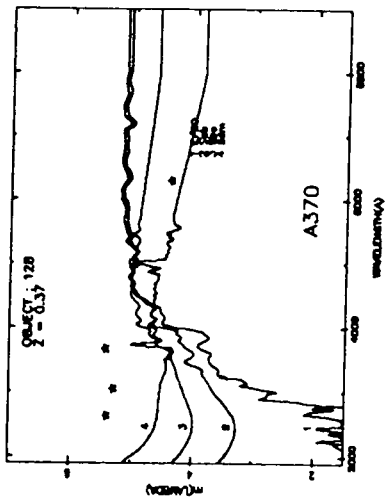


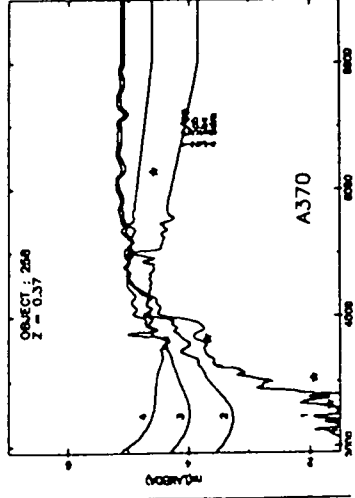
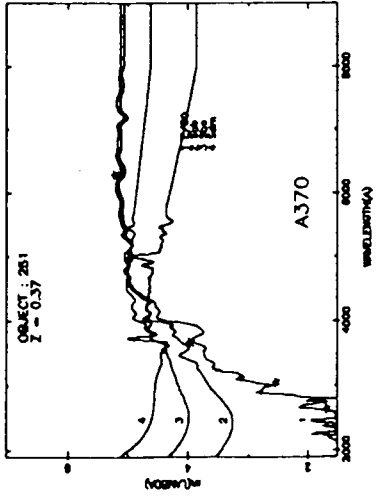
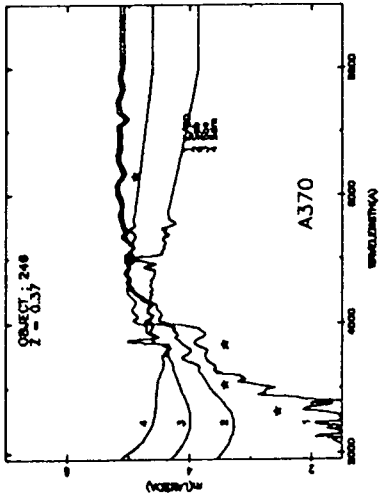
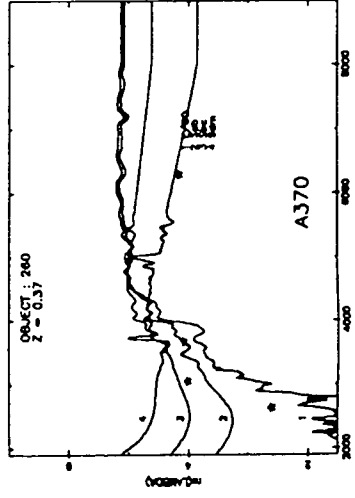
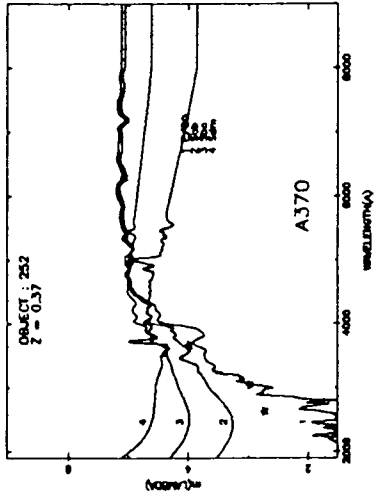
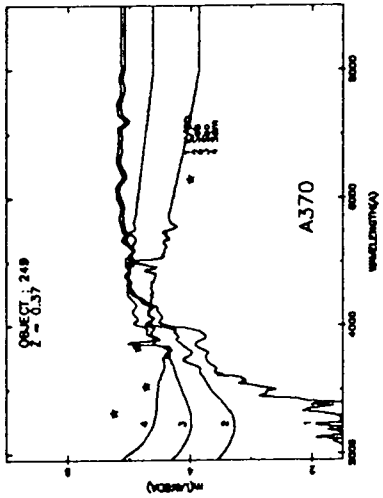
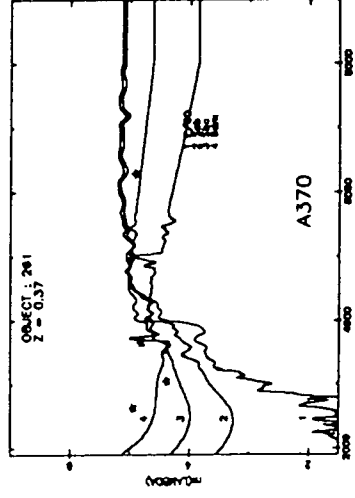
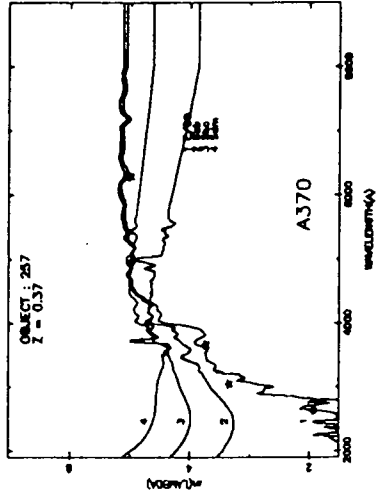
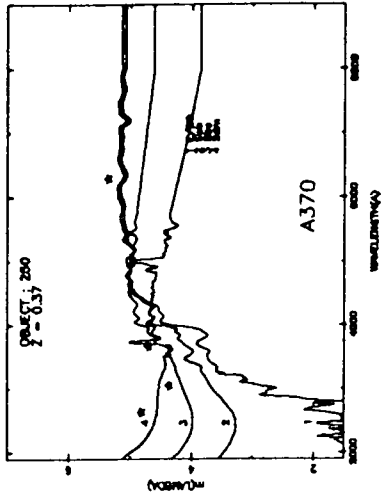












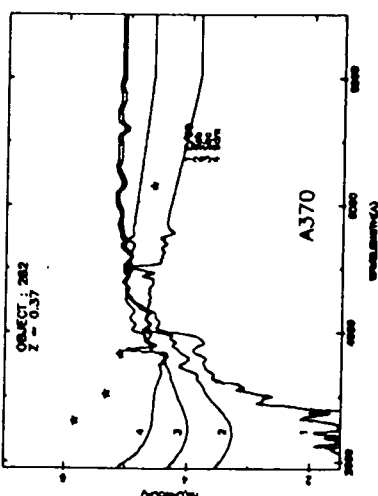
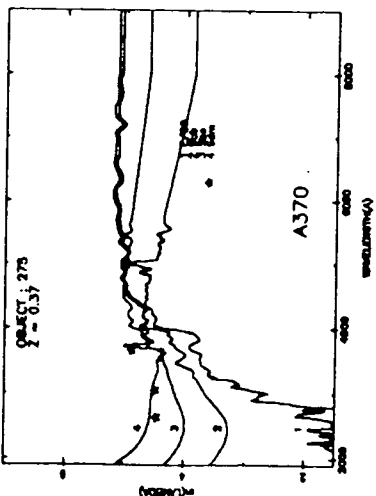
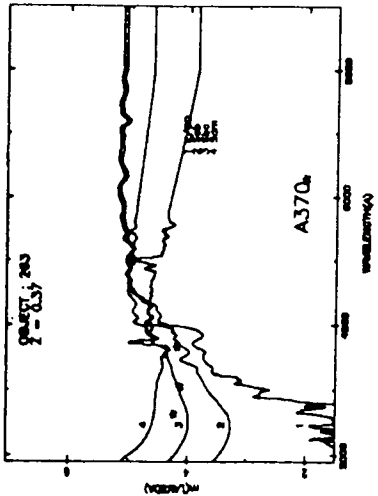
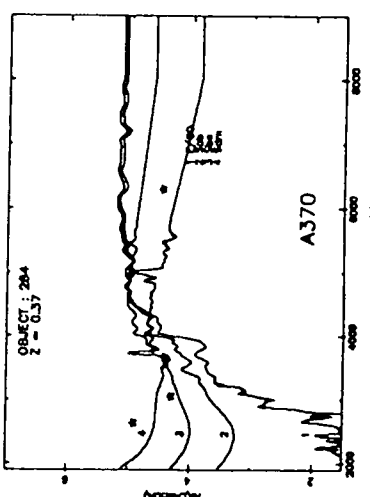
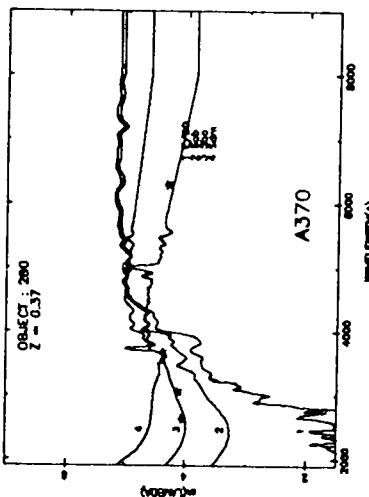
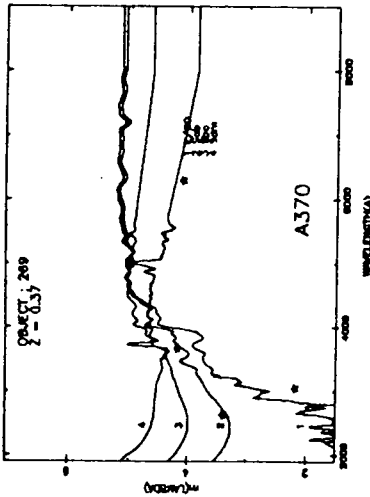
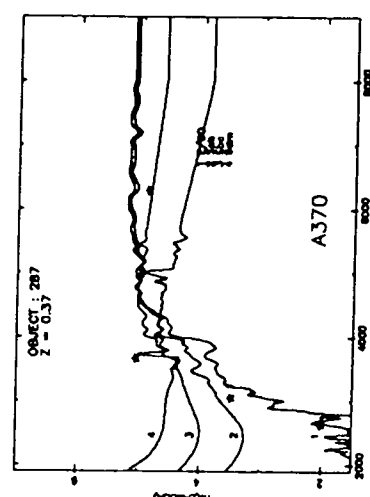
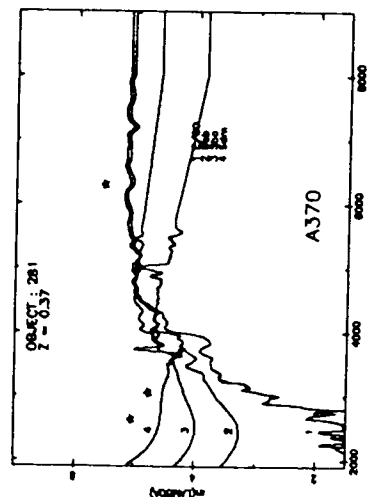
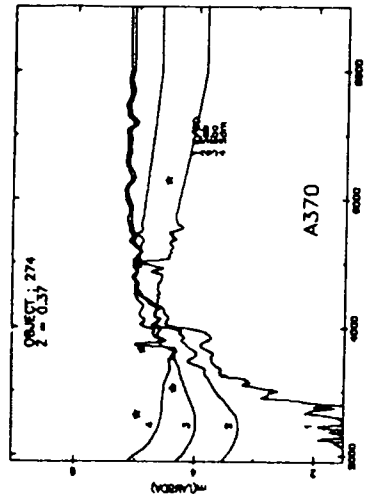


Table 4.3: A370 Object Classifications

CCD#	BO#	RA(1950)			Dec(1950)			R_F	z	Type
128	16	02	37	13.9	-01	48	2.8	17.845	0.00	Star
107	9	02	37	20.6	-01	47	48.1	18.453	~0.37	E/S0
1	10	02	37	20.2	-01	47	10.6	18.470	~0.37	E/S0
53	15	02	37	15.9	-01	46	32.1	18.621	~0.25	E/S0
81	-	02	37	24.0	-01	47	18.5	18.820	~0.37	E/S0+uv
125	21	02	37	16.2	-01	47	25.5	18.880	~0.37	E/S0
20	29	02	37	18.8	-01	47	43.5	18.901	~0.37	E/S0+uv
47	34	02	37	18.3	-01	46	45.0	18.992	~0.37	E/S0
42	24	02	37	20.0	-01	46	33.9	19.028	~0.37	E/S0
31	26	02	37	22.8	-01	46	57.2	19.044	~0.37	E/S0
32	43	02	37	22.1	-01	46	47.1	19.124	~0.37	E/S0
66	39	02	37	21.9	-01	46	27.8	19.166	0.2-0.4	Scd
29	41	02	37	23.3	-01	47	11.1	19.193	~0.37	E/S0
49	45	02	37	17.2	-01	46	48.1	19.265	~0.37	E/S0
137	56	02	37	11.7	-01	47	1.5	19.294	~0.37	Sab
94	-	02	37	21.7	-01	48	0.6	19.306	~0.37	E/S0
15	61	02	37	19.3	-01	47	11.6	19.331	~0.37	E/S0
3	-	02	37	20.2	-01	47	16.5	19.341	~0.37	E/S0
55	37	02	37	17.7	-01	46	21.5	19.358	~0.37	E/S0
80	-	02	37	23.9	-01	47	20.7	19.376	~0.37	E/S0
102	49	02	37	20.8	-01	47	55.8	19.377	~0.37	E/S0+uv
36	245	02	37	21.5	-01	46	43.6	19.396	~0.37	E/S0
68	66	02	37	19.0	-01	46	33.5	19.407	~0.37	E/S0
22	63	02	37	20.0	-01	47	34.9	19.442	~0.37	E/S0
83	70	02	37	25.3	-01	47	26.2	19.455	~0.37	E/S0
54	-	02	37	15.6	-01	46	24.1	19.486	~0.37	Scd
105	-	02	37	20.2	-01	47	53.3	19.535	~0.37	E/S0
14	84	02	37	19.1	-01	47	8.5	19.571	~0.25	E/S0
12	80	02	37	20.4	-01	47	1.0	19.628	~0.37	E/S0
46	256	02	37	18.6	-01	46	48.5	19.668	~0.37	E/S0+uv
27	544	02	37	22.1	-01	47	32.3	19.730	~0.37	E/S0+uv
86	106	02	37	24.2	-01	47	56.8	19.739	~0.37	E/S0+uv
28	111	02	37	23.0	-01	47	13.5	19.785	~0.37	E/S0
144	-	02	37	12.7	-01	46	29.0	19.796	0.3-0.4	Sab
4	58	02	37	19.9	-01	47	20.7	19.801	~0.37	E/S0
50	99	02	37	16.9	-01	46	51.1	19.827	~0.37	E/S0
70	128	02	37	18.4	-01	46	37.0	19.833	~0.37	Scd
110	94	02	37	19.7	-01	48	4.1	19.834	~0.37	E/S0
82	115	02	37	25.0	-01	47	23.8	19.838	0.2-0.4	Scd/Sdm
133	113	02	37	11.8	-01	47	41.0	19.854	~0.37	Sab
2	-	02	37	20.5	-01	47	13.7	19.880	~0.37	E/S0
127	148	02	37	10.9	-01	48	9.5	19.903	~0.37	E/S0
126	102	02	37	15.3	-01	47	32.0	19.915	~0.37	E/S0
106	-	02	37	20.4	-01	47	53.4	19.926	~0.37	E/S0
6	124	02	37	19.1	-01	47	24.4	19.945	0.3-0.4	E/S0
108	176	02	37	20.7	-01	47	41.3	19.964	~0.37	Scd
124	151	02	37	17.5	-01	47	48.2	19.966	0.2-0.4	Scd/Sdm
93	128	02	37	22.0	-01	47	56.7	19.978	~0.37	Scd
91	119	02	37	22.0	-01	47	46.6	19.982	~0.37	E/S0
26	-	02	37	22.0	-01	47	27.1	19.986	~0.37	E/S0
18	166	02	37	17.5	-01	47	7.3	20.028	~0.37	E/S0
90	165	02	37	22.2	-01	47	44.9	20.033	~0.37	Scd

CCD#	BO#	RA(1950)			Dec(1950)			R_F	z	Type
79	149	02	37	23.8	-01	46	51.5	20.043	~0.37	E/S0
138	145	02	37	13.6	-01	46	56.5	20.047	~0.37	Sbc
69	131	02	37	18.1	-01	46	34.2	20.049	~0.37	E/S0+uv
109	142	02	37	19.2	-01	48	1.5	20.100	~0.37	E/S0+uv
16	-	02	37	18.9	-01	47	12.9	20.154	~0.37	E/S0
88	161	02	37	22.9	-01	47	37.7	20.161	~0.37	E/S0
33	153	02	37	22.7	-01	46	42.9	20.187	~0.37	E/S0
23	133	02	37	21.5	-01	47	28.1	20.195	~0.37	E/S0
21	154	02	37	19.0	-01	47	40.9	20.243	~0.37	E/S0
103	-	02	37	20.5	-01	47	56.7	20.302	~0.37	E/S0+uv
19	164	02	37	17.8	-01	47	15.0	20.330	~0.37	Sbc/Scd
9	232	02	37	21.0	-01	47	23.4	20.332	~0.37	Sab
252	-	02	37	6.9	-01	47	46.6	20.334	~0.37	E/S0
84	203	02	37	25.0	-01	47	33.8	20.376	~0.37	E/S0+uv
35	55	02	37	21.7	-01	46	41.1	20.399	~0.37	Scd
89	226	02	37	22.7	-01	47	39.0	20.401	~0.37	Scd
30	213	02	37	23.1	-01	47	6.7	20.416	~0.3	E/S0
250	-	02	37	4.9	-01	48	5.0	20.433	0.2-0.4	Scd
71	168	02	37	18.8	-01	46	32.8	20.445	~0.37	E/S0
140	201	02	37	14.3	-01	46	34.9	20.473	~0.37	Scd/Sdm
24	247	02	37	22.1	-01	47	18.8	20.475	0.2-0.4	Scd?
11	219	02	37	21.3	-01	47	15.5	20.496	~0.37	E/S0+uv
52	-	02	37	15.8	-01	46	40.4	20.499	~0.37	E/S0
292	314	02	37	20.9	-01	50	5.7	20.511	>0.5	Scd
85	239	02	37	25.4	-01	47	48.1	20.529	~0.37	Scd
275	329	02	37	17.2	-01	49	41.9	20.573	0.2-0.4	Scd
25	-	02	37	22.4	-01	47	21.6	20.583	~0.37	Scd
274	-	02	37	9.5	-01	46	54.8	20.599	0.2-0.4	Scd/Sdm
245	235	02	37	9.4	-01	48	8.0	20.604	>0.5	Sab
5	230	02	37	19.8	-01	47	23.4	20.609	~0.37	E/S0
77	-	02	37	24.8	-01	46	56.4	20.663	0.2-0.4	Scd
101	-	02	37	21.2	-01	47	54.9	20.664	0.2-0.4	Scd
10	238	02	37	21.0	-01	47	28.5	20.702	~0.37	E/S0
100	136	02	37	20.5	-01	48	4.6	20.712	~0.37	Scd
139	231	02	37	14.8	-01	46	49.2	20.736	~0.37	Scd
13	255	02	37	19.7	-01	47	2.5	20.782	~0.37	E/S0
57	293	02	37	20.1	-01	46	17.3	20.796		Steep spectrum
17	308	02	37	18.1	-01	47	10.9	20.801	~0.37	E/S0
45	256	02	37	18.8	-01	46	50.7	20.802	0.2-0.4	Scd
87	311	02	37	23.1	-01	47	34.5	20.840	~0.37	E/S0
40	220	02	37	20.4	-01	46	43.3	20.865	~0.37	E/S0 (no U)
8	363	02	37	20.7	-01	47	20.9	20.872	~0.3	E/S0
78	257	02	37	23.5	-01	46	42.0	20.882	~0.37	E/S0-Sab
123	249	02	37	17.1	-01	47	39.1	20.884	~0.37	Sab
56	280	02	37	19.6	-01	46	16.3	20.927	0.5-0.6	Sbc
37	-	02	37	21.6	-01	46	52.1	21.092	~0.5:	E/S0:
122	316	02	37	16.7	-01	47	41.9	21.108	~0.37	E/S0
41	251	02	37	20.2	-01	46	39.8	21.113	~0.37	E/S0
44	372	02	37	19.7	-01	46	53.3	21.139	0.2-0.4	Scd
51	409	02	37	16.3	-01	46	52.5	21.197	~0.6	Sbc
39	227	02	37	20.5	-01	46	49.3	21.203	~0.37	E/S0

CCD#	BO#	RA(1950)			Dec(1950)			R_F	z	Type
249	-	02	37	6.5	-01	48	0.3	21.215	~0.37	Sdm
132	-	02	37	12.7	-01	47	44.3	21.299	~0.37	Sab
257	53	02	37	9.4	-01	47	5.2	21.332	~0.37	E/S0
261	-	02	37	7.0	-01	46	47.7	21.344	~0.37	Scd/Sdm
67	303	02	37	19.1	-01	46	41.7	21.385	0.5-0.6	E/S0
246	126	02	37	10.1	-01	48	1.4	21.473	~0.37	E/S0
251	183	02	37	5.7	-01	47	42.7	21.478	~0.37	E/S0
290	427	02	37	22.6	-01	50	17.6	21.506	>0.5	Scd/Sdm
258	78	02	37	8.5	-01	47	7.2	21.582	>0.45	E/S0
141	-	02	37	14.5	-01	46	29.9	21.619	0.75?	Sab
263	-	02	37	5.0	-01	47	1.8	21.664	~0.37	Sbc/Scd
280	262	02	37	17.8	-01	49	55.4	21.697	0.4-0.6	Sbc
284	208	02	37	24.3	-01	49	41.2	21.782	~0.37	Scd
297	187	02	37	19.0	-01	50	39.5	21.822	~0.37	Scd
295	-	02	37	18.2	-01	50	30.5	21.879	~0.37	Scd
282	425	02	37	18.8	-01	49	40.3	21.943		Steep Spectrum
287	40	02	37	24.7	-01	50	4.9	22.184	~0.37	E/S0
281	-	02	37	19.0	-01	49	43.1	22.211	~0.37	Scd/Sdm

He found that of 184 galaxies measured within a 2.6 arcmin radius, 34% were classified as blue or 'spiral' types. This is equivalent, approximately, to a blue fraction, $f_b \sim 0.19$ in Butcher and Oemler's scheme (Couch, 1986, private communication).

Using the SED method we should be able to independently check these conclusions. This present sample covers a smaller area than Couch's previous work. From the SED classifications of table 4.3 the relative proportions of each class of object (those identified as cluster members) are as follows:

$$E/S0 : 76\%, Sab : 6\%, Sbc : 2\%, Scd : 15\%, Sdm : 1\%.$$

Couch, however, observed a 66%:34% division between E/S0s and spirals within his data. The difference between this result and the CCD populations could be due to the different sizes of region sampled. Consequently, Couch (1987, private communication) has determined the local galaxy density for the present sample and finds that it is a factor two higher than in his more extended sample. This analysis results in an expected spiral fraction of 11% within the CCD area compared with 15% in the photographic sample. The reduced spiral fraction observed in the CCD data ($\frac{24}{34} = 0.70$) is in very close agreement with the expected difference ($\frac{11}{15} = 0.73$), implying that we observe the same spiral excess as did Couch.

In terms of Butcher and Oemler's method, a rest-frame $B - V$ blueing of 0.2 magnitudes compared to an E/S0 galaxy corresponds approximately to Sbc and later type galaxies. In the CCD sample there are some 13 objects which fall into this blue category out of a membership of 78, ie a blue fraction of 18%. This is in good agreement with Butcher and Oemler's value of $21 \pm 5\%$ for the blue fraction.

However, not only does our SED method find a large spiral fraction, but interestingly, as table 4.3 verifies, most of these blue galaxies are late-type spirals, which are rarely seen in a cluster environment at the present epoch. In this context we should also remember, as we discussed in chapter 2, the error on galaxy classifications is greater for bluer objects. Nevertheless this is an important result which we shall refer to in the following chapter when we discuss possible evolutionary models for galaxies in high redshift clusters.

4.5 Spectral Evolution of Early-type Galaxies in A370.

In our previous work we have used the colour-magnitude (CM) effect (eg. Visvanathan and Sandage, 1977) for early-type galaxies as a diagnostic tool for galaxy evolution. As, for example, in the case of 0016+16 the CM effect enabled us to select a very clearly defined sequence of early-type galaxies in the optical colours. We were then able to study the behaviour of these as we moved into the rest frame uv. We will now undertake a similar analysis for the present data.

For comparison of the observed CM-relation with that expected from studies of nearby early-type galaxies we have to firstly consider the amount of foreground reddening in the field of A370.

(a) Foreground Reddening.

Two estimates of the foreground reddening to A370 are available to us through (i) the work of Couch (1981) who, from a study of the colour distribution of field galaxies in the vicinity of A370, derived a reddening of $E_{(B-V)} = 0.12 \pm 0.05$, and (ii) the method we have used for 0016+16 in chapter 3 and originally developed in Ellis *et al* (1983), for measuring the reddening directly from the observed SEDs using the information redward of ~ 550 nm.

In the latter case we are able to follow the procedure of the previous chapter where the reddening estimation is based on both our intermediate-band data and also infra-red (ir) photometry. This is made possible through AAT photometry that Couch and Sharples (1986,

unpublished) have obtained in H (and sometimes J and K) using a 4.5 arcsec aperture for 11 of the galaxies in our sample. These measures together with the 685 and 862 magnitudes observed throughout the same sized aperture are converted to fluxes via our white dwarf calibration and then compared with the redshifted present-day SED for the morphological class into which the object was classified above (10 of the 11 galaxies are E/SO). The difference between the two at each wavelength point is converted to an $E_{(B-V)}$ value using Seaton's (1981) reddening law and the mean over all points is taken to be the $E_{(B-V)}$ for the object. Due to the photometric errors involved (the ir-magnitudes alone have a scatter of ± 0.07 mag) the precision of the method (per individual measurement) is $\sim 10\%$.

The large number of objects available for measurement in A370 allows us to derive a mean $E_{(B-V)}$ for the cluster with a small uncertainty. Surprisingly, however, we find the reddening to be negative with $\langle E_{(B-V)} \rangle = -0.104 \pm 0.020$. We stress this is not the result of a spurious $E_{(B-V)}$ value being obtained at one of the wavelength points in each object; even when 3 ir-magnitudes were available all points gave consistently negative values. It would therefore appear that some systematic error is the reason for this erroneous reddening. It is conceivable that the zero-point of our 685 magnitude scale is in error. Since our data are standardised at the 685 point it would, for example, require our 685 magnitudes to be too bright by only 0.16 mags to account for the difference between the $E_{(B-V)}$ derived here and Couch's value. However, the fact that we find very good agreement between the observed E/SO CM-sequence and that predicted in 418-685 and 502-685 (see below) makes this latter explanation somewhat unlikely. We regard the most likely source of this error to be the near-ir to ir regions of the present-day SEDs which are very poorly defined.

Having not been able to obtain a satisfactory measurement of the reddening in A370 from Couch and Sharples' data we shall adopt the value estimated by Couch. It will also be seen that our CM-data provide support for making a reddening correction of this size; without the correction the 418-685 and 502-685 CM-sequences appear far too red with respect to the predictions.

(b) *Luminosity Evolution.*

The method we defined in chapter 3 to investigate the effects of luminosity evolution in distant galaxy clusters, can readily be applied to our present data. Once more we use Metcalfe's Coma luminosity function (LF) to define the no-evolution case. The normalised cumulative LFs of Coma (at $z = 0.37$) and A370 are plotted in fig. 4.5, where it is evident that the bright end of the A370 LF is substantially enhanced over that of Coma. Indeed, the implicit luminosity evolution of some $M_V = 0.5$ mags, is quite considerable, although, as we noted in the previous chapter, we must be cautious of over-interpretation of such results. In particular, as we have discussed in the previous chapter, the validity of adopting the Coma LF as a 'standard' for rich clusters is somewhat suspect, the very notion of there being such a 'standard' form at bright magnitudes is probably unrealistic (Dressler, 1978).

A370 is a very rich cluster and as such it is not clear that it possesses an obvious nearby counterpart. We should note also that the dynamical structure of the cluster, as implied from its visual appearance, is that of two rich galaxy concentrations. Over the lookback time to $z = 0.37$, dynamical processes, such as cannibalism (eg, Ostriker and Tremaine, 1977) may be expected to modify the top of the cluster LF by depleting the numbers of bright galaxies as they are consumed by the dominant members.

We conclude, then, as in the previous chapter that this method is dependent on the LFs of nearby rich clusters being similar to Coma at the bright end. Since Dressler's results cast doubt on such an assumption we should view the present result as being only an indicator of the possible presence of luminosity evolution, but that another indicator, such as M^* should be considered for more detailed study.

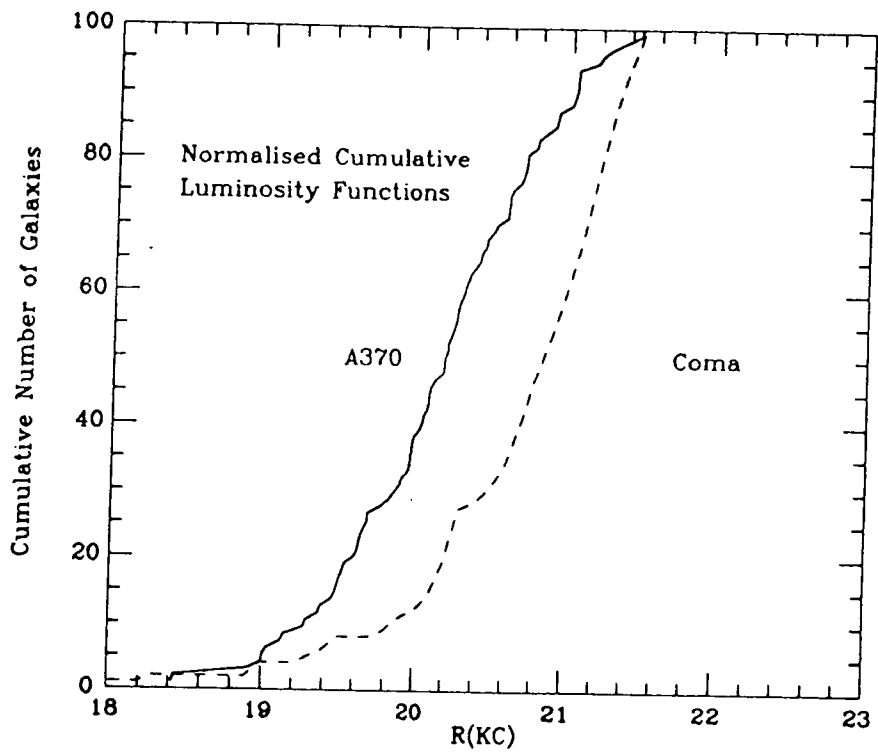


Figure 4.5: Normalised Cumulative LFs for A370 and Coma (Metcalf, 1983).

(c) Colour Evolution.

The technique we have developed in earlier chapters to investigate spectral evolution of galaxies in distant clusters is based on monitoring the behaviour of the observed colour-magnitude relation as we move shortwards in wavelength from optical to ultraviolet colours. The 502-685 (restframe U-V) vs R_F CM-relation for A370 is shown in figure 4.6(a), where we have represented different galaxy types by various symbols (see figure caption), the classifications being taken from table 4.3. From the figure we can see exactly how well-defined the CM-relation for early-type galaxies (filled circles) is with such a tight scatter about the mean relation. Note that the predicted CM line (denoted by the solid line in the figures), defined by the simple method described earlier and including the adopted reddening, lies very close to the observed relation. If the effect is universal (at least in clusters) as is implied here and in the earlier work of Visvanathan and Sandage (1977), any evidence for significant deviations from the mean relation may well be indicative of evolutionary changes, as we shall discuss shortly.

Reaching rest wavelengths of $\sim 3000\text{\AA}$ in the 418-685 colour (Fig. 4.6(b)) the relation shows more scatter, as we expect from increasing errors. However, in the $U-685$ CM diagram this scatter is considerable (Fig. 4.6(c)). As we discussed earlier (section 3.2), the errors in this colour are dependent on the exact location of the given object on the CM-plane. Using our repeat frame analysis we have plotted representative error bars for many of the objects in different regions of the diagram. We have also indicated the predicted slope and scatter determined using Couch's(1981) method of simulating the CM-effect by using combinations of ultraviolet-optical spectra of M31 and M15 described in chapter 3 and re-examined in chapter 5. It can now be seen that the scatter in Fig. 4.6(c) is not purely random, but rather there is a class of blue object with errors that are small in comparison to their separation from the predicted relation. The implication, then, is that such objects have uv colours significantly bluer than those of nearby E/S0 galaxies. Some ~ 10 galaxies have significant ($> 4\sigma$) ultraviolet excesses when compared with the predictions. Figure 4.7 shows typical SEDs of two of these objects. Note that although in both cases the 418-685 colour is very close to that expected of an E/S0 galaxy, the uv colours are very blue.

In the previous chapter we interpreted similar results as being due to increased levels of star formation being present in these galaxies, either as a result of a 'passive' evolution in star formation such as in Bruzual type models, or some more dramatic event, occurring perhaps in disc galaxies. We shall discuss these effects in considerably more detail in the following chapter, but for the present we shall briefly outline the implications of our current observations of A370.

Firstly, we can compare the colours of our uv-excess galaxies with predictions made on the basis of Bruzual's evolutionary models. The expected colours from a single initial burst of star formation (c-model) and that of an exponentially decreasing star formation rate ($\mu = 0.5$) are indicated in figures 4.6(a)-(c). Neither of these models may be capable of explaining the colours of the bluest of our uvx galaxies. In particular the observations tend to suggest a steeper rise in uv colour than would be expected, suggesting that the star formation occurring in such objects is perhaps, more vigorous than that due to such a gradual decline in star formation. However, this result is not entirely clear as the errors in these passbands are fairly large.

The key fact to note is that rather than all of the galaxies evolving in this manner, we find a range in colours, with most (80%) of our early-type members having colours compatible with no-evolution at all over the past 5 Gyr. In other words only a subset of the early-type galaxies have evolved significantly over this period.

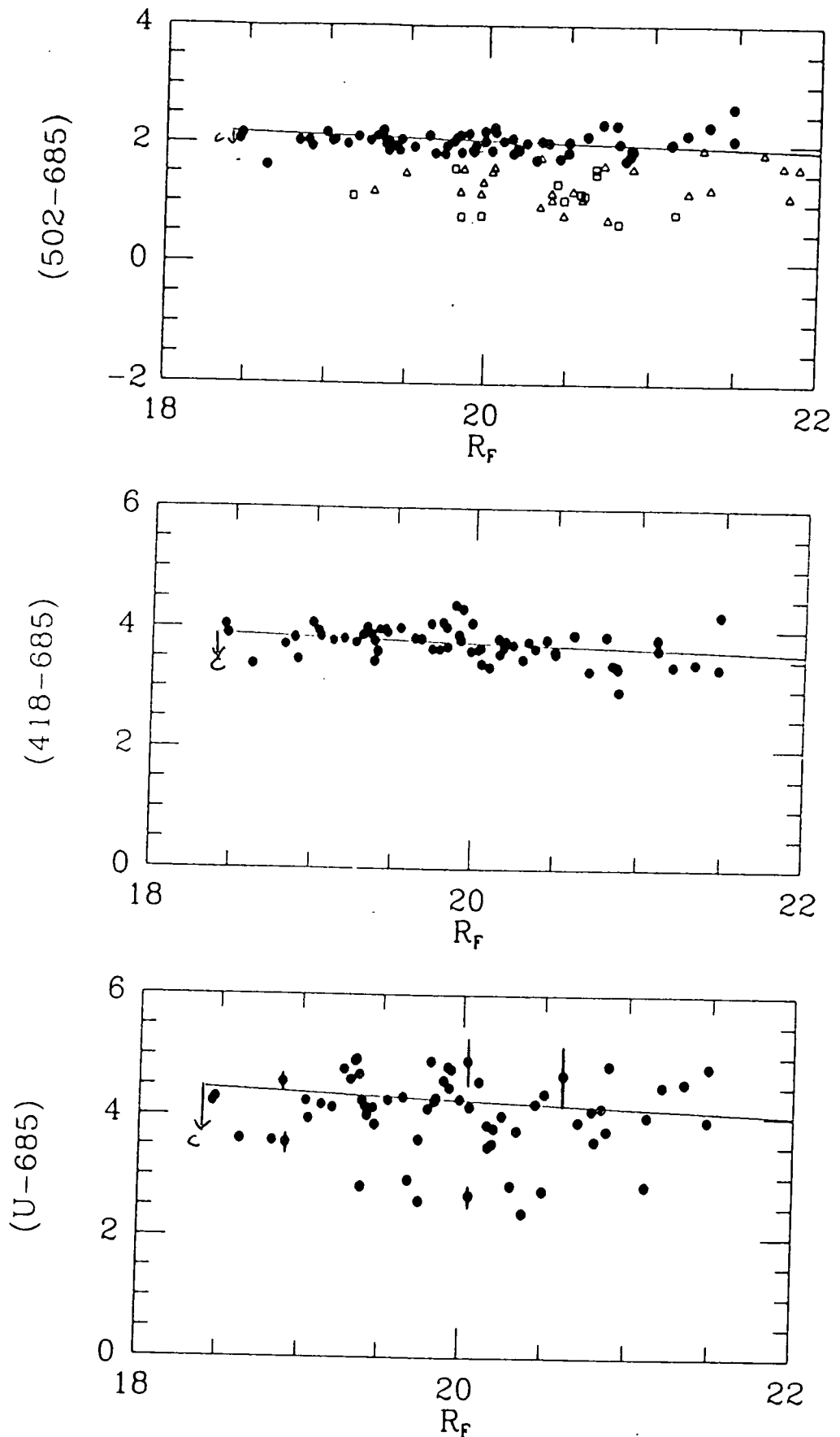


Figure 4.6: Colour-magnitude diagrams for galaxies classified via the SEDs as being members of A370. Solid lines represent the expected relations from present-day galaxies. (a) 502-685, all members: E/S0s (filled circles), spirals (triangles), and unclassified possible members (squares). (b) 418-685, E/S0s only. (c) U-685, E/S0s with representative error bars.

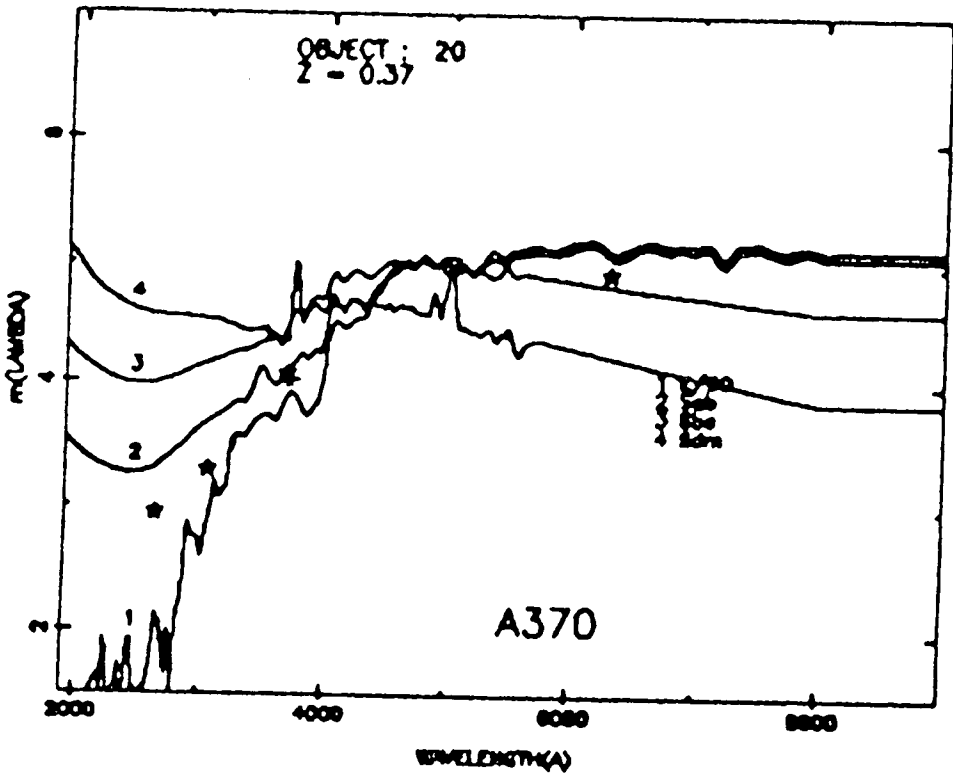
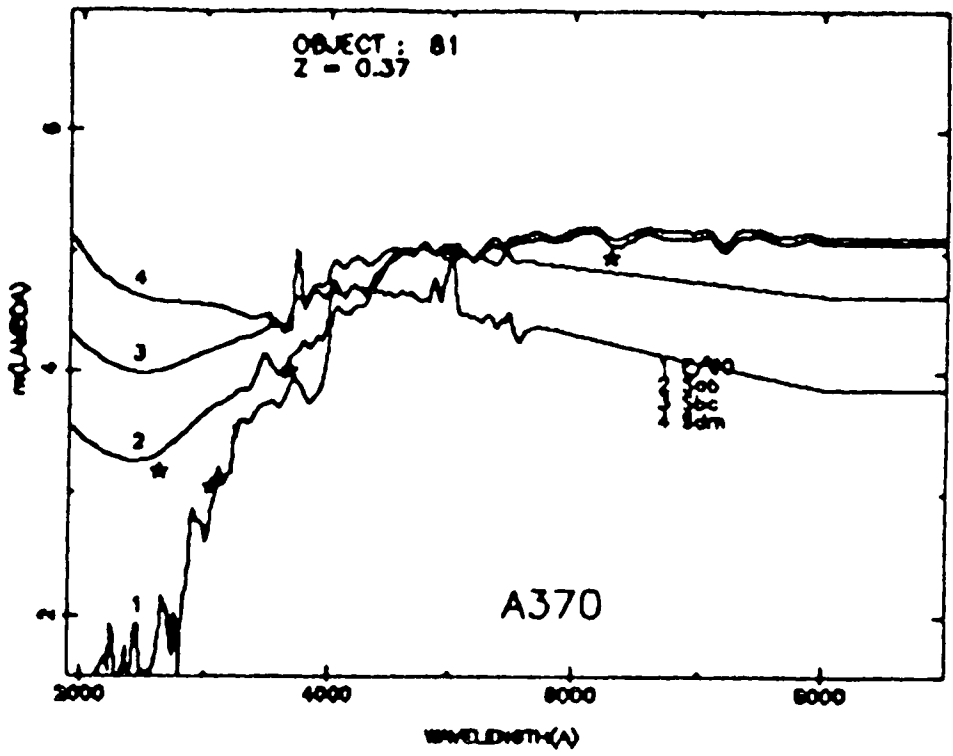


Figure 4.7: SEDs of two examples of 'uvx' galaxies found in the cluster A370.

A further two possible clues as to the underlying mechanism for such apparent evolution can be obtained from these CCD observations. Firstly, important information may reside in the detailed structure of the individual galaxy images, ie, are there any suggestions of discs in these objects? Unfortunately this approach cannot be further studied in detail using the present data since we lack the necessary spatial resolution (see eg, Thompson, 1986). However, at the simplest level we should be able to say whether the galaxies show extended or centrally-concentrated images in the individual uv image frames. Figure 4.8 shows image profiles of some of the uvx and E/S0 galaxies in comparison to stellar profiles constructed in the manner described in the previous chapter. It would appear, then, that the uv light from the uvx galaxies is not discernably different from that of non-uvx galaxies. We should note that the seeing during these observations was rather poor.

Another suggestive property of the present data may also provide us with a further clue. If we consider the spatial distribution of the uvx galaxies within the cluster, as shown in Fig. 4.1., we note that there is a tendency to avoid the cluster core, as well as a congregation of blue and uvx galaxies associated with the arc-like structure observed by Lynds and Petrosian (1986). Such a result could be interpreted as tentative evidence for an environmental process (eg, ram-stripping or shock induced pressure on galaxy as it passes through the cluster core regions).

I shall discuss the implications of these observations in the context of evolutionary models in greater detail in chapter 5 and so shall suspend further discussion of these topics until then.

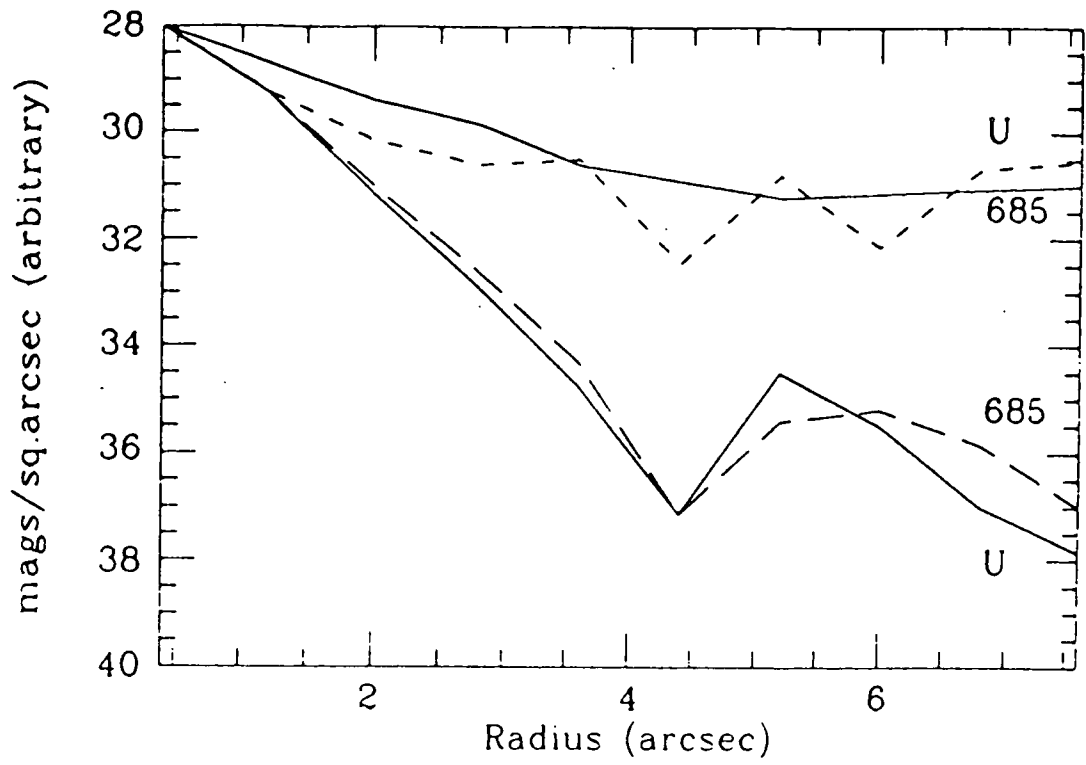
4.6 Spectroscopy.

Whilst this cluster is one of our targets in a planned program of multi-object spectroscopy, at the present time we have only a limited number of spectra available. However, Bernard Fort and Yves Mellier at the Observatoires du Pic-du-Midi et de Toulouse, have used A370 to test their recently developed multi-aperture spectrograph at the Canada-France-Hawaii Telescope on Mauna Kea. Although their results are only of a preliminary nature, they have very kindly provided us with their spectroscopic identifications for a number of galaxies in our CCD field (now also in Mellier *et al*, 1987). Furthermore, Henry and Lavery(1987) have also observed this cluster.

Table 4.4 lists all the available spectroscopy of A370 from the above references and also from the limited observations of Couch, Ellis and D'Odorico (1986, private communication). We should note the various selection methods used by these different authors in compiling their lists of target objects. Henry and Lavery, being interested in the Butcher-Oemler effect, selected primarily blue objects. Fort and Mellier have similar selection methods. Couch, Ellis and D'Odorico selected, in a single multi-slit exposure with the ESO 3.6m EFOSC system, a number of E/S0s classified via the SED technique as having an ultraviolet excess.

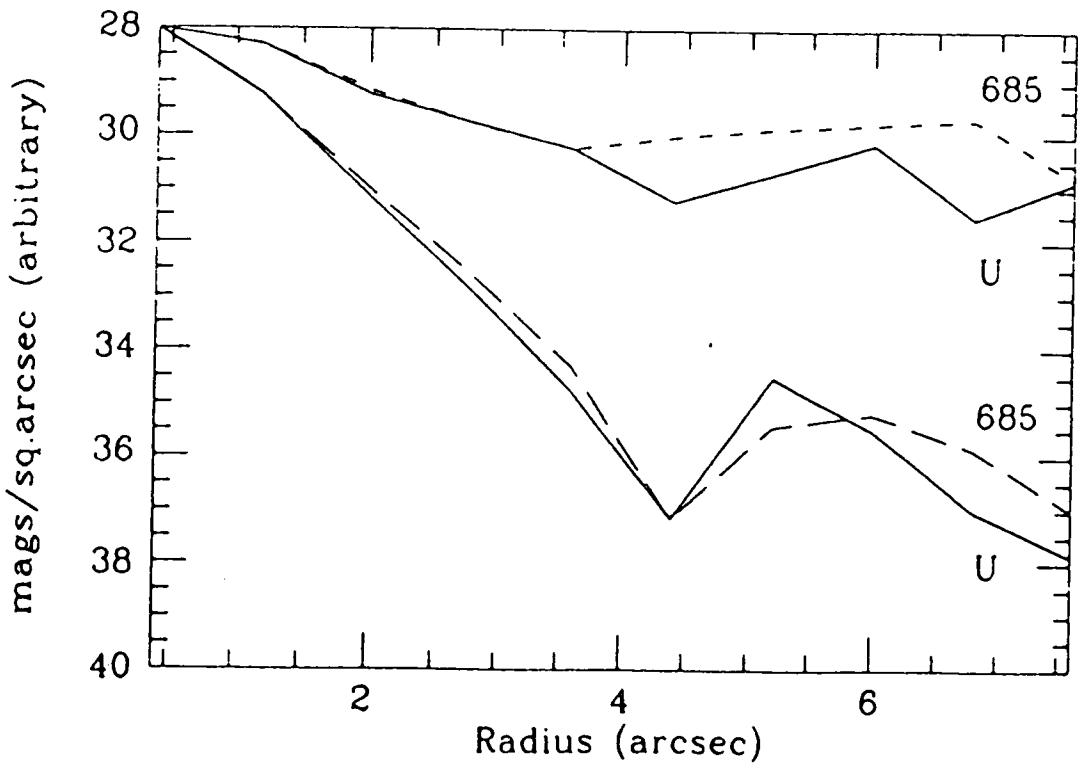
There are some 23 galaxies in common to the SED and spectroscopic samples to $R = 20.0$. The agreement is excellent despite the spectroscopy being biased to blue objects where the SED method is intrinsically less accurate. Only six galaxies have SED classifications discrepant with the spectroscopy, which we shall now examine in detail.

Firstly, there is some confusion over objects #4 and #50, which Mellier *et al* claim are background E/S0s, whereas the SED classification very clearly puts these two objects at the cluster redshift. With such red colours the SED method should be accurate enough to distinguish redshift differences of this order (indeed the SEDs are very good fits for $z = 0.37$), so this result is very surprising.



E/S0(10)

Star(128)



UVX(102)

Star(128)

Figure 4.8: Surface brightness profiles (in arbitrary units) with radius for the brightest representative uvx and non-uvx galaxies in A370.

Table 6: Spectroscopy of A370.

CCD	BO	R_p	z	Source	Features	SED class
107	9	18.45	0.374	M	E	E/S0
			0.365	BO	sp	
1	10	18.47	0.379	M	E	E/S0
53	15	18.62	0.201	HL	-	$z = 0.25$ E/S0
			0.250	M		
81	-	18.82	0.37	M	E	E/S0+uv
125	21	18.88	0.366	HL	-	E/S0
			0.370	M	E	
20	29	18.90	0.370	HL	-	E/S0+uv
			0.371	M	E+A	
			0.37	CED	E	
47	34	18.99	0.378	M	E	E/S0
42	24	19.03	0.375	M	Sp	E/S0
31	26	19.04	0.382	M	E	E/S0
32	43	19.12	0.383	M	E	E/S0
66	39	19.17	0.374	HL	sp	Scd
			0.375	M	sp	
			0.375	BO	sp	
29	41	19.19	0.375	HL	-	E/S0
			0.377	M	E	
49	45	19.27	0.368	M	E	E/S0
137	56	19.29	0.177:	HL	-	Sab
			0.17	M	sp	
102	49	19.38	0.378	M	sp	E/S0+uv
46	256	19.67	0.37	M	sp(weak)	E/S0+uv
68	66	19.41	0.370	M	sp	E/S0
			0.361	HL	E+A?	
			0.37	CED	E	
27	105	19.73	0.37	M	sp(weak)	E/S0+uv
86	106	19.74	0.371	M	sp(weak)	E/S0+uv
4	58	19.80	0.460	M	E	E/S0
50	99	19.83	0.548	M	E	E/S0
70	128	19.83	0.358	HL	sp	Scd
62	107	19.85	0.37	CED	E	E/S0+uv
108	176	19.96	0.222	HL	-	Scd
124	151	19.97	0.253	HL	-	$z = 0.2 - 0.4$ Scd/Sdm
93	128	19.98	0.358	HL	sp	Scd
90	165	20.03	0.386	HL	?	Scd
79	149	20.04	0.382	M	sp	E/S0-Sab
69	131	20.05	0.37	M	sp(weak)	E/S0+uv
138	145	20.05	0.376	HL	sp	Sbc
19	164	20.33	0.227	HL		Sbc/Scd
140	201	20.47	0.230	HL		Scd/Sdm
85	239	20.53	0.384	HL	sp	Scd
139	231	20.74	0.31	HL		Scd
56	280	20.93	0.328	HL		E/S0+uv

Sources:

HL - Henry, JP and Lavery, RJ (1987) preprint.

M - Mellier, Y, Fort, B, and Soucail, G (1987) preprint.

BO - Butcher and Oemler (private communication)

CED - Couch, WJ, Ellis, RS and D'Odorico, S (unpublished)

Features:

E - E/S0 with no emission, large 4000 A break, red spectrum

E+A - as E/S0 with Balmer absorption lines

sp - [OII] emission or Balmer absorption lines

General notes:

- (i) Spectral features for HL have been deduced from their published spectra.
- (ii) All SED classifications have $z = 0.35 - 0.40$ unless otherwise indicated.

Another two of the discrepancies are objects #42 and #68 which are identified as E/S0s by the SED approach, but Mellier *et al* classify as spirals. Again this is surprising, particularly since both the SEDs show that these galaxies have uv colours typical of bright red E/S0s. Other than being a result of object misidentification these results are difficult to understand.

Galaxy #137 is classified as a spiral member by the SED approach whereas Henry and Lavery conclude from a weak spectrum that this is a foreground object. The only way to reconcile the SED with the lower redshift would be by ignoring the 502 point. However, we have no reason to do this and this case cannot be resolved until a better spectrum can be obtained.

Henry and Lavery have also obtained a redshift of $z = 0.22$ for galaxy #108, which is classified as a blue cluster member from its SED. Of the 5 late type galaxies in the spectroscopic sample to $R = 20.0$ this is the only discrepancy. Re-examining this and the two similar cases fainter than $R = 20$ (#19, 140), it is clear that the error in redshift from the SED method is a strong function of colour. When the 418-502 colour is very blue, the near uv minimum is removed, the SED becomes linear and a representative error for redshift precision seems to be about ± 0.15 .

Since there are these apparent discrepancies with some of the bluest objects (although not statistically significant) and Henry and Lavery also identify some 4 late-type galaxies in a foreground clump at $z \sim 0.20 - 0.25$ it may be worthwhile to re-address the question of foreground contamination.

The SEDs have classified 25 galaxies in our prime sample as being late type spirals, 10 of which also have spectroscopic redshifts (with 4 being non-members). Re-analysing the SEDs of the remaining objects to examine the possibility that they could be associated with a lower redshift of $z = 0.23$ rather than being cluster members, it can be seen that it is impossible to decide for, at most, 5 of these galaxies (less than half the number of definite blue members). At most the blue fraction can be as uncertain as $\sim 30\%$. It should be stressed, however, that this is the worst case possible and assumes that all 5 of these ambiguous objects are not in the cluster. We should note also that the SED sample is statistically complete and much larger than the spectroscopic one. In conclusion the spectroscopy still confirms that there are about twice as many blue galaxies in the cluster as expected for its richness and central concentration.

Of particular interest in this comparison is the spectroscopy of objects that the SED technique classified as being uvx galaxies. Some 9 such galaxies have available spectroscopy. Mellier *et al* have observed 7 of these galaxies, all of which they find to lie at the cluster redshift. Galaxy #81, which shows the weakest uv excess, has an optical spectrum which is apparently typical of an E galaxy at the cluster redshift. Object #20 is classified as an 'E+A' type spectrum and the remaining 5 galaxies are noted as having weak spiral absorption features in their spectra. Only one (#102) is noted as having emission lines present, this object has the largest uv excess in the sample and is associated with the arc-like feature near one of the central galaxy condensations (see figure 4.1).

Object #56 is observed by Henry and Lavery to have a redshift close to the cluster but does not actually constitute a member, nor do they classify this spectrum. The remaining galaxy, #62, has been observed by Couch, Ellis, and D'Odorico who have classified the spectrum as being that of an E galaxy.

In summary; of the 8 uvx galaxies confirmed spectroscopically as being cluster members, 6 display Balmer absorption lines, and two (which display only weak uv excesses) are noted as having E/S0 type spectra. Thus it would appear then that the uvx galaxies show signs of enhanced levels of past star formation, a suggestion to which we shall return in the next

chapter.

4.7 Summary and Conclusions.

In summary, then, our photometric investigation of the distant cluster A370 has revealed this object to be quite remarkable in comparison with nearby rich clusters. Not only is the cluster very rich in luminous members, but a large fraction of the constituent galaxies are found to be very blue, possessing SEDs typical of rather late-type spirals. Furthermore, we have discovered that a subset of the cluster's early-type population possesses enhanced levels of emission in the rest frame uv region, as was found in our earlier study of the cluster 0016+16.

These observations, taken together, are suggestive of an evolutionary explanation for the cluster's properties, with the blue galaxies (undergoing large amounts of star formation at the observed epoch) being the precursors of the red early-type galaxies which dominate such environments at the present epoch — ie the classical Butcher-Oemler effect. In such a picture then, our uvx galaxies may be those objects which have undergone a decline in blue luminosity, after a recent period of star formation, ie at an intermediate evolutionary stage between the blue and red members. This is a rather exciting possibility, and consequently we have decided to consider it in greater detail in the next chapter, collating all our available observations in 0016 and A370, and comparing the results with other published work and theoretical models.

5. Ultraviolet Colours and the Spectral Evolution of Galaxies in Distant Clusters.

5.1 Introduction.

In chapters three and four of this thesis we have presented observations of galaxy spectral energy distributions (SEDs) in rich clusters at high redshifts. Reaching to rest wavelengths of ~ 270 nm with samples of ~ 50 and ~ 100 galaxies per cluster we have thus assembled the largest set of ultraviolet photometry of galaxies published to date, providing an insight into the extent and possible nature of the spectral evolution of galaxies over the past 5–7 Gyrs.

The primary tool in such investigations is the ultraviolet colour-magnitude (CM) effect. In the previous two chapters the CM-diagrams revealed the presence of an unexpected difference in the uv brightness of some distant early-type galaxies when compared with their present-day counterparts. Whilst most of the distant early-type galaxies were found to lie near to the relation expected in the absence of significant amounts of spectral evolution, a subclass of objects was easily identifiable which exhibited enhanced uv luminosities, despite having the optical colours appropriate to red E/S0s.

I aim to address these topics in greater detail in this chapter. I begin by considering the available uv data on nearby galaxies. In section 5.2 I present satellite observations of a sample of nearby elliptical galaxies and discuss their implications for the present work. Following these results, section 5.3 addresses the comparison of our photometric observations of distant galaxies with a series of possible evolutionary models.

5.2 The Ultra-violet Colour-Magnitude Relation.

1. Introduction.

The interpretation of colour-magnitude diagrams of distant clusters is clearly dependent on our knowledge of the uv-SEDs of nearby galaxies. Whilst the relationship found by Visvanathan and Sandage (1977, and chapter 1) was observed down to $\sim 3200\text{\AA}$, shortward of this we have to rely on satellite-based observations. In the past, this study has been subject only to somewhat limited investigation. Couch (1981), for example, devised a method for producing the 'expected' uv CM relation based on satellite uv spectra of M31 (Coleman *et al*, 1980) and M15 (Dupree *et al*, 1979). Using the former to represent the bright, metal-rich end of the relation and the latter as the faint end, he mixed these two spectra together in different proportions to mimic the behaviour of galaxies of intermediate brightness/metallicities ($M_V = -22.4, -20.0, -18.0, -16.0, -14.0, -9.0$). These spectra (see figure 5.1) can then be used to evaluate the CM slope for any chosen colour. In the wavelength region at which these predictions overlap those of Visvanathan and Sandage very good agreement was found.

This was the approach adopted in chapters 3 and 4, Couch *et al* (1983), and also in Ellis *et al* (1985), but since it is based only on two uv spectra its validity may be somewhat suspect. Furthermore, its range of applicability should be limited by the observations of Oke *et al* (1981) that show large variations in the uv brightnesses in different E/S0 galaxies whose nature is not well understood (see e.g., Rocca-Volmerange, 1986, and discussion in chapter 1). In the light of such uncertainties and because our analysis of observations at high redshifts are so dependent on these effects, it is important to collate information on the present day uv uv-SEDs of early-type galaxies.

The International Ultraviolet Explorer (IUE) satellite has proven to be an outstandingly successful mission. Originally expected to have an operational lifetime of 3–5 years, today, some 8 years after launch, the satellite continues to be available to observers and is still producing many high quality spectra. The satellite consists of a 45 cm telescope for

exclusively spectroscopic observations and separate cameras allow the possibility of high resolution spectroscopy ($\sim 0.2\text{\AA}$) of bright objects or low resolution spectra ($\sim 7\text{\AA}$) of fainter sources.

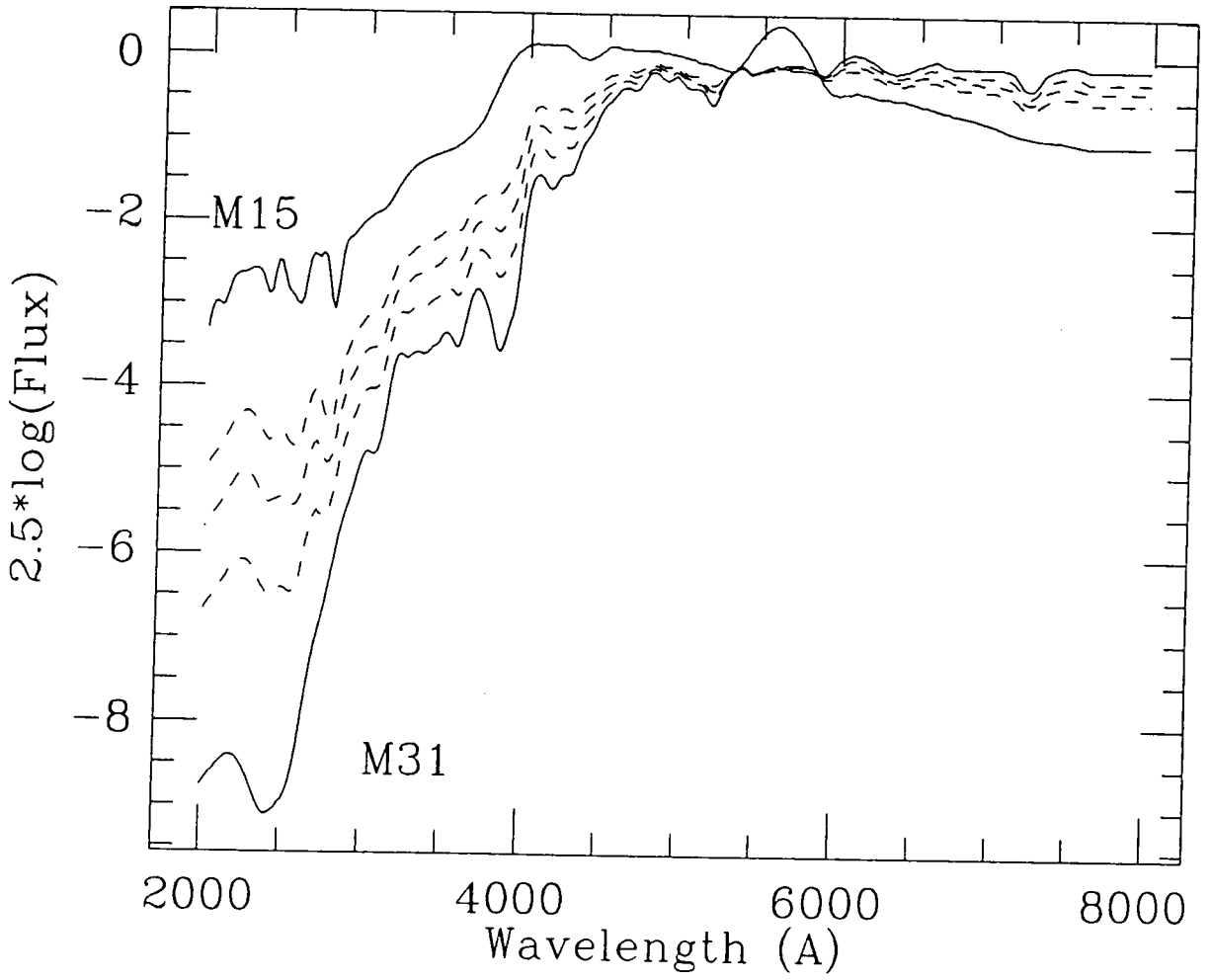


Figure 5.1: Couch's (1981) interpolated SEDs for use in colour-magnitude predications, based on M31 and M15.

The spectra are divided into two regions, short wavelength (1150Å–2000Å), and long wavelength (1800Å–3200Å), each spectrum being recorded on an imaging device (image converter plus SEC Vidicon television tube).

Although the detectors and instrumentation are particularly well suited to stellar observations, IUE has been successfully used for studies of nearby galaxies. Here we shall discuss our analysis of the spectra of several early-type galaxies taken from the IUE data archive as well as our own observations of the elliptical galaxy, NGC4621.

(2) *Observations and Data Reduction.*

The intention here is to study the extension of the CM effect into the uv of these nearby galaxies in order to predict the form and scatter about the CM relation for galaxies at high redshifts. The large intrinsic uv variations discussed above arise at wavelengths shortward of $\sim 2200\text{\AA}$, ie primarily in the short wavelength region. In our observations of distant galaxies, then, we have probed into the rest-frame uv only down to $\sim 2500\text{\AA}$ (our 418 nm filter is at 270 nm at $z = 0.54$). We will therefore be concerned only with observations obtained in the long wavelength cameras.

Three basic criteria determined the selection of spectra from the IUE data archives.

- (1) The spectra had to be of sufficiently good quality to allow reasonable uv colour determinations.
- (2) The objects selected should be in some sense representative of 'typical' E/S0 galaxies. Unfortunately, because of the low uv brightnesses of early-type galaxies, many of those studied by IUE were selected because of unusual blue colours caused by various mechanisms (eg. radio emission, ongoing star-formation).
- (3) Since it is important to use the same aperture in both passbands in any colour determination, the sample had to be further limited to those galaxies for which optical aperture photometry is available. This is an important point since the IUE aperture is fairly small in extent (approximately 10×20 arcsec oval), covering only the nucleus of each galaxy. However, as part of another research program, D. Burstein (Burstein, private communication) has very kindly provided his V band CCD photometry for many of these galaxies determined in the IUE aperture.

In addition to these archive observations I have also observed the elliptical galaxy NGC4621 using the IUE LWP camera on May 1st 1986 at the ESA VILSPA tracking station at Villafranca del Castillo. The final list of our chosen objects is presented in Table 5.1, where we include Burstein's V magnitudes and extinction estimates.

All the spectra were reduced using the IUEDR software package available on STARLINK (see Starlink User Note 72), which enables flux and wavelength calibrations determined from the known response of the IUE cameras. The procedure is fairly straightforward and the finally reduced spectra of these galaxies are shown in figure 5.2. We note however, that because of the low brightnesses of these galaxies the TRAK program had difficulty in tracing the centroid of most of the spectra below about 210–230 nm, just shortward of our adopted wavelength limit.

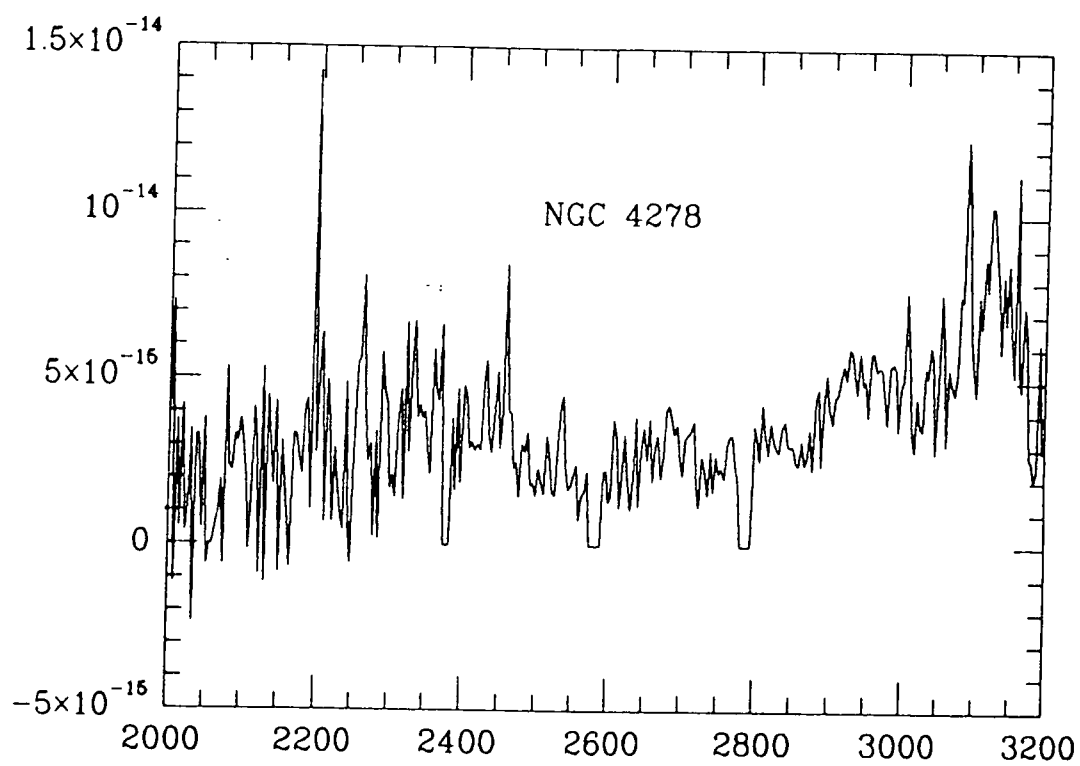
(3) *Analysis.*

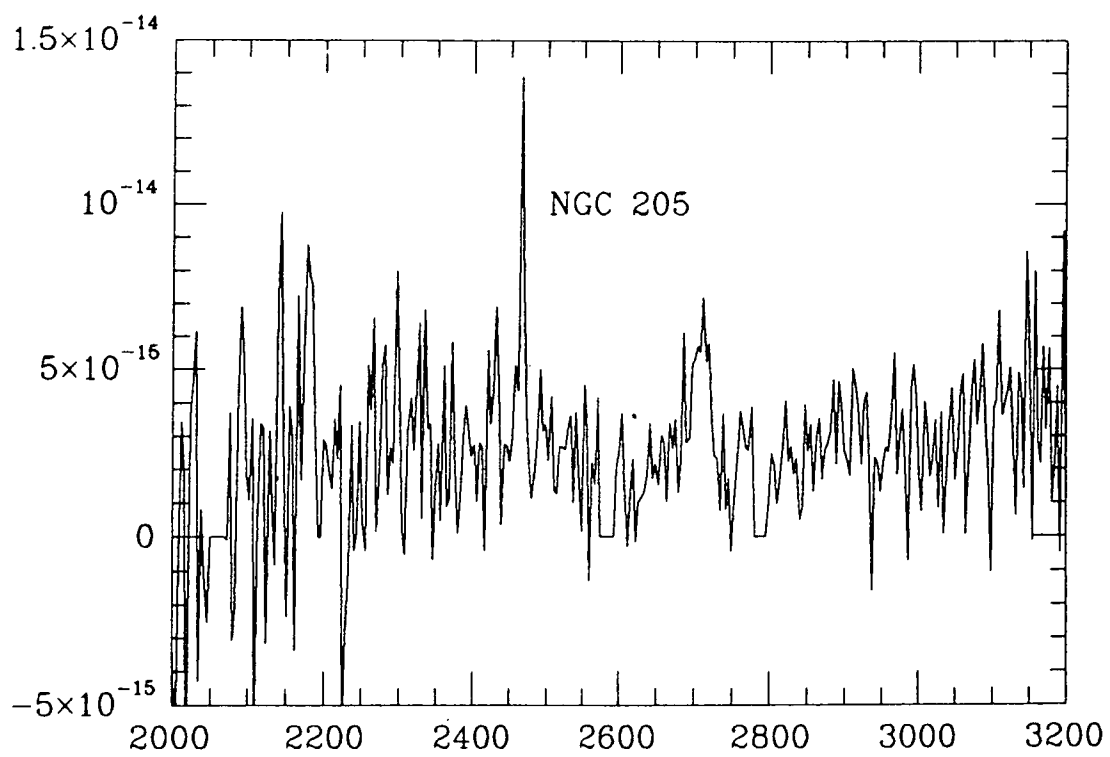
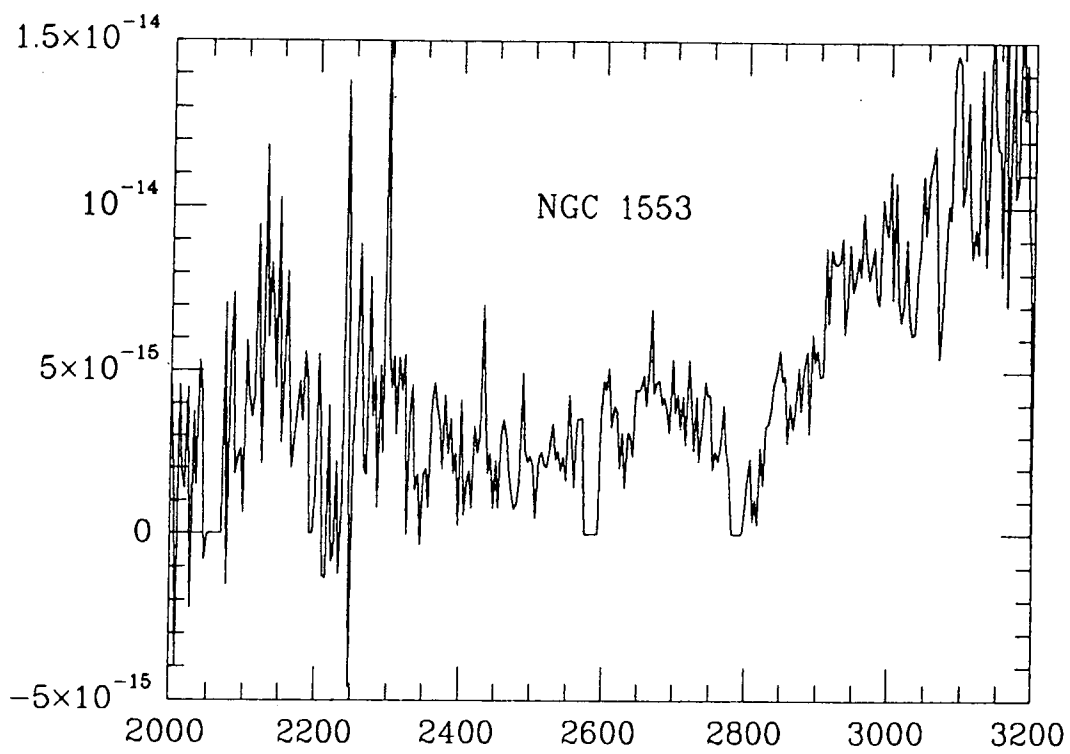
After de-redshifting all the spectra to the rest frame, it is then possible to make colour estimates by passing the spectrum of each of these galaxies through the simulation programs we discussed in chapter 2. This allows estimates of the magnitudes in any specified filter/detector system for a chosen redshift. Thus the expected uv colours of non-evolved early-type galaxies can now be directly compared with the photometry of the two distant clusters A370 and 0016+16.

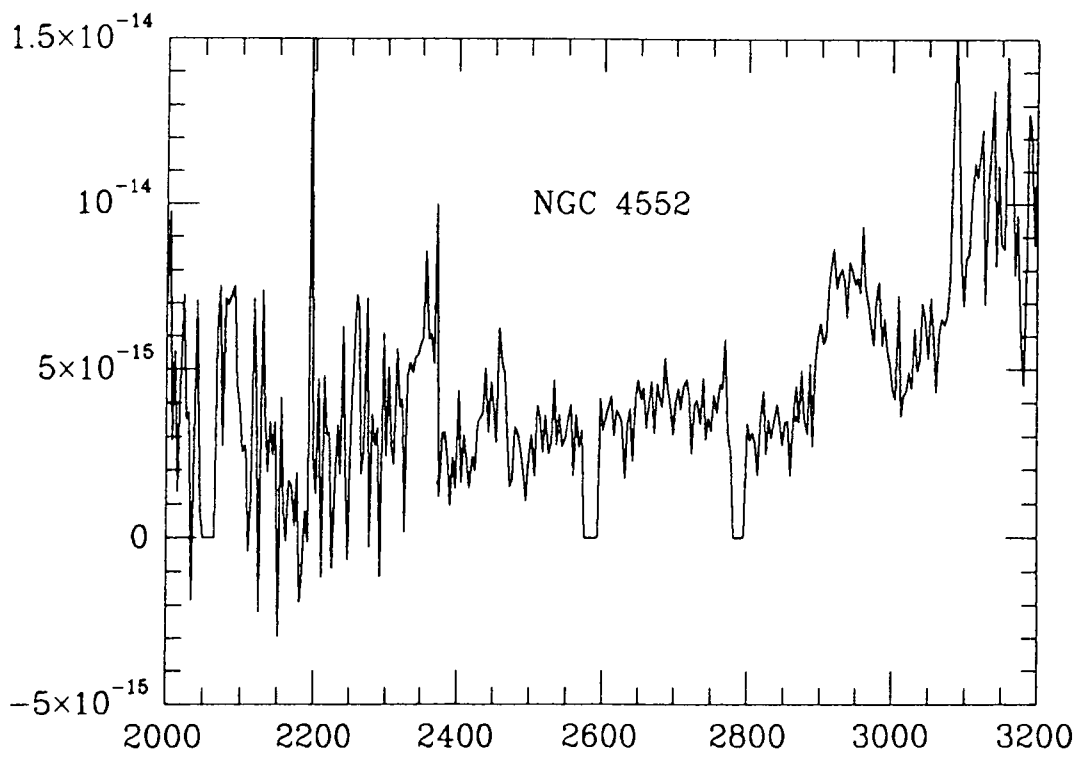
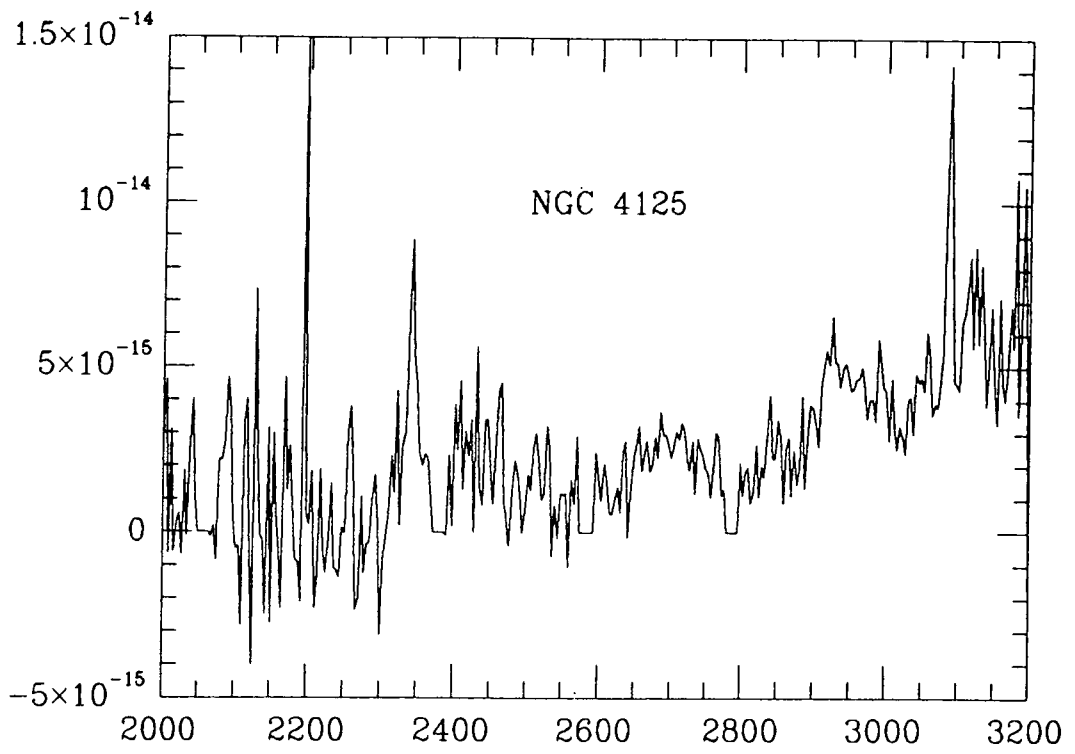
Table 5.1: *Ultraviolet Colour—Magnitude Effect*

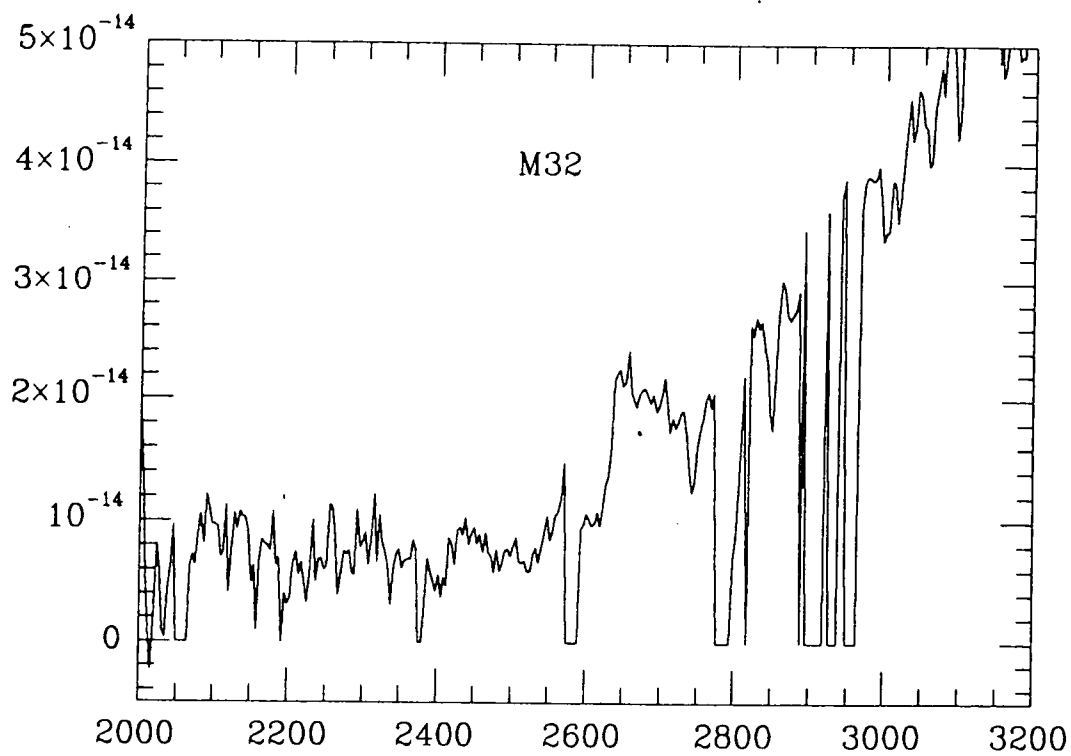
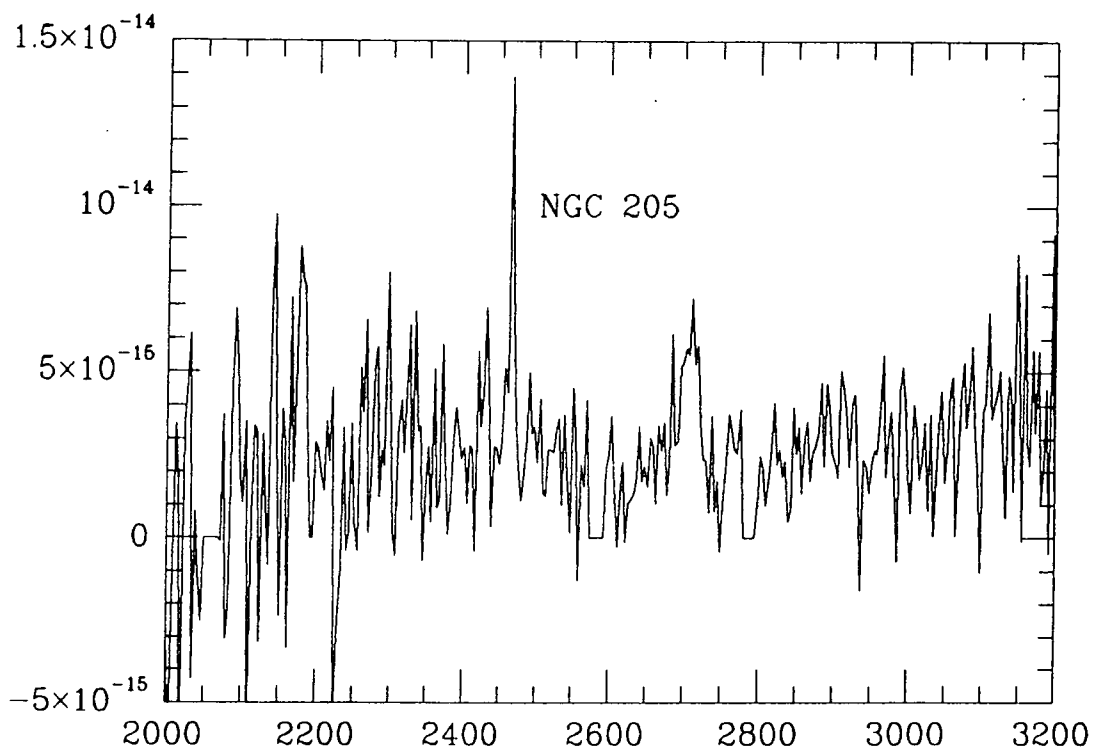
IUE #	NGC #	m_B	A_B	V	U(0.37)	418(0.54)	M_V
LWR15381	1553	10.47	0.00	11.78	29.62	30.28	-22.17
LWR11055	4278	11.15	0.10	12.18	29.89	30.60	-20.32
LWP1524	4889	12.45	0.05	13.49	31.44	32.03	-24.06
LWR13025	4125	10.70	0.04	12.59	30.07	30.68	-22.62
LWR13622	4552	10.81	0.14	12.01	29.56	30.18	-17.64
LWR17019	205	8.85	0.14	13.49	29.77	30.37	-14.54
LWR3111	221/M32	9.15	0.31	10.30	27.99	28.44	-14.13
LWR4777	4374	10.31	0.13	11.83	29.66	30.21	-21.72
LWR6343	224/M31	4.36	0.31	10.28	28.51	28.98	-22.40
LWR6877	4472	9.31	0.00	11.62	29.46	29.97	-22.76
LWR6912	4472	9.31	0.00	11.62	29.35	29.97	-22.76
LWP8129	4621	10.75	0.07	12.10	29.18	29.72	-19.35
LWR1372	6166	13.05	0.00	14.65	30.69	31.30	-24.24
LWR9381	4382	10.10	0.04	11.84	29.30	29.83	-21.69

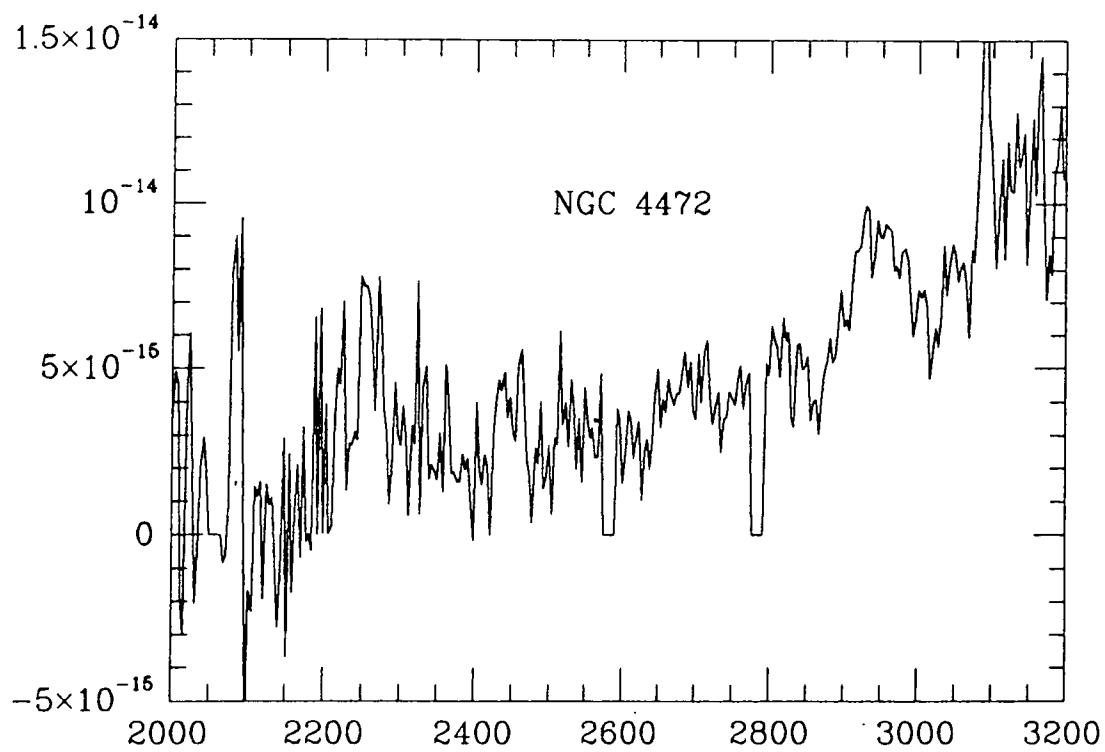
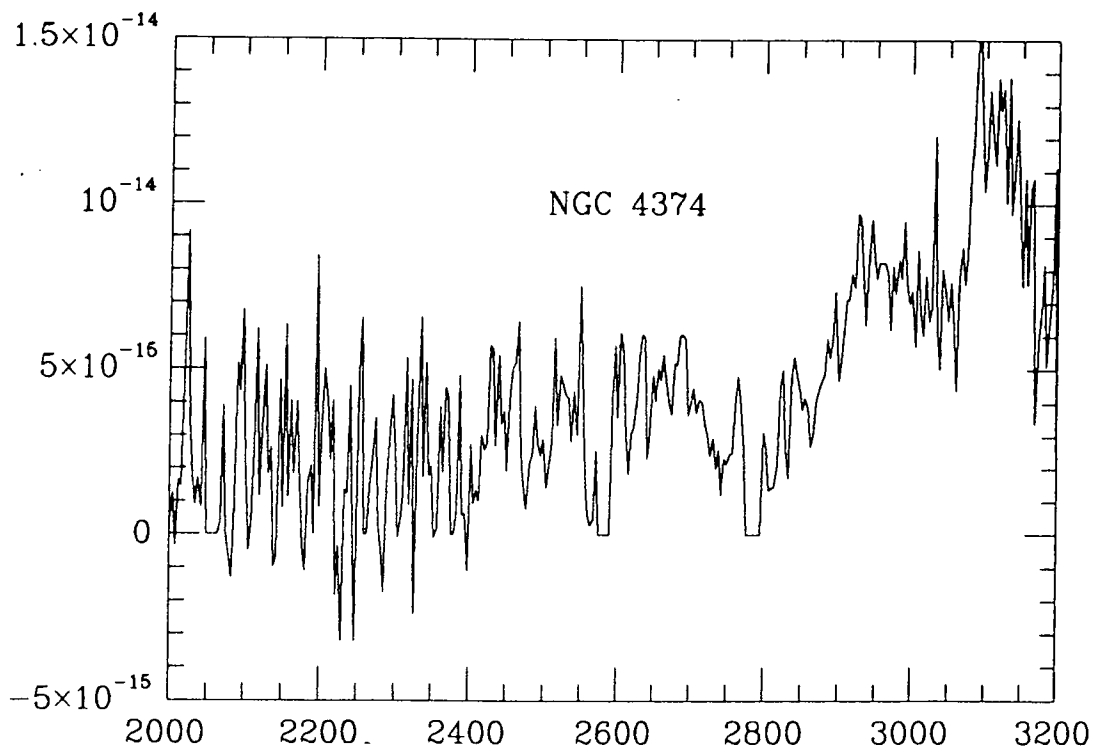
Figure 5.2: Reduced spectra of early-type galaxies observed using the IUE satellite. Note that NGC 4621 was observed by the present author, and has not been published earlier.

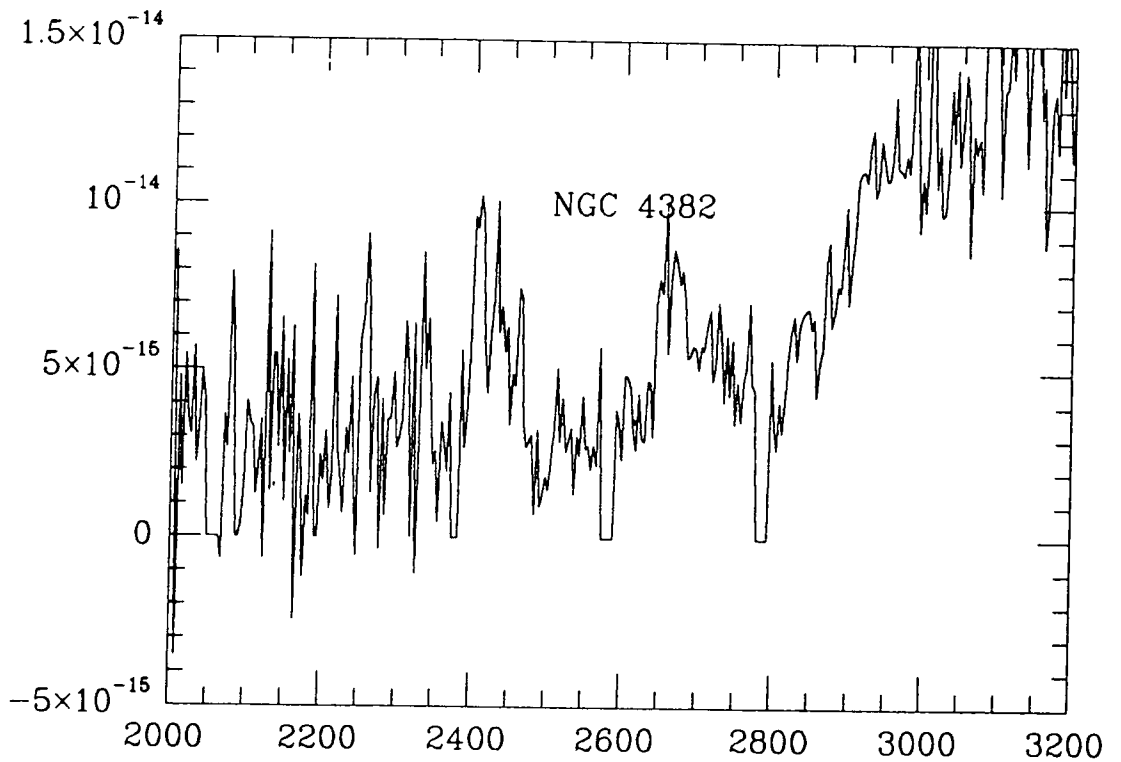
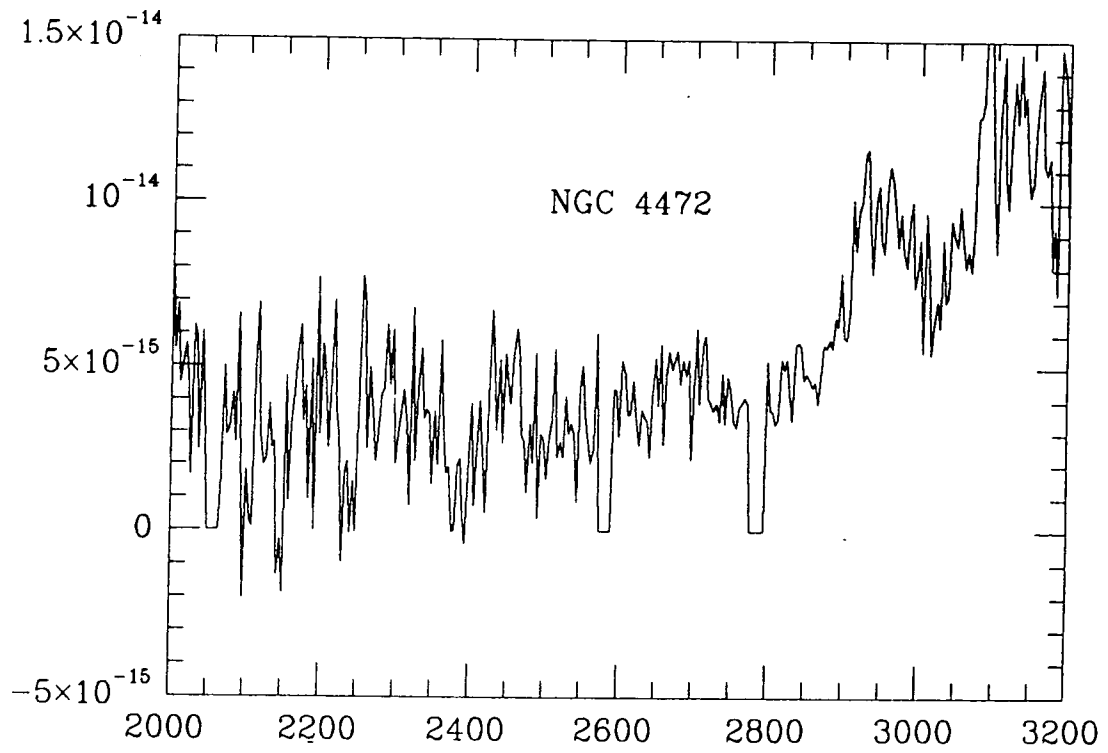


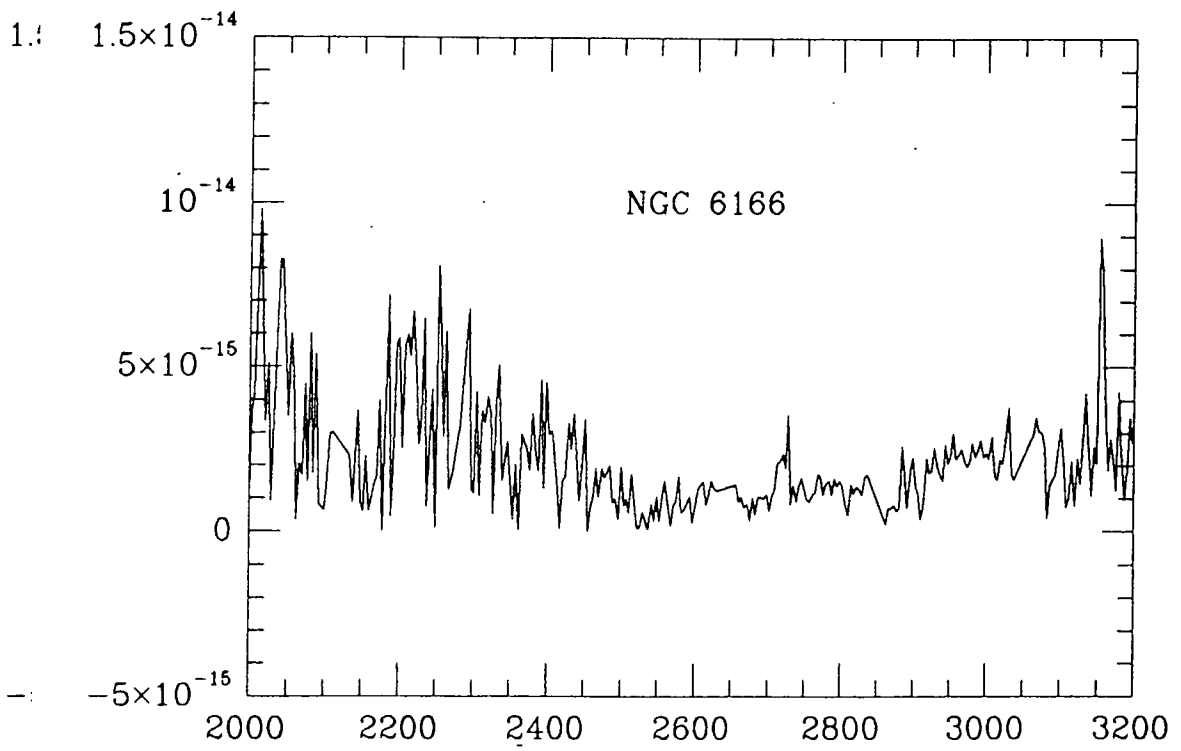




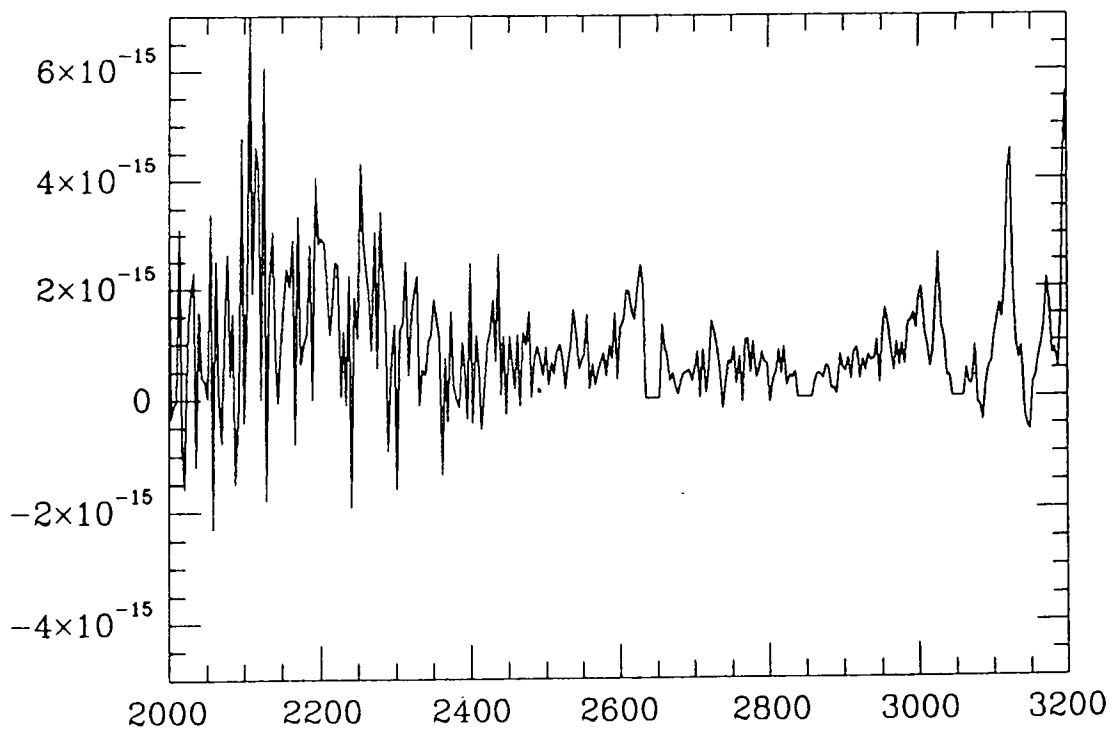


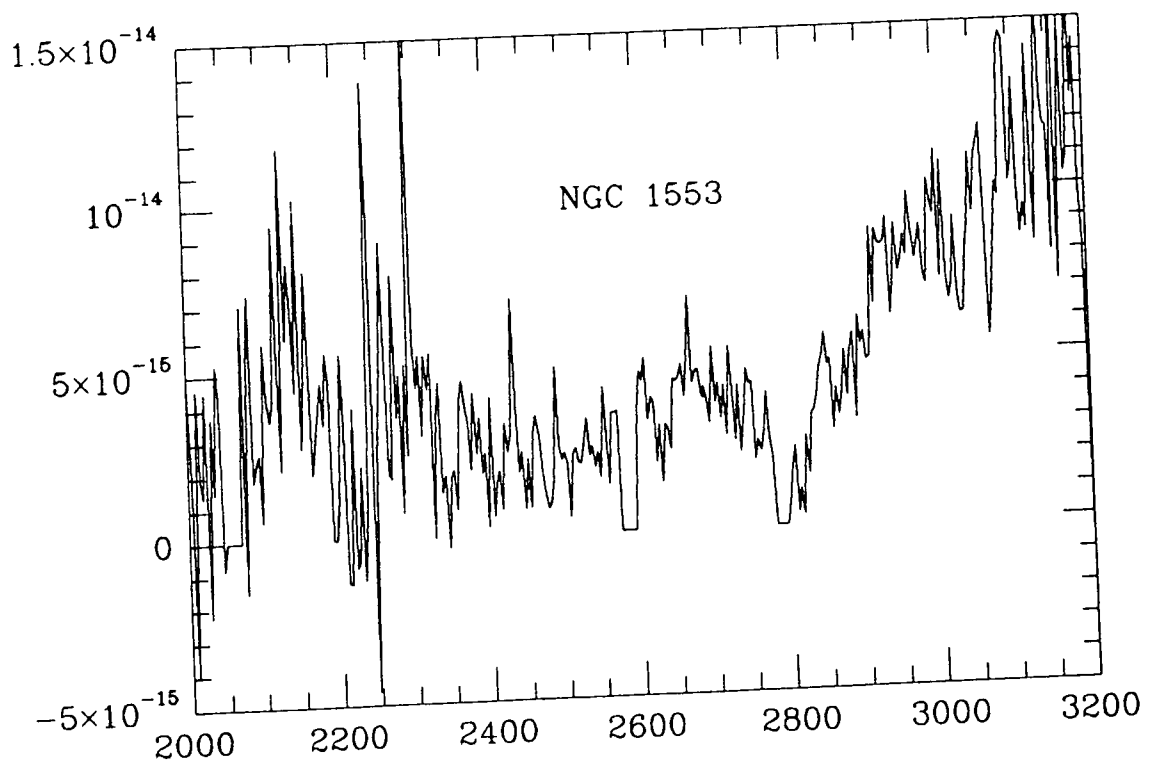
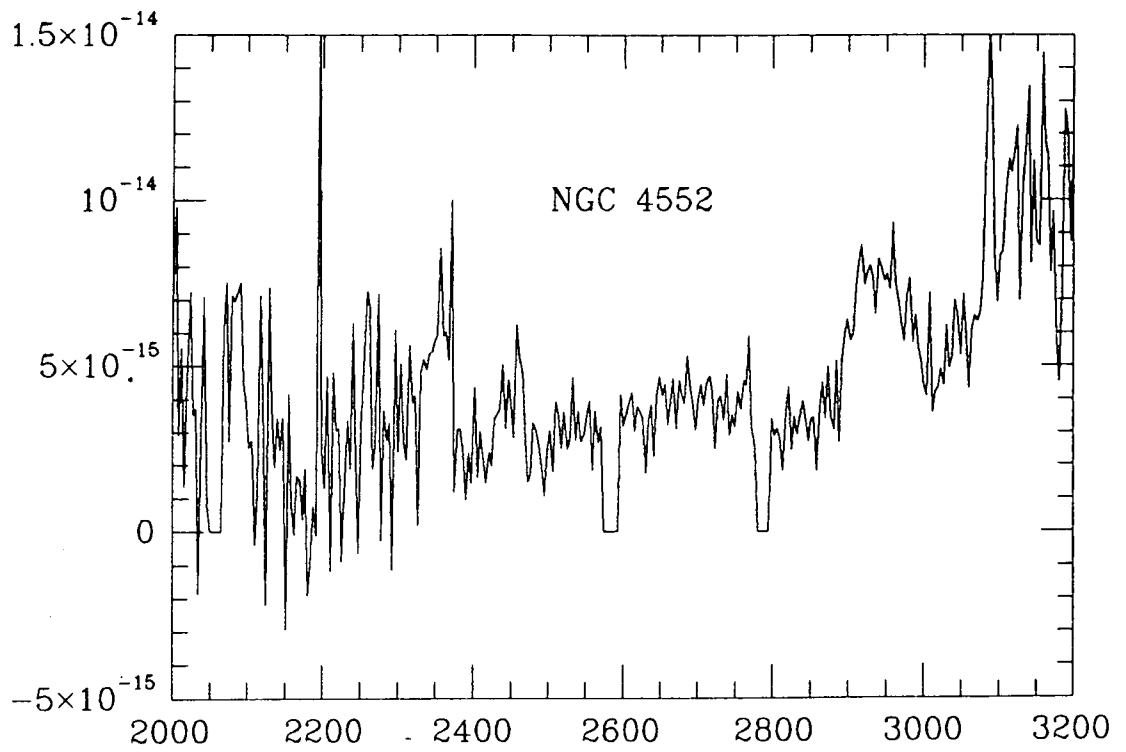


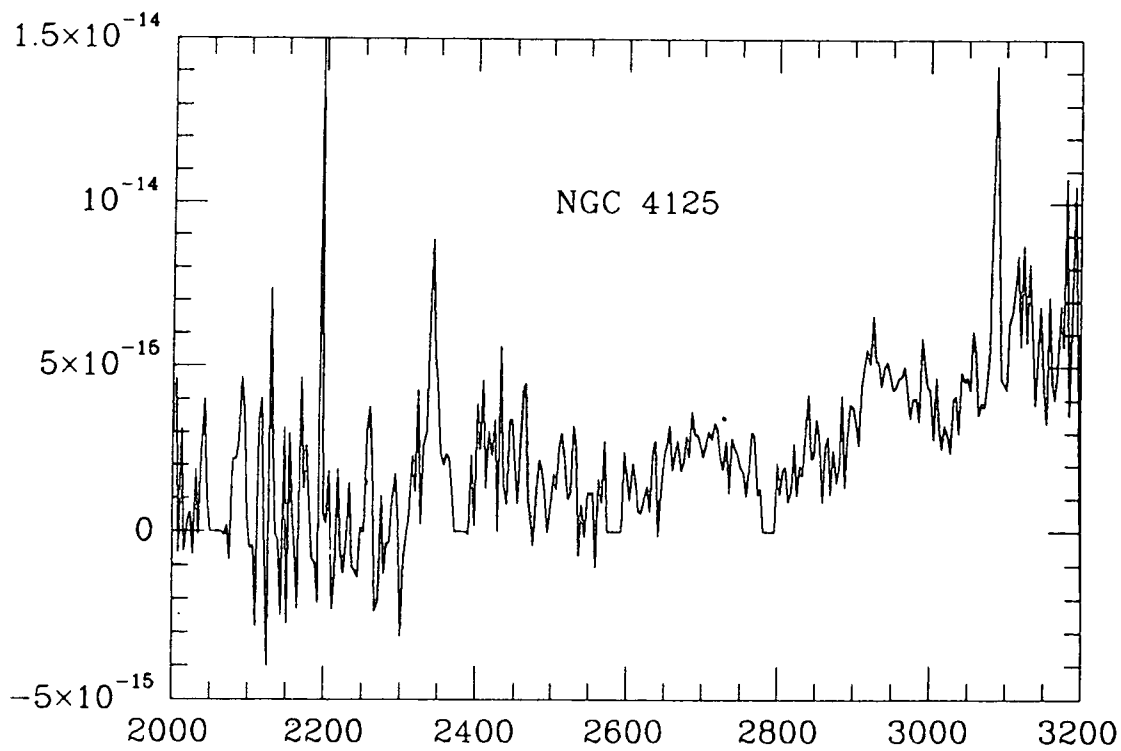
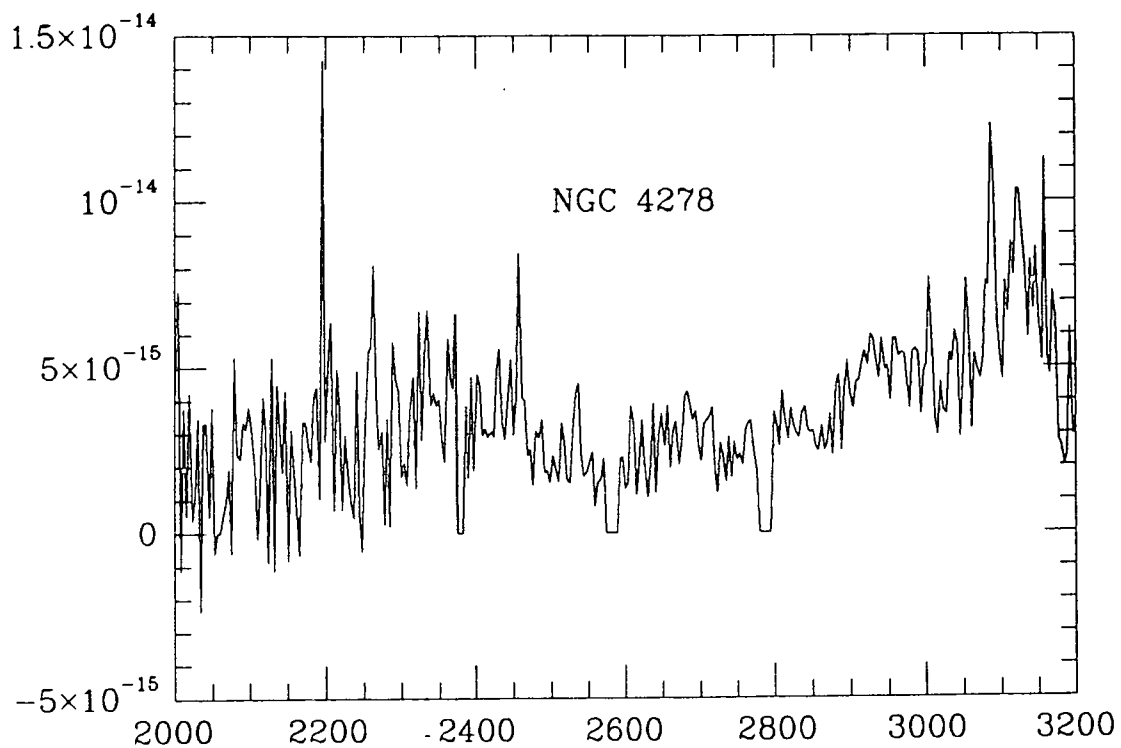


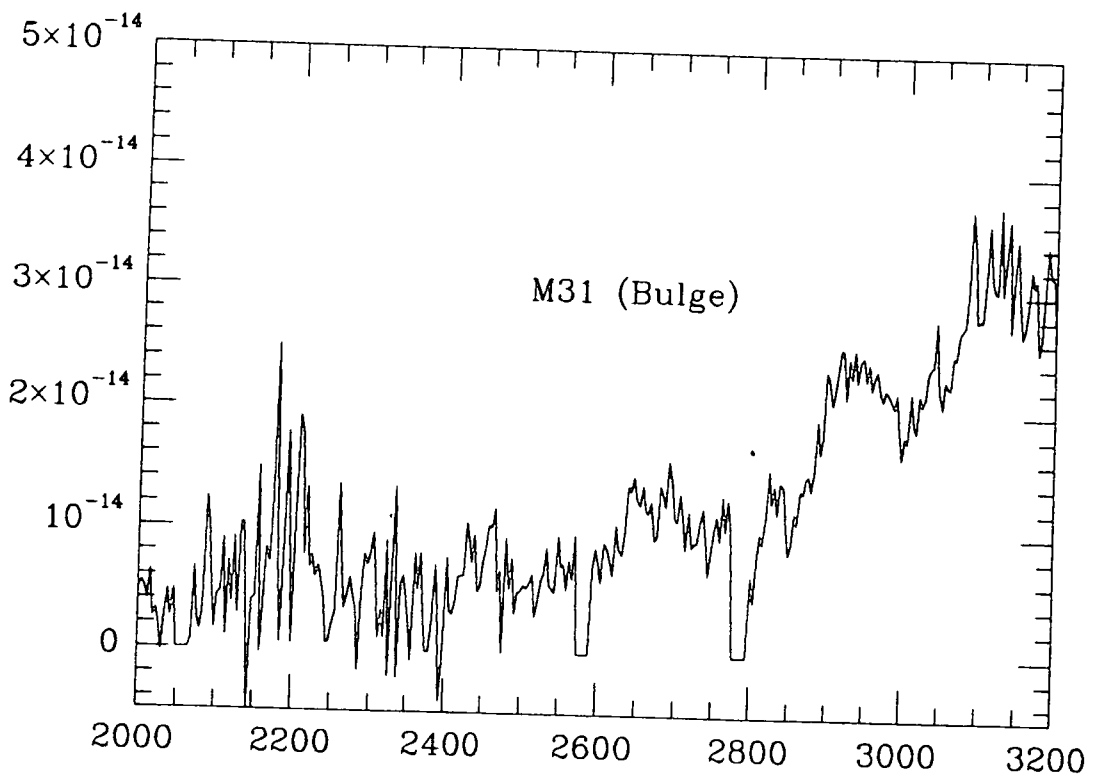
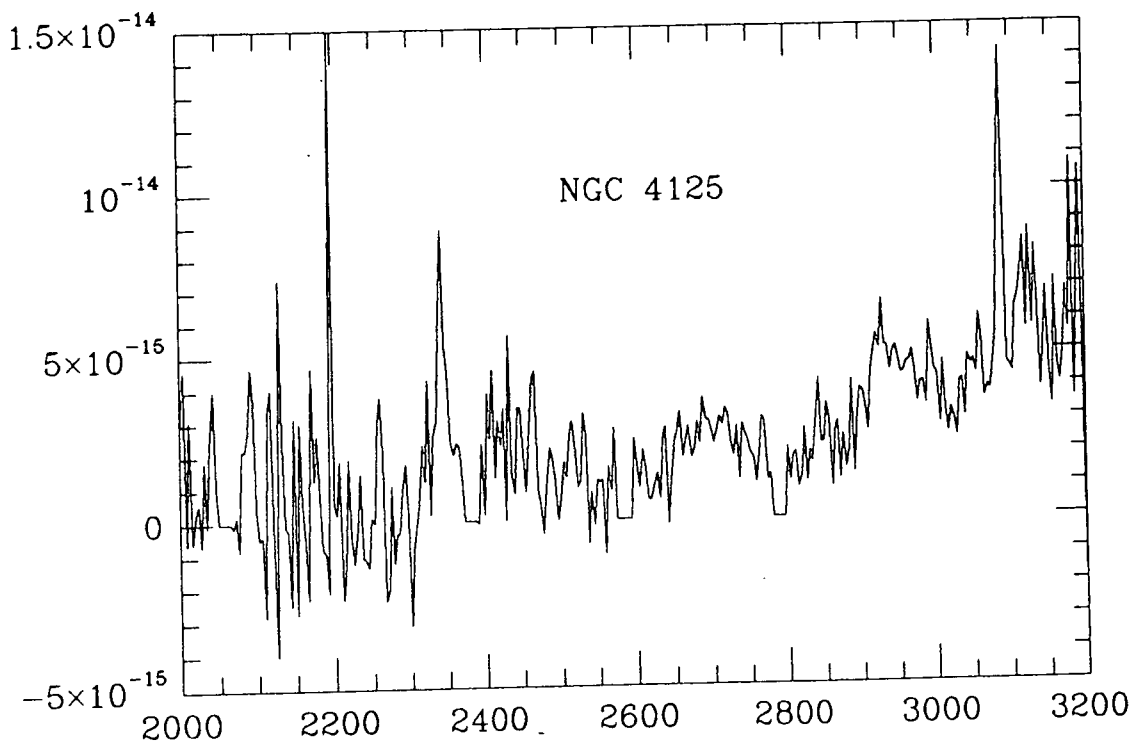


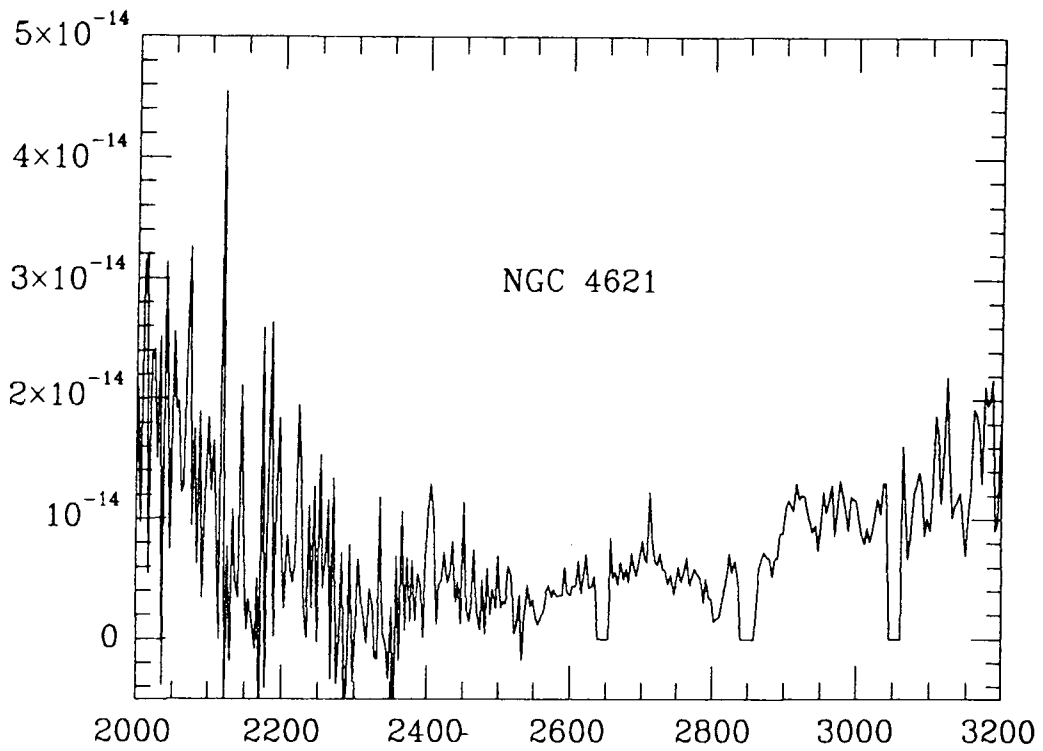
NGC 4889



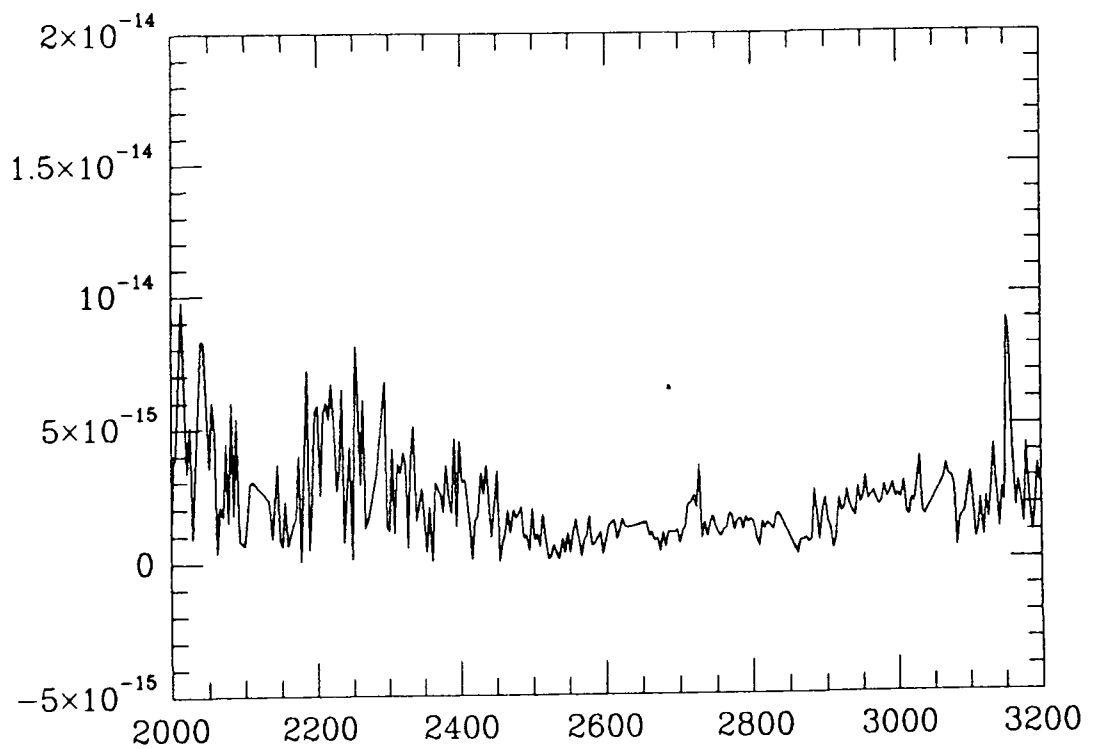








NGC 6166



These predicted colours are plotted against galaxy absolute magnitude, M_V (estimated using the B_T values in de Vaucouleurs and de Vaucouleurs, 1976), in figure 5.3, revealing that the CM-relation is still well-defined down to these rest wavelengths (~ 270 nm). Further, the excellent agreement between the observed data and Couch's simulations (represented by the solid line in the figure) is gratifying. The scatter about the predicted relation is some 0.29 mags for the 418-685 colour at $z = 0.54$, and 0.25 mags for U-685 at $z = 0.37$. The galaxies that were discovered in the previous two chapters to display enhanced uv luminosities possess uv colours which lie significantly blueward of the expected CM-slope, i.e. beyond the 1σ boundary of the relation defined by the present data.

From the published short wavelength ($\lambda < 220$ nm) observations of nearby early-type galaxies we can see that there are large object-to-object variations and that the simple CM effect is no longer apparent. The explanations attributed to such behaviour have been varied and discrimination between the different possibilities is not easy. We may ask, however, is it possible that these variations are somehow related to the uvx phenomenon, that is, do such galaxy-to-galaxy differences occur at longer wavelengths at the earlier epochs at which our distant clusters are observed? One possibility is an additional component of young stars. At the present epoch such objects will be scarce (if at all present) in early-type systems, but should be more common when these galaxies were younger. We shall return to these considerations in the next section.

In summary, we have shown that it is a valid approach to examine the form of the uv CM relation down to wavelengths ~ 220 nm, since available IUE spectra of early-type galaxies reveal that not only is the relation still well defined here, but that it is in excellent agreement with Couch's crude simulations. The implication then for our uv photometry of galaxies in 0016+16 and A370 is as we originally postulated in the previous chapters, that is that the uvx objects most probably represent an evolutionary difference between the early-type galaxies at the present epoch and at these high redshifts.

5.3 Galaxy Evolution in Distant Clusters.

(a) Introduction.

We should now analyse our observations of galaxy SEDs in A370 and 0016+16 in the context of a series of possible star formation histories. Firstly, however, it is informative to review relevant observations by other authors to place our work in a more general perspective.

From the available, published spectroscopy of member galaxies of distant clusters, summarised in table 5.2, we can basically distinguish four main object types.

- (1) Firstly, there are the red early-type galaxies whose rest-frame optical colours and spectral line strengths are very similar to those of nearby E/S0s. Such galaxies predominate in the rich cluster environment at the present epoch and are the largest single population of object even in the high redshift clusters so far studied. Little attention has been focussed here in spectroscopic surveys, especially since their red colours and their scarcity in the low-density field mean that there is less ambiguity in their associated redshift, ie such red objects can fairly safely be assumed to lie at the cluster redshift. The emphasis, then has tended to concentrate on the blue 'Butcher-Oemler' objects, which provide the interesting contrast with nearby clusters.
- (2) 'Normal' spirals constitute the second most common object type in all the spectroscopic surveys of distant clusters. A galaxy is classified as spiral-type if its colours and line strengths indicate levels of ongoing star formation consistent with nearby late-type galaxies. Dressler and Gunn (1982) determined a relation between the strength of the [OII] 3727 Å line and galaxy colour $(B - V)_0$, which provides a comparison of the amount of current star formation with the past average. The distant spectra were found to

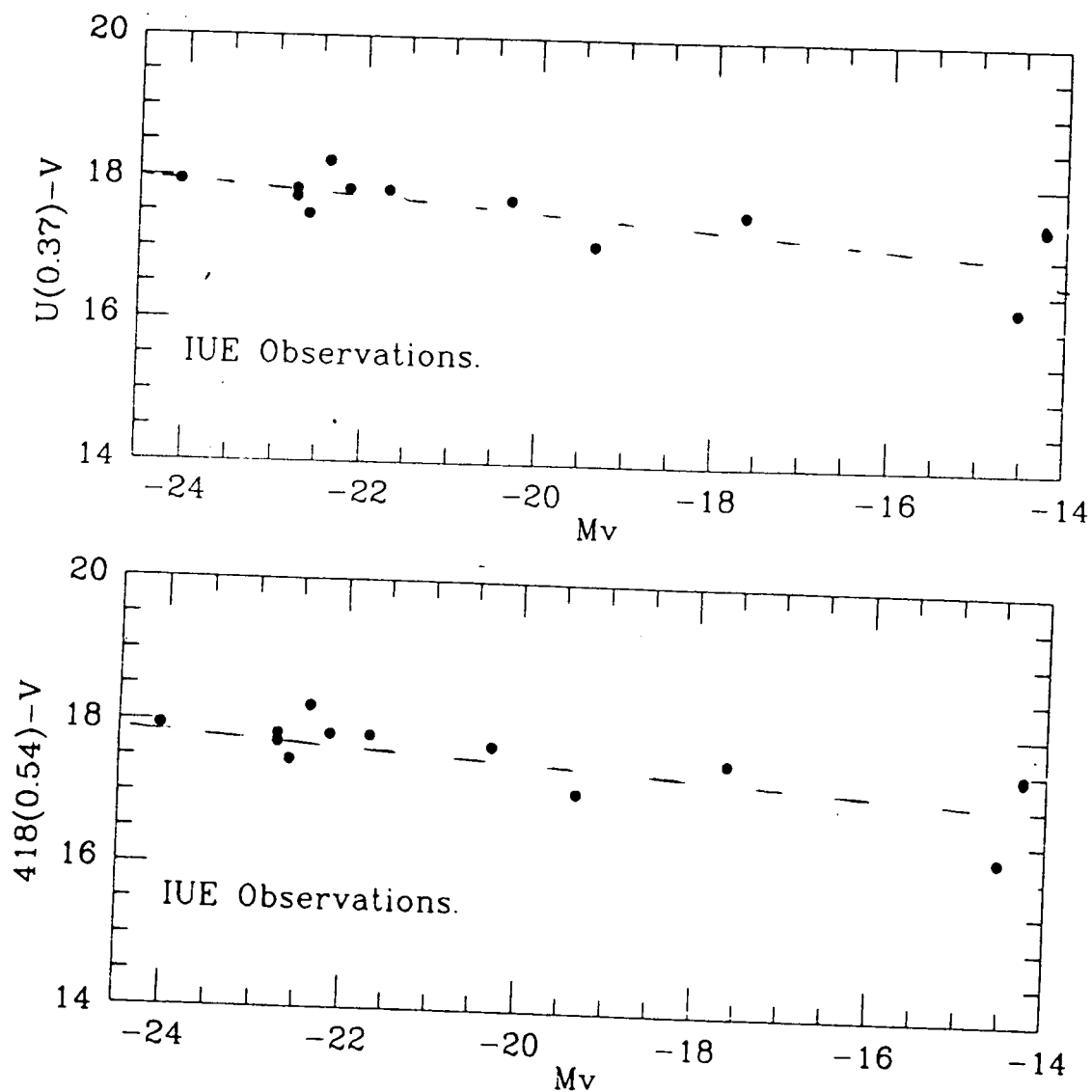


Figure 5.3: Ultraviolet-optical colour-magnitude relation for present-day early-type galaxies derived from the IUE spectra. Colours are corrected for effects of redshift and Galactic extinction. The dashed line is the predicted relation derived using Couch's synthesis method.

Table 5.2: Spectroscopy of Distant Clusters.

Cluster	z	Red	Spiral	PSGs	AGN	Source
0024	0.39	16	14	(1)		Dressler <i>et al</i> ,1985
3C295	0.46	6		3	3	Dressler, Gunn,1983
1447	0.38	7	4	4		Butcher,Oemler,1984
AC103	0.31	7	9	2		Sharples <i>et al</i> ,1985
A223	0.2	2		2		Lavery, Henry,1986
A963	0.2	7	3	4	2	Lavery, Henry,1986
A2111	0.2	5	4	5	1	Lavery, Henry,1986

display a similar relation indicating that such galaxies may also be characterised as having undergone star formation at a constant rate with no significant deviations in the recent (\sim few Gyrs) past.

- (3) Many of these distant clusters have been found to contain blue galaxies with high excitation emission spectra, implying identification as active galactic nuclei. This is an interesting result which may prove indicative of evolutionary change, since such objects are rare in the rich cluster environment at the present epoch (Dressler *et al*, 1982). Progress in this area, however, will require more detailed statistical analyses of nearby and distant systems with due regard being paid to selection biases.
- (4) Half of the blue objects in the preliminary spectroscopy of 3C295 (three galaxies!) by Dressler and Gunn (1982) were found to exhibit Balmer absorption lines which were unusually strong ($W_\lambda \sim 7-8\text{\AA}$) compared with spiral galaxies of a similar colour ($W_\lambda \sim 2-3\text{\AA}$). Such line strengths indicate an A-star spectrum which implies an intermediate age for the system of only a few Gyrs. However, the spectra also show the underlying characteristics of an older red population, and also, importantly, do not show the [OII] 3727 \AA line. This feature arising in HII regions is the most obvious indicator of ongoing (within the last $\sim 10^7$ yrs) star formation. The implication is that these galaxies are thus no longer forming stars, but, unlike the redder early-types, have only very recently ended a period of significant star-forming activity. The best fit that Dressler and Gunn obtained to their observations was that of a galaxy which is observed some 1-1.5 Gyr after it had undergone a short burst of star formation, hence their adopted nomenclature, 'Post Starburst Galaxy' (PSG).

Similar objects have now been claimed to be present in all other distant clusters of galaxies (note the case of 0024+1654, referred to in chapter one), although authors have tended, largely because of the low quality of such spectra, to be somewhat 'loose' in their classification criteria. For example, Butcher and Oemler's (1984) study of the cluster 1447+26, reveals a large number of 'E+A type' spectra, but, importantly, many of these galaxies still exhibit [OII] emission, so that star formation may not yet have completely finished. We shall return to these detailed points in section 5.3(b).

Perhaps, finally, a further class of object discovered in distant clusters, should also be added to this list. I refer to the actively star-forming galaxies discovered by Lavery and Henry (1986) which have extremely strong [OII] emission (up to $W_\lambda \sim 100\text{\AA}$), but are not AGN. Although such objects are claimed to be present in three clusters at $z \sim 0.2$, no other examples have yet been reported by other authors.

A major survey of galaxy spectra in distant clusters, which is substantially more detailed than most of the previous work has recently been completed by Couch and Sharples (1987, and private communication) encompassing some ~ 180 spectra of galaxies in three clusters (AC103, AC114, AC118) around $z \sim 0.3$. In conjunction with detailed evolutionary models these observations will provide a valuable insight into the evolutionary status of each of the observed galaxy types.

As we have seen, one of the contributions of our rest-frame uv photometry to the study of distant clusters of galaxies has been to introduce yet another type of object for which it has not yet been possible to find nearby equivalents, viz, the uvx galaxies. However, rather than merely further complicating the issue, we should ask whether these observations can in some way be linked to the previous spectroscopic and photometric results and perhaps point the way to a more complete and united picture. In particular, the fact that most members of nearby rich galaxy clusters are red E/S0 galaxies, with blue objects being only a very minor component, suggests an evolutionary transformation from blue to red galaxies, and it is therefore tempting to associate the other types of galaxy found at high redshifts with

some intermediate stage.

This is of course only one possibility and there is as yet no evidence that convincingly demonstrates that such a simple evolutionary sequence exists. However, since it constitutes the simplest interpretation of the available data it is worthwhile pursuing in some detail. In the next section I shall make use of a series of galaxy SEDs and spectra produced using Bruzual's (1981, 1983) simulations by way of illustrating the expected behaviour in such a scenario.

(b) Modelling Galaxy Evolution.

Tinsley (1972) suggested that the red colours and lack of star formation in nearby elliptical galaxies could be well matched by a history that involved a single burst of star formation at the epoch of galaxy formation (16 Gyrs ago). This is represented by the Bruzual c-model, whose evolution is illustrated in figure 5.4. Using the programs developed in chapter 2, I have simulated the colour measurements expected on the basis of our intermediate-bandwidth filter system at the redshifts of the two clusters, $z = 0.37$ and 0.54 . This provides, then, a direct comparison between our observations and theory. For convenience and ease of reference, we have also predicted the rest-frame B-V colours and expected V band luminosity change.

Directly after the initial burst, colour evolution is extremely rapid, as shown in figures 5.4. During the epoch of large scale star formation, the spectrum is dominated by the blue light of the massive hot young stars. The main-sequence lifetimes of these O and B type stars are fairly short so that after only a few gigayears the optical light becomes dominated by the less massive, later stellar types, eventually acquiring the K-type spectrum of nearby E/S0 galaxies. Since the evolution is most dramatic in the rest-frame ultraviolet region, we can see that our use of the U and 418 filters at $z = 0.37$, and 0.54 , should indeed provide an ideal indication of the level of any ongoing star formation in such systems.

We can compare the colours of the c-model with our photometric observations by constructing mean red galaxies from the CM-sequence objects (ie, excluding the uvx galaxies) in A370 and 0016+16. In this way we find reasonable agreement with ages of 7-10 Gyrs in both cases. The inadequacies of the Bruzual models soon become apparent when we consider the colours of a 16 Gyr age for a present-day galaxy. As discussed in chapter 1, the models are too red compared with the observations, with such an inconsistency most likely being due to the absence of various stellar populations (e.g. Asymptotic Giant Branch, Horizontal Branch) from Bruzual's evolutionary tracks.

Progress to date on a theoretical understanding of late stellar evolution (beyond double-shell hydrogen burning and He core ignition) has been somewhat limited (see Renzini, 1986). An approach that has been followed in practice by most workers is to add the colour change between each age of the model galaxy and the 16 Gyr spectrum to an observed present-day galaxy. This differential approach does not bypass the difficulty but provides a means of calibrating the calculated colours onto the present-epoch values. The colours of the models, and our observed mean red sequence galaxies are presented in table 5.3.

Whereas in 0016+16, there is a more pronounced displacement between the observed and predicted no-evolution colours (see Fig. 3.11), for A370, the situation is possibly more complex. In this case we see that the predicted CM-relation for (502-685) lies somewhat redward of the observed sequence, implying the possibility of an evolution in colour of order 0.15 mags. However, in the case of (418-685) the predictions apparently agree more closely with the observed slope, implying overall a lesser amount of evolution. We should note, though, that there are a number of possible uncertainties in such comparisons, for example, those arising from the zero-pointing of the CM-relation and the exact level of reddening present in this field.

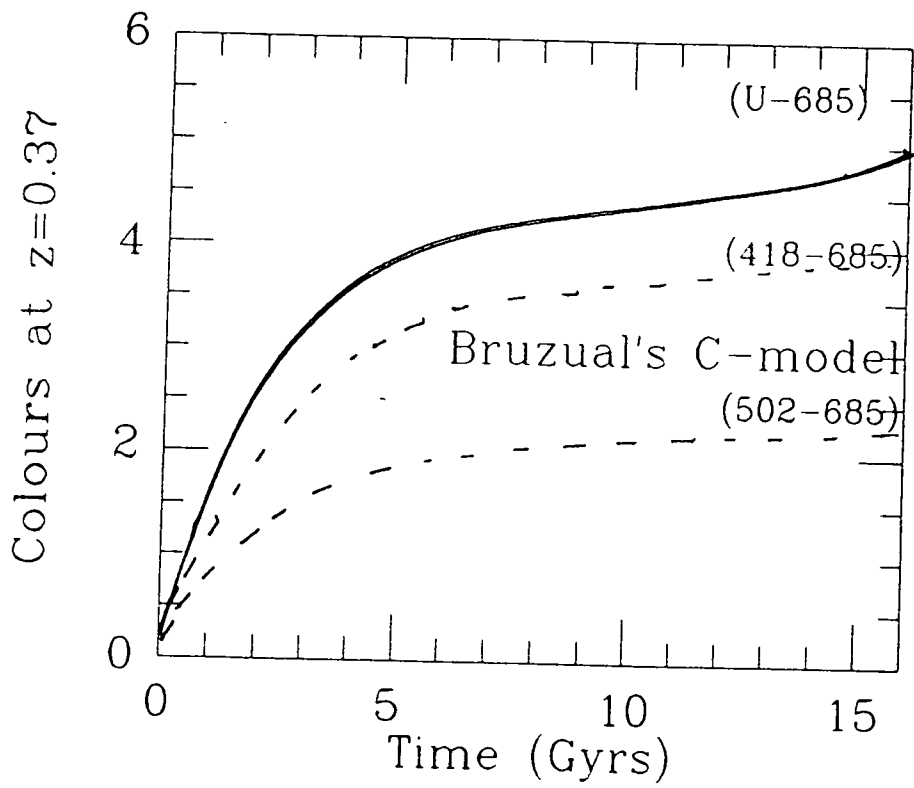


Figure 5.4: Colour changes as a function of time, predicted by Bruzual's c-models.

Table 5.3(a): $z = 0.37$ Colours from c-model

Age(Gyr)	418-685	U-685	502-685
0.01	0.509	-0.300	0.211
0.75	1.486	0.809	0.888
1.00	1.584	0.932	0.938
1.20	2.465	2.186	1.367
1.60	2.600	2.526	1.415
2.00	2.835	2.883	1.595
2.60	3.151	3.369	1.813
3.00	3.437	3.798	2.006
4.00	3.062	3.455	1.807
5.00	3.561	4.187	2.097
6.00	3.549	4.306	2.016
8.00	3.646	4.419	2.140
10.0	3.581	4.336	2.120
11.0	3.732	4.532	2.175
12.0	3.783	4.605	2.211
16.0	4.116	5.135	2.347
Pence	3.798	4.376	2.176
A370	3.70	4.12	2.02

Table 5.3(b): $z = 0.54$ Colours from c-model

Age(Gyr)	418-685	502-685	578-685
0.01	0.642	0.374	0.-0.146
0.75	1.547	1.089	0.347
1.00	1.669	1.168	0.394
1.20	2.779	1.807	0.742
1.60	3.074	1.877	0.782
2.00	3.317	1.965	0.871
2.60	3.671	2.090	0.986
3.00	3.996	2.223	1.102
4.00	3.704	2.045	0.967
5.00	4.319	2.252	1.163
6.00	4.437	2.176	1.098
8.00	4.518	2.202	1.192
10.0	4.443	2.152	1.177
11.0	4.625	2.332	1.222
12.0	4.690	2.306	1.251
16.0	5.183	2.505	1.361
Pence	4.563	2.245	1.189
0016	4.4	2.0	1.0

Such a situation will only be more firmly resolvable when (a) we obtain a better understanding of the CM-relation via more detailed observations of a larger number of galaxies in both nearby and distant clusters; (b) the evolutionary models themselves are made more realistic by, for example, accounting for the full range of stellar populations in galaxies; (c) and also in this case, when we manage to unravel the level of reddening present.

In summary, we can conclude that the red galaxies observed in our samples have colours consistent with only a mild amount of spectral evolution over the appropriate lookback times, with the non-evolving colours of nearby galaxies still acceptable within our errors. There is though, an indication of more evolution (bluer uv colours) in these galaxies at the higher redshift, $z = 0.54$. Furthermore, the $\mu = 0.5$ -model can be ruled out as a viable description of the history of these red galaxies since the amount of predicted evolution is too large to be compatible with the observations. The ultraviolet colours of even the more passive c-model are also bluer than the observations, indicative perhaps of a large age for our galaxies, if the inconsistencies in the models do not dominate. These red colours imply that the galaxies are already several Gyrs old at these redshifts.

The blue galaxies observed in the clusters have uv and optical colours that are consistent with a range of nearby spiral types. Note however, that these colours are also expected of any galaxy that is undergoing ongoing star formation on a large scale, independent of its morphological appearance. The significant fact to draw from this data is not the form of the average SED, but rather, the proportion of such galaxies in the cluster. Whereas in 0016+16 the blue fraction is no larger than may be expected from a nearby cluster of similar richness. The case of A370 provides a dramatic example of the Butcher-Oemler effect.

Following the results of section 5.2 we were able to conclude that the uvx objects observed in the two distant clusters were most likely a genuine new population of galaxy and were unaccountable for on the basis of our observations of nearby early-type galaxies. Their enhanced uv brightness is more consistent with an excess number of young stars. We may, therefore, ask is it conceivable that the explanation for the distinction between the uvx and the red CM-sequence galaxies can be described simply in terms of differences in star formation rates as we originally suggested in the earlier chapters?

As in the Dressler and Gunn model for the PSGs in the 3C295 cluster, we can attempt to simulate the observed colours of the uvx galaxies by using a combination of a red underlying galaxy and an added burst of star formation of varying age and strength. We can, once again make use of the Bruzual models for comparison with our observed SEDs (see table 5.4). The uvx galaxies in both clusters occupy a range of colours in the CM-diagram, from almost Sab-type uv colours to just slightly bluer than 'normal' red galaxies. From the models then we can conclude that if this is a valid history (15% burst at 8 Gyr age) for these galaxies, then the last epoch of significant star formation occurred some 1.5–2.0 Gyrs prior to observation for the bluest galaxies, and earlier (2–3 Gyr) for the weaker examples. In other words, we are observing these galaxies during their decline from a recent burst of star formation prior to their attainment of the red colours typical of E/S0 galaxies. Indeed, there is sufficient time during the period from $z = 0.37$ to the present epoch for there to be little trace of such activity in nearby galaxies as indicated in figures 5.4.

An age of 1.5–3.0 Gyr is older than that proposed by Dressler and Gunn to explain their observations of the PSGs (1 Gyr). It is therefore important to check whether these two sets of quite different observations are consistent with each other. We should therefore attempt to refine our models for the uvx galaxies in order to predict measurements of spectral line strengths at various stages in the galaxy's evolution to examine the possibility that a single model can explain both phenomena.

Bruzual's standard models use only the crude low-resolution stellar SEDs of Straižys

and Sviderskeine (1972) to construct synthetic galaxy colours. These are able to reasonably simulate broad-band colours but are of insufficient resolution to monitor the evolution of spectral lines. Thus, as in Hamilton (1985), we have replaced Bruzual's stellar library with the high resolution (2.5Å) stellar spectroscopy presented by Jacoby, Christian, and Hunter (1984, obtained from World Data Centre A).

However, two obvious inadequacies exist in this approach. Firstly, this stellar library consists primarily of stars of solar metallicity, whereas elliptical galaxies are largely considered to be of two to three times this metallicity (Burstein *et al*, 1984). Secondly, during the active star-forming phases, and so long as hot O and B stars are present, we can expect emission lines to be produced in galaxy HII regions, as is manifest in spiral galaxy spectra via the [OII] 3727Å line and the Balmer series of hydrogen. This emission may lead to a 'filling in' of the absorption lines measured in our models, thus decreasing the equivalent widths. However, this will only be of importance during the period of active star formation.

Couch and Sharples (1987, and private communication) have managed to circumvent this latter difficulty by combining the model galaxy spectrum with that of an HII region, obtained by using an image-slicer on the spiral arm of a nearby galaxy. The strengths of the emission features are determined from the expected Ly α flux calculated from the numbers of O and B stars. However, we have not included such a scheme in our present models, although the effect should not produce too great a difference, particularly when we consider only short bursts of star formation.

The spectral lines that would prove of particular interest to our work, bearing in mind the observations of the PSGs are the Balmer absorption lines. In figure 5.5 we plot the strength of the $H\delta$ line as a function of stellar type, showing the clear peak for A stars. In practice the $H\delta$ line is the least contaminated of the Balmer series in galaxy spectra (Hamilton, 1985) and thus we shall use it as our indicator rather than, for example, Dressler and Gunn's mean strength $H = \langle H\beta + H\gamma + H\delta \rangle$. Since the $H\epsilon$ line coincides with CaII H, the ratio of CaII H + $H\epsilon$ to CaII K can provide an indication of the number of young stars present. This approach was developed by Rose (1985), who has found in a nearby sample of early-type galaxies, that the number of young stars is very low and typically can at most contribute a few percent of the light at 4400Å.

Figure 5.6 shows some examples of the resulting composite galaxy spectra at a range of ages. As the galaxy evolves the Balmer lines weaken in strength so that after an age of about 5 Gyr the CaII K line dominates over CaII H+ $H\epsilon$. Using the SPICA software package, I have measured the equivalent widths of the CaII lines and $H\delta$ in a series of models from the epoch of formation to an age of 16 Gyr. The results are given in table 5.5, which includes three basic models: (a) the standard c-model with a 1 Gyr initial burst; (b) a model incorporating constant star formation for 8 Gyr, followed by a sudden cessation of activity; and (c) a c-model galaxy with an additional burst of star formation (involving ~15% of the mass of the galaxy) at an age of 9 Gyr. Also included in the tables are the rest frame B-V colours and V magnitudes.

The absorption line equivalent widths measured during any period of ongoing star formation will be over-estimated due to the missing emission line spectrum of the star-forming regions. Nevertheless the models provide a useful illustration of the behaviour of spectral properties with age.

Our photometry can only provide us with somewhat limited information regarding the nature of the true star formation histories of these galaxies. In particular, the visible/blue light from each galaxy will be dominated by the most recent epoch of significant star formation. The behaviour of the galaxy prior to these epochs is thus difficult to ascertain. Spectroscopy can provide somewhat more detailed information if we can accurately model

the line strengths.

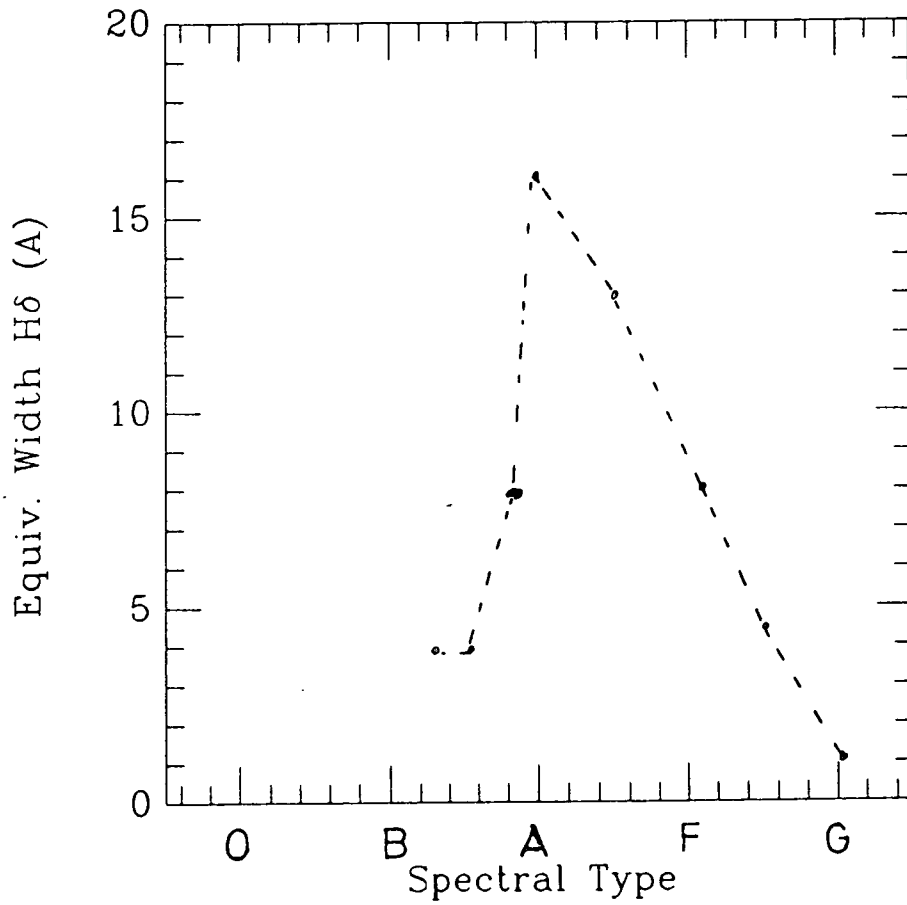
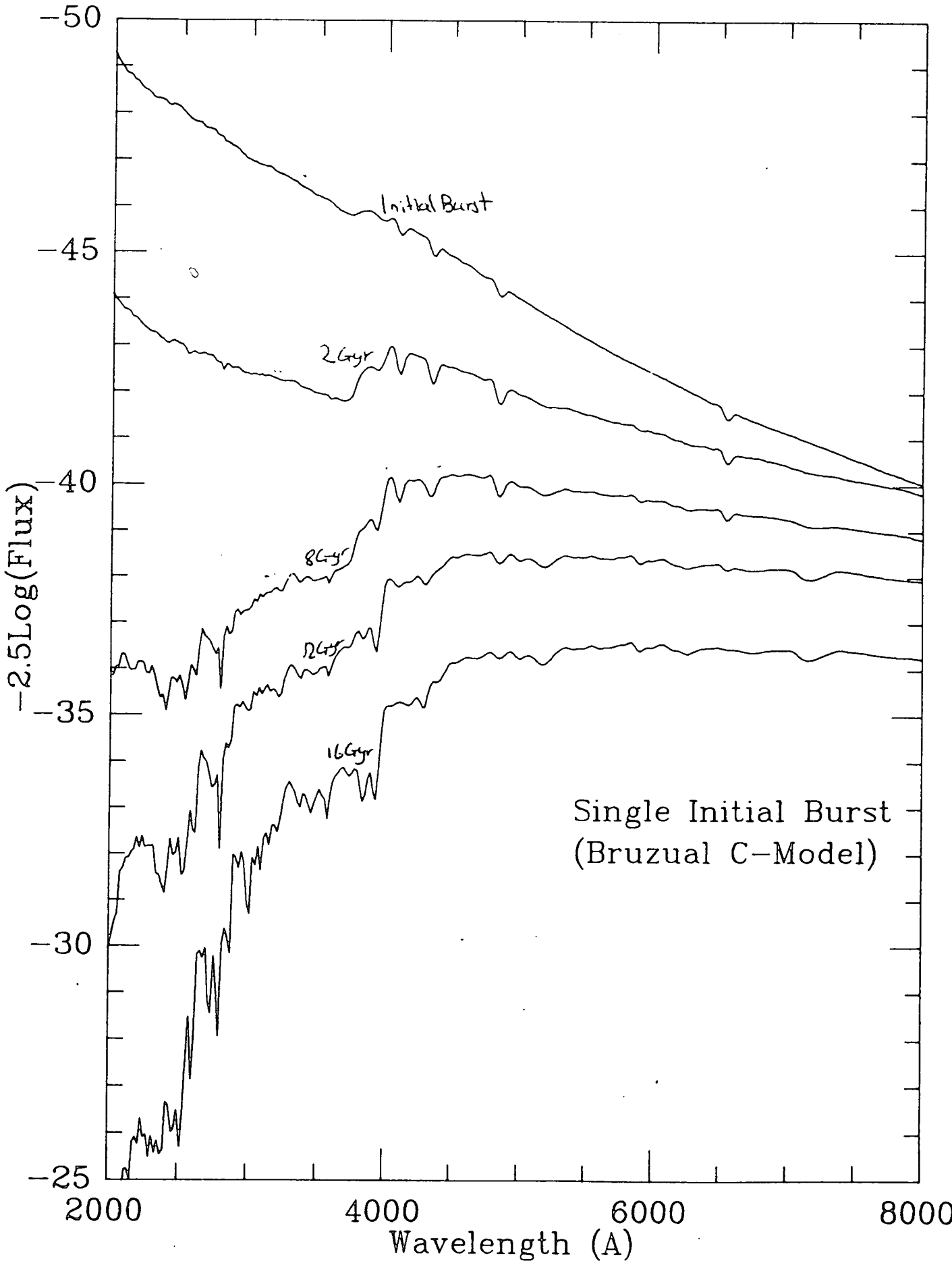
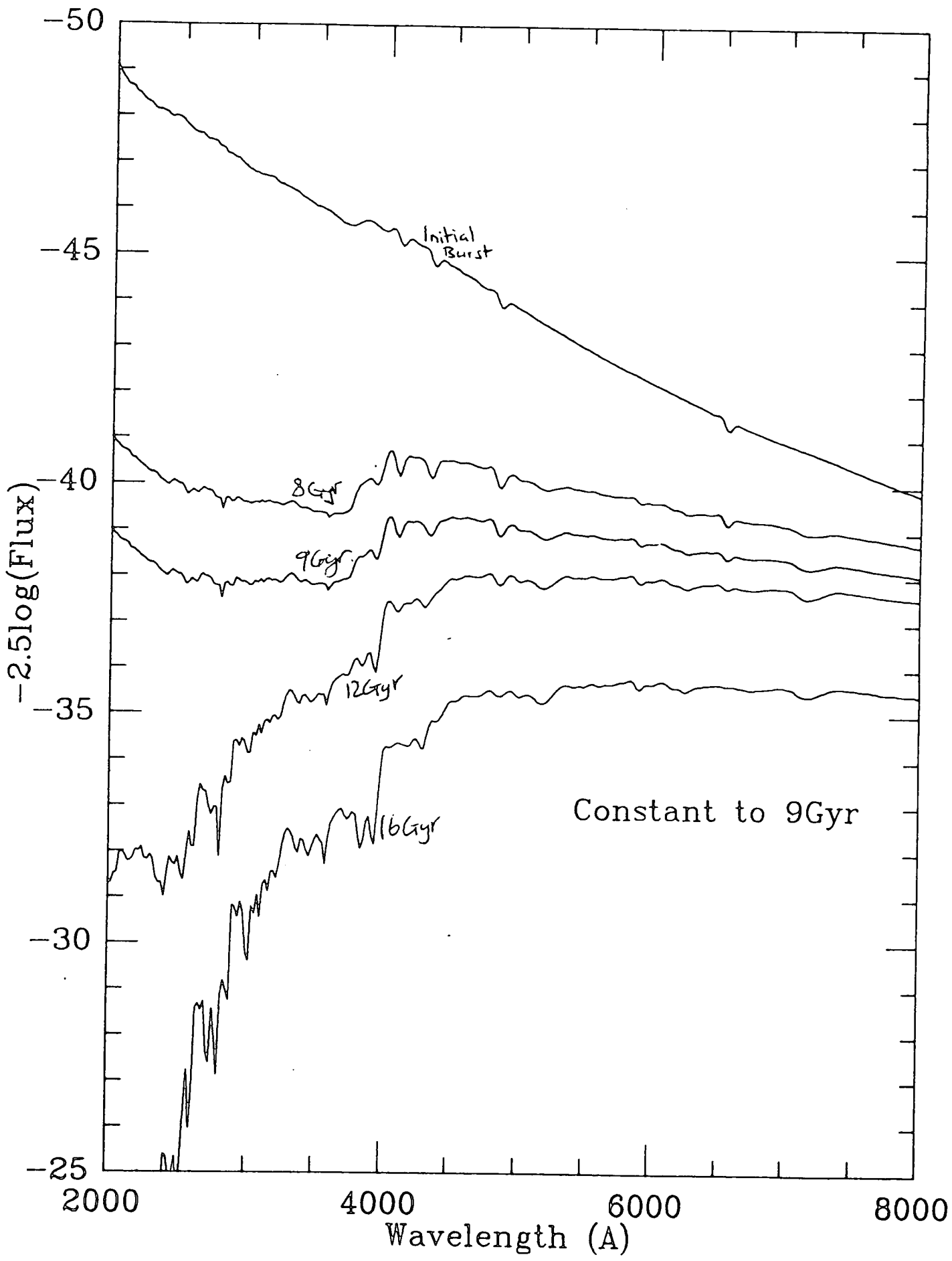


Figure 5.5: The variation in strength of the $H\delta$ absorption line with stellar type (from Kurucz, 1979).

Fig. 5.5(b) Bruzual SEDs for a variety of ages.





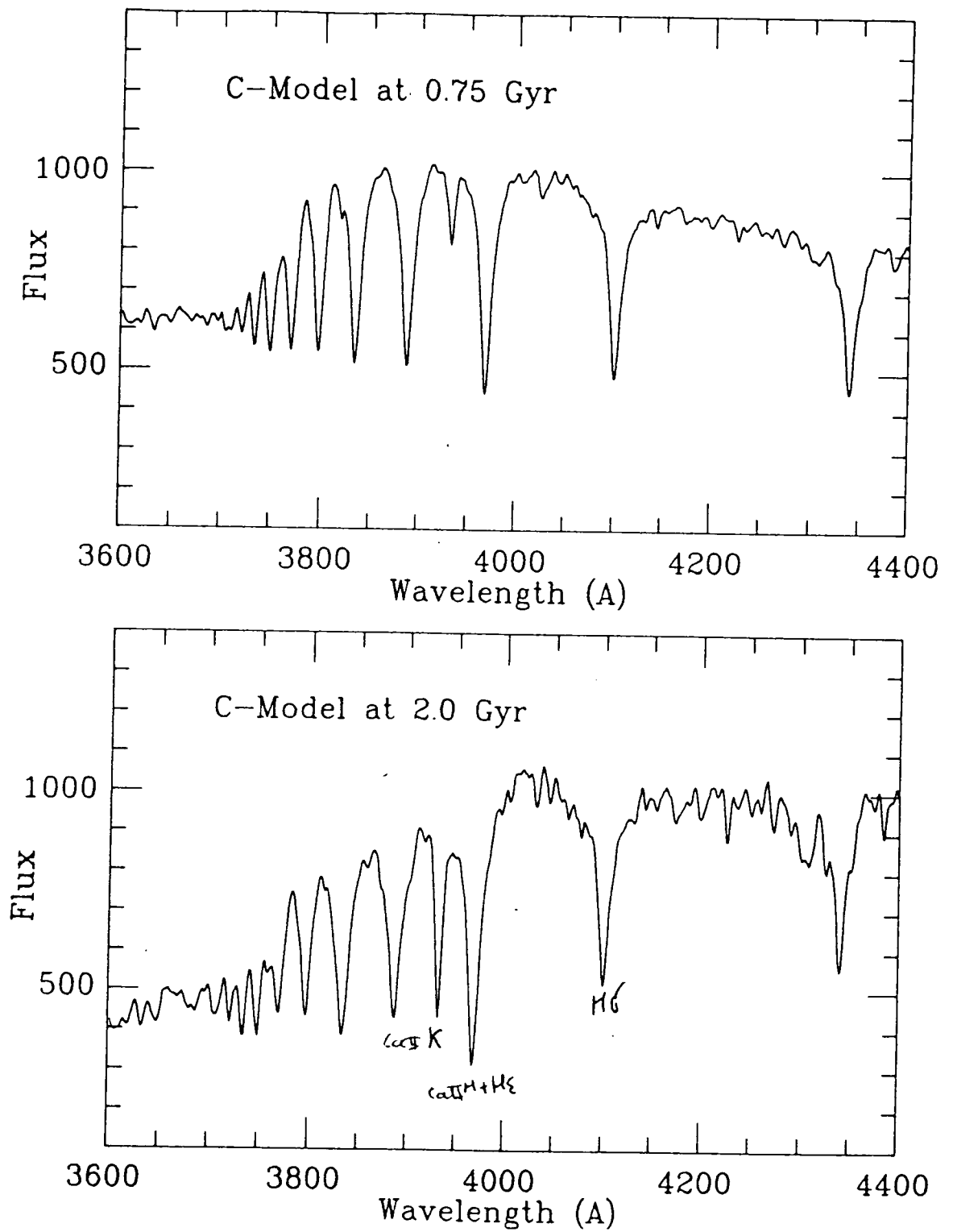


Figure 5.6: Modelled galaxy spectra using Bruzual models and Jacoby *et al*'s detailed library of stellar spectroscopy, shown at different ages after the initial burst of star formation.

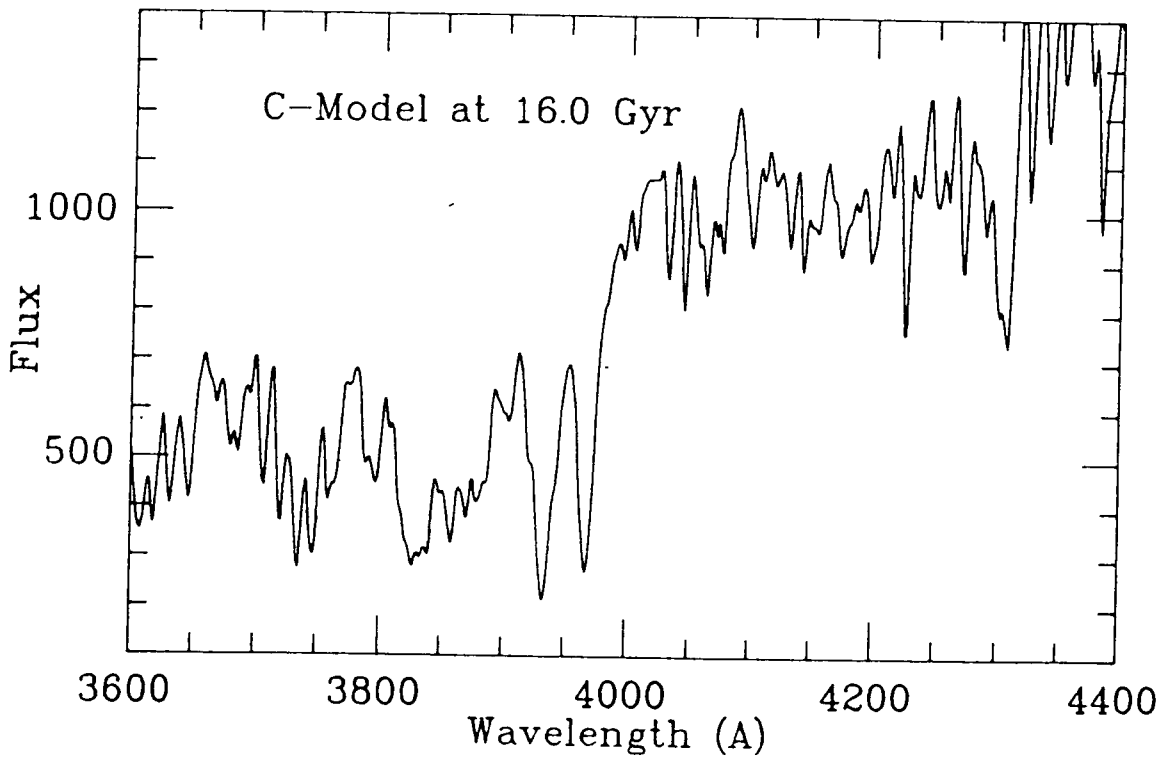
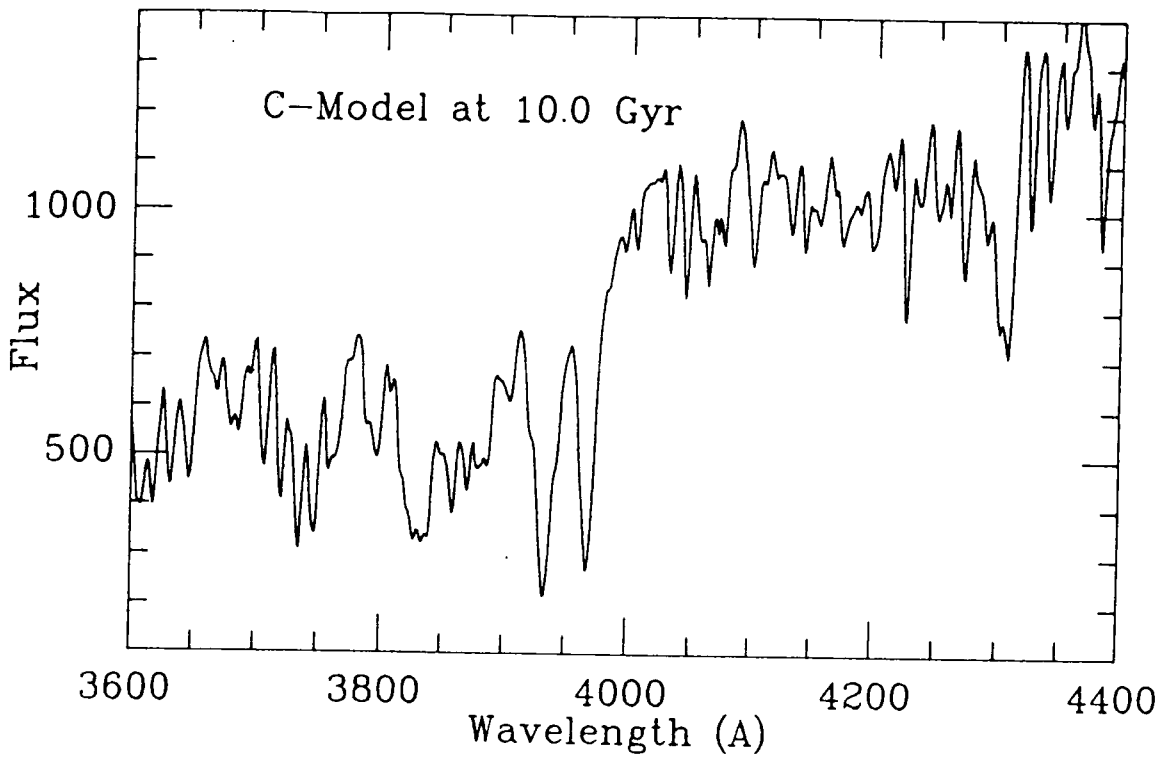


Table 5.4(a): $z = 0.37$ Colours from burst model

Age(Gyr)	418-685	U-685	502-685
6.0	3.731	4.498	2.147
7.0	3.812	4.562	2.196
8.0	3.810	4.501	2.257
8.4	1.512	0.817	0.964
9.0	2.825	2.765	1.605
9.4	2.901	2.997	1.657
10	3.254	3.539	1.903
11	3.694	4.244	2.170
12	3.617	4.181	2.147
16	4.133	5.051	2.392

Table 5.4(b): $z = 0.54$ Colours from burst model

Age(Gyr)	418-685	502-685	578-685
6.0	4.585	2.287	1.187
7.0	4.640	2.327	1.226
8.0	4.582	2.312	1.272
8.4	1.476	1.025	0.342
9.0	3.219	1.941	0.875
9.4	3.396	1.948	0.900
10	3.800	2.096	1.042
11	4.365	2.304	1.212
12	4.299	2.292	1.195
16	5.080	2.513	1.383

Table 5.5: (1) Bruzual's *c*-Model, Equivalent Widths.

Age	H δ	H + H ϵ	K	(B - V) _o	ΔV_o
0.01	4	5.5	0.9	-0.208	0.696
0.75	7	8.7	1.3	0.176	-2.738
1.0	7.5	9.4	1.6	0.179	-2.909
1.6	8.0	10.6	3.2	0.343	-2.313
2.0	6.5	9.3	4.2	0.505	-2.167
2.6	3.6	8.3	6.1	0.672	-1.849
3.0	2.4	8.0	8.8	0.802	-1.744
4.0	3.3	8.0	8.0	0.695	-1.546
5.0	1.7	8.1	11.5	0.850	-1.014
6.0	2.0	8.2	12.2	0.818	-1.070
8.0	1.5	8.1	12.8	0.891	-0.691
10.0	1.4	8.4	12.9	0.860	-0.576
11.0	1.3	8.2	12.6	0.882	-0.427
12.0	1.2	8.4	12.6	0.896	-0.322
16.0	1.1	8.5	13.3	0.946	0.0

(b) Decay Model, Equivalent Widths.

Age	H δ	H + H ϵ	K	(B - V) _o	ΔV_o
0.01	4.0	4.8	0.6	-0.209	3.282
1.0	6.9	9.2	1.6	0.180	-0.324
3.0	5.9	8.4	2.2	0.358	-0.990
5.0	5.3	8.1	2.6	0.426	-1.231
8.0	4.7	7.9	3.0	0.487	-1.435
9.0	3.1	7.8	6.5	0.351	-1.031
10.0	1.6	7.6	9.4	0.806	-0.786
11.0	1.4	7.8	9.2	0.811	-0.600
12.0	1.2	8.1	10.8	0.852	-0.420
13.0	1.2	8.0	11.0	0.856	-0.268
14.0	1.2	8.1	11.5	0.870	-0.207
16.0	1.3	8.0	11.7	0.891	0.0

(c) Burst Model (15% at 9.0 Gyr).

Age	H δ	H + H ϵ	K	(B - V) _o	ΔV_o
0.01	4.1	4.9	0.6	-0.209	-2.335
1.0	7.9	9.1	1.6	0.180	-1.592
2.0	6.2	8.7	4.0	0.504	-0.971
4.0	3.2	7.3	7.4	0.694	-0.440
5.0	1.3	8.0	9.8	0.850	-0.117
8.0	1.2	8.1	11.0	0.871	-0.169
9.0	1.3	7.9	10.8	0.840	-1.436
10.0	6.1	9.4	3.0	0.454	-0.978
11.0	3.6	7.9	5.9	0.686	-0.630
12.0	1.4	7.7	9.2	0.857	-0.414
13.0	1.5	7.6	9.3	0.847	-0.365
16.0	1.2	8.1	11.4	0.928	0.0

For example if we consider the reported Balmer line strengths of the PSGs in the 3C295 cluster in comparison with these models, we find that the decay scenario, whereby a blue galaxy suddenly ceases star formation, will not produce strong enough absorption lines. As with Dressler and Gunn, we are led to the conclusion that to match such spectra the last active star-forming period must have represented a considerable increase over the past average SFR. In other words, the models suggest that we require an additional burst of star formation on our pre-existing galaxy. However, we are still unable to tell whether that pre-existing galaxy was of an early-type containing a large gas fraction which suddenly underwent a burst of star formation, or whether the galaxy was of a 'spiral' type, with a constant level of star formation.

Returning to the current observations, if this 'burst' scheme is appropriate, then the galaxies exhibiting the strongest uv excess should also display strong Balmer absorption lines. Figure 5.7 shows the relation between uv colours and absorption line strength calculated for a single added starburst. Indeed, from the preliminary spectroscopy reported to us by Fort and Mellier (1987, and private communication), this result would appear to be confirmed, for example, in the case of galaxy # 102 in A370.

To conclude this section we must stress that it is probably unwise to pursue our models much beyond the largely qualitative stage of the present discussion, but that our discovery of the enhanced uv brightnesses of optically red galaxies using the narrow-band imaging technique has played a significant role in our progress towards an overall evolutionary model for distant galaxies. In particular, the class of uvx galaxies is not inconsistent with the picture envisioned by Dressler and Gunn, whereby some galaxies, for reasons yet to be discussed (see next section), undergo short but significantly large bursts of star formation in the recent past (1-3 Gyrs ago). This would lead to an evolutionary progression from blue, actively star-forming galaxies, via the PSG phase, to uvx galaxies, and thence to the red colours appropriate to early-type cluster members. Although the question that arises is, do all galaxies go through such a phase at different epochs, or do only certain types of galaxies behave in this way? For a definitive answer to this we must deduce the 'trigger' mechanism responsible for the observed star-forming phase.

5.4 Discussion.

In the previous section we attempted to address our current observations in the context of the 'starburst' model of galaxy evolution. However, we have, as yet, to consider the fundamental question, viz, what possible physical mechanisms can be responsible for such behaviour?

Gunn and Gott (1972) originally noted that in the rich cluster environment, the hot intracluster medium (ICM) may be sufficiently dense that the pressure it causes a galaxy to experience on its orbit through the cluster's central regions is larger than the binding force of the galaxy's gaseous material to its disc. This ram-pressure effect received a lot of attention and was embraced by many authors as a possible explanation for the change of blue fraction with redshift. The blue, star-forming galaxies then lose their gas as they move through the ICM and consequently their star-formation is truncated. Whilst the simplicity of such a process is attractive it may only be illusory, since subsequent work has revealed that the actual dominating mechanism responsible for the Butcher-Oemler effect is most probably more complex.

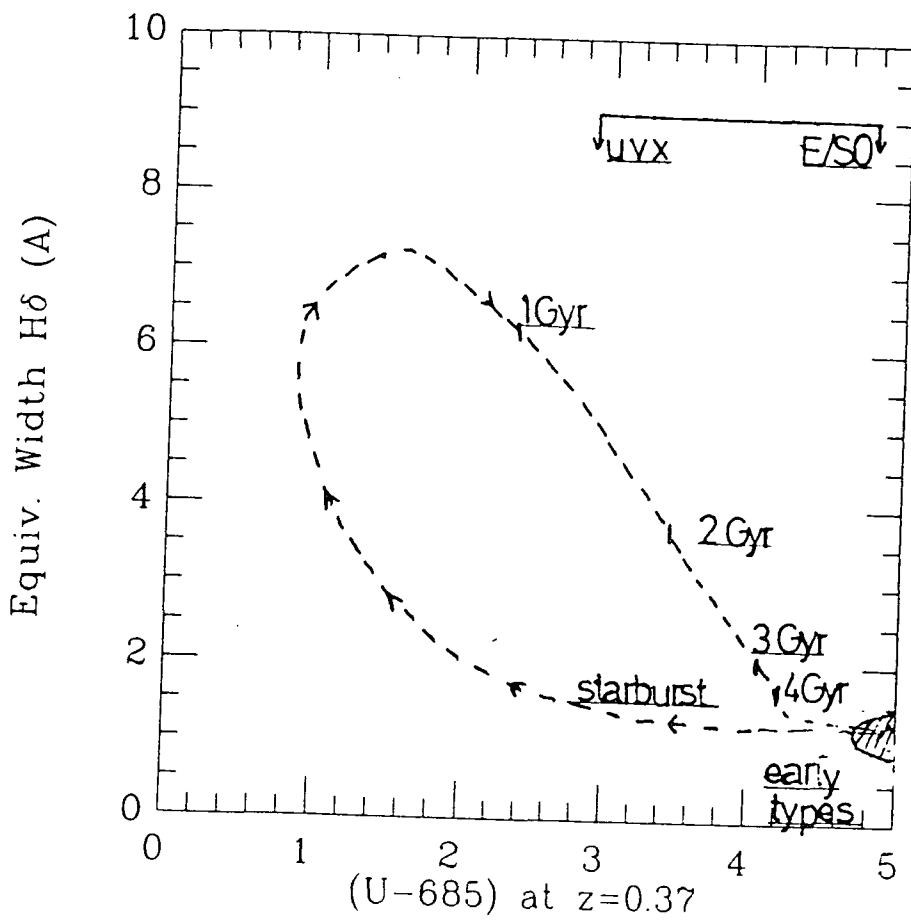


Figure 5.7: Relation between uv colour and $H\delta$ absorption line strength, estimated using the second burst model in figure 5.6 The times shown are measured from this second burst.

Whilst we shall not be concerned, too greatly, with the arguments regarding ram-pressure stripping, here, it is important to outline a few key aspects of the debate. Haynes *et al.* (1984) provide a fairly detailed discussion of the process in their studies of the gas-content of galaxies. The focus of many of the arguments has been the likely efficiency of the stripping and its dependence, for example, on galaxy morphology or bulge-to-disc ratio (Gisler, 1980). Studies of large samples of nearby galaxies seemed to indicate that the removal of gas from discs by simple stripping, or indeed other ablation schemes (evaporation, see Cowie & Songaila, 1977), is quite difficult to achieve, at least to the extent necessary to explain the Butcher-Oemler effect.

Larson, Tinsley, and Caldwell (1980) proposed a scheme whereby material was not stripped from galaxy discs, but rather from surrounding gaseous halos which supply fuel to the star-forming disc via infall. This rather simple scheme removed many of the previous difficulties, yet its realism is in doubt since such infall has not been observed. So we must only consider it as being speculative.

However, these arguments should not imply that ram-pressure stripping does not occur, since clearly the ICM densities in rich cluster cores are very high. Indeed, van den Bergh's (1976) discovery of 'anemic' spirals in cluster cores, ie galaxies containing very little hydrogen content, may very well testify to the presence of the effect. The only question is to the efficiency of the stripping process.

Considering the observations of galaxies in distant clusters, a model of simple cessation of star formation due to a sudden removal of gas content is incapable of explaining the line strengths claimed for the PSGs. However, a galaxy moving through the dense ICM could cause a sudden compression of the gas in the galaxy's disc leading to a rapid burst of star formation which rapidly consumes the available gas. As Bothun & Dressler (1986) discuss; when one seriously considers the gas dynamics of these systems many complications arise, such as the formation of bow-shocks around the galaxy which could even inhibit star formation or lead to a redistribution of material within the galaxy.

Advocating ram-pressure or other environmental processes as a means of transforming spiral galaxies into S0s, may also be unsatisfactory, since we must then ask why it is that S0 galaxies are observed to have similar properties whether they are found in the field or in rich cluster cores.

Aside from such a cluster-dependent mechanism, an alternative possible cause of star-formation is galaxy-galaxy interactions. This type of behaviour has received a lot of consideration recently from studies of local galaxies, particularly with the results of IRAS observations (see, eg, de Jong, 1986, for a review). However in the rich cluster environment, such interactions are unlikely to occur due to the large velocity dispersions. A larger degree of substructure within galaxy clusters at these epochs could lead to the possibility of interaction with the lower internal velocity dispersions of each subcluster. From the observations of our two distant clusters we can see that some of the blue galaxies do have apparent close neighbours, but many appear to be isolated. this question however cannot be answered in the absence of detailed velocity information.

Lavery and Henry (1987) have studied this possibility using a series of observations of three clusters at $z = 0.2$. They prefer this method to the stripping process since they claim that many of the actively star-forming galaxies in their samples have close companions.

The observations of the distant clusters, A370 and 0016+16, presented in the previous two chapters may provide further clues to the evolutionary process. For example, we have compared the observed proportions of each type of galaxy with the expected populations estimated by Couch (1981), in earlier.

As first mentioned in chapter 3, it is notable that the proportions of galaxies in 0016+16

that display enhanced uv luminosities as compared to the red CM-sequence galaxies is close to the expected elliptical to S0 ratio. Placing significance on this result leads to the conclusion that the S0 galaxies constitute the evolving component at high redshifts (see Couch, 1981). If this were the case, we must then be observing the cluster A370 at a time at which most of the S0-precursors are undergoing large amounts of star formation (and hence display the colours of spiral types), or have recently ceased such activity (Balmer absorption lines, uvx galaxies).

Valuable information will also lie in the light profiles of high redshift galaxy images, indicating the presence or otherwise of disc structure. As discussed earlier, the present observations can only indicate that the individual galaxy uv images are extended rather than centrally-concentrated. Thompson (1986) has obtained detailed, high spatial resolution images of the core of the cluster 0024+1654 and claims to be able to estimate bulge-to-disc ratios. Unfortunately, however, few of the blue Butcher-Oemler objects were included in his sample. Nevertheless, he claims that most of the images show moderate to large ratios, suggesting that these galaxies are of earlier type than present-epoch colour equivalents, the spirals.

The spatial distribution of the star-forming galaxies is also of relevance to a discussion of the potential effects of environment on galaxy evolution. In the case of 0016+16, the small sample of objects considered in chapter 3 revealed no evidence for any such structure, but we do note that one of the central members of the cluster was classified as a uvx galaxy, highlighting the possibility of galaxy interactions being of significance.

In A370, as can be seen in figure 4.1, there is a hint of a circular distribution over $150h_{-1}$ kpc from the cluster centre. Also of possible relevance is Lynds and Petrosian's (1987) recent discussion of the large arc-like structure present in A370, and which they also note in another (presumed) distant cluster. Conjecture as to the origin and nature of this feature has been wide-ranging, but one favourable possibility is that a cluster-scale shock wave has swept up the ICM or stripped gas to form a large star-formation region. The arc is present in our observations of the cluster and is the feature stretching from galaxy # 100 to # 101. Unfortunately, the resolution of our CCD images is rather limited and we cannot easily separate the arc from the nearby galaxies. Whilst we find that of the four galaxies that lie along (or are projected on) this arc, two have blue spiral-type SEDs and the others are uvx-type, the arc itself is likely to lead to colour contamination. However, this may well indicate that cluster-scale dynamical effects and star-formation are related. Further observations are obviously vital to this particular point, specifically spectroscopy and detailed photometry of the arc itself.

In the dynamical approach (ie rather than assuming that the observed evolution is due to an internal mechanism in each galaxy), the explanation for the apparent low blue fraction of 0016 in comparison to A370 and other clusters at this redshift would be that the former is in a dynamically more evolved state and collapsed at significantly earlier epochs. Thus we observe few or no ongoing starbursts and only the 'tail-end' of evolution in the uvx galaxies. A370 on the other hand, is currently in an active star-forming phase (large blue fraction) and the evolution from blue to red galaxies is ongoing over a range in epoch since not all galaxies are observed in a single state. Furthermore, the cluster is apparently more 'clumpy' in that there are two bright central condensations of galaxies in the core region, although we have as yet insufficient spectroscopy available to study velocity structure.

This section should only serve as a guide to the variety of possibilities available for explaining the observed evolution of galaxies in distant clusters. Clearly we are at the forefront of this field with such imaging uv techniques, but before we can make any further headway as to any general theory or model, we must ensure that our interpretations are

well-founded. Specifically, we must ensure that we compare like with like, and that reality is not obscured by a lack of regard for selection effects.

6. A Catalogue of Distant Clusters of Galaxies.

In the previous chapters we have seen that distant clusters of galaxies can serve as excellent probes of galaxy evolution, providing large samples of galaxies over a range of luminosities at each redshift. The first problem we face in undertaking such studies however, is rather basic, namely that of cluster selection, the requirement of a homogeneous, well-defined catalogue of distant galaxy clusters being difficult to fulfil.

In this chapter I shall briefly discuss previously published catalogues of clusters of galaxies and stress the difficulties encountered when extending such searches to higher redshifts. I shall then describe a technique that has been devised to detect and categorise distant clusters before presenting the results of applying the method to deep 4 m photographic plates. Finally I shall summarise the current observational status of our catalogue.

6.1 Introduction.

Definitions in astronomy are seldom free of a degree of subjectivity. Clusters of galaxies prove no exception, causing difficulty both in their detection and the specification of their various structural properties. The discovery of clusters on photographic plates and other panoramic detectors is hampered by the lack of almost any 3-dimensional information. For example, overlapping statistical fluctuations in the galaxy field distributions can mimic clusters on the projected 2-dimensional plane, when no genuine physical association exists in the redshift distribution.

In order to avoid, or at least minimise, such difficulties, attention is usually focussed on the core regions of the richest of systems. Such was the approach of, for example, Abell (1958) during the compilation of his catalogue of rich clusters. Abell provided a sample of 2712 clusters of galaxies selected from red Palomar Plates using well-defined selection criteria and covering a large area of the Northern Sky unaffected by galactic obscuration ($\sim 3 \times 10^4$ square degrees). To be included in the catalogue a cluster had to contain at least 50 members in the magnitude range m_3 to m_{3+2} , these members lying within a circle about the cluster centre of radius $3h_{50}^{-1}$ Mpc. Cluster distances were estimated from the brightness of the 10th brightest member and largely lay in the range $0.02 \leq z \leq 0.20$. Of the 2712 clusters in the sample, 1682 constitute a complete sample, making the Abell catalogue a useful statistical tool. The success of the Abell Catalogue has led to current attempts by Abell and Corwin to extend its coverage to the southern hemisphere using U.K. Schmidt Survey plates (Abell and Corwin, 1983).

The importance of carefully specifying selection criteria can be demonstrated quite vividly by comparing the Abell catalogue with that of Zwicky (1961-68) whose definitions were somewhat less strict. Rather than specifying a fixed diameter within which the cluster members should lie, Zwicky used the isopleth where the projected density of galaxies was about twice that for the neighbouring field. On the whole, Zwicky tended to pick less rich clusters than Abell and the use of the contour method resulted in the selection of quite different structures from the same observational material (see figure 1 of Flin (1981) for an example).

The Abell catalogue has been extensively used and so it is important to be aware of its limitations. Lucey (1983) has analysed the selection criteria of the catalogue in some detail. Using computer produced galaxy distributions he attempted to simulate, as near as was possible, the selection methods of Abell on artificial 'plates' (projections of the real spatial distribution on the two-dimensional plane, including magnitude limits, etc.). He was able to estimate the number of 'false' clusters (projection effects) that would be found to satisfy the selection criteria, thus providing an estimate of the probable correctness of the catalogue.

In conclusion, Lucey states that the Abell Catalogue contains “ 70 to 85 per cent of the rich clusters within $z = 0.19$, and also a significant fraction of false (i.e. non-physical) clusters.” Obviously, the reality of a given cluster as a true physical association can only be finally resolved by detailed spectroscopy of the supposed members.

If our aim is to compare galaxies at high redshifts with their nearby counterparts in order to gain insight into evolutionary processes, then we must probe to somewhat greater depths than that attained by the Abell catalogue.

There are two possible approaches to the detection of distant galaxy clusters, either by ‘direct’ or ‘indirect’ means. By ‘direct’ I refer to those methods which make use of the definition of a cluster as an enhancement in galaxy number density above the background. A set of specified criteria are used to select only those candidates which are statistically significant at a chosen limit. The Abell Catalogue then is a prime example of this approach. Since I use such a method in this work I shall defer detailed discussion of its merits and disadvantages to a later section, but note here that, because of the low density contrast of distant clusters on photographic plates at redshifts in excess of $z \sim 0.3$, numerous other ‘indirect’ techniques for cluster detection have been used.

An ‘indirect’ approach is typified by using any detection methods that are based only on some secondary property associated with the cluster. For example, we can examine the environments of known distant radio sources to test whether such objects inhabit clusters, groups, or the field (see, eg., Prestage, 1984). The implication of using radio techniques to search for distant clusters is that such methods will only find certain types of objects whose physical properties (i.e. radio emission) may be due to both their specific evolutionary stage and also the conditions in the cluster environment itself, thus creating a serious bias in the sample and perhaps confining the spread of possible cluster properties to an artificially narrow range.

Each of the techniques used to date has its own characteristic advantages and disadvantages in comparison to the others. However, the issue which is of concern here is that we must be wary about collating together clusters from a variety of *different* sources to form any single sample of objects for evolutionary investigations.

In the past, authors have indeed studied clusters selected from a wide range of sources, the emphasis having been on trying to find increasingly distant objects with little regard paid to the intrinsic biases of each method. In table 6.1 I present a list of all clusters of galaxies with redshifts greater than $z \sim 0.3$ that have been used for previous investigations of galaxy evolution with a brief description of how each was originally found.

The fact that the cluster around 3C295 contains many blue ‘active’ objects whereas the other original Butcher-Oemler cluster 0024+16 is dominated by galaxies with spiral-type spectra, may not be at all surprising when we remember that the former was discovered by virtue of its radio source. Similarly the difference in constituent populations of the 0024+16 and 0016+16 clusters may simply be a reflection of the use of blue and red photographic plates in respective cases.

The most substantial work that has been done in this area is the compilation of a large sample of clusters over the past ten years by Gunn and co-workers. Their final catalogue as presented in Gunn, Oke and Hoessel (1986) consists of positions of some 400 potential distant clusters. Despite the scale of such an undertaking, the catalogue as it is presented still suffers from some drawbacks. In particular, none of the publications to date has presented any strict definition of what constitutes a ‘cluster.’ A simple eyeball search for an ‘apparent cluster’ without any refining semi-quantitative criteria is fraught with complications. This must surely cast doubts on the possible reality of many of the candidates and indeed on the completeness limits, making the catalogue considerably less systematic than the authors

Table 6.1: *Detection Techniques for Previously Observed Distant Clusters.*

Cluster	z	Detection Method	References
0024+1654	0.39	Bright members visible on blue plates.	Humason and Sandage(1957)
3C295	0.46	Optical id. of radio source.	Minkowski(1960)
Abell 370	0.37	No. density enhancement.	Abell(1958)
1447+26	0.37	enhancement?	Gunn and Oke(1975)
AC103 AC114 AC118	0.3	No. density enhancement.	Abell and Corwin(1983)
0016+16	0.54	No.density enhancement on red plates	Kron(private communication to Koo, 1981)

claim.

We can illustrate the nature of the expected problems in searches for distant clusters of galaxies by using the models of Couch *et al* (1983). The simplest definition of a cluster of galaxies is that of an over-density in the distribution of galaxies against the field within a fixed area. Using a specified luminosity function in conjunction with field counts and k-corrections, it is possible to simulate the density contrast of a cluster of a given richness in a chosen passband.

The density contrast at a fixed redshift will obviously be greater for richer clusters, so this simple model made use of Couch and Newell's (1984) B_J and R_F luminosity functions for Abell 1942 which is of richness class 3. The k-corrections of Ellis (1982) were applied, along with a modelled field distribution based on the counts of Couch and Newell (1984), Koo (1981), and Peterson *et al* (1981). To define an area over which the density contrast was measured, a metric diameter of some ~ 1.5 Mpc ($H_0 = 50, q_0 = 0.1$), was used for convenience with the available photometry.

Such a model must be accepted as being fairly crude, based on a number of simplifying assumptions. Nevertheless, it provides a useful indication of the likely appearance of a cluster as a function of redshift. We can define the contrast, σ , such that it represents the *excess* number of galaxies found in a given area ($N - N_f$), above that expected from the field distribution (N_f),

$$\sigma = \frac{N - N_f}{\sqrt{N_f}} \quad (6.1)$$

whose redshift dependence is shown in figure 6.1. In the absence of any spectral evolution of galaxies it can be seen that clusters are more significant in the red (R_F), whereas the inclusion of Bruzual $\mu = 0.5$ evolution (chapter 1), enhances the cluster contrast in the blue.

By increasing our redshift range much beyond the limits of the Abell catalogue, we shall become more susceptible to the difficulties caused by the behaviour of the field galaxy distributions. Furthermore, by subtending a larger volume of space, there is a much increased probability of finding overlapping of clusters at very different redshifts, where the combined density contrast may be mistaken for a single rich system at one redshift.

The need then is for us to impose an acceptable cut-off in the contrast necessary for inclusion in our catalogue. A useful limit will be determined by the size of the contrast that minimises these spurious effects whilst allowing us to probe to reasonably high redshift. Using these simple models for example, a 3σ cut-off corresponds (in the no-evolution case) to $z = 0.55$ in J, or $z = 0.65$ in F, for richness class 3 clusters.

In this chapter we shall consider a new approach to finding possible distant clusters from existing photographic plates. We are primarily interested in selecting clusters at redshifts beyond those of the Abell clusters, $z > 0.3$, pushing the plate material to its limits, hopefully reaching as deep as $z \sim 0.7$. A large sample of candidate clusters selected by a well-defined set of criteria from a single homogeneous source, should prove an invaluable tool in our quest to unravel the true nature of galaxy evolution since these early epochs.

6.2 Detection Method.

Exploiting the fact that whilst faint images form in the upper layers of photographic emulsions, noisy fog grains are randomly distributed throughout the emulsion, Malin (1978) has developed a technique for enhancing the prominence of extremely faint images on photographic plates without also boosting the noise. Such high contrast films (HCFs) made from photographic plates have already been used to much effect in the study of faint nebulosities

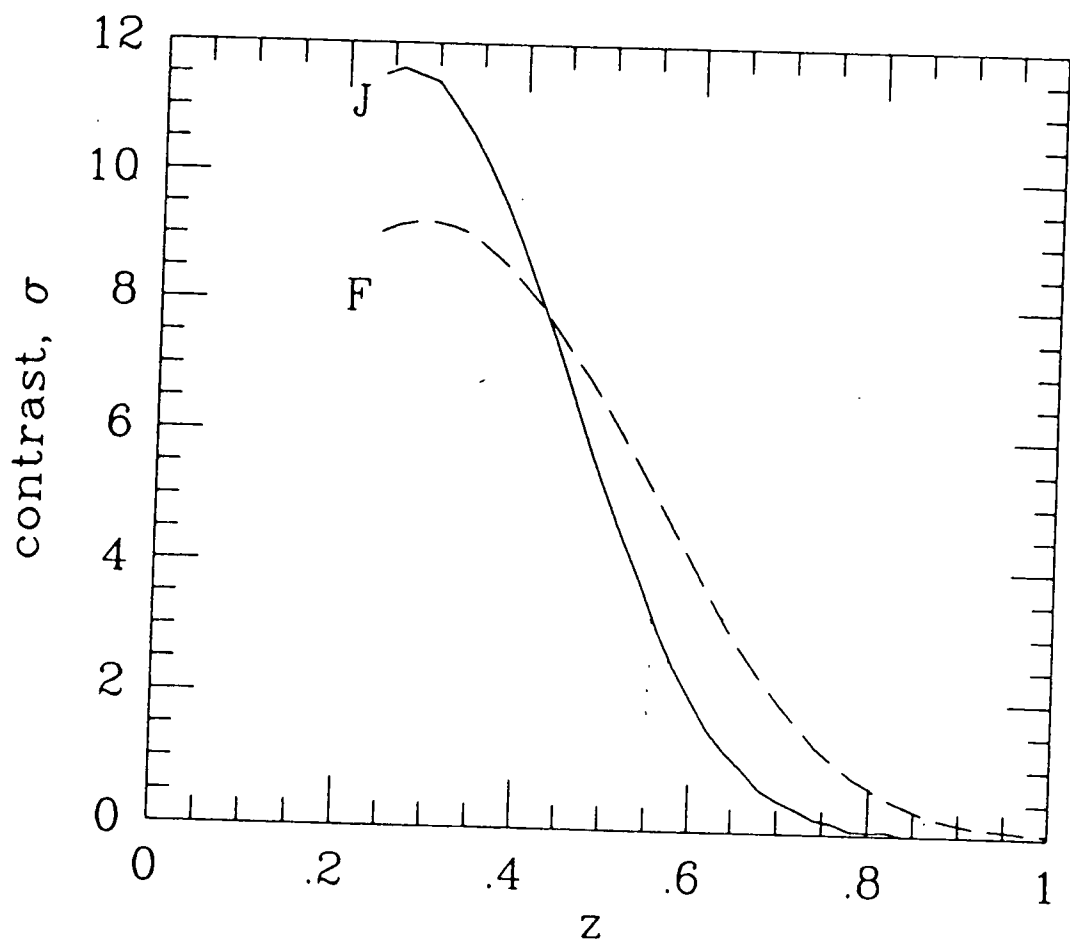


Figure 6.1: Cluster contrast as a function of redshift (from Couchet *al*, 1983).

and, for example, led to the detection of faint shell like structures surrounding elliptical galaxies (Malin and Carter,1980).

Such a technique obviously holds much promise for the detection of faint clusters of galaxies whose brightness lies so close to the detection threshold that their discovery on untreated plates would have proven extremely difficult. Indeed it is this possibility which we shall now consider. Firstly, however, it is important to check the reliability of the HCFs.

Couch *et al* (1984) have compared the results of a search for faint objects on one HCF with APM (Kibblewhite,1980) reductions of the original AAT plate. They concluded that the high-contrast technique could reliably detect images down to the faint limits of the original plate. We have subsequently undertaken a similar analysis on a number of other fields and find that their results are generally applicable.

As an example, we consider the AAT plate J1836 for which photometry has been obtained using the COSMOS plate-measuring machine at the Royal Observatory, Edinburgh (Stobie *et al*, 1979). As well as mapping the original plate we have obtained deep CCD frames in a selected area of this field. Figure 6.2 is a print of the region under consideration produced using the high contrast technique. The area is dominated by an enhancement in the surface density of galaxies which we classify as a candidate distant cluster, using criteria which we shall discuss later. For the present we shall only be concerned with individual object detection and, in particular, a comparison between machine measurements and eyeball searches.

Jones (1986, private communication) has reduced the COSMOS scans of the original plate material, calibrating the magnitude system using CCD photometry of standard stars. We have used these results to map the region under consideration and count the number of objects in magnitude intervals down to the limits of the sky threshold. An example of such a map, produced using software supplied by Shanks and co-workers (1986, private communication), is given in figure 6.3. Comparisons of these counts with the previous eyeball search of the HCF of this plate are presented in table 6.2. Column (a) is the number of objects found by COSMOS, whilst column (b) is the number of these objects which were also found in the eyeball search.

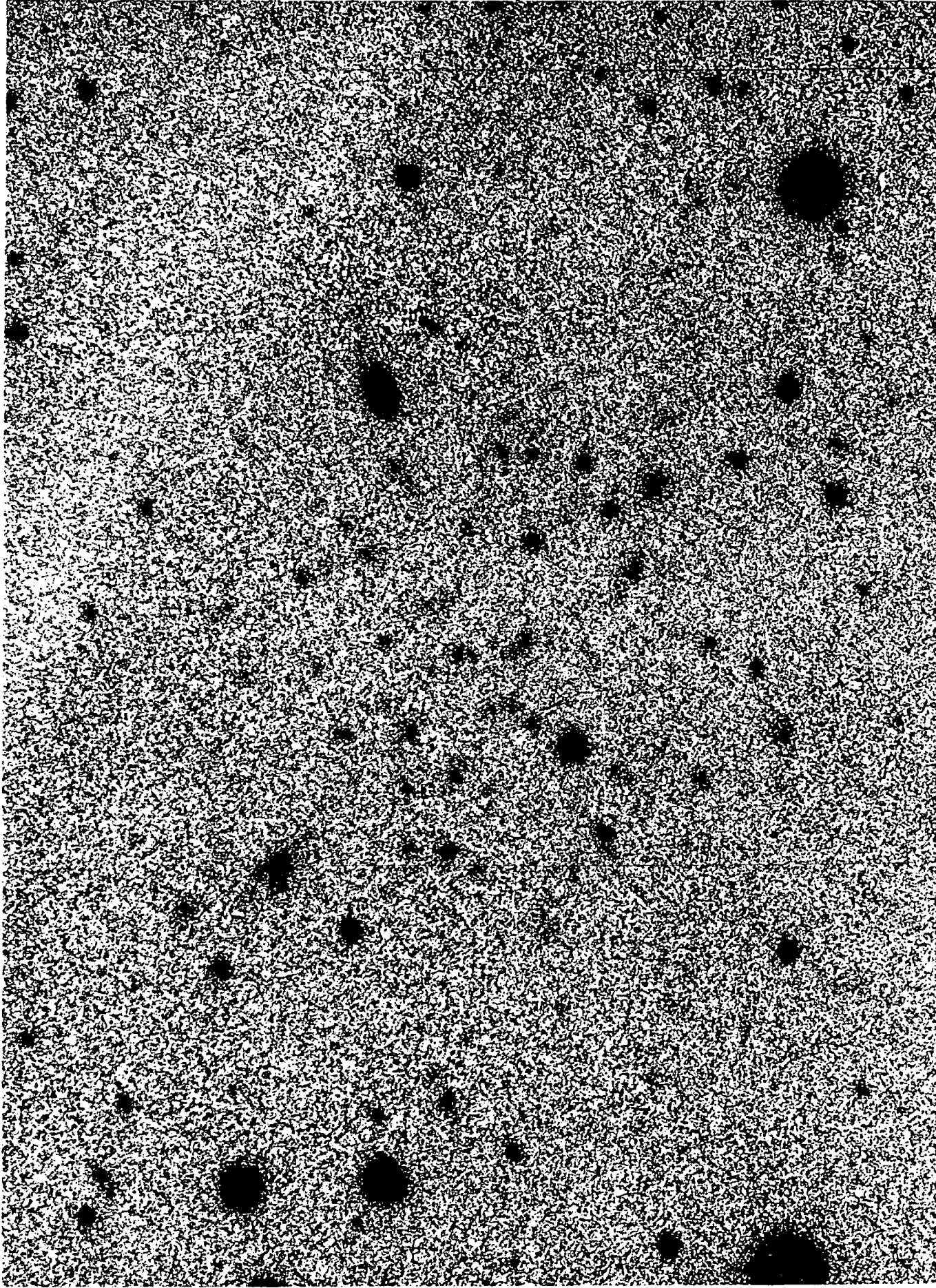
Whilst agreement is relatively good between the two methods, we also find some disagreement, particularly at faint limits. Indeed, beyond $B_J = 24.5$, there is an increasing number of objects found by COSMOS but not identified by eye. Furthermore, in the eyeball search, we also identified a large number of objects which the COSMOS scans did not detect. Fortunately, further study of each of these discrepant cases can be effected by comparison with our CCD images of the area. Although these frames are relatively deep, they have not been obtained in exactly the same passband as the photographic material. However, the effective wavelength (~ 418 nm) is fairly close to that of B_J (~ 440 nm).

We find that of the excess objects found by eye on the HCF but not by COSMOS, almost all (17/19) were also present on the CCD frames, proving that these constitute genuine objects and are not spurious effects caused by either the HCF technique or the subjective nature of the eyeball searches. Column (d) of table 6.2 reveals, however, that most of the objects that were detected only by COSMOS are not present in the CCD data, but rather, are spurious effects in the sky background that were identified as objects by the adopted threshold of the COSMOS analyser.

It is worthwhile considering here some of the problems that machine-scanning techniques can be prone to. For example, varying definitions of what constitutes a genuine image in such digitised data can lead to differing results. Altering the threshold above the sky background intensity at which an object is accepted as real, can introduce problems. Images that are near to each other may be merged and identified as only a single object by the analyser program, or very bright images may be fragmented into a large number of smaller objects.

N

E



1"/mm

Figure 6.2: High contrast print of the candidate cluster J1836.23t, produced by D. Malin.

f

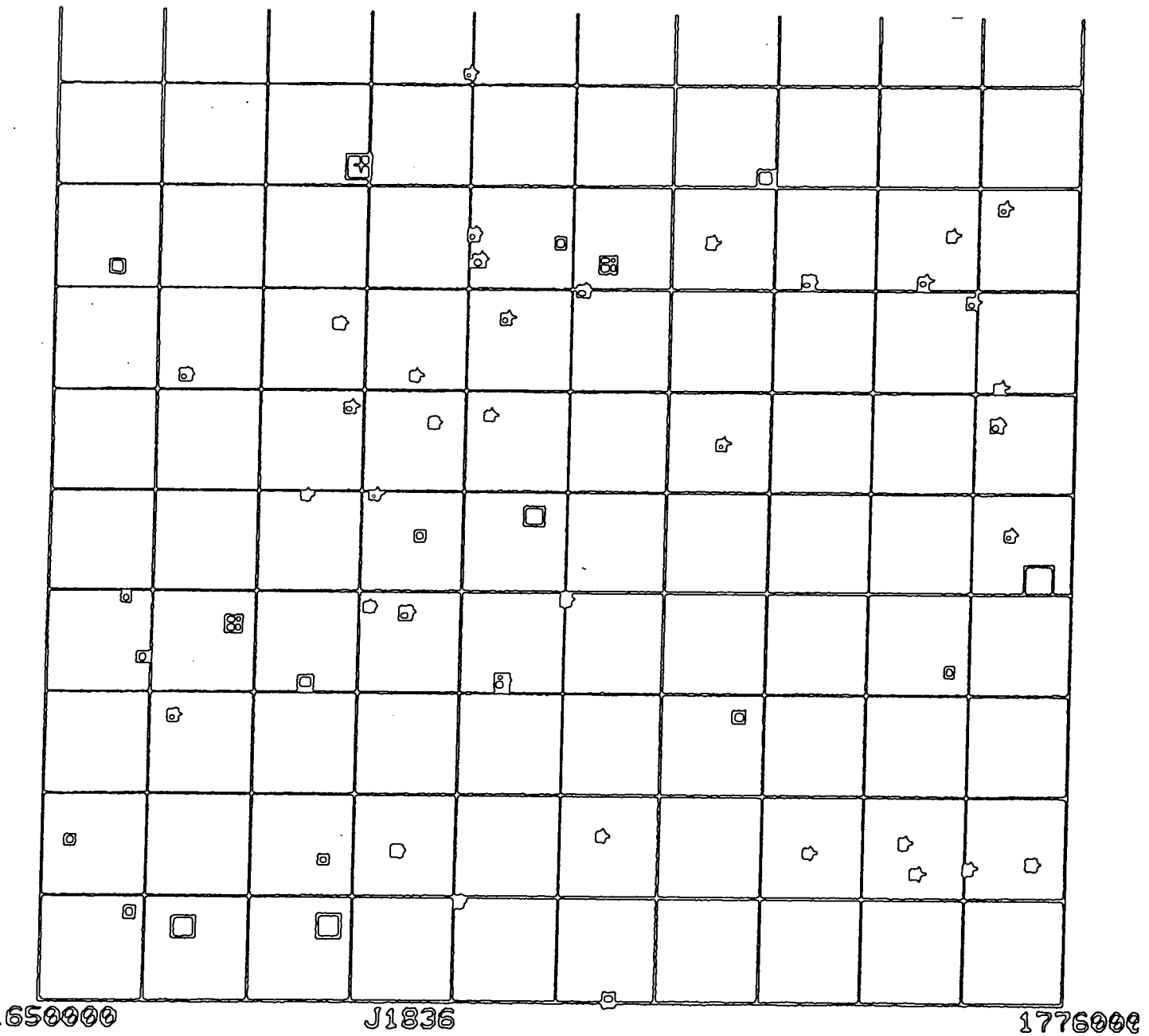
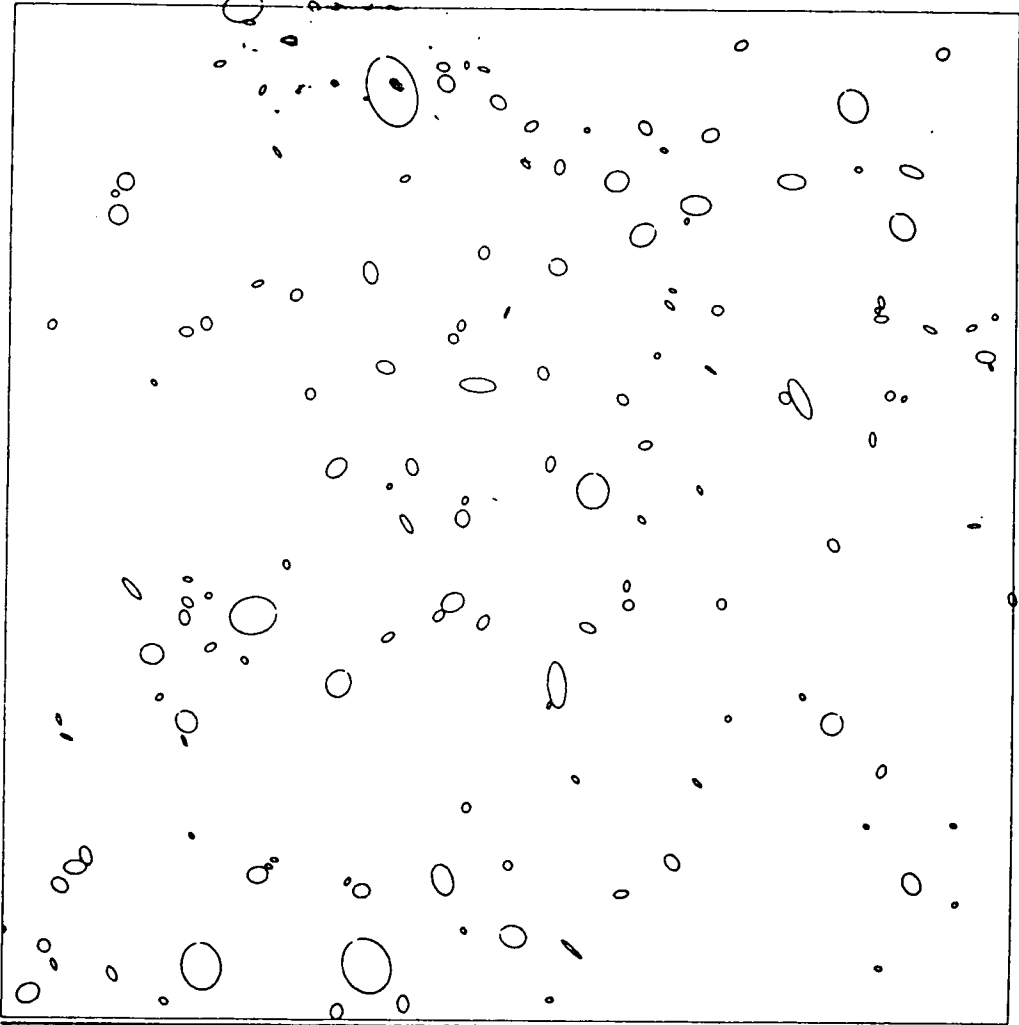


Figure 6.3: COSMOS map of the region around J1836.23t.

f

I.D.P.U. ROYAL OBSERVATORY EDINBURGH (COSMOS GROUP)



JOB: 731
PLATE: 1836
DATE: 30 10 19
PCUT: 15
XMIN: 1416800
YMIN: 2200000
XMAX: 1526050
YMAX: 2309200

ACUT: 10
PLATES: 1

TAKE COP

Table 6.2: Comparison of eyeball search of HCF and COSMOS scans of original plate material. AAT plate # J1836: 8arcmin² region centred on cluster 23T.

B_Jrange	(a)	(b)	(c)	(d)
23.50 – 24.00	31	30	1	1
24.00 – 24.25	14	12	2	0
24.25 – 24.50	19	17	2	1
24.50 – 24.75	21	17	4	1
24.75 – 25.00	35	22	13	3
> 25.00	27	8	19	2

(a) number of objects on COSMOS scans

(b) number of COSMOS objects confirmed on HCF

(c) excess objects on COSMOS only

(d) number of COSMOS excess objects confirmed on CCD frame

Excess number found on HCF only = 19

Furthermore, lowering the threshold too much can lead to the inclusion of spurious noise spikes arising in the random noise from the sky.

Let us now summarise these points. We have seen that, rather than being less reliable than machine-measurements, as our initial prejudices may have supposed, we find that, in practice, eyeball searches of the HCFs can effectively detect images down to very faint limits. Whilst machine-measurements are undoubtedly invaluable for photometry and statistical analyses, they can themselves be subject to problems at limits close to the sky threshold. For the present purpose, we are initially only interested in cluster detection and not detailed photometry, so that eyeball searches of HCFs have the advantage in that they are relatively quick to perform (even when we include the time needed to produce an HCF), whereas machine scanning requires large amounts of computer processing.

So far we have only addressed the detection of individual objects on HCFs. Considering the problem of cluster detection, the situation becomes rather more complex, and possibly more subjective. I shall now outline the method that I have chosen to employ for the construction of the proposed cluster catalogue.

As discussed in section 6.1, the simplest definition of a potential cluster is that of an enhancement in the density of objects counted in a specified area, above the mean background. That is,

$$\sigma_{cl} = \frac{(N_{cl} - N_f)}{\sigma_f} \quad (6.2)$$

where σ_{cl} is the significance of the enhancement, N_{cl} is the number of objects in the cluster area, N_f the mean field counts, and σ_f is the deviation of the field counts. It is fairly well established that the background counts can vary across the area of the photographic plate by amounts greater than simple Poisson scatter. Thus σ_f should be determined from a large sample of background areas across the plate, and is not merely $\sqrt{N_f}$, but often considerably larger.

As regards the area within which we obtain our cluster and background number counts, we should reiterate the arguments at the beginning of this chapter. Essentially we should select a small area appropriate to the scale size of cores of rich clusters in the redshift range with which we are concerned. Specifically we choose a metric cluster core diameter of 1.5 Mpc (Bahcall 1977, Couch *et al*, 1983) as in section 6.1. Since we are hoping to detect clusters of galaxies in the redshift range, $z \sim 0.4 - 0.7$, using $H_0 = 50$, $q_0 = 0.1$, this corresponds to an angular diameter range of ~ 2.8 to 3.4 arcmin, which on the AAT plate (scale is 15.3 arcsec per mm) is ~ 10 to 14 mm. We adopt a mean value of 12 mm for our survey.

The actual detection and classification of clusters proceeded as follows.

- (a) The film being searched was divided into square sections of side 10 arcmin by means of an overlay grid. As well as enabling the eyeball search to be carried out more efficiently, this also provided a convenient simple coordinate system.
- (b) Within each section a circular aperture of diameter 3 arcmin was randomly placed and the number of objects lying within this aperture was recorded as an estimate of the local background. Note that comparison of these background counts in fields for which photometry has already been obtained can give an indication of the magnitude depth of the HCF surveys.
- (c) Each section was scanned by eye and the locations of any apparent density enhancements of faint objects above the background were noted.
- (d) The aperture was then used to count the number of objects in each density enhancement, providing a significance level for the candidate cluster.

Suspicion has often been placed on purely visual examination of photographic material for its reliability in terms of completeness and uniformity, and for the subjective nature of searches for possible structure in galaxy distributions. With care, and the adoption of quantitative selection criteria these difficulties may be minimised, but should still be borne in mind. As we have discussed earlier, measuring machines also are prone to their own idiosyncratic difficulties.

Whilst I have already shown that careful eyeball counts of objects on HCFs can yield reliable results, I have as yet said little about the ability of the eye to find density enhancements above the mean background. To further investigate this problem we shall make use of COSMOS scans of the HCF of the plate F1652, which had been scanned originally for astrometric purposes. We may expect to find some possible disagreements with the comparison of COSMOS and eyeball searches. In particular, the problem of image-merging could be expected to occur in the dense regions of rich clusters and thus possibly lead to a lower ascribed contrast over the field. In the case of the present data the threshold for image identification was chosen empirically (by H. MacGillivray) by comparison of small areas of the film with COSMOS maps of the same regions, selecting the value that minimised the merging problems without introducing substantial numbers of noise spikes.

Consequently, using the COSMOS data, I have counted the number of galaxies in bins (1.5×1.5 arcmin) over the area of this film, providing a detailed map of the number count variations across the fields. Figure 6.4 is a contour map of these scans, which reveals that the counts are reasonably well-behaved over this film with no evidence for any significant gradients. The lowest contour is plotted at the 3σ level above the mean, with 4 and 5 σ being the subsequent levels. The procedure has managed to isolate a few discrete structures with significances of $\geq 4\sigma$.

Because of the possibility of any, or all, of these enhancements being due to some algorithm-induced spurious effect, such as the fragmentation discussed above, it is important that we produce COSMOS analyser maps for the neighbourhood of each density peak. We can then re-examine the original plate material to verify the reality or otherwise of the detected structures. In this particular case many of the bright star images display a slight trail, which closer scrutiny reveals to be the cause of some of the number density enhancements by exactly this fragmentation. In figure 6.4 we have identified those density peaks which were found to be genuine, or at least not artificially induced by any obvious such processes.

If we now compare this contour map with our original eyeball search of the HCF, we see that the density enhancements delineated in figure 6.4 correspond to candidate clusters that were independently identified by eye. Furthermore, we can also compare the machine scans with our eyeball number counts to examine possible inconsistencies in our cluster significances.

These counts are shown in table 6.3. Note that here we have measured the numbers in the cluster in the same manner as in the eyeball survey, i.e., by counting within a 3 arcsec aperture centred on the cluster. The excellent agreement between the eye and machine counts is gratifying, and shows that (a) our eyeball counts are reliable, and (b) that the expected merging problems in the COSMOS scans are not, in this case, too severe a problem. The difficulties may have been alleviated in this case by our use of the HCFs, since on the original plates each of the faint images' photographic intensity contrast above the sky will be lower. Thus detection will require a lower image threshold and merging will become more important.

This method is fairly crude and really only suited to large scale structures, but provides a useful illustration of the concepts we are considering here. For detailed cluster searches on lower angular scales, a method such as that developed by Stevenson (1986) may be more appropriate, but it is considerably more expensive of computing time.

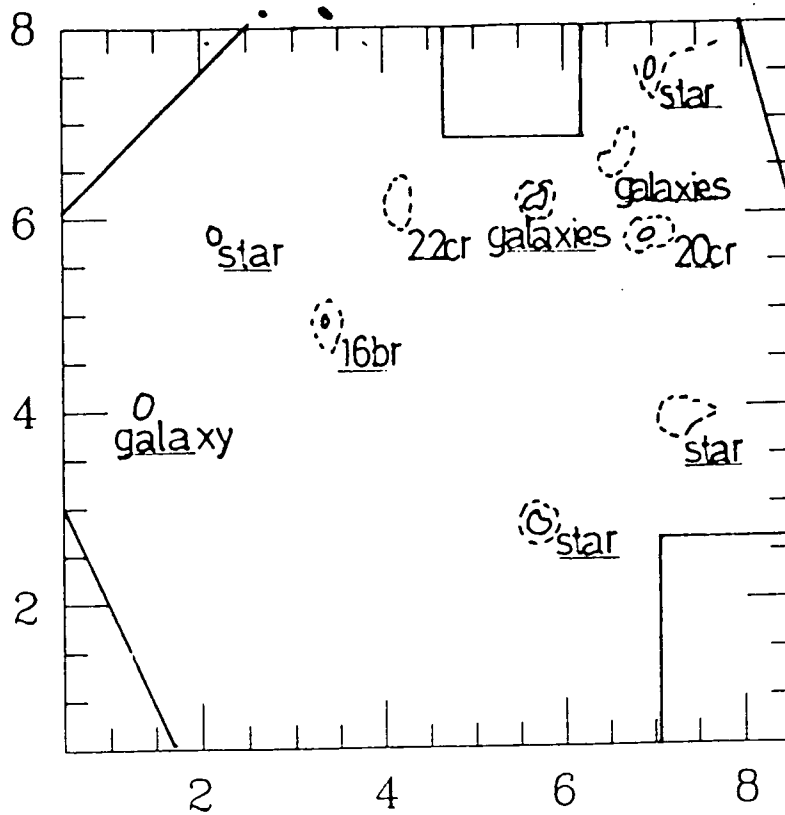


Figure 6.4: Contour map of COSMOS number counts across the film F1652. Each high density peak was subsequently identified as marked in the figure.

Table 6.3: COSMOS and Eyeball Number Counts on F1652

Method	Mean Number	σ	Cluster	Significance (σ)
COSMOS	38	7.6	22cr	3.7
			20cr	6.4
			16br	3.2
Eye	41	6.8	22cr	4.2
			20cr	> 4
			16br	3

Note: The number counts compared here were both measured in the same area aperture and σ refers to variation in counts over the area of the film.

Although discrepancies can arise between clusters found using machine scans and eye searches, these occur at the $1 - 2\sigma$ level, where observer-to-observer differences also, unsurprisingly, arise. Based on these few simple experiments then, we feel it is worthwhile to attempt to construct the proposed catalogue of distant clusters from the available HCF material.

6.3 The AAO Deep Cluster Catalogue.

Dave Malin of the Anglo-Australian Observatory (AAO) has supplied us with a large number of HCF copies of high quality (seeing less than 2 arcsec FWHM) AAT plates. The sample amounts to some 56 films, effectively randomly sampled from the southern sky, and covering both J and F passbands (including 6 J and F plate pairs). Using the techniques and selection criteria described in the previous section I have compiled a catalogue of candidate distant clusters from this sample of HCFs.

The catalogue is presented in table 6.4. The cluster identifications refer to the position of each candidate on our crude co-ordinate grid. The number immediately following the plate name is the 10×10 arcsec box in which the cluster was found and the subsequent letters describe its position within that area (t -top, b -bottom, l -left, etc). This is of little relevance here and detailed astrometry will be presented later for spectroscopic targets and in a future publication. Note that many of these films were searched by eye by three independent observers (Ian MacLaren, Richard Ellis, Warrick Couch) and those clusters common to all three are included here (discrepancies between the observers only arose for the clusters identified as having contrasts of $\leq 1\sigma$).

As an indication of the average magnitude depth reached by the catalogue, figure 6.5 shows the number counts on each film with the expected magnitude limits from our study of J1836 superposed. With the original plates and the HCFs produced under similar circumstances, the spread in this figure provides an indication of the effects of galactic absorption on the number counts, as well as the uniformity of the fields under study. This is particularly evidenced by the larger scatter found in the blue counts when compared to those in the red passband.

Regarding the surface density of clusters in the survey, we find 2-3 clusters per $1^\circ \times 1^\circ$ film, on average. It is worth noting that not all of the films are of deep field regions, however, since many were originally used to investigate faint outer structures of nearby galaxies, thus obscuring a large portion of the plate. In other words, our density may be a slight underestimate; indeed, many of the films contain some 5 or 6 clusters over their full area.

Figure 6.5(b) shows the distribution of cluster σ s for the total catalogue, revealing that we have found many candidates with the appropriate significances expected of rich clusters in the redshift range 0.4 - 0.7. We shall address the details of the catalogue in further depth in section 6.6. As a preliminary study of the catalogue, we decided to undertake some initial spectroscopy of a number of the candidate clusters, which we shall discuss in the following section.

6.4 Spectroscopy and Further Observations.

(a) Introduction.

Now that we have compiled our catalogue of candidates we should address ourselves to the major question in hand. Are these objects truly distant clusters, and if so, just how distant are they? Specifically, we should like to obtain an empirical estimate of how likely our candidates are to be the rich clusters we so enthusiastically seek at redshifts of 0.3 to 0.7. We decided, therefore, to use a simple single-slit spectrograph to acquire a few spectra for as many cluster candidates as possible in the available observing time, rather than concentrating on obtaining a large number of spectra of galaxies in only one or two clusters.

Table 6.4: Catalogue of HCF Clusters

Plate	R.A.	Dec.	Clusters	Contrast(σ)
J2172	00 35 00	-34 00 00	17C	6
J1742	00 44 34	-21 01 08	18BL	7
			9CL	3.8
			14BR	1.9
J1739	00 45 04	-25 34 11	5CB	2.8
			13BR	1.1
J1888	00 54 48	-27 54 46	16CL	5.3
			28CL	4
J1763	01 34 08	-13 10 20	14C	3.4
			21CR	2
			16BC	1
J1566	02 00 02	-50 00 02	24TL	3.5
			11C	3.2
			29BR	3
			26TR	2.4
			21TL	2
J1779	02 44 18	-30 29 01	23TL	4.2
			9BL	3.7
			13BC	2.8
			3CR	2.7
			29CR	2
J1780	03 20 30	-51 28 00	5BL	4.2
			22CL	4.2
			2TC	2
J2073	03 26 18	-31 14 24	9/10C	4.3
			17BC	1.9
J2175	03 33 15	-39 10 02	15TR	5.1
			23C	4.5
			22C	3.6
			29CR	2.2
			26TR	0.7
J1727	03 36 50	-26 32 51	23T	4
			24TL	3.6
			13C	3.2
			14CL	3.1
			30C	2.9
J1556	03 36 36	-35 38 07	15BL	5.6
J2059	03 41 41	-53 48 02	28TR	8

Catalogue of HCF Clusters (contd.)

Plate	R.A.	Dec.	Clusters	Contrast(σ)
J2183	03 44 45	-34 32 02	27TL	7
			15CR	4.5
			4TC	4
			10TC	3.7
			11BC	3.5
J1765	03 53 46	-74 16 06	24TL	1.7
J2000	04 00 30	-18 08 44	8LC	2.6
			3C	1.4
			9TR	1.3
			9C	< 1
J2089	04 14 56	-55 48 00	11TC	5.3
			28BC	4.1
			9TC	4
			5TR	4
			21TC	2.7
			3C	2.3
J1766	04 46 49	-20 49 56	10C	2.4
			8BC/BR	2
J2001	05 11 27	-48 27 47	21C	4.0
J1772	05 11 39	-30 31 36	19CR	1.1
			29TC	3.3
			3BR	2.1
J2077	09 21 16	-22 56 50	11TC	1.5
			16C	2.2
J1789	09 43 17	-14 05 50	-	-
J2082	09 51 43	-27 03 04	-	-
J2090	10 02 48	-07 28	7CL	7
			9/10BC	4
			3BR	3.1
			4C	2.9
J1816	10 39 12	-28 33 17	23BC	2.4
			11C	2.3
			16BR	1.7
			9BR	< 1
			4CL	< 1
J1834	10 43 38	-00 04 49	5BC	4.6
			8BL	4.4
			3TC	4.1
			28BR	3.7
			2TC	2.8
			23CL	2.1
			22C	2.0
			28C	2
			28BL	1.4

Catalogue of HCF Clusters (contd)

Plate	R.A.	Dec.	Clusters	Contrast(σ)
J1604	10 49 25	-09 04 04	10C	3
J2091	11 10 54	-26 29 01	27TL	1.8
			4BRX	1.8
			9BCX	< 1
			11LC	< 1
J2026	11 48 30	-28 31 20	20C	1.1
J1614	12 00 41	-21 15 11	13C	1
J1872	12 19 26	-00 51 21	10C	3
J2092	12 56 42	-14 45 58	17CL	2.7
J1665	13 09 00	-01 06 00	-	-
J2093	13 17 04	-26 46 08	23CL	5.3
J2233	13 17 34	-21 34 00	10CL	3
			4C	1.9
			17TR	< 1
J1836	13 41 14	-00 00 30	3CR	7.0
			23TR	4.8
			14RC	5
			10RC	4.6
			11TL	1.5
J1824	13 41 14	-26 59 28	-	-
J2094	15 04 00	+01 48 01	7CR	1.5
J1631	15 04 16	-16 40 54	-	-
J1884	20 48 13	-57 15 24	3TL	3.8
J2056	23 21 46	-00 24 00	25/26	4
F2262	00 54 48	-27 54 02	16CL	5.5
			28CL	2.5
F2057	02 00 00	-50 01 01	20C	4.6
			26TR	3.3
F1557	04 08 58	-65 53 01	19TC	5.2
			11BR	5.0
			18BL	3.6
			5C	2.9
			9BL	1.9
			14BL	1.3
			23BL	< 1
F1652	04 46 49	-20 49 57	20CR	> 4
			22CR	4.2
			16br	3.0
F1767	08 44 04	+18 03 50	10TC6	

Catalogue of HCF Clusters (contd)

Plate	R.A.	Dec.	Clusters	Contrast(σ)
F1612	09 44 24	-08 34 15	22BC	3.5
			22LC	2.3
			27C	2
			3C	< 1
			22TC	< 1
F1835	10 43 38	-00 04 49	3TC	6.9
			2CL	5.0
			22CR	4.9
			28BR	4.6
			5/11	3
F1613	12 00 41	-21 15 11	13C	2.5
F2097	13 34 18	-29 36 58	-	-
F1837	13 41 14	-00 00 30	23C	7.0
			3C	6.3
			15	3.8
			10C	3.2
			30BLX	2.5
			28BR	2.2
			11	2
			1CR	1.9
F2110	16 17 04	-15 31 14	-	-
F1896	19 54 49	-32 33 49	-	-
F1636	22 26 56	-21 02 37	28/29CT	4.1
			14BR	3.5
			11CR	3.1
			24BR	2.5
F1746	22 50 48	-33 58 04	24C	4.8
			11C	3.6
			9CT	2
F1637	23 56 00	-32 39 40	23TL	5.2
			23BC	5.1
			20C	1.9
			17BC	1.3
			29CR	< 1

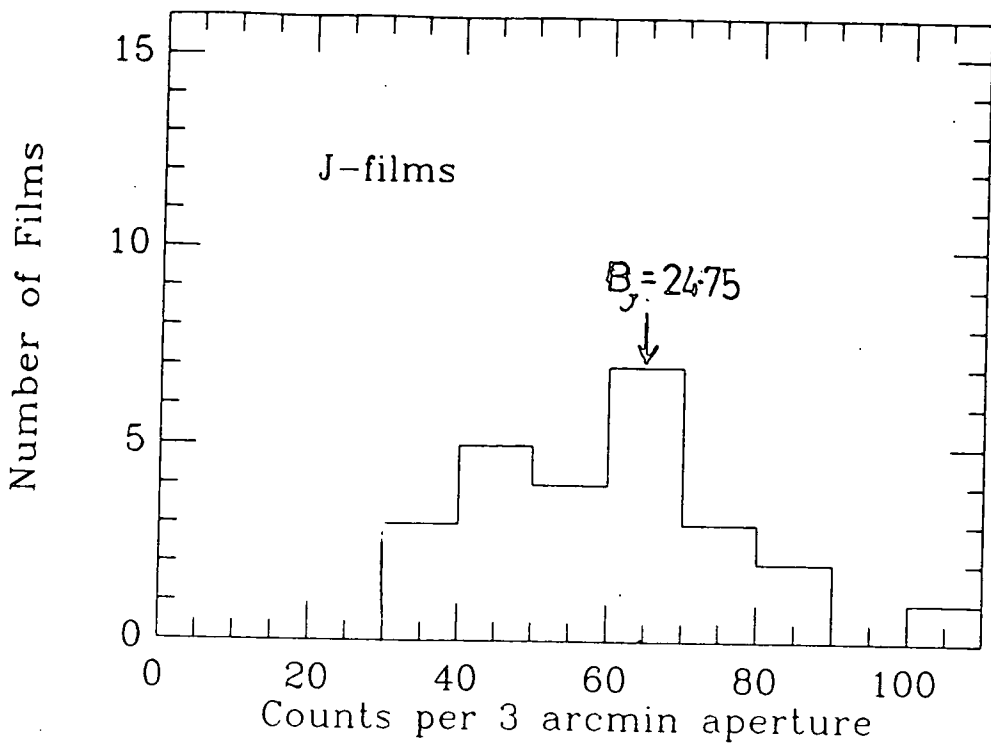
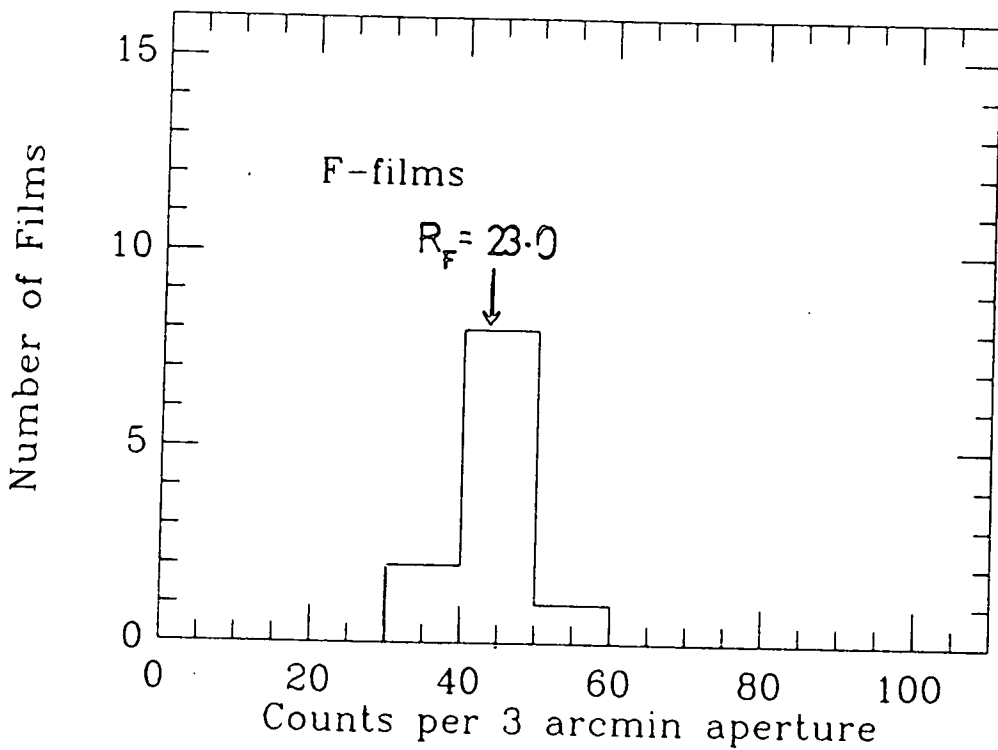
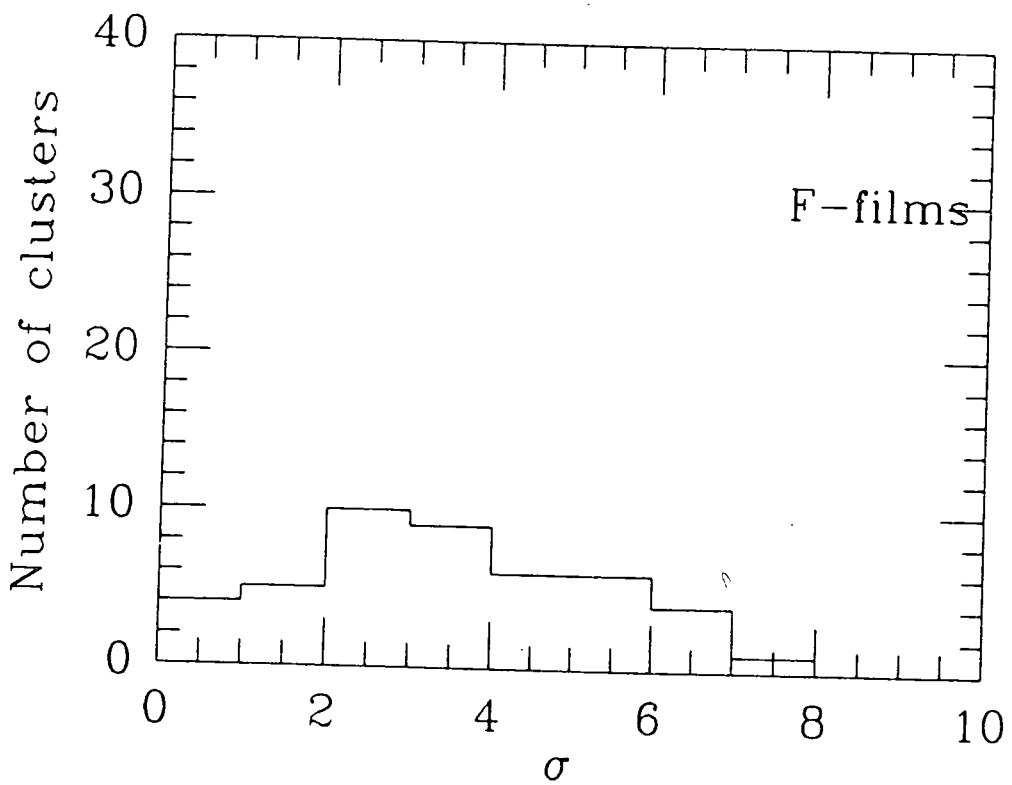
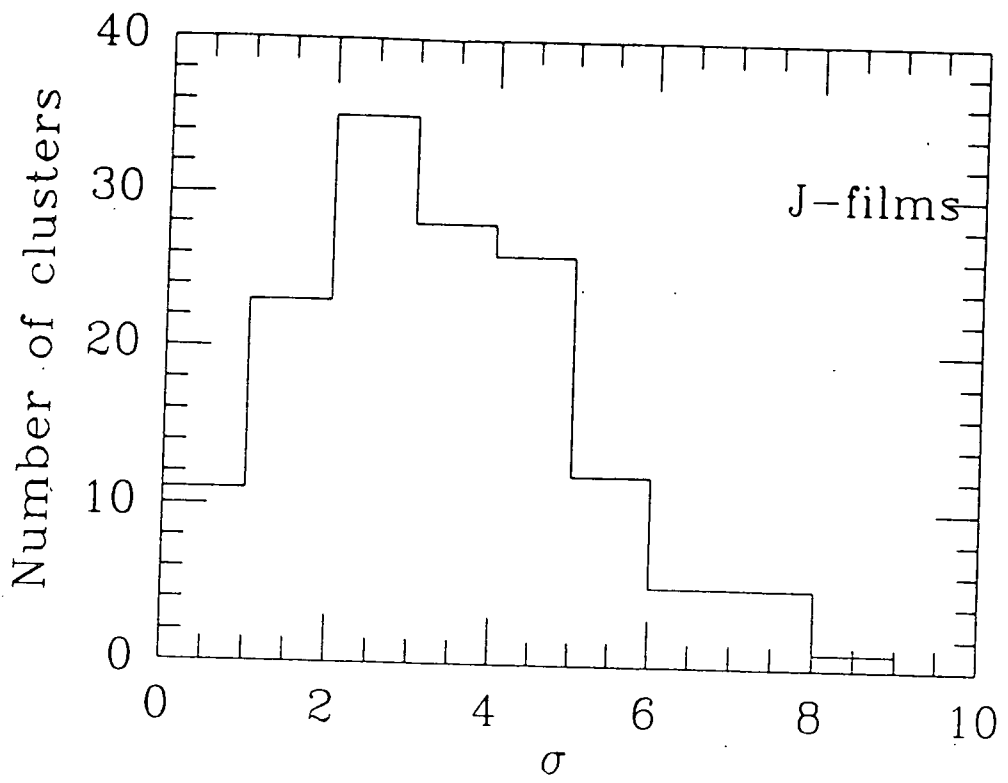


Figure 6.5: (a) Number counts on each film in the cluster catalogue. Superposed are the estimated magnitude limits from the study of J1836. (b) Distribution of cluster contrasts over the whole catalogue. This point is further discussed in section 6.5.





Indeed, multi-object spectroscopy requires a great deal of preparation (drilling of aperture plates, etc) and was viewed as a secondary objective of the programme to be undertaken once we had determined a simple redshift estimate for each candidate.

In this section I shall discuss our observations and the results of a preliminary investigation of some 16 candidates. We have, thus far, obtained spectroscopy for only $\sim 30\%$ of those clusters with $\sigma \geq 4$ in B_J . These candidates were initially chosen to test the feasibility of embarking upon a much larger and potentially difficult survey of even more distant objects.

We should note here, that, independently of this general survey, Couch, Shanks, and Pence (1985) have studied one particular candidate from our catalogue, J1888.16cl. Their spectroscopy has revealed this cluster to have a redshift of 0.57. The implication of this redshift and the large value of the cluster contrast in the B_J passband compared to R_F , is that we may well expect to see evidence for galaxy spectral evolution in this cluster. Indeed, Couch, Shanks, and Pence's photometry in B,V,R,I does apparently suggest that this cluster possesses an unexpectedly large fraction of blue members (see earlier chapters). These results, certainly add confidence to our basic approach of using such a survey for evolutionary studies.

(b) Observations and Data Reduction.

Absorption line spectroscopy of objects as faint as even the brightest members ($R \geq 21.0$) of our candidate clusters requires long exposure times and a sensitive detector system with as little light loss as possible. In this section I shall present preliminary spectroscopy of a small subset of our catalogue, all of which was obtained using spectrographs specifically designed for such faint magnitudes.

The bulk of the redshifts were obtained using the Faint Object Red Spectrograph (FORS) at the Anglo-Australian Telescope. This is a high throughput, collimator-less spectrograph with a GEC CCD located on a cold finger within a fast Schmidt camera. The dispersing element is a grism blazed at 7500\AA , giving a resolution of 15\AA from $5000\text{\AA} - 10500\text{\AA}$. A further advantage is provided by the long slit length of FORS, which can be exploited, using a judicious slit orientation, to provide more than one object spectrum per exposure.

During three clear nights in March 1985, we obtained spectroscopy in nine of our candidate clusters, with typically 4 galaxies per field. Details of the observations are given in table 6.5. The astrometry used was obtained from measurements of the galaxy images on the high contrast films using the Packman XY-carriage at the Royal Observatory Edinburgh and the CHART and ASTROM software available via STARLINK. This astrometry is listed in table 6.5. The positions were sufficiently accurate (to within 0.5 arcsec) to enable us to confidently employ blind offsets for the positioning of the FORS slit. Good seeing allowed us to narrow the slit width to 1.6 arcsec during these observations.

Absorption line identifications and measurements are often difficult to attain on such faint galaxies. Experience has shown (see Parry, 1986) that exposures long enough to reach a high continuum signal to noise (typically $\simeq 20$) can be sufficient to observe such weak features in early type galaxies. Consequently our typical total exposure times (including several shorter co-added exposures) per slit position were several thousand seconds.

The data reduction was achieved using a software package developed by Parry (1986), originally conceived for use with the Durham/AAO FOS instrument but suitably modified for use with FORS data. Firstly, each spectrum was extracted from the CCD image frame by means of a cursor on an ARGS interactive image display system. The next stage, which often proves to be of great importance in such work, is the subtraction of the contribution of the night sky's spectroscopic features from the observed object spectrum. The user defines the width of the object spectrum on the CCD frame. The software then interpolates the sky spectrum under the object using the available spectrum on either side of the object

(weighting the object columns according to Robertson's (1985) scheme). An example of the night sky spectrum in the wavelength range under consideration here is shown in figure 6.6(a) and further details can be found in Parry (1986). The useful wavelength range, defined as that region where the sky features are of little effect and easily removable, and where the detector has a reasonable sensitivity, is in this case from 5500\AA to 8000\AA .

The final stage then is the fluxing of the spectra which is achieved using a calibration based on observed spectra of standard stars, and correcting for the sensitivity variations of the detector. The finally reduced spectra for this observing run are presented in figs 6.6 with identifiable features labelled. Table 6.5 contains a summary of these observations.

Couch, Ellis and D'Odorico (1987, private communication) have observed a further sample of clusters using the European Faint Object Spectroscopic Camera (EFOSC) at the European Southern Observatory at La Silla in Chile and their redshift values are also given in table 6.6.

Importantly, we have shown that absorption-line spectroscopy of faint galaxies is entirely feasible using existing telescopes and instrumentation. Indeed, we were able to determine redshifts from absorption line spectra in the present work as far as $z = 0.68$, using the FORS plus AAT combination. This bodes well for future studies, in which we shall be considering the lower σ , and hence presumably more distant, clusters. Our work has shown that given reasonable observing conditions, with a sufficient integration time (several thousand seconds), we can readily probe to the expected distant end of our catalogue (ie $z \geq 0.7$).

6.5 Discussion.

As remarked earlier, at the present time only preliminary observations have thus far been carried out on the HCF catalogue candidate clusters. We have obtained spectroscopy for only a small sample of the highest contrast clusters. Nevertheless, these results do enable us to make several important conclusions, both about the nature of individual clusters, and the catalogue as a whole.

- (a) Firstly, most of our supposed clusters are 'well-behaved' in that most, if not all, of the spectroscopic targets in each candidate cluster lie at the same redshift. This is the case for 10 candidates out of the sample of 14 for which more than 1 redshift is available. This gives us confidence that we have indeed, largely found genuine clusters of galaxies and not just spurious superpositions.
- (b) Of those clusters for which an unambiguous redshift was determined, most lie at $z \sim 0.4 - 0.5$ (mean value, $z = 0.41$), which is consistent with their high contrast values ($\sigma \geq 4$ in B_J). It is possible, at a very crude level, to attempt to model the expected distribution of clusters in terms of redshift and σ , by extending Couch *et al's* (1983) modelling scheme. In the no-evolution case, we can adopt the spatial density of clusters and the relative proportions of each richness class from Lucey's (1983) study of the Abell catalogue, assuming that we can extend these values to higher redshifts. Estimating contrast levels and expected numbers of clusters over a range of richness classes (Abell classes 1-3) allows a prediction of the expected redshift distribution for any chosen cut-off in density contrast. For a sample of clusters with $\sigma \geq 4$ we estimate $z \simeq 0.37$ and $\sigma \simeq 5.1$ from such models (see figure 6.6). Such limited numbers of observations and crude simulations can serve as very little other than illustrative at this stage. For effective detailed studies of the cluster distributions, we require not only considerably more redshift observations (extended over a range of σ values), but also more detailed models, which include the effects of contamination of distant clusters with overlapping foreground systems. At the high redshifts with which we shall be concerned, these effects will become increasingly important, as we shall now discuss.

Table 6.5: FORS Spectroscopy Run, March 1985 — Summary

Cluster	σ	i.d.	R.A.	Dec.	z	Comments	$R_{\text{ slit}}$	Dwell(s)	
J2233.10cl	5.5(J)	c	13 16 53.064	-21 33 26.76	0.424	Seyfert?	20.6	3000	
		g	13 16 52.650	-21 33 03.05	0.424	absorpt.	20.0		
		s	13 16 52.350	-21 32 41.21		blue	22.4		
		t	13 16 52.137	-21 32 27.41		very blue	21.9		
J1836.3cr	7.7(J)	a	13 42 28.09	-00 05 51.47	0.415	absorpt.	20.7	7000	
		n	13 42 27.20	-00 05 46.87	0.415	[OIII] 5007Å only 1 line	23.7		
	6.3(F)	d	13 42 28.31	-00 05 52.81	0.412	Mgb red, 1 line	22.5		
		k	13 42 26.84	-00 05 44.18	0.319	[OIII] 5007Å only 1 line	21.7		
J1836.14rc	5(J)	a	13 41 10.62	-00 15 46.10	0.283	absorpt.	19.4	3000	
		l	13 41 10.65	-00 15 26.31	0.283	absorpt.	20.3		
	3.8(F)	z	-	-	0.284	H α em	21.0		
		u	-	-	0.583	absorpt.	22.4		
J1834.23t	5.2(J)	a	13 40 32.40	+00 13 59.64	0.400	absorpt.	20.6	15000	
		e	13 40 33.97	+00 13 26.36	0.685	absorpt.	21.8		
	7.1(F)	p	13 40 33.37	+00 13 40.14	0.587?	very poor	21.4		
		x	-	-	0.417	absorpt.	20.6		
J1834.3tc	4.1(J)	a	10 42 06.30	+00 01 19.86	0.150	absorpt.	19.6	8000	
		f	10 42 06.72	+00 01 46.08	0.274	em. lines	21.6		
	7.4(F)	m	10 42 03.74	+00 01 20.05	0.560	absorpt.	21.4		
		y	-	-	0.231	em. lines blue	22.2		
F1835.22c	5(F)	a	10 44 28.44	-00 11 17.26	0.424	absorpt.	21.1	8000	
		b	10 44 28.44	-00 11 21.51	0.465	H+K?	21.7		
		d	10 44 28.47	-00 11 39.89		M star	21.9		
		x	-	-	0.576	H+K, [OII] 3727Å	21.0		
		y	-	-	0.229	em. lines	22.8		
J1834.2cl	5.4(J)	a	10 42 11.21	+00 15 12.41	0.379	absorpt.	20.2	5000	
		2.8(F)	b	10 42 11.28	+00 15 07.81	0.500	absorpt.		21.4
			u	-	-	0.375	absorpt.		21.0
F1835.28br	4.6(J)	a	10 45 04.05	-00 07 30.71	0.346	absorpt.	20.0	7000	
		3.7(F)	b	10 45 03.80	-00 07 28.78	0.346	absorpt.		21.2
			f	10 45 06.29	-00 07 47.10	-	very poor		22.5
F1767.10tc	7(F)	g	08 44 51.997	+18 04 36.93	0.667	absorpt.	21.4	8000	
		j	08 44 56.900	+18 05 07.23	0.438	absorpt.	22.4		
		y	08 44 53.596	+18 05 01.91	-	M star	19.9		

Table 6.6: Spectroscopy of HCF clusters - other sources

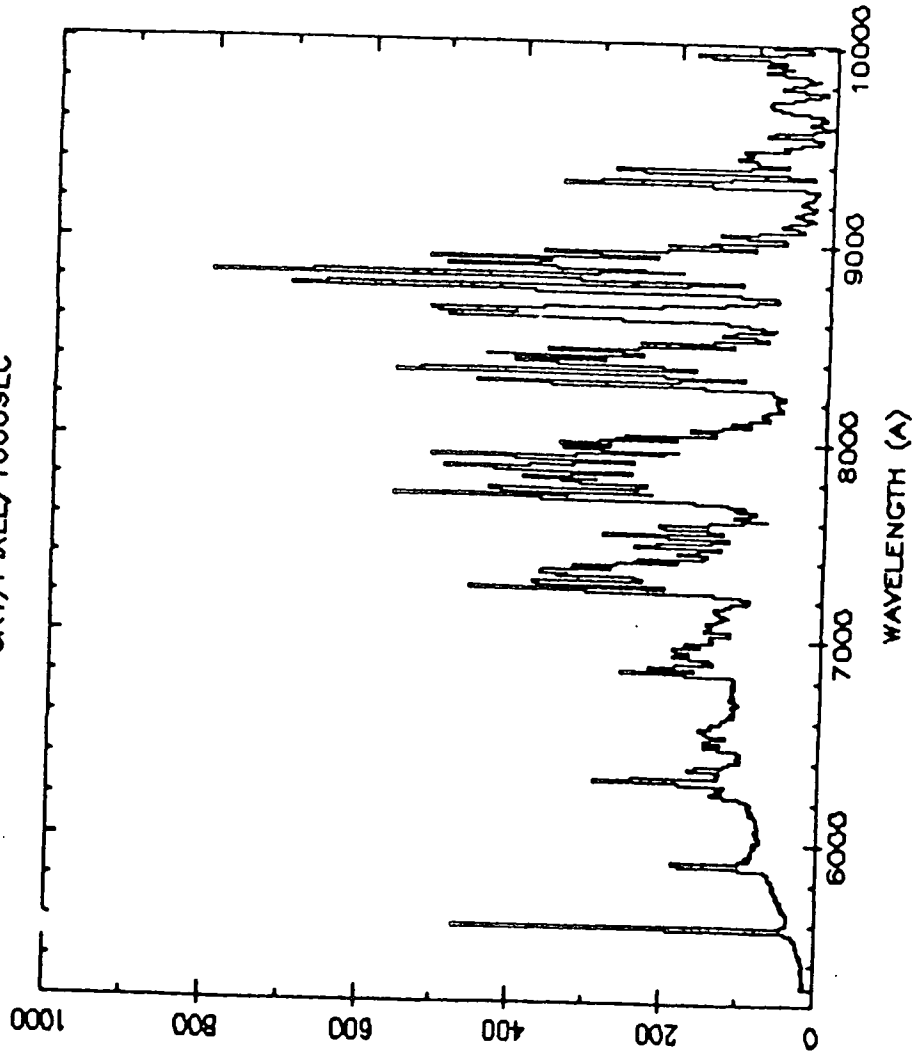
Cluster	σ	i.d.	R.A.	Dec.	Source	z	Features
J1556.15bl	5.6(J)	2	03 37 30.964	-35 38 53.39	AAT Dec 1985	0.457	E
		8	03 37 30.977	-35 39 16.87		0.457	E+A
F1557.11br	5.3(F)	b	04 05 38.164	-65 43 44.11	AAT Dec 1985	-	-
		a	04 05 39.651	-65 43 58.33		0.151	E
J2001.21c	4.7(J)	5	05 12 17.143	-48 21 47.12	AAT Dec 1985	0.414	-
		1	05 12 14.386	-48 21 53.93		0.406	-
J1884.3tc	4.0(J)	4	20 45 38.260	-57 06 19.10	ESO Sep 1986	0.381	E
		5	20 45 37.420	-57 06 18.96		-	-
		1	20 45 39.300	-57 06 24.35		0.380	E
		3	20 45 37.420	-57 06 31.63		0.380	E
J2172.17c	6.0(J)	c	00 35 01.275	-34 09 55.82	ESO Sep 1986	0.348	E
		a	00 35 01.984	-34 09 46.71		0.348	E
J1779.9bl	4.7(J)	3	02 43 19.133	-30 34 54.20	ESO Sep 1986	0.37	E
J1888.16cl	5.5(J)	x	-	-	ESO Sep 1986	0.28	-
		1	00 54 31.51	-27 56 44.00		0.563	E
		5	00 54 30.35	-27 56 38.03		0.56	E

Sources:

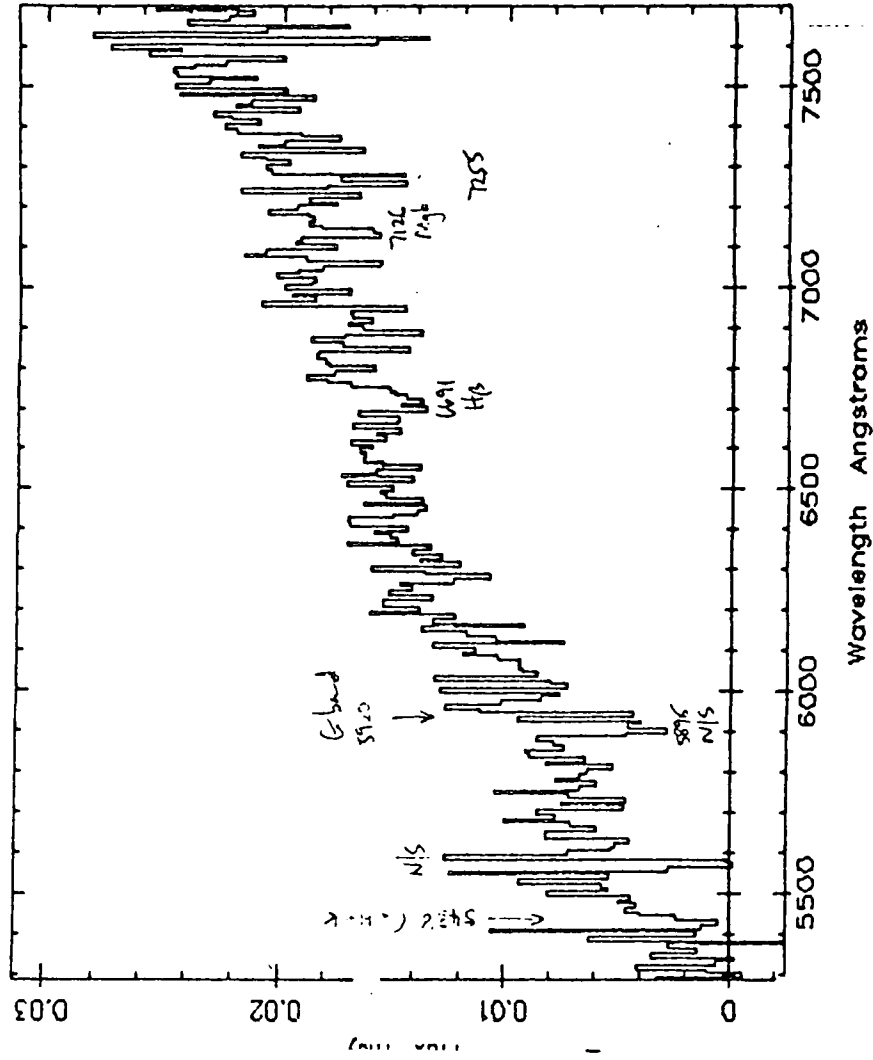
- (a) AAT Dec 1985, Couch, Sharples, and Gray (private communication)
 (b) ESO Sep 1985, Couch, Ellis, and D'Odorico (private communication)

Figure 6.6: (a) Observed night sky spectrum, using FORS at the AAT. (b) Spectra of galaxies listed in table 6.5.

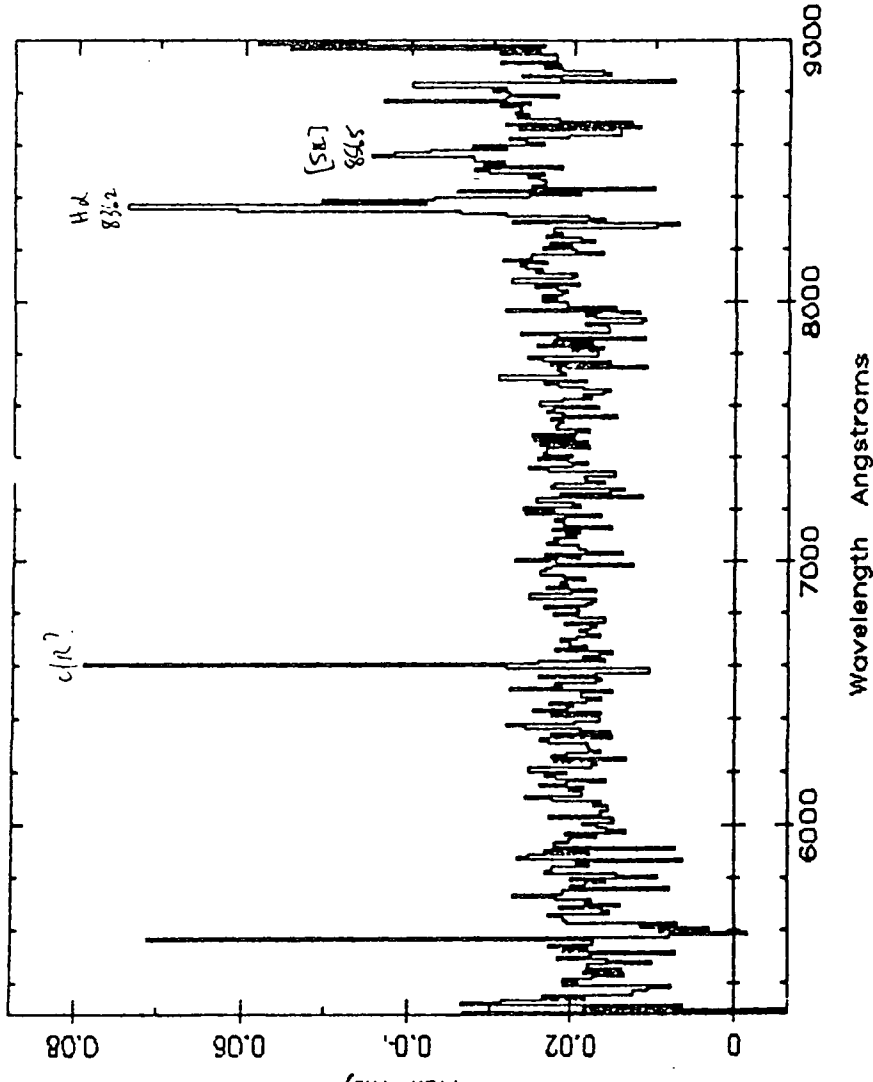
SKY/PIXEL/1000SEC



J1834.2CL/U FLUXED(CALIB3B) SMC DIV'D

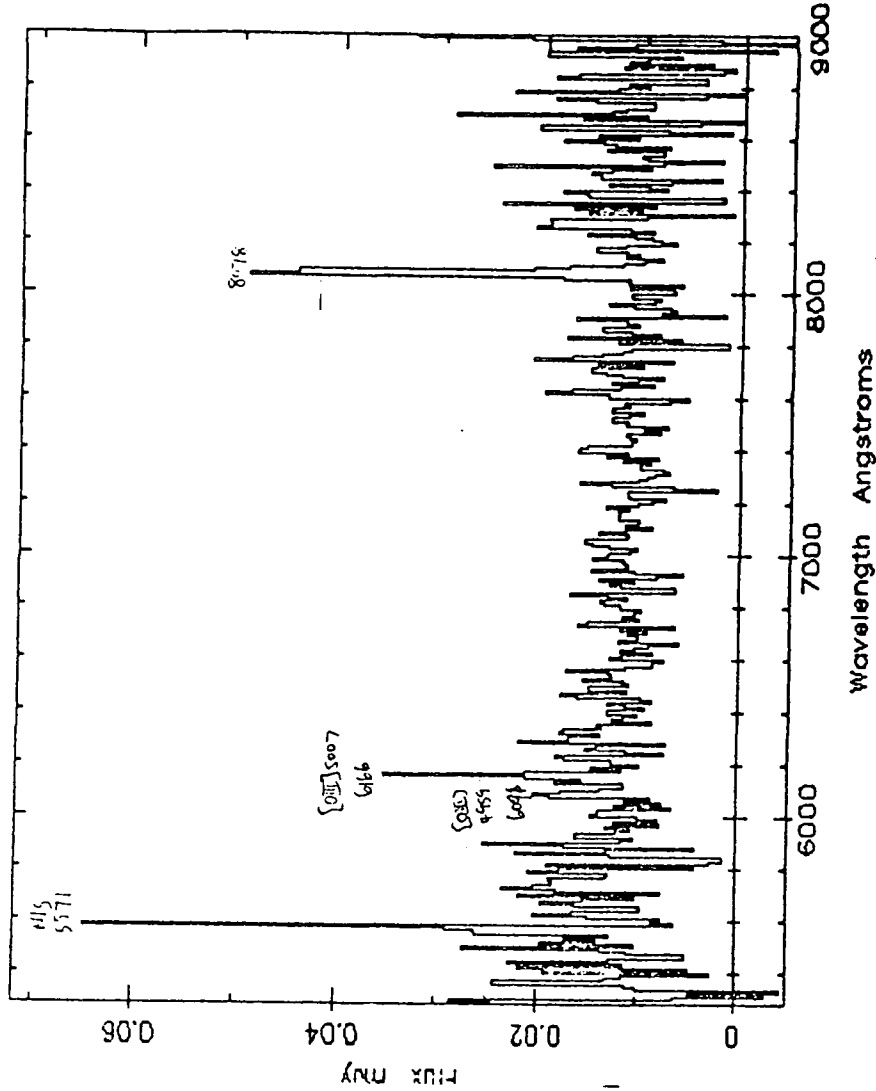


J1834.3TC/F(N3) FLUXED(CALIB4) SMC DIV'D



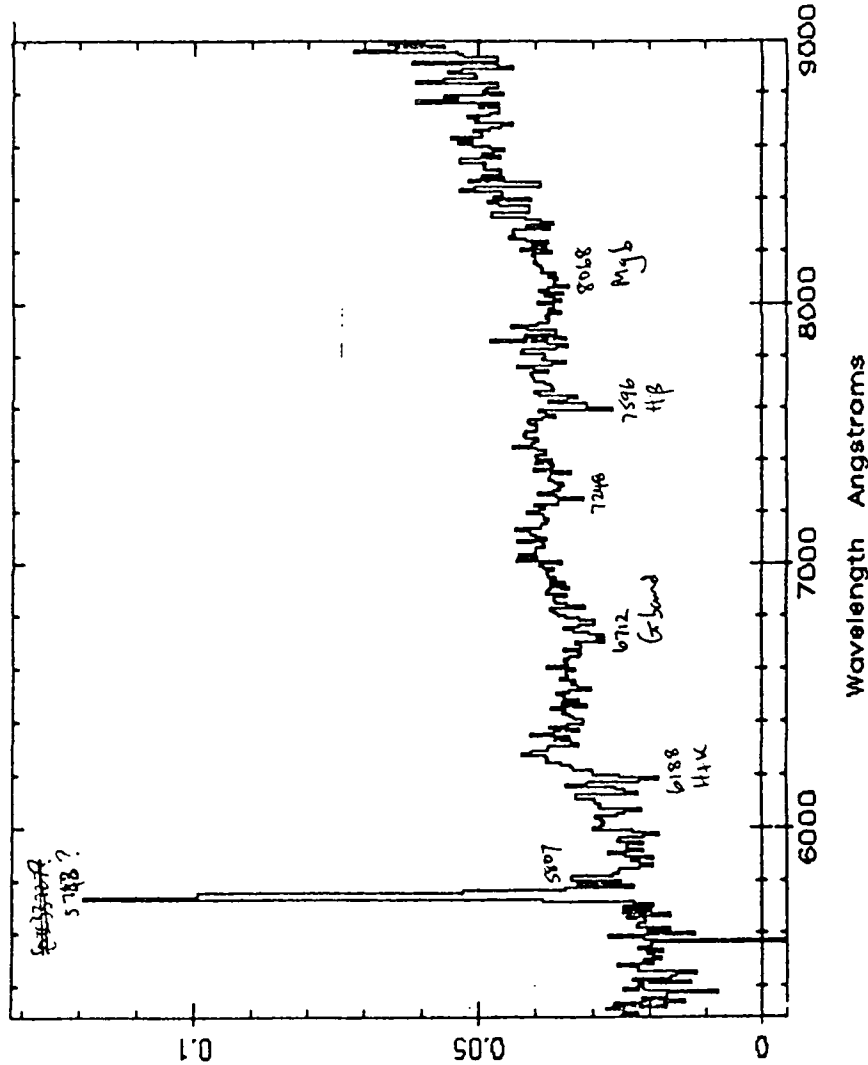
1834.3TC/F(N3) FLUXED(CALIB4) SMC DIV'D

J1834.3TC/Y(N3) FLUXED(CALIB4) SMC DIV'D



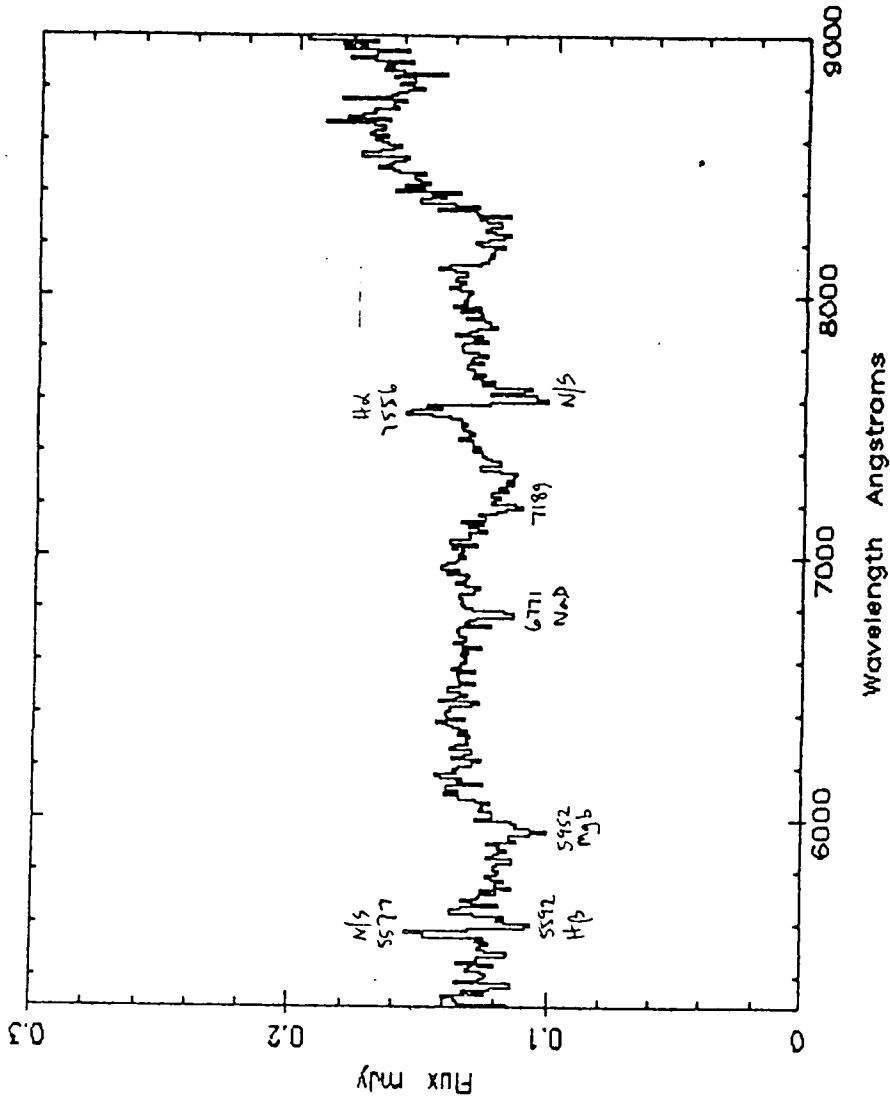
1834.3TC/Y(N3) FLUXED(CALIB4) SMC DIV'D

J1834.3TC/M(N1+N3) FLUXED(CALIB4) SMD DIV'D



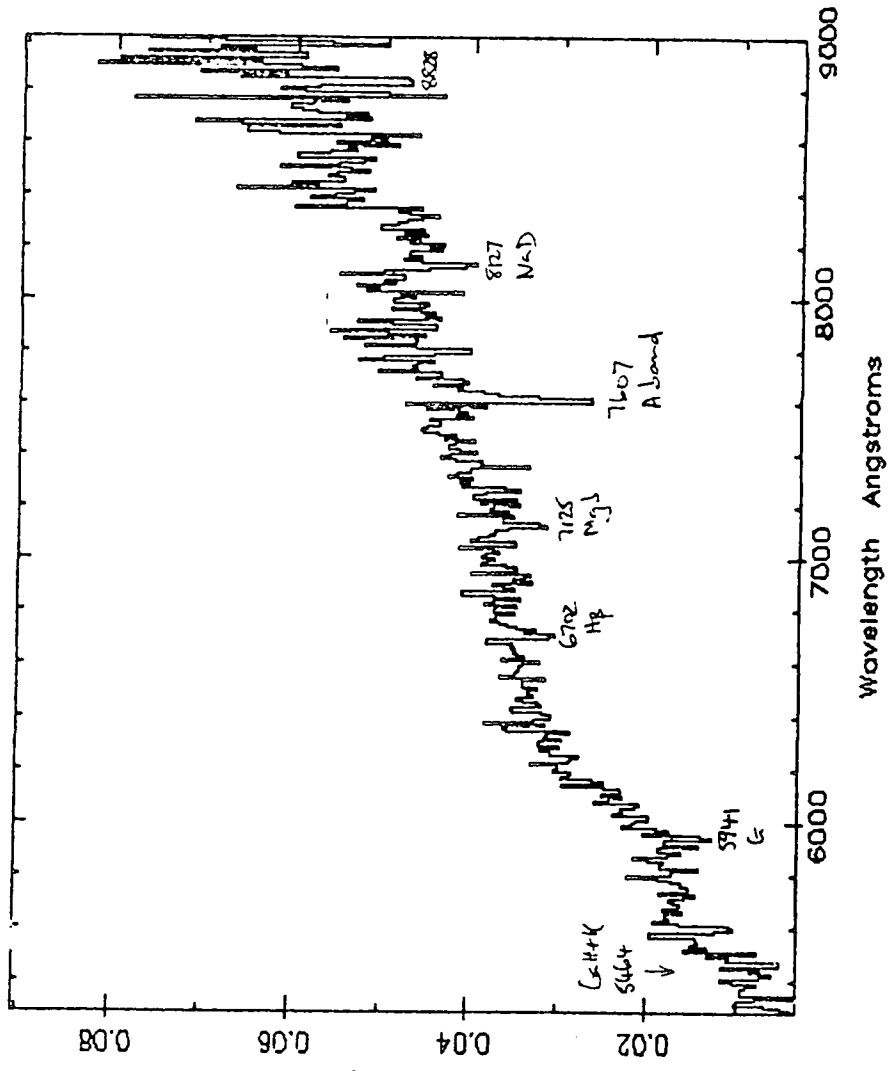
J1834.3TC/M(N1+N3) FLUXED(CALIB4) SMC DIV'D

J1834.3TC/A FLUXED9(CALIB4) SMC DIV'D



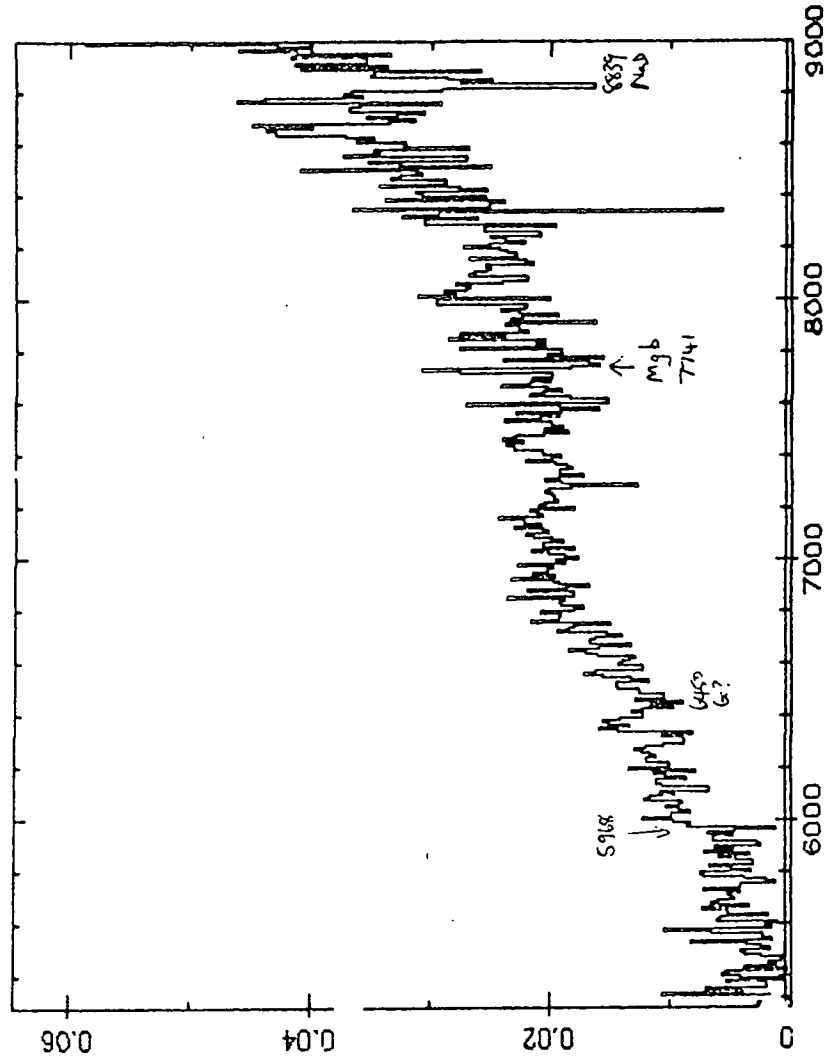
J1834.3TC/A(N1) FLUXED(CALIB4) SMC DIV'D

J1834.2CL/A FLUXED(CALIB3B) SMC DIV'D



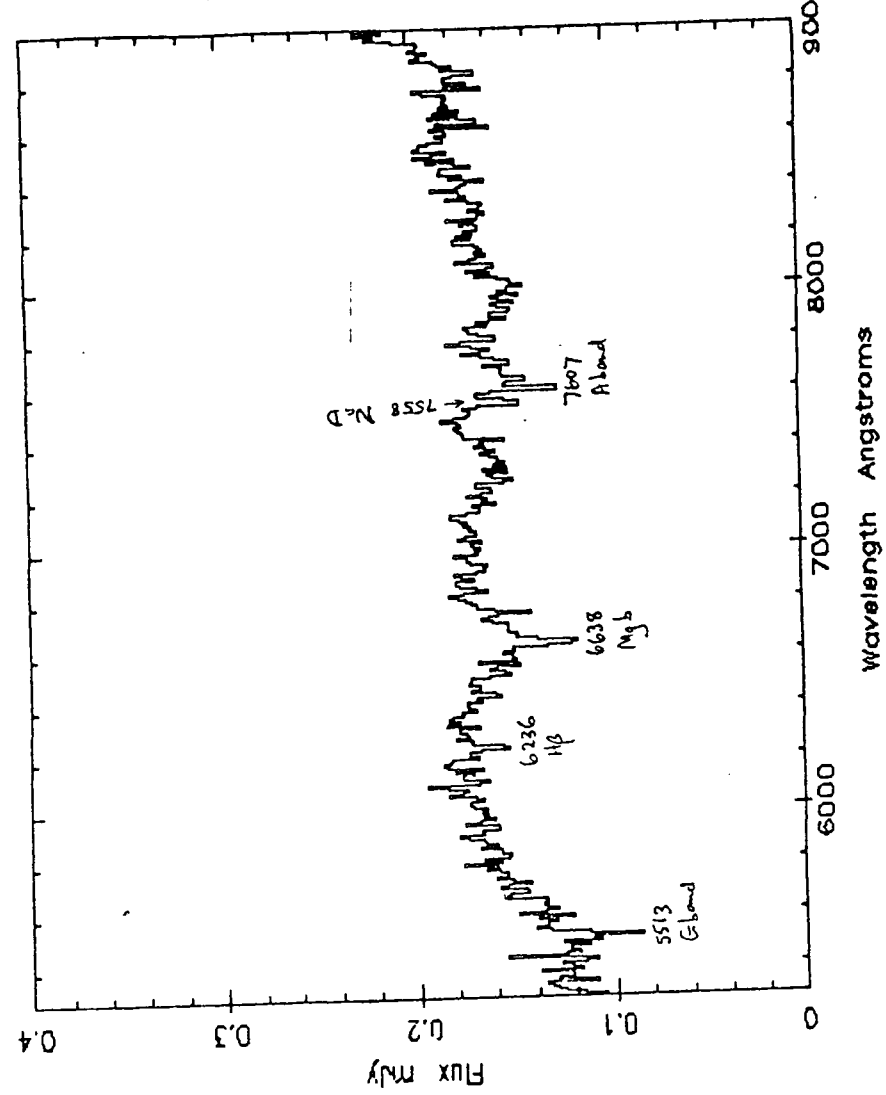
34. 2CL/A FLUXED(CALIB3B) SMC DIV'D

J1834.2CL/B FLUXED(CALIB3B) SMC DIV'D



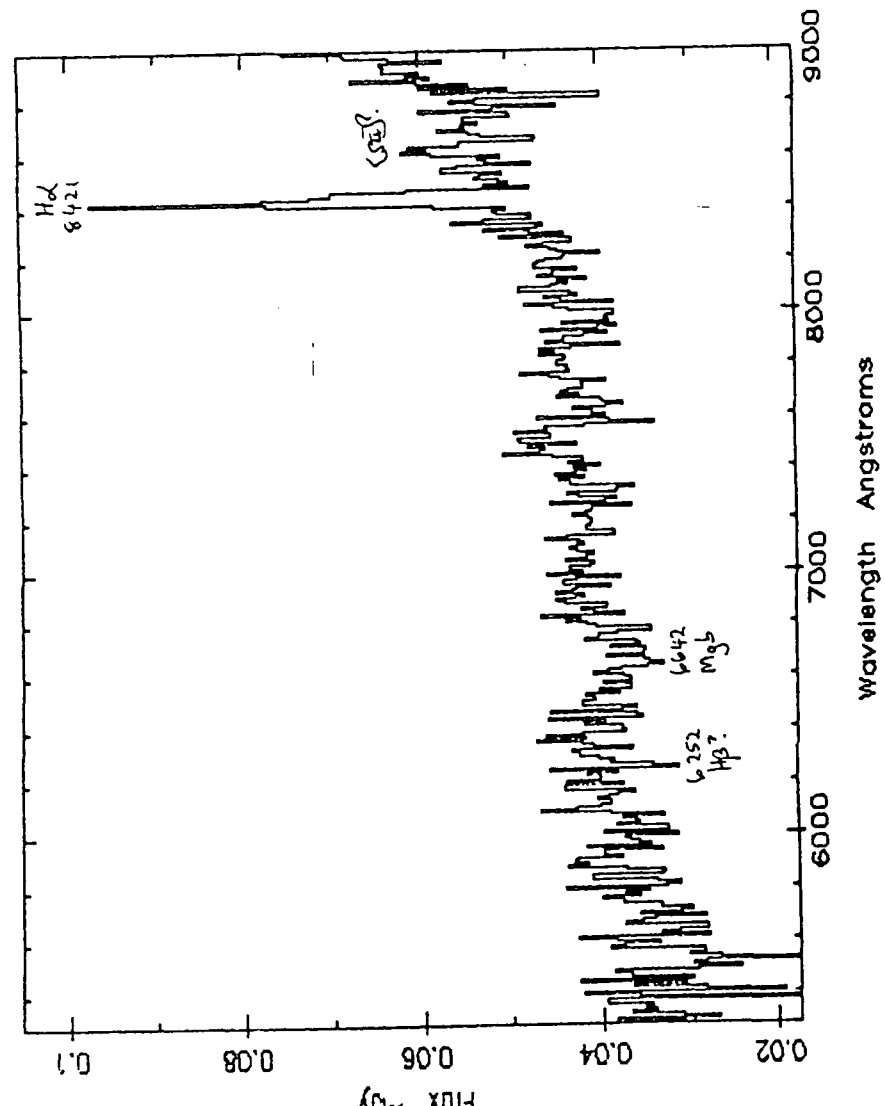
34. 2CL/B FLUXED(CALIB3B) SMC DIV'D

J1836.14RC/A FLUXED(CALIB4) SMC DIV'D



J1836.14RC/A FLUXED(CALIB4) SMC DIV'D

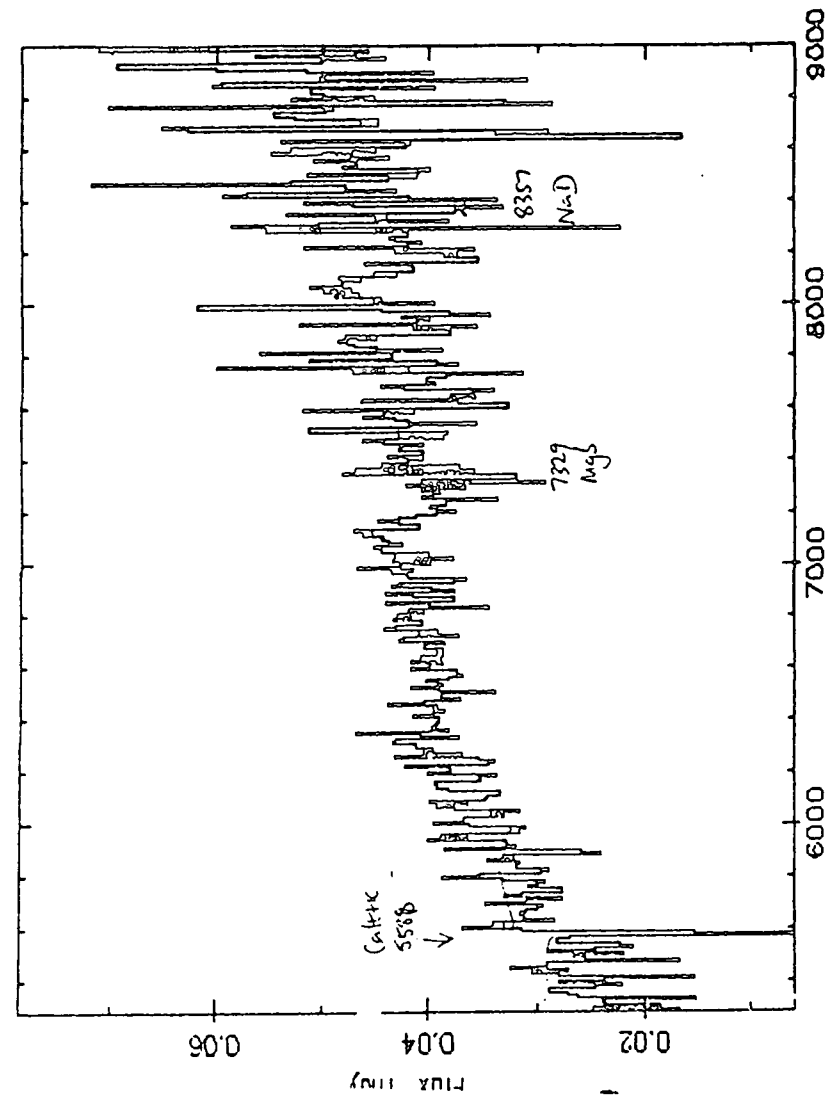
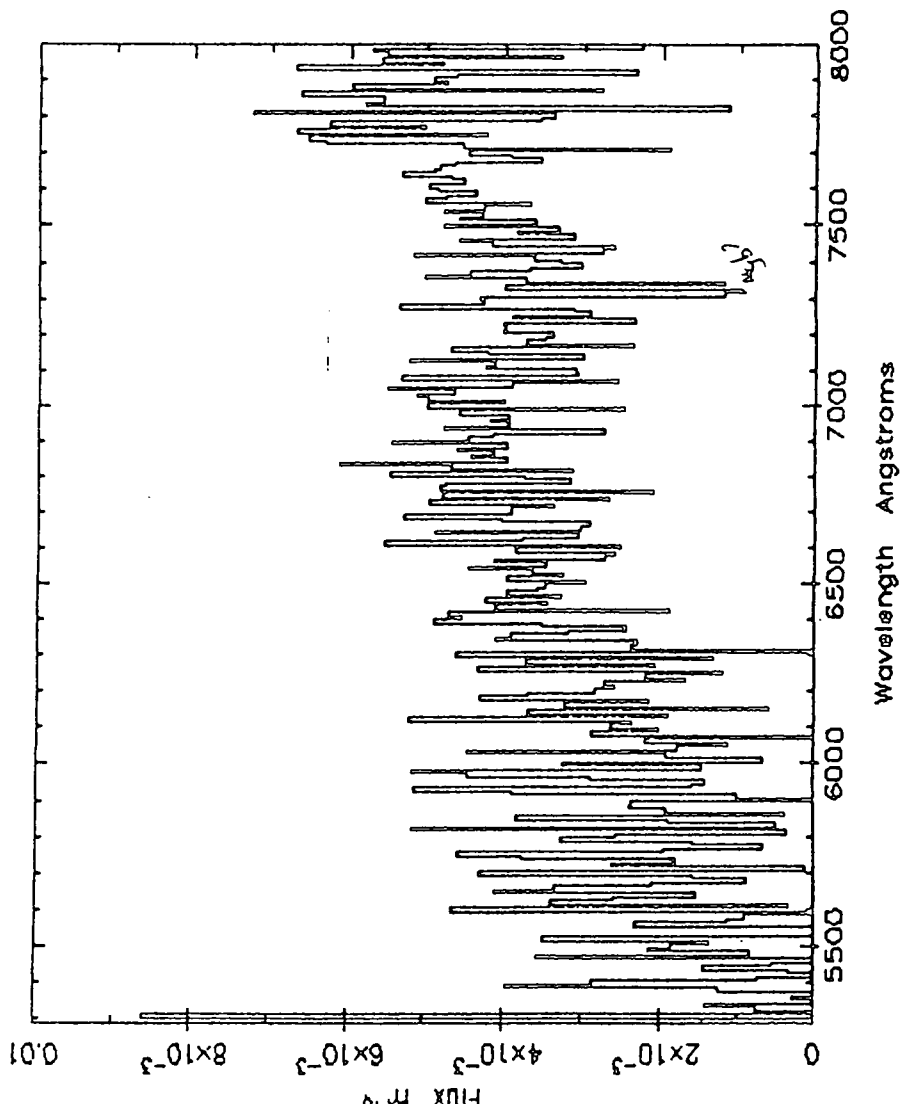
J1836.14RC/Z FLUXED(CALIB4) SMC DIV'D



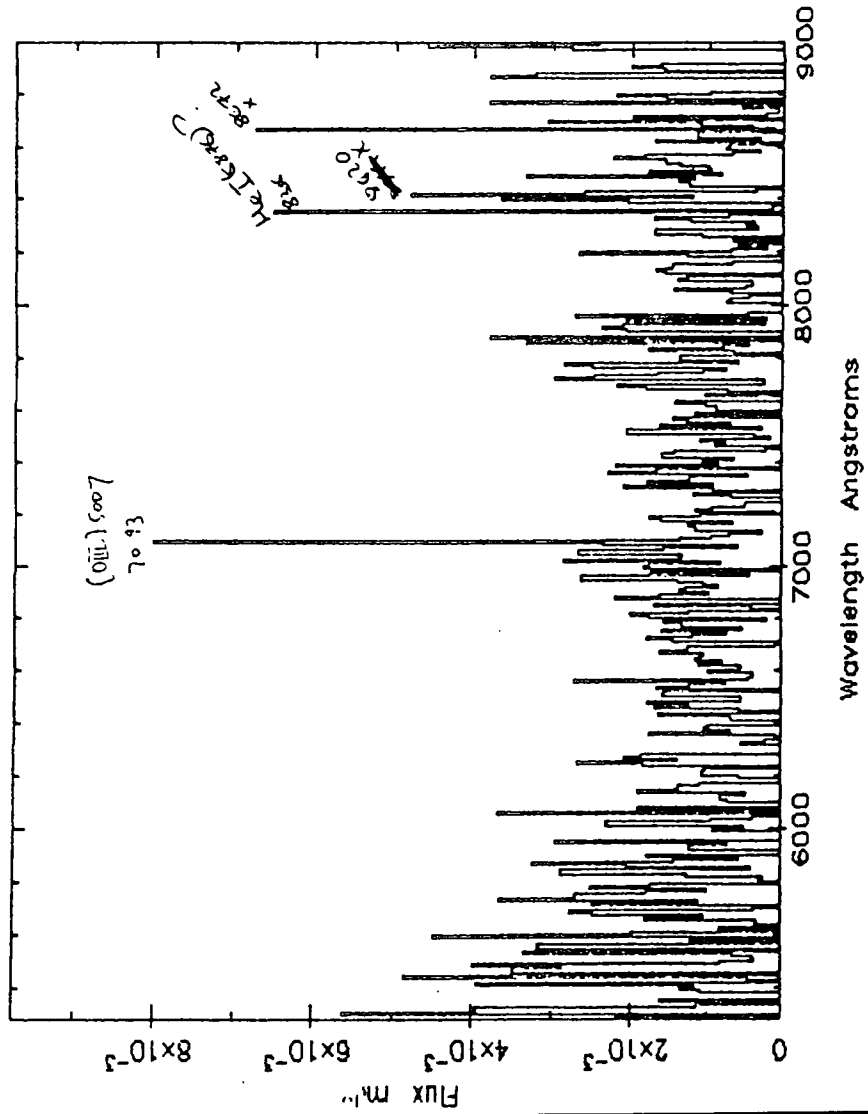
J1836.14RC/Z FLUXED(CALIB4) SMC DIV'D

J1836.3CR/D FLUXED(CALIB4) SMC DIV'D

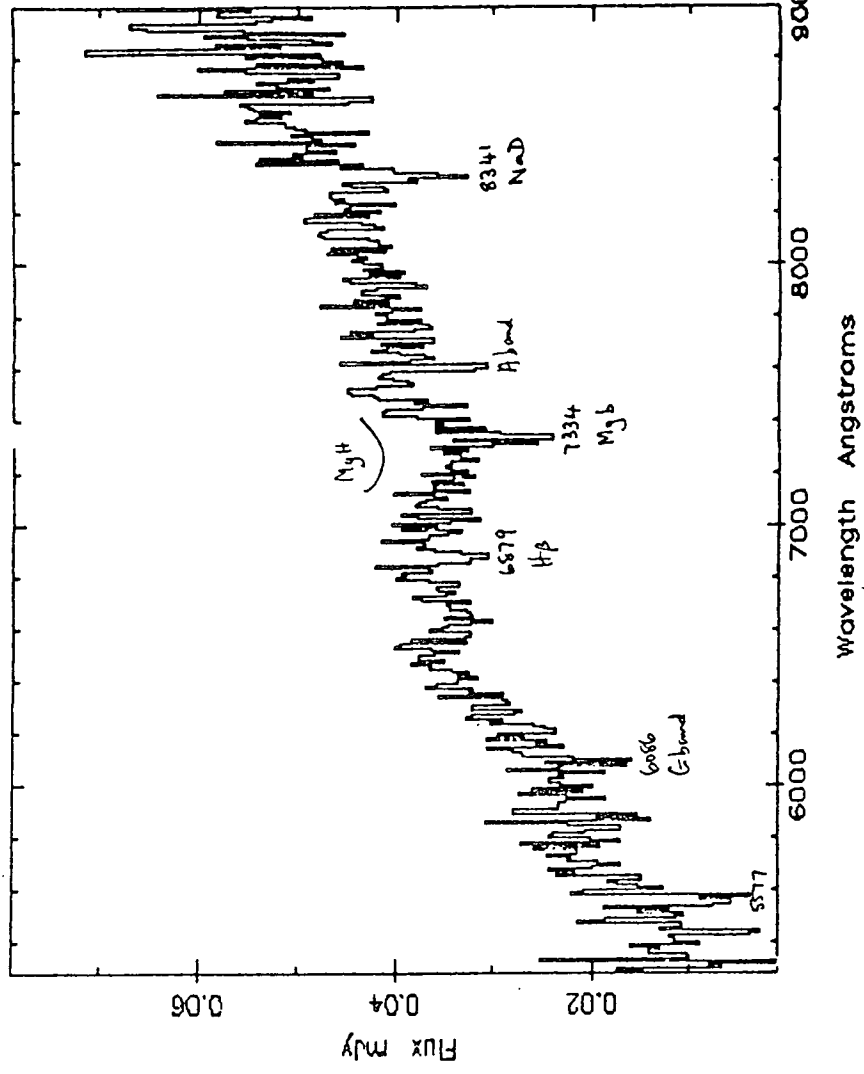
J1836.23TR/X FLUXED(CALIB3B) SMC DIV'D



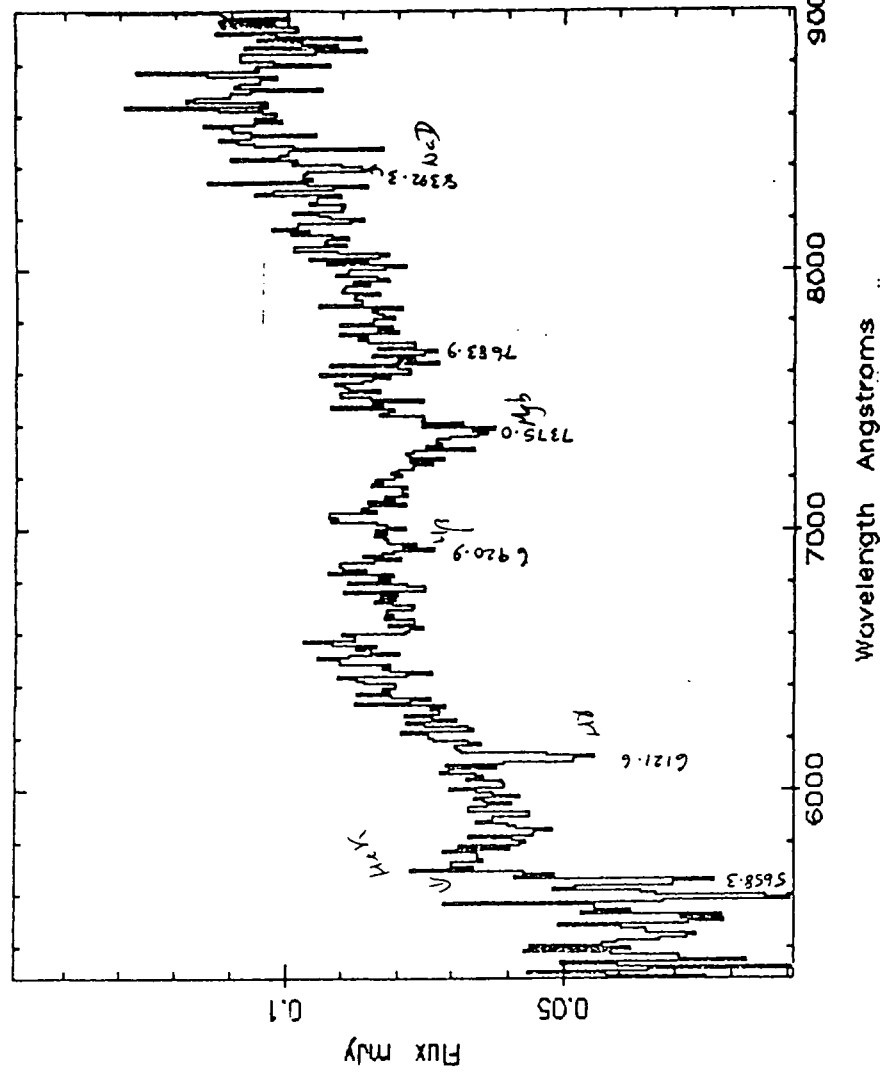
J1836.3CR/N FLUXED(CALIB4) SMC DIV'D



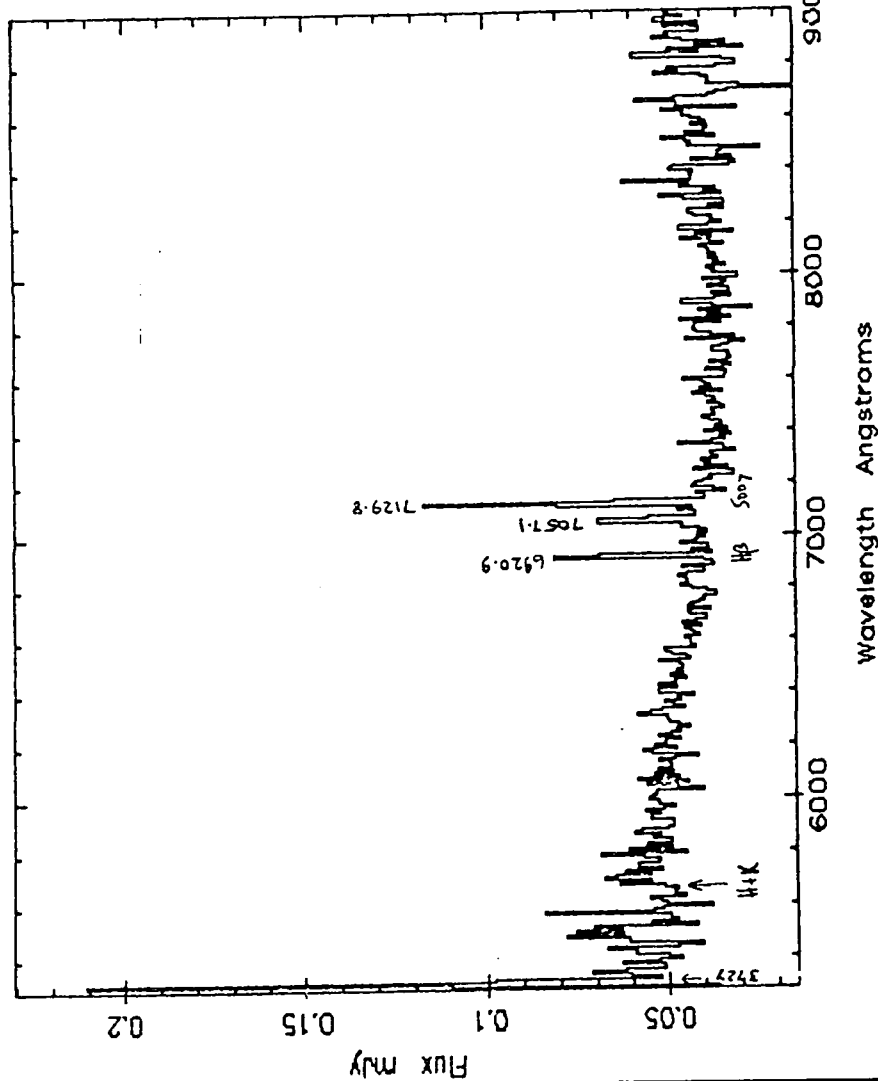
J1836.3CR/A FLUXED(CALIB4) SMC DIV'D



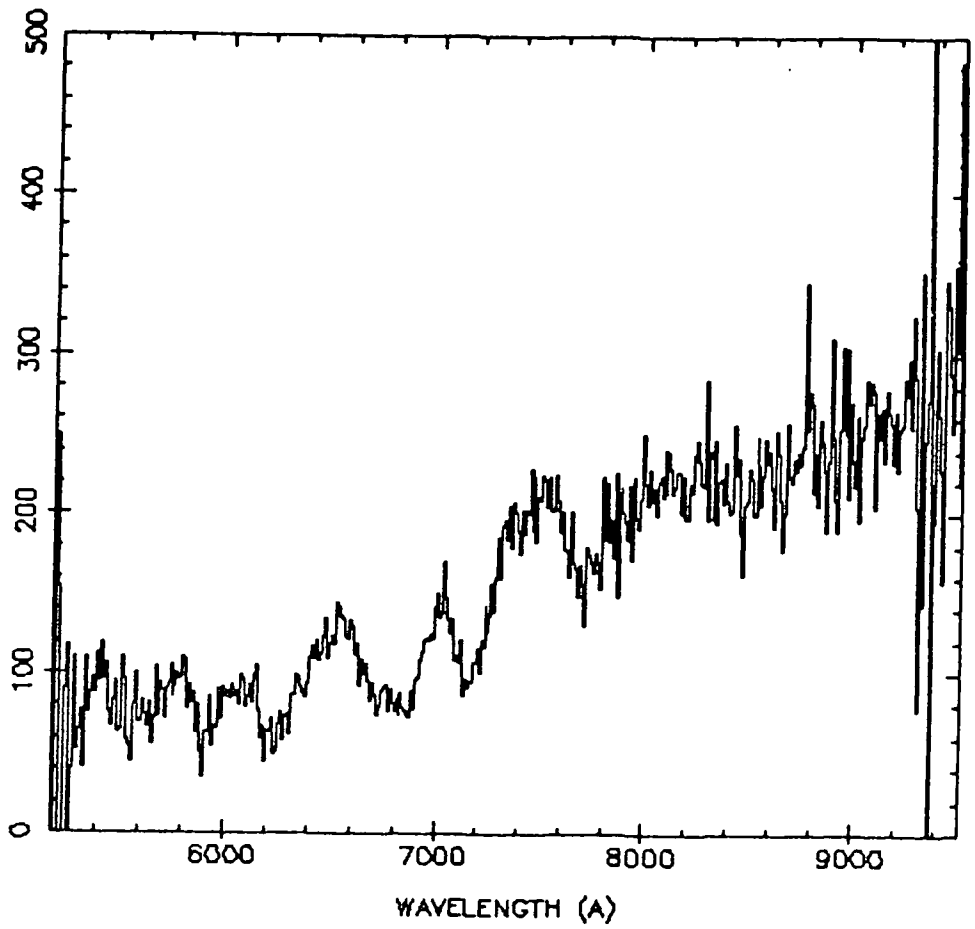
J2233/G FLUXED(CALIB4) SMC DIV'D



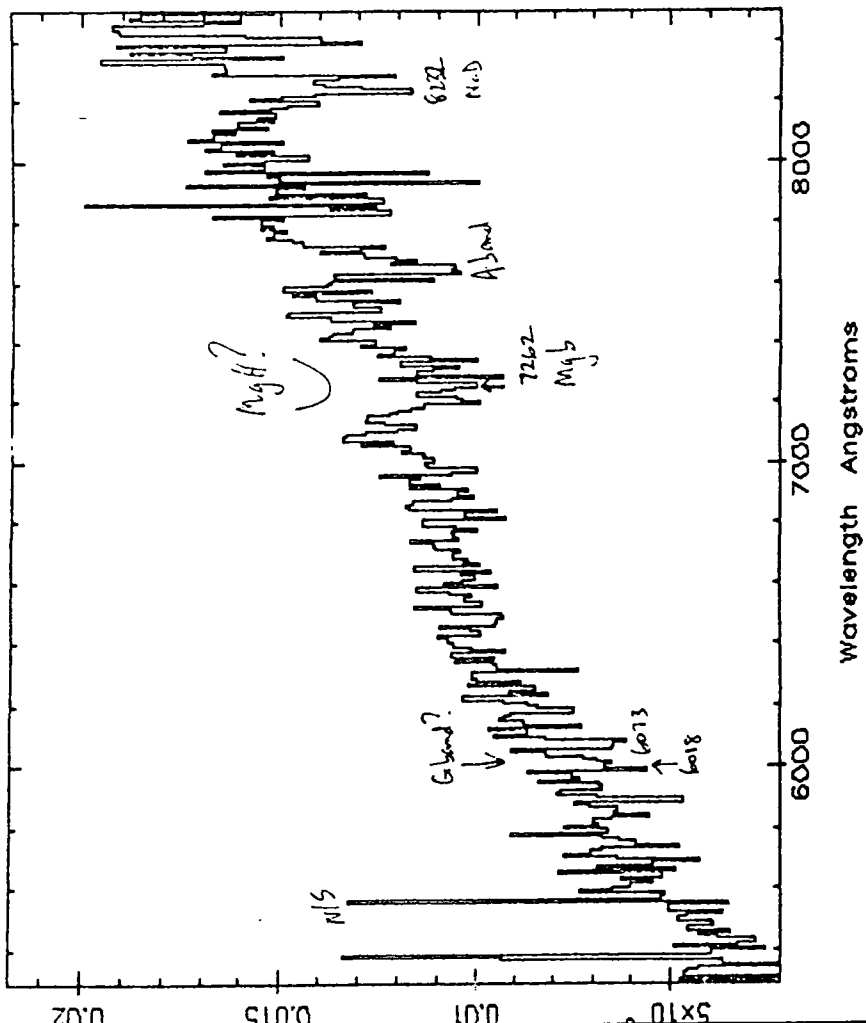
J2233/C FLUXED(CALIB4) SMC DIV'D



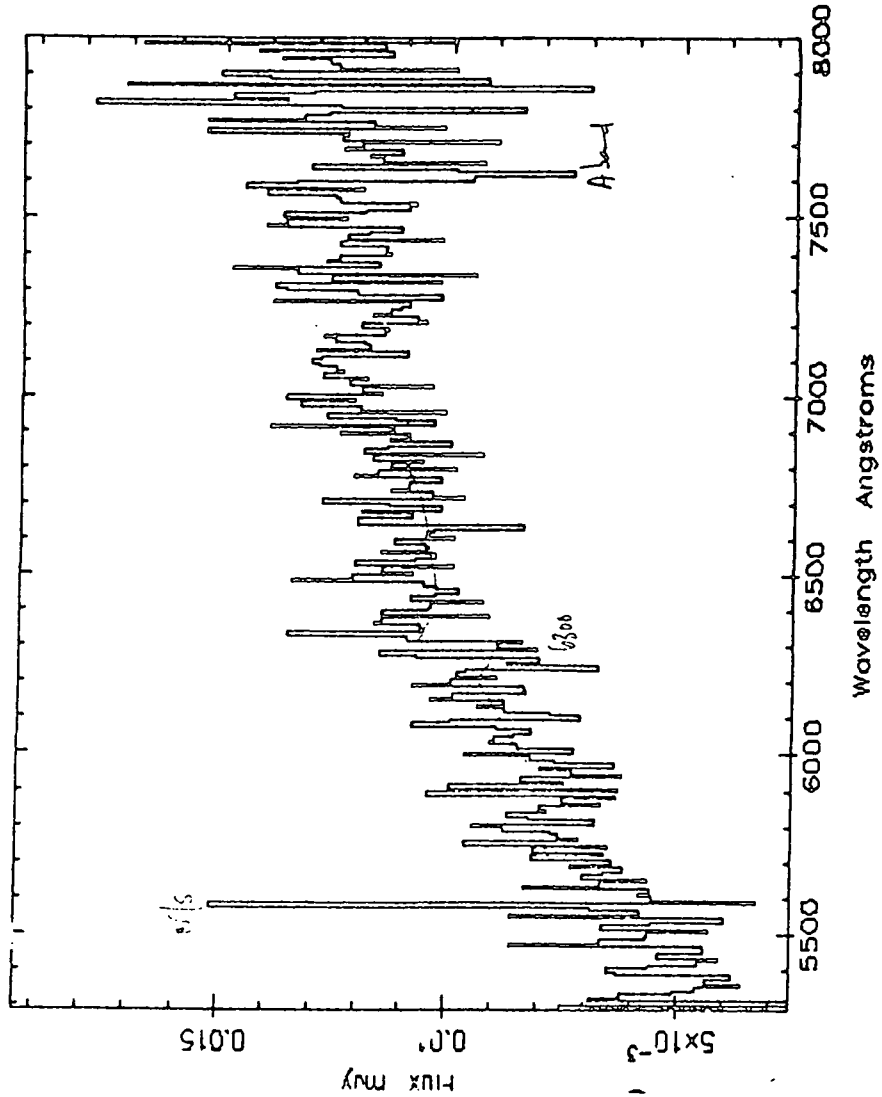
F1767.10TC YFLUX



J1836.23TR/A(N1+N2) FLUXED(CALIB3B) SMC DIV'D

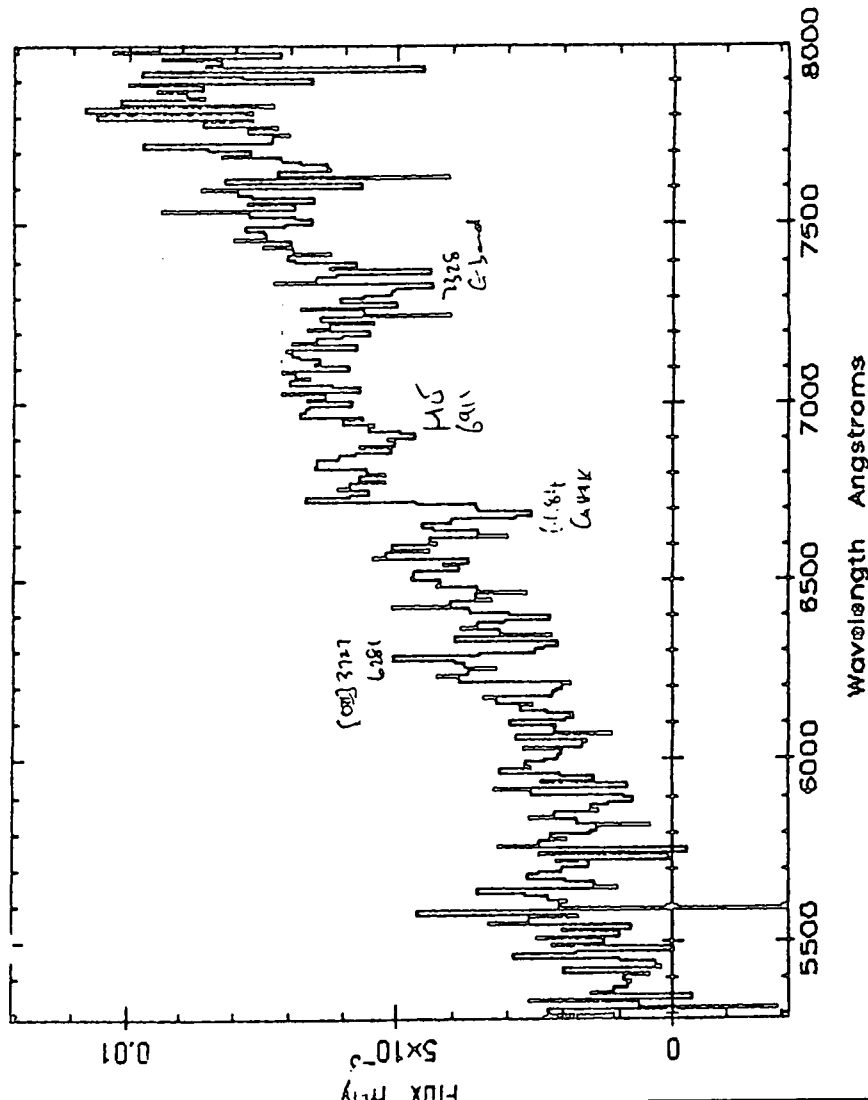


J1836.23TR/P(N2) FLUXED(CALIB3B) SMC DIV'D



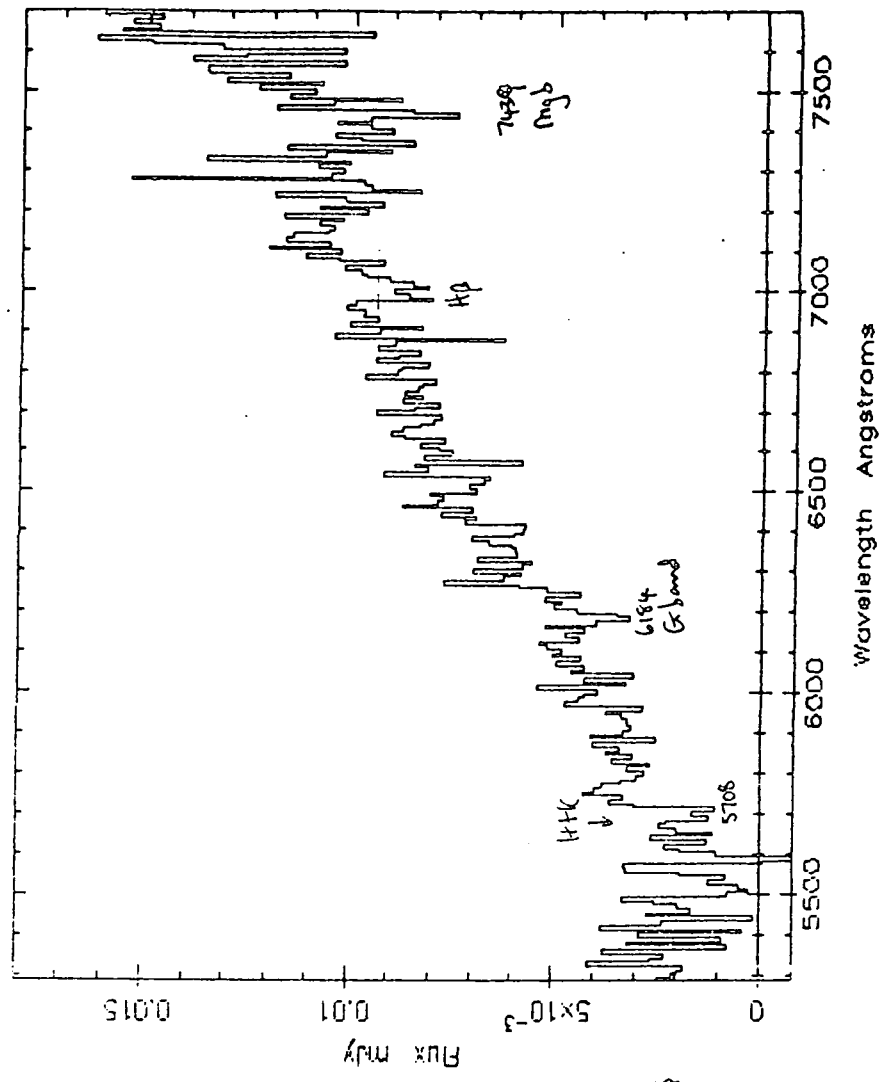
1836.23TR/P(N2) FLUXED(CALIB3B) SMC DIV'D

J1836.23TR/E(N1+N2) FLUXED(CALIB3B) SMC DIV'D



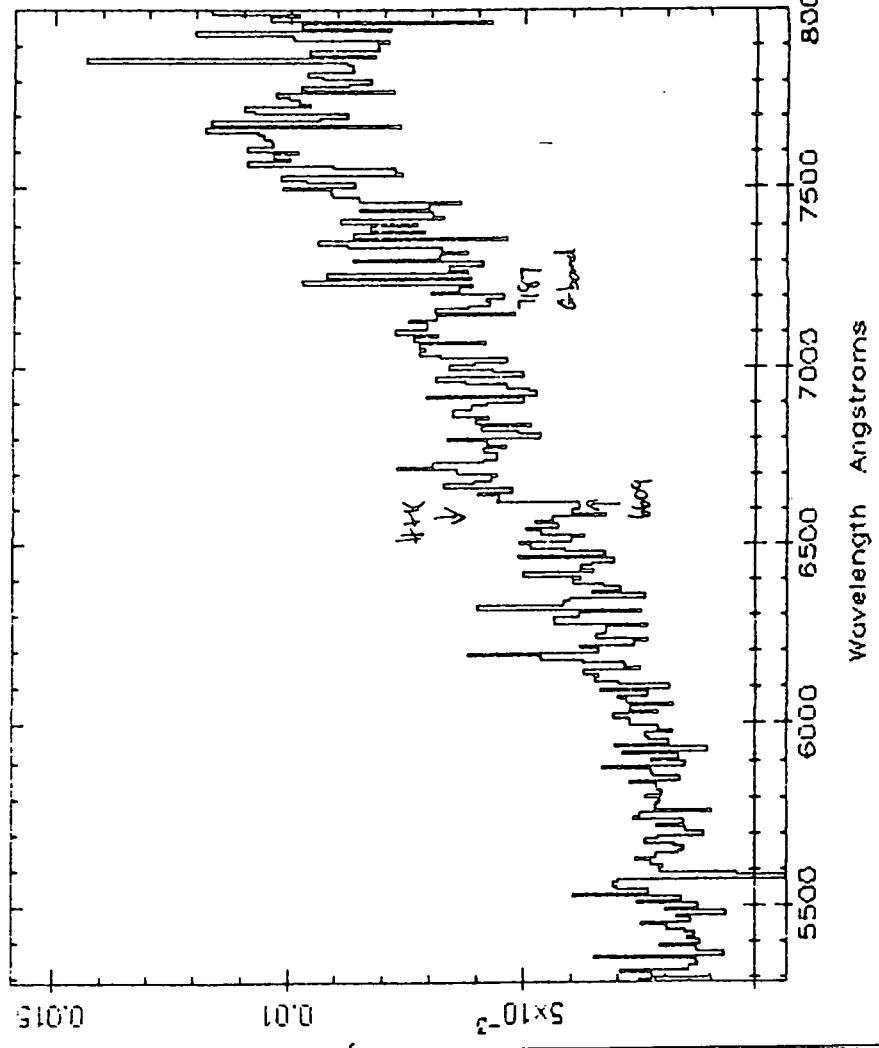
1836.23TR/E(N1+N2) FLUXED(CALIB3B) SMC DIV'D

F1767.10TC/J FLUXED(L745-46A) SMC DIV'D



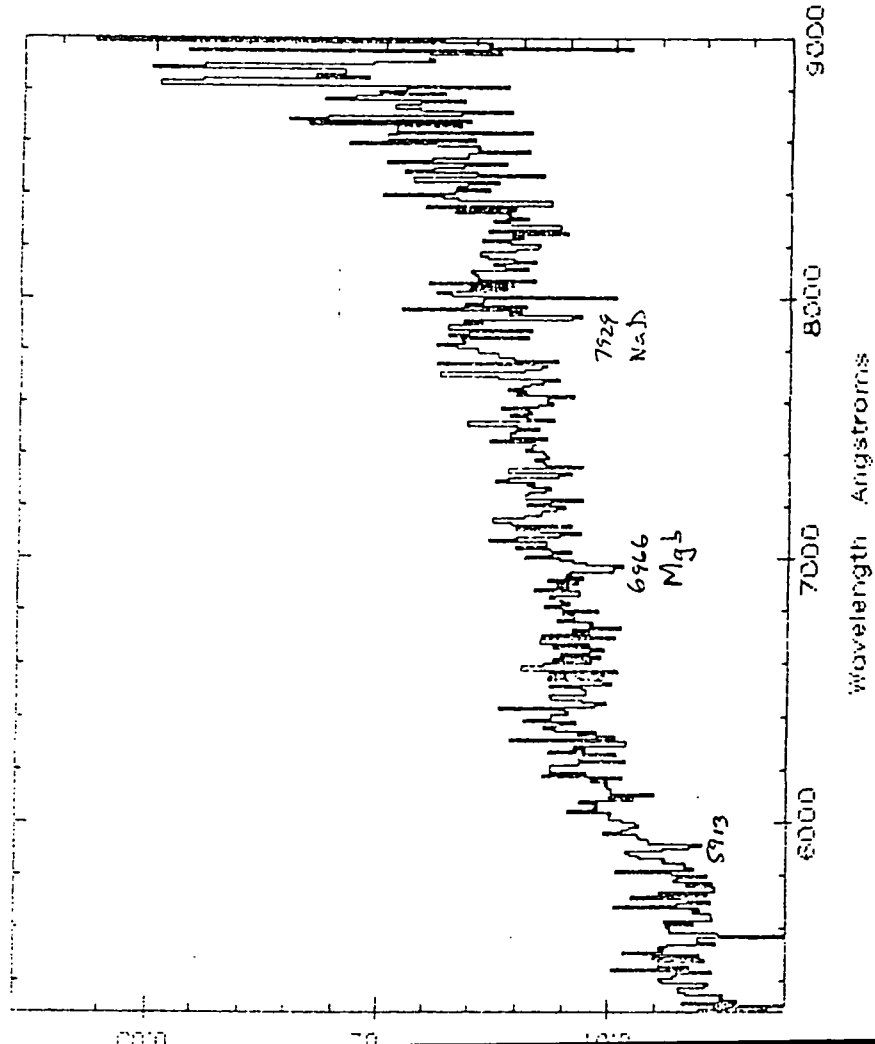
F1767.10TC/J FLUXED(L745-46A) SMC DIV'D

F1767.10TC/G(NOT OLD) FLUXED L745-46A) SMC DIV'D

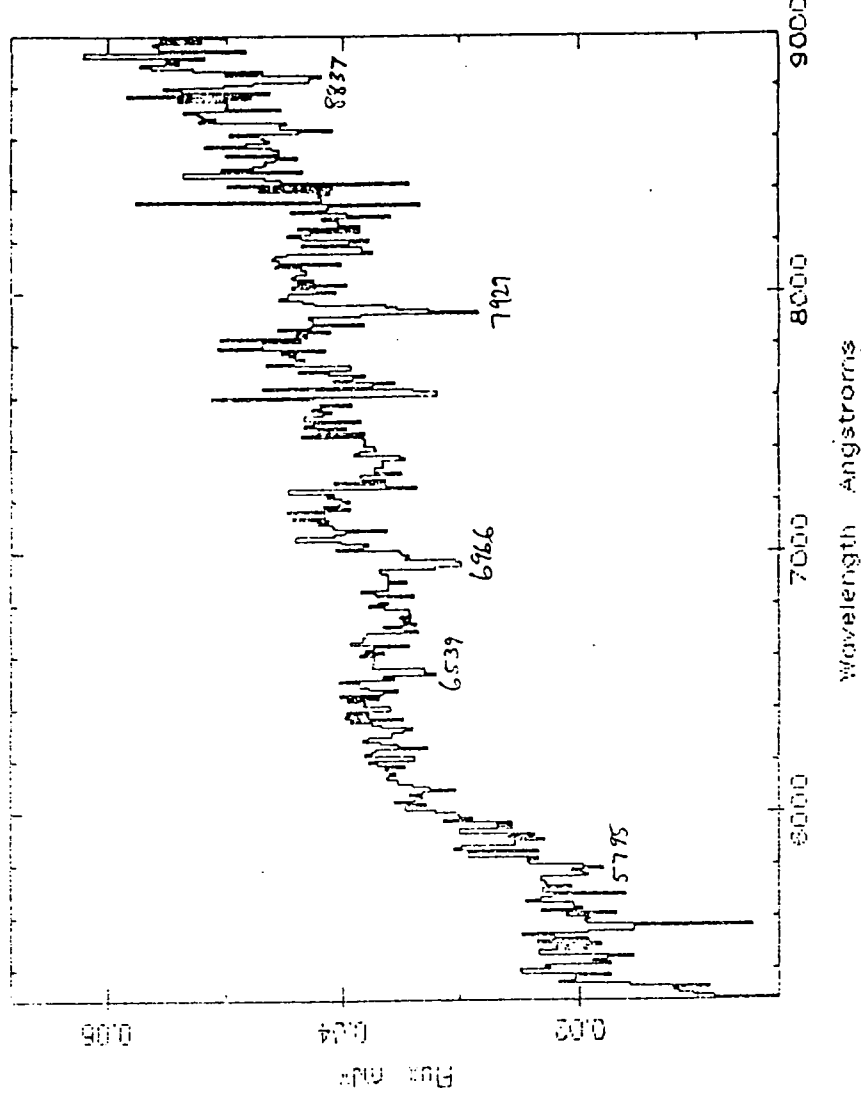


F1767.10TC/G(NOT OLD) FLUXED(L745-46A) SMC DIV'D

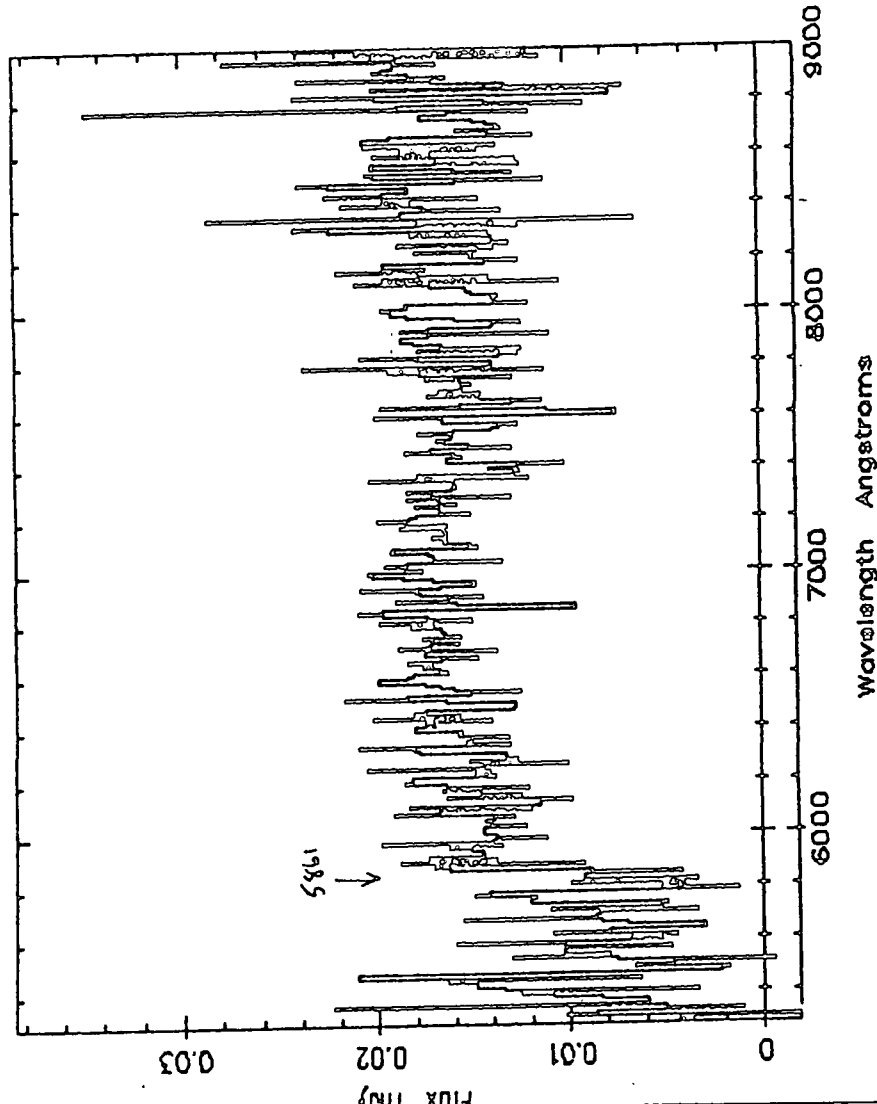
F1835.286R/B FLUXED(CALIB38) SMC DIV'D



F1835.286R/A FLUXED(CALIB38) AND SMC DIV'D



F1835.22C/B FLUXED(CALIB4) SMC DIV'D



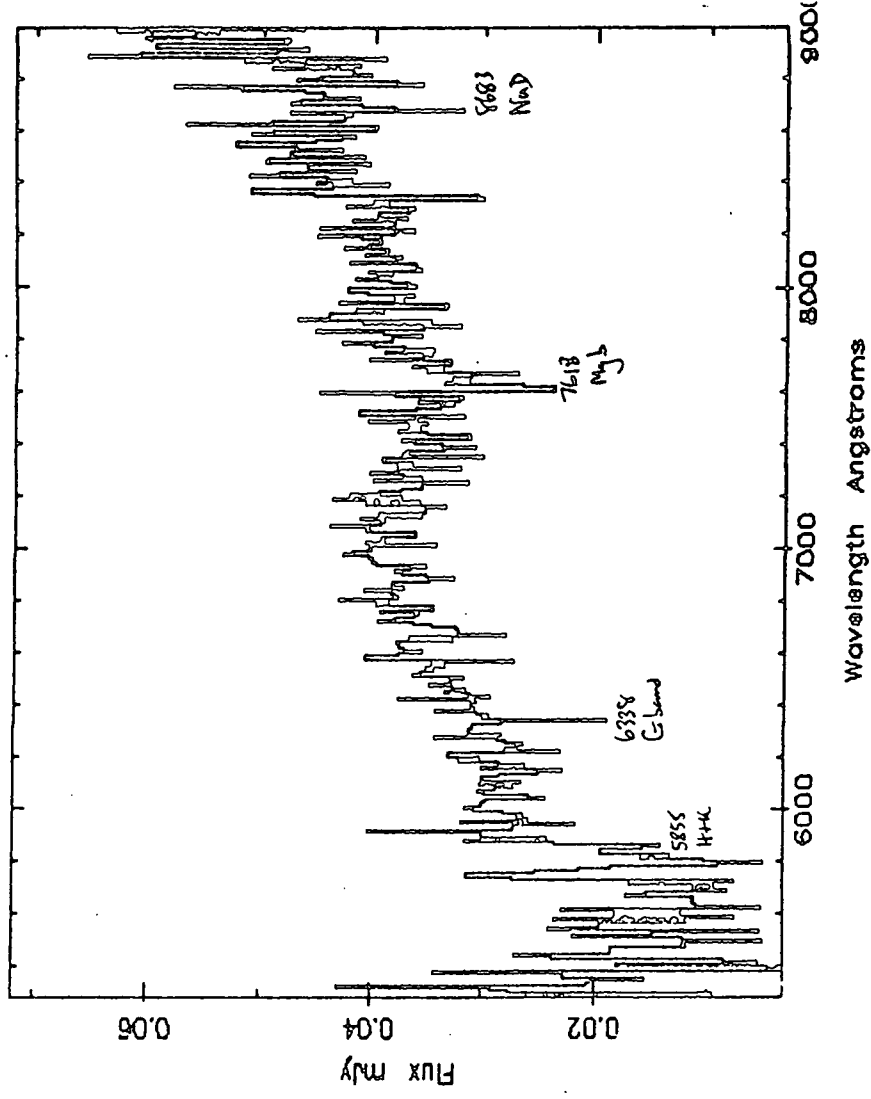
F1835.22C/B FLUXED(CALIB4) SMC DIV'D

LIS, 1

17-APR-1989 17:35

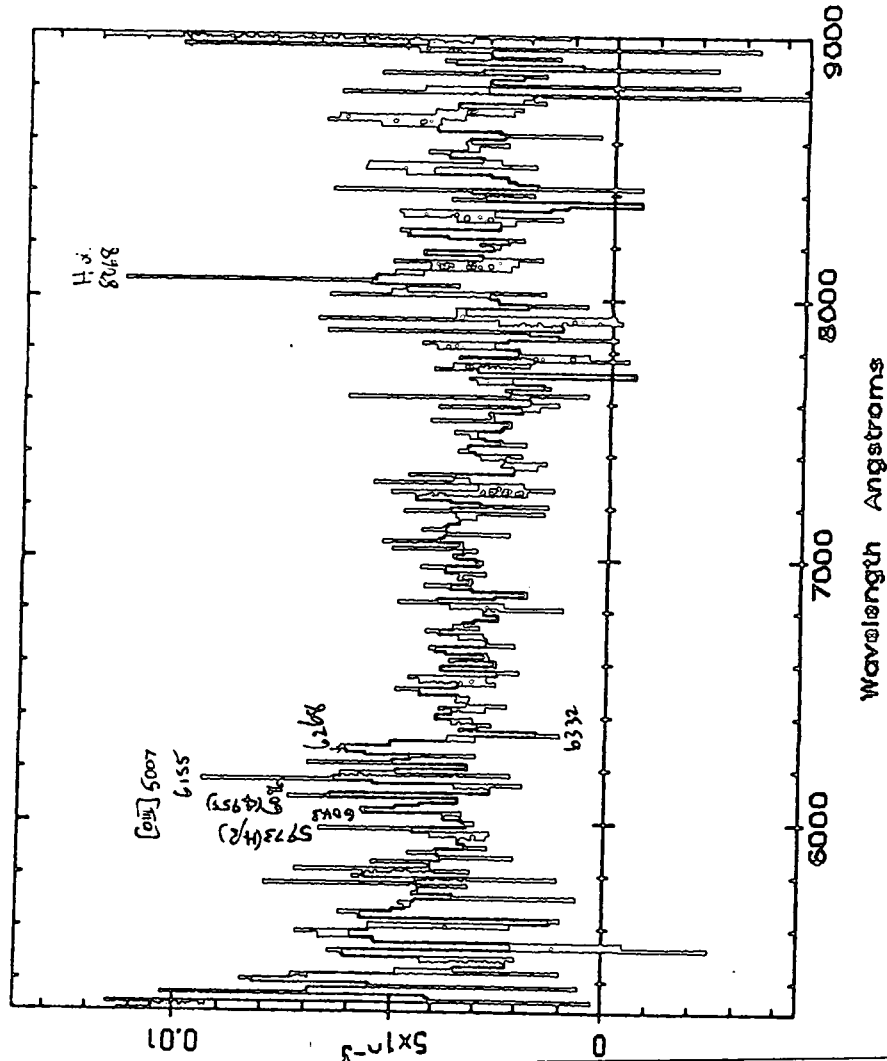
Page 1

F1835.22C/A FLUXED(CALIB4) SMC DIV'D



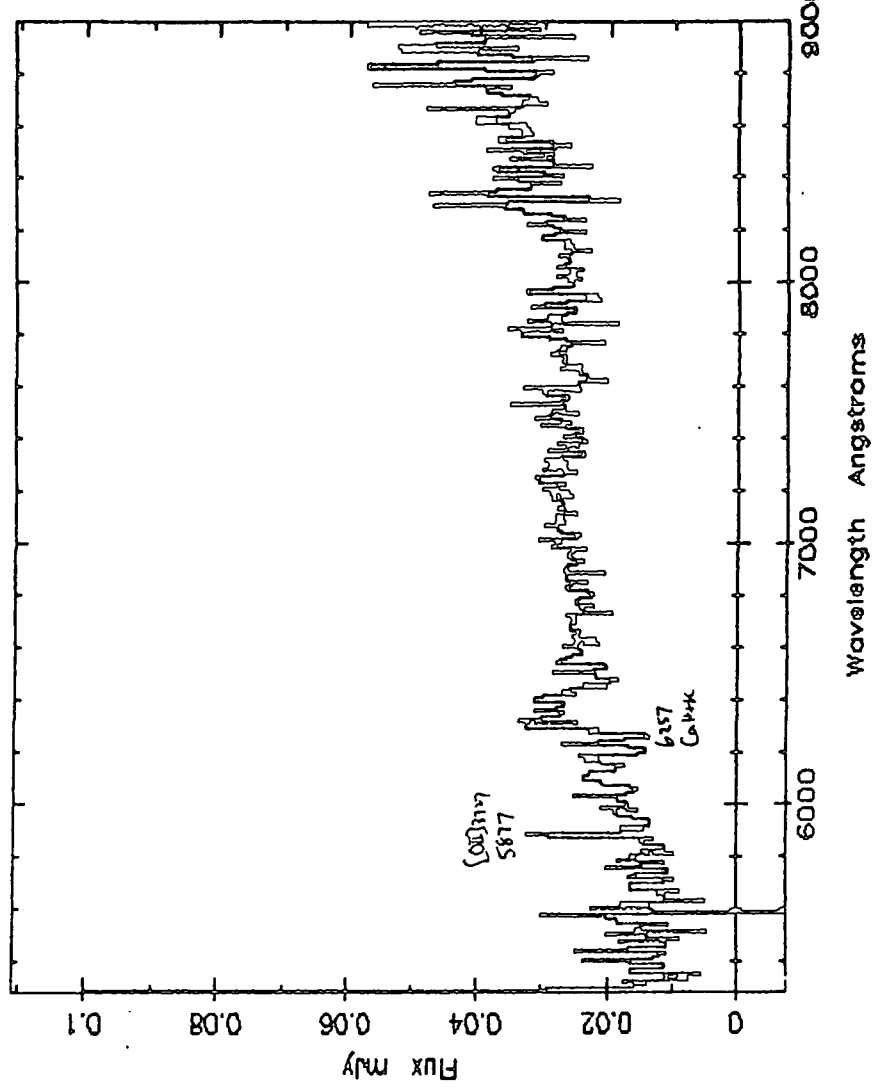
F1835.22C/A FLUXED(CALIB4) SMC DIV'D

F1835.22C/Y FLUXED(CALIB4) SMC DIV'D



F1835.22C/Y FLUXED(CALIB4) SMC DIV'D

F1835.22C/X FLUXED(CALIB4) SMC DIV'D



F1835.22C/X FLUXED(CALIB4) SMC DIV'D

f

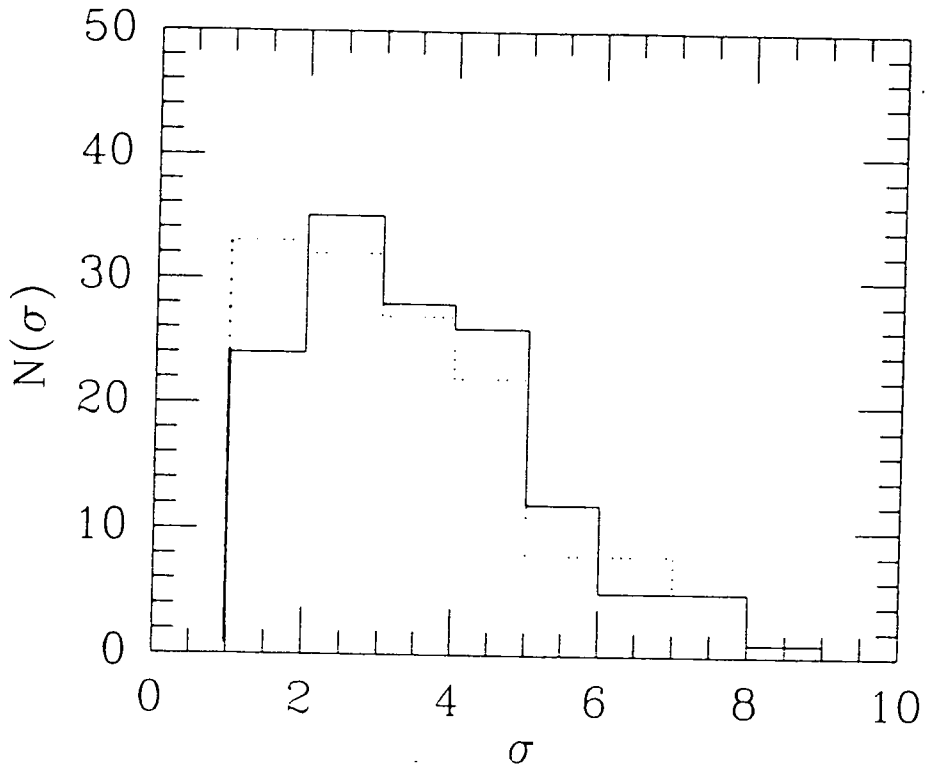
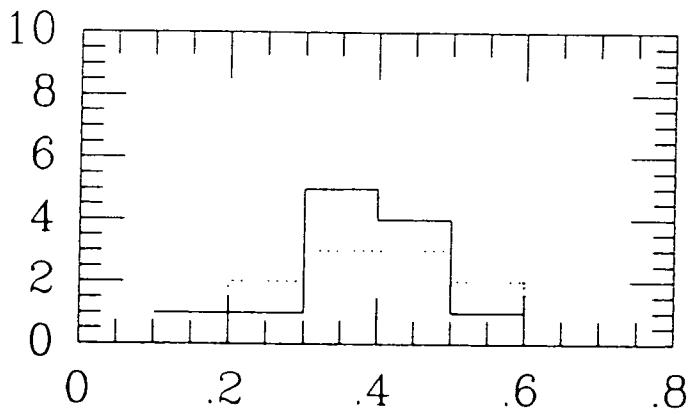


Figure 6.7: (a) Observed $N(\sigma)$ distribution for clusters selected on J film (solid line) compared with the expected distribution estimated from the crude models, normalised to the catalogue total (dotted line). (b) Observed redshift distribution (solid line) for clusters with unambiguous z values, with the expected distribution from the simulations, with a 4σ cut-off (dotted line).



- (c) Two candidates, J1836.3TC and F1835.22c, have different redshift values for each galaxy observed, providing important examples of field density enhancements conspiring to mimic distant clusters. Even at this high σ level, therefore, such problems are not totally preventable. However, as noted earlier, the fact that is the only clear example of such a 'false' cluster we have so far found, is reassuring, although we expect the detection of such objects to increase at lower σ levels.
- (d) Having noted these points, we must now consider two further specific cases, those of J1836.23T, and F1767.10TC. Both of these clusters have two conflicting redshifts, with one component at $z \sim 0.4-0.5$ and, in each case, a further object conclusively at $z \geq 0.65$. This result, particularly when viewed in conjunction with the fact that both these clusters have high catalogued σ values, may provide possible examples of the projected overlap of clusters. In the case of F1767.10TC, we only have two redshifts, one at 0.44 and the other at 0.67. Such a result is of course inconclusive, but we should certainly not expect a cluster with such a very high σ to lie predominantly at the higher z , since this would require a combination of a very rich cluster and extremely large amounts of galaxy evolution.

These results have shown that, ideally, as many spectra as possible are desired to unravel the true redshift and three-dimensional structure of our candidates. However, a minimum of three or four redshifts can tell us whether the candidate is most probably a genuine single cluster, a spurious field enhancement, or a superposition of clusters of different redshifts.

One of the implications of the large apparent effects of contamination and overlap is that simple two band photographic photometry of these candidates is likely to be fraught with difficulty in terms of assigning membership for those clusters with ambiguous redshifts.

6.6 Conclusions.

In conclusion, we can summarise the results of this chapter as follows.

- (1) We have demonstrated the use of a photographic contrast enhancement technique to enable the detection of distant clusters of galaxies with relative ease, using eyeball searches.
- (2) From a sample of some 56 HCFs we have constructed a catalogue of distant clusters of galaxies, classified in terms of their contrast against the background field counts within a fixed aperture.
- (3) A small subset of these candidates has now been observed spectroscopically and the results do indeed confirm that we are selecting galaxy clusters in the redshift range ~ 0.3 to 0.7 .
- (4) We recognise the importance of further detailed observations to properly examine the characteristics of this catalogue and note the importance of effects such as overlapping of clusters at different redshifts at these faint limits.

Encouraged by these preliminary results, we plan to extend multi-object spectroscopy to the catalogue as a whole, whilst also embarking upon a programme of multicolour photometry. With accurate photometry and spectroscopy the HCF catalogue will provide an invaluable resource for investigations of galaxy evolution. Some possibilities for future investigation are discussed in the next chapter.

7. Summary and Future Work.

7.1 Summary.

In this thesis I have addressed a wide range of topics, based on the principle of using member galaxies of distant clusters in studies of galaxy evolution. Here we shall draw these various strands together in an attempt to construct a more global view of the subject, highlighting those areas ripe for development in the immediate or near future.

Firstly, we have discussed the problems associated with the detection and identification of distant ($z > 0.3$) clusters. The principal difficulties are the low contrast of such faint objects against the background and the often severe selection effects that have dominated most previous work. The AAO Deep Cluster Survey is an attempt to construct a catalogue of clusters from a single source whose selection properties could be understood. Further, a great deal of effort has been expended in attempts to overcome the technical difficulties associated with observations at such very large distances. Using a CCD photometric system based on a set of intermediate bandwidth filters, we have been able to construct low resolution spectral energy distributions (SEDs) for each galaxy in the CCD field. This method has been able, to some extent, to alleviate the important problem of cluster contamination by foreground galaxies, since the SEDs allow us to estimate whether or not each object is likely to be a genuine cluster member. As we have seen, independent spectroscopy has, on the whole, shown that this approach is an effective one.

Considering astrophysical, rather than 'technical,' questions, the photometry of distant galaxies has revealed the presence of a range of galaxy types in each cluster. The SEDs enable the selection of various populations of galaxy for further study. For example, we have exploited the effect of redshift and imaged these distant galaxies in their rest-frame ultraviolet. This resulted in the detection of a distinct class of object at these early epochs, which, whilst displaying the rest-frame optical colours associated with the cluster's colour-magnitude relation, also exhibit enhanced uv luminosities.

Attempting to reconcile such galaxies with other spectroscopic observations of these and other clusters, we have proposed a simple evolutionary progression for the progenitors of the red early-type galaxies observed in rich clusters at the present-day. This scenario envisages some mechanism for the stimulation of significant levels of star formation in these galaxies. Spectroscopic observations and modelling imply that this star-forming activity takes place in a short burst. After this period, the galaxy's spectrum evolves redwards, passing through a phase in which Balmer absorption lines are highly prominent, and then becoming the uvx galaxies that are observed via our multicolour work, before eventually acquiring the red colours of nearby E/S0 galaxies.

The 'trigger' mechanism for such behaviour is as yet unresolved, but could arise either from dynamical considerations such as galaxy-galaxy interactions, or more large scale effects, such as shocks generated as galaxies pass through the cluster's core. Alternative hypotheses could be based on the presence of some internal mechanism within each galaxy, or some connection with the discs of SO galaxies.

A further significant observation was that the uvx galaxies only constitute a sub-sample of the total cluster 'red' population (ie., those galaxies that follow the colour magnitude relation in the rest-frame visible colours). Many galaxies at high redshift have spectral properties little different to those of their nearby counterparts. An issue to be settled, then, is what is the reason for these differences in evolutionary behaviour. Do all galaxies undergo such bursts of star-forming activity, but at different epochs, or does one specific type only behave in this manner? If so, is there a preferred epoch, and what determines this? The

relative proportions of galaxies at each evolutionary stage may provide some clue to these questions, as we suggested in chapter 5.

Two key points are crucial to our understanding of these evolutionary effects. Firstly, our knowledge of nearby galaxies is still somewhat limited, particularly with regard to ultraviolet wavelengths. Whilst we have seen that the satellite observations so far accumulated seem to indicate a simple extension of the colour-magnitude effect down to short wavelengths, we should re-emphasise that the number of such observations is, at present, extremely limited.

Furthermore, the work carried out by O'Connell (1983,1986) and Rose(1985), in determining the constituent populations of nearby early-types in an attempt to unravel some indication of their last period of star-forming activity, is a significant contribution to the subject. It is vital to extend this type of investigation to cover a larger range of galaxy absolute magnitudes and environments.

In conclusion, then, the work presented in this thesis has highlighted some of the key problems in studying galaxy evolution at high redshifts; provided some useful new approaches and interesting results; and, finally, has indicated possible lines of enquiry for subsequent future studies. In the next section I shall present a range of possible topics, which currently available, or proposed, detectors and facilities will enable us to address.

7.2 Suggestions for Future Work.

(a) *Cluster Redshifts.*

Further development of the catalogue of distant clusters can be effected by the determination of redshifts for each candidate cluster. At present we have only a limited amount of spectroscopy available, but with further allocation of observing time to such a project we should be able to remedy this situation, making use of presently available spectroscopic detector systems. The combination of the cluster redshifts and further photometry of each candidate will allow a quantitative investigation of the detection parameters of the survey, and the problems of foreground contamination and superpositions of clusters at different redshifts.

(b) *Multicolour Photometry.*

Once again we can use the photometric technique developed in this thesis to isolate particular galaxy types in each cluster for detailed investigation. Extending this approach to the catalogue as a whole, will allow us to probe the evolutionary questions in considerably more detail than has been possible using only the two clusters, A370 and 0016+16, that we thus far imaged. Having a range of clusters should reveal whether or not effects such as the uvx phenomenon are universal at earlier epochs or only arise in some clusters.

(c) *Extending the Photometry.*

As Lilly and Gunn (1985) and Lilly (1987) have shown, extension of these studies into the near infrared can yield more information on the nature of the underlying stellar populations in each galaxy. Combining ultraviolet, optical, and infrared observations allows direct monitoring of the contributions of young, main-sequence, and giant branch stars, enabling analysis of the star formation rates and evolutionary status of each galaxy. With the development of new two-dimensional infrared cameras, these observations will become considerably easier and less expensive in terms of telescope time in the very near future.

(d) *Multi-Object Spectroscopy.*

Multi-object spectroscopy of galaxy clusters is a rapidly expanding field of study, particularly with the devices such as the AAT fibre-optic system and the other new instruments that are currently becoming available (eg., Parry, 1986). As I have discussed in chapter 5,

analysis of the strengths of various spectral features (eg., emission lines, Ca II H and K, Balmer absorption lines, etc.) can be used to great effect in evolutionary studies. Couch and Sharples (1987) have, for example, undertaken such observations for three clusters at $z \sim 0.3$, and have constrained possible evolutionary scenarios in conjunction with detailed spectral evolution models (see chapter 5). Finally, detailed spectroscopy will also allow us to study the dynamical properties of these clusters, and examine such possibilities as substructure, etc.

(e) *High Resolution Imaging.*

High resolution imaging of galaxies at high redshifts is another exciting prospect for the near future, both using the Hubble Space Telescope and the ground-based techniques that are presently being developed by several groups (eg, Thompson, 1986). Imaging should reveal whether the blue members of distant clusters have, for example, bulge-to-disc ratios typical of nearby spiral-type galaxies, or indeed, possibly even if they possess spiral structure. This determination of the location of the ongoing star-formation within each galaxy will be essential to our overall picture of such behaviour. It would also be of great interest to attempt imaging of the galaxies classified by our photometric method as being uvx galaxies in an attempt to morphologically distinguish these from the red colour-magnitude sequence objects in these clusters.

(f) *Nearby Galaxies.*

One of the important consequences of the many interesting results to have arisen from the observations of distant galaxy clusters is an awareness of just how limited is our understanding of even nearby galaxies in similar environments. As discussed earlier, techniques such as that of Rose (1985) will prove invaluable if extended to cover a larger range in absolute magnitude, and if used to examine possible differences between galaxies in different environments. Furthermore, we have also noted the limitations of the available information on the rest-frame ultraviolet properties of nearby early-type galaxies, and this situation must also be remedied. Unfortunately significant progress in this field will only be achieved via space-borne detector systems, and thus we await the launch of the Hubble Space Telescope, to enable uv imaging.

As we noted in chapter one, spectroscopy of nearby galaxies is usually only obtained for the nuclear regions of each object, whereas for large redshifts, the spectrum is obtained from a much larger area of the galaxy. For proper comparisons, we should attempt to acquire integrated galaxy spectra from a larger spatial area in the nearby galaxies, some work is currently being done in this area (eg, Dressler *et al*, 1982). This again highlights one of the important points in such a research programme, in that our observations of distant galaxies are not usually equivalent to the available information on more nearby systems, with which we attempt to compare them. Thus much of the impetus in future work should be towards standardising the observations of our nearby template galaxies. We should also consider carefully, as in Butcher & Oemler (1983), the differences in observed properties between nearby galaxies that are in clusters or the field.

7.3 Postscript.

In this thesis I have shown how a variety of observational methods can be used in the unravelling of the evolutionary history of star forming activity in galaxies. We have seen how, by reaching to fainter magnitude limits, we can probe further back into the history of the universe, enabling us to directly observe the past, as it happened several Gigayears ago. The nature of this work has been exploratory, to investigate the difficulties present in the field and to attempt some minimisation of their consequences. Even so, we have been able to conclude that we have seen strong evidence for the evolution of a substantial

number of early-type galaxies between the present epoch and a period some 6–7 Gyrs ago. Such lookback times are now readily accessible with large telescopes, and we can begin to undertake large scale systematic investigations of galaxies at high redshifts ($z > 0.3$) given sufficient allocation of observing time.

Much of this work has only become possible due to the many innovations and development of a wide range of astronomical detectors and telescope systems that have occurred over the past several years. This rapid advance in technology and ingenuity of application continues apace to date, and thus holds much promise for the near future. Indeed it is worth noting that we can begin to make headway in revealing the answers to many of the important topics outlined above using technology that is available at the present day. Thus, although the launch of the Hubble Space Telescope will have a major impact in our understanding not only of this particular subject but of many fields in astronomy, the current level of progress in ground-based techniques will ensure the significance of the role played by earthbound astronomers in extragalactic astronomy over the decades to come.

References:

- Abell,G.O., 1958, *Astrophys. J. Suppl.*, **3**, 211.
- Abell,G.O., & Corwin,H.G., 1983, *Early Evolution of Universe*, IAU Symp 104, Reidel, Holland.
- Allen,C.W., 1973, *Astrophysical Quantities*, Athlone Press, London.
- Arimoto,N., Yoshii,Y., 1987, *Astron. Astrophys.*, **173**, 23.
- Bahcall,N., 1977, *Ann. Rev. Astr. Astrophys.*, **15**, 505.
- Baum,W.A., 1962, *Problems of Extragalactic Research*, IAU Symp. 15, ed. McVittie,G.C., MacMillan, New York.
- Bautz,M., Loh,E.D., & Wilkinson,D.T., 1982, *Astrophys. J.*, **255**, 57.
- Bertola,F., Capaccioli,M., & Oke,J.B., 1982, *Astrophys. J.*, **254**, 494.
- Birkinshaw,M., & Gull,S.F., 1984, *Mon. Not. R. Astr. Soc.*, **206**, 359.
- Bothun,G.D., & Dressler,A., 1986, *Astrophys. J.*, **301**, 57.
- Bruzual,G.,1980, *PhD thesis*, University of California,Berkeley.
- Bruzual,G., 1983, *Astrophys. J.*, **273**, 105.
- Bruzual,G.,& Spinrad,H.,1980, *The Universe at Ultraviolet Wavelengths*, Reidel, Dordrecht, Holland.
- Burstein,D., Faber,S.M., Gaskell,C.M., Krum,N., 1984, *Astrophys. J.*, **287**, 586.
- Burstein,D., & Heiles,G., 1978, *Astrophys. J.*, **225**, 40.
- Butcher,H, & Oemler,A., 1978a, *Astrophys. J.*, **219**, 18.
- Butcher,H. & Oemler,A., 1978b, *Astrophys. J.*, **226**, 559.
- Butcher,H. & Oemler,A., 1984a, *Astrophys. J.*, **285**, 426.
- Butcher,H., & Oemler,A., 1984b, *Nature*, **310**, 31.
- Butcher,H., & Oemler,A., 1984, *Astrophys. J. Suppl.*, **57**, 665.
- Butcher,H., Oemler,A., Wells,D.C., 1983, *Astrophys. J. Suppl.*, **52**, 183.
- Ciardullo,R.B., & Demarque,P., 1977, *Trans. Astr. Obs. Yale Univ.*, **35**.
- Coleman,G.D., Wu,C.C., & Weedman,D.W, 1980, *Astrophys. J. Suppl.*,**43**, 393.
- Couch,W.J., 1981, *PhD thesis*, Australian National University.
- Couch,W.J, & Newell,E.B., 1984, *Astrophys. J. Suppl.*,**56**, 143.
- Couch,W.J., Ellis,R.S., Godwin,J., & Carter,D., 1983, *Mon. Not. R. Astr. Soc.*, **205**, 1287.
- Couch,W.J., Ellis,R.S., Kibblewhite,E.J., Malin,D.F., Godwin,J., 1984, *Mon. Not. R. Astr. Soc.*, **209**, 307.
- Couch,W.J., Shanks,T., Pence,W.D., 1985, *Mon. Not. R. Astr. Soc.*, **213**, 215.
- Couch,W.J., & Sharples,R.M., 1987, *Mon. Not. R. Astr. Soc.*, in press.
- Cowie,L.L., & Songaila,A., 1977, *Nature*, **266**, 501.
- De Gioia-Eastwood,K., & Grasdalen,G.L., 1980, *Astrophys. J.*, **239**, L1.
- de Jong,T., 1986, *Spectral Evolution of Galaxies*, eds. Renzini,A., & Chiosi,C., Reidel, Holland.
- de Vaucouleurs,G., de Vaucouleurs,A., Corwin,H.G., 1976, *Second Reference Catalogue of Bright Galaxies*, Austin, University of Texas Press.
- Dodd,R.J., & MacGillivray,H.T., 1987, *Astron. J.*, **92**, 706.

- Dressler, A., 1978, *Astrophys. J.*, **223**, 765.
- Dressler, A., 1980, *Astrophys. J.*, **236**, 351.
- Dressler, A., 1984, *Ann. Rev. Astron. Astrophys.*, **22**, 185.
- Dressler, A., & Gunn, J.E., 1982, *Astrophys. J.*, **263**, 535.
- Dressler, A., & Gunn, J.E., 1983, *Astrophys. J.*, **270**, 7.
- Dressler, A., Gunn, J.E., Schneider, D.D., 1985, *294*, 70.
- Dressler, A., Thompson, I.B., Schectman, S.A., 1985, *Astrophys. J.*, **288**, 481.
- Dressler, A., Lynden-Bell, D., Burstein, D., Davies, R.L., Faber, S.M., Terlevich, R.J., 1987, *Astrophys. J.*, **313**, 42.
- Dupree, A.K., Hartmann, L., Black, J.H., Davis, R.J., Matilsky, T.A., Raymond, J.C., Gursky, H
 1979, *Astrophys. J.*, **230**, L89.
- Ellis, R.S., 1982, *Origin & Evolution of Galaxies*, eds. Jones, B.T. & Jones, J.E., Reidel, Holland.
- Ellis, R.S., 1983, *Clusters & Groups of Galaxies*, eds. Mardirossian, F., Giaricin, G., Mezetti, M., Reidel, Holland.
- Ellis, R.S., 1987, *Observational Cosmology*, IAU Symposium 124, Beijing, eds. Burbidge, G.R., & Hewitt, A., Reidel, in press.
- Ellis, R.S., & Allen, D.A., 1983, *Mon. Not. R. Astr. Soc.*, **203**, 685.
- Ellis, R.S., Couch, W.J., MacLaren, I., & Koo, D.C., 1985, *Mon. Not. R. Astr. Soc.*, **217**, 239.
- Flin, P., 1981, *Origin & Evolution of Galaxies*, eds. Jones, B.T. & Jones, J.E., Reidel, Holland.
- Gisler, G.R., 1980, *Astron. J.*, **85**, 623.
- Godwin, J., 1976, *D.Phil. thesis*, University of Oxford.
- Gull, S.F., Birkinshaw, M., Moffet, A.T., 1981, *Astrophys. J.*, **251**, L69.
- Gunn, J.E., & Gott, J.R., 1972, *Astrophys. J.*, **176**, 1.
- Gunn, J.E., Hoessel, J.G., Oke, J.B., 1986, *Astrophys. J.*, **306**, 30.
- Gunn, J.E., & Oke, J.B., 1975, *Astrophys. J.*, **195**, 255.
- Hamilton, D., 1985, *Astrophys. J.*, **297**, 371.
- Hamilton, D., 1986, *Spectral Evolution of Galaxies*, eds. Renzini, A., & Chiosi, C., Reidel, Holland.
- Hausman, M.A., & Ostriker, J.P., 1978, *Astrophys. J.*, **224**, 320.
- Haynes, M.P., Giovanelli, R., Chincarini, G.L., 1984, *Ann. Rev. Astron. Astrophys.*, **22**, 445.
- Heckmann, T.M., Balick, B., Crane, P.C., 1980, *Astron. Astrophys. Suppl.*, **40**, 295
- Jacoby, G.H., Hunter, D.A., & Christian, C.A., 1984, *Astrophys. J. Suppl.*, **56**, 278.
- Jorden, P.R., Thorne, D.J., van Breda, I.G., 1982, *Proc. SPIE*, **331**, 87.
- Keeping, E.S., 1962, *Introduction to Statistical Inference*, Princeton; Van Nostrand.
- Kibblewhite, E.J., 1980, *APM Facility Manual*, Institute of Astronomy, Cambridge.
- King, C.R., & Ellis, R.S., 1985, *Astrophys. J.*, **288**, 456.
- Koo, D.C., 1981a, *Astrophys. J.*, **251**, L75.
- Koo, D.C., 1981b, *PhD thesis*, University of California, Berkeley.

- Koo,D.C., 1985, *Astron. J.*, **90**, 418.
- Koo,D.C., 1986, *Astrophys. J.*, **311**, 651.
- Kristian,J., Sandage,A., Westphal, 1978, *Astrophys. J.*, **221**, 383.
- Kron,R.G., 1978, *PhD thesis*, University of California, Berkeley.
- Larson,R.B., Tinsley,B.M., Caldwell,C.N., 1980, *Astrophys. J.*, **237**, 692.
- Lavery,R.J., & Henry,J.P., 1986, *Astrophys. J.*, **304**, L5.
- Lavery,R.J., & Henry,J.P., 1987, *Preprint*.
- Lilly,S.J., 1983, *PhD thesis*, University of Edinburgh.
- Lilly,S.J., & Gunn,J.E., 1985, *Mon. Not. R. Astr. Soc.*, **217**, 551.
- Lilly,S.J., & Longair,M.S., 1984, *Mon. Not. R. Astr. Soc.*, **211**, 833.
- Loh,E.D., & Spillar,E.J., 1986, *Astrophys. J.*, **303**, 154.
- Lucey,J.R., 1983, *Mon. Not. R. Astr. Soc.*, **204**, 33.
- Lynds,C.R. & Petrosian,V., 1986, *Bull. Am. Astr. Soc.*, **18**, 1014.
- Malin,D.F., 1978, *Nature*, **276**, 591.
- Malin,D.F., & Carter,D., 1980,...
- Matthieu,R.D., & Spinrad,H., 1981, *Astrophys. J.*, **251**, 485.
- Mellier,Y., Soucail,G., Fort,B., & Mathez,G., 1987, preprint.
- Metcalfe,N., 1983, *DPhil thesis*, University of Oxford.
- Mihalas,D., & Binney,J., 1981, *Galactic Astronomy*, W.H. Freeman & Co., San Francisco.
- Miller,G.E., & Scalo,J.M., 1978, *Astrophys. J. Suppl.*, **41**, 513.
- Newell,E.B., 1979, *Image Processing in Astronomy*, eds. Sedmak,G., Capaccioli,M., & Allen,R.J., Observatorio Astronomica di Trieste.
- Newell,E.B., 1982, *Occassional Report of the ROE*, **10**.
- O'Connell,R.W., 1973, *Astrophys. J.*, **78**, 1074.
- O'Connell,R.W., 1976, *Astrophys. J.*, **206**, 370.
- O'Connell,R.W., 1980, *Astrophys. J.*, **236**, 430.
- O'Connell,R.W., 1983, *Astrophys. J.*, **267**, 80.
- O'Connell,R.W., 1986, *Spectral Evolution of Galaxies*, eds. Renzini,A., & Chiosi,C., Reidel, Holland.
- Oemler,A., 1974, *Astrophys. J.*, **194**, 1.
- Oke,J.B., 1974, *Astrophys. J. Suppl.*, **27**, 21.
- Oke,J.B., 1983, *Clusters & Groups of Galaxies*, eds. Mardirossian,F., Giarcin,G., Mezetti,M., Reidel, Holland.
- Oke,J.B., Bertola,F., & Capaccioli,M., 1981, *Astrophys. J.*, **243**, 453.
- Ostriker,J.P., & Tremaine,S.D., 1975, *Astrophys. J.*, **202**, 413.
- Parry,I.R., 1986, *PhD thesis*, University of Durham.
- Pence,W.D., 1979, *Astrophys. J.*, **203**, 39.
- Peterson,B.A., Ellis,R.S., Kibblewhite,E.J., Bridgeland,M.J., Hooley,T., Horne,D., 1979, *Astrophys. J.*, **233**, L109.
- Pickles,A.J., 1985, *Astrophys. J.*, **296**, 340.
- Pickles,A.J., & Visvanathan,N., 1985, *Astrophys. J.*, **294**, 134.

- Press, W.H., Flannery, B.P., Teukolsky, S.A., Vetterling, W.T., 1986, *Numerical Recipes*, Cambridge University Press.
- Prestage, R., 1984, *PhD thesis*, University of Edinburgh.
- Richstone, D., 1976, *Astrophys. J.*, **204**, 642.
- Robertson, G., 1985, *Preprint*.
- Rocca-Volmerange, B., & Guiderdoni, B., 1986, *Spectral Evolution of Galaxies*, eds. Renzini, A., & Chiosi, C., Reidel, Holland.
- Rose, J.A., 1984, *Astron. J.*, **89**, 1258.
- Rose, J.A., 1985, *Astron. J.*, **90**, 10.
- Schneider, D.P., Dressler, A., Gunn, J.E., 1986, *Astron. J.*, **92**, 523.
- Seaton, M.J., 1981 *Mon. Not. R. Astr. Soc.*, **187**, 75p.
- Shanks, T., Couch, W.J., McHardy, I.M., Cooke, B.A., Pence, W.D., 1986, *Preprint*.
- Shanks, T., Stevenson, P.R.F., Fong, R., MacGillivray, H., 1984, *Mon. Not. R. Astr. Soc.*, **206**, 767.
- Sharples, R.M., Ellis, R.S., Couch, W.J., & Gray, P.M., 1985, *Mon. Not. R. Astr. Soc.*, **212**, 687.
- Sparke, L.S., Kormendy, J., Spinrad, H., 1980, *Astrophys. J.*, **235**, 755.
- Spinrad, H., 1980, *IAU Symp. 92*, p39, eds. Abell, G.O. & Peebles, P.J.E., Reidel, Holland.
- Stevenson, P.R.F., 1986, *PhD thesis*, University of Durham.
- Stobie, R.S., Smith, G.M., Lutz, R.K., Martin, R., 1979, *Proc. Int. Workshop on Image Processing in Astronomy.*, Trieste.
- Straižys, V., & Sviderskiene, Z., 1972, *Bull. Vilnius Astron. Obs.*, 35.
- Thompson, L.A., 1986, *Astrophys. J.*, **300**, 639.
- Thompson, L.A., 1986, *Astrophys. J.*, **306**, 384.
- Thompson, L.A., & Gregory, S.A., 1980, *Astrophys. J.*, **242**, 1
- Tinsley, B.M., 1972, *Astrophys. J.*, **178**, 319.
- Tinsley, B.M., 1979, *Physical Cosmology, Les Houches*, eds. Balian, R., Andouze, J., Schramm, D.N., North Holland Publ.Co.
- van den Bergh, S., 1976, *Astrophys. J.*, **206**, 883.
- Visvanathan, N., & Sandage, A., 1977, *Astrophys. J.*, **216**, 214.
- White, S.D.M., Silk, J., & Henry, J.P., 1981, *Astrophys. J.*, **251**, L65.
- Wyse, R.F.G., 1985, *Astrophys. J.*, **299**, 593.
- Yates, M.G., Miller, L., Peacock, J.A., 1987, *Preprint*.
- Zwicky, F., Herzog, E., Karpowicz, M., Kowal, C., Wild, P., 1961-1968, *Catalogue of Galaxies and Clusters of Galaxies*, Vol I-VI, Pasadena, Calif. Inst. Tech.

Acknowledgements.

During the period over which research was undertaken for this thesis I have received a great deal of valuable help and advice from many people. I should firstly like to acknowledge my supervisor Prof.R.S. Ellis, and also Dr.W.J. Couch, both of whose assistance was invaluable. I have also greatly appreciated discussions with Dr.s J.R. Lucey, T. Shanks, N. Metcalfe, R. Fong, B.J. Boyle, P.R.F. Stevenson, R.M. Sharples, and L.R. Jones. Special gratitude is also due Dr.B. Mobasher, for putting up with me sharing an office with him for two years.

I have also visited a number of observatories and research establishments during this period and I thank everyone I met for their help, particularly Dr.L.A. Thompson at the University of Hawaii. Further, I acknowledge the use of data from the *International Ultraviolet Explorer* archives and observations made at the European Space Agency tracking station at Villafraanca del Castillo. The library of stellar spectra used in the models of chapter 5 was obtained from the Astronomical Data Center at the NASA Goddard Space Flight Center.

I acknowledge the support of the Science and Engineering Research Council for the award of a postgraduate research studentship during this period. I thank also the Department of Physics of Durham University for the use of its facilities including the local STARLINK node.

A great deal of the present work (including the printing of this thesis using T_EX!) would simply not have been possible without the patience and helpfulness of Mr.A.P. Lotts and Mr.R.M. Myers, whose knowledge of the intricacies of computing is matched only by my ignorance.

The completion of the work discussed here would have been impossible were it not for the encouragement and support of all of my friends, both Celtic and otherwise. In particular I wish to thank Gillian, Graeme, John, Stephen and John for allowing me to exploit their hospitality to a great degree whilst 'on the run' from Durham. Also, Janey Cringean, Brian Houston, David Lambrick, Dave Mannion, Michael Trueman, Gill Cooper, Anthony Lewis, and everyone else I've complained to in Durham. The Scottish National and Communist Parties also served as stimulants in promoting a critical, dialectical approach.

Finally, my family in Paisley, should be thanked for their patience over all these years in which I've hidden in the sheltered, over-privileged world of academia.

